Numerical simulation of compressible multiphase flows with or without phase transition. Application to laser plasma interaction

Vincent Perrier

N° d'ordre: 3394

THÈSE

présentée à

L'UNIVERSITÉ BORDEAUX 1

ÉCOLE DOCTORALE DE MATHÉMATIQUES ET INFORMATIQUE

par **Vincent Perrier**

POUR OBTENIR LE GRADE DE

DOCTEUR

SPECIALITÉ: MATHÉMATIQUES APPLIQUÉES

Modélisation et simulation d'écoulements multiphasiques compressibles avec ou sans changement de phase. Application à l'interaction laser–plasma.

Soutenue le 10 Juillet 2007.

Après avis de

M. Allaire, Grégoire, Professeur à l'École Polytechnique	Rapporteur
M. Kröner, Dietmar, Professeur à l'Université de Freiburg	Rapporteur

Devant la commission d'examen formée de

M. Abgrall, Rémi, Pr. à l'Université de Bordeaux 1	Directeur de thèse
M. Allaire, Grégoire, Pr. à l'École Polytechnique	Rapporteur
M. Colin, Thierry, Pr. à l'Université de Bordeaux 1	Président
M. Coquel, Fréderic, C.R. au Laboratoire Jacques-Louis Lions	Examinateur
M. Kröner, Dietmar, Pr. Dr. à l'université de Freiburg am Breigsbau	Rapporteur

Contents

List of Figures

Remerciements

Je remercie en premier Rémi Abgrall pour m'avoir proposé ce sujet, pour avoir suivi le déroulement de mes travaux, ainsi que pour m'avoir permis de pouvoir présenter ceux-ci dans plusieurs conférences. Je remercie également Ludovic Hallo, qui a tout d'abord eu la lourde tâche de partager mon bureau lorsque j'étais au CELIA, et avec qui j'ai pu avoir de nombreuses discussions sur le changement de phase, ainsi que sur d'autres aspects de l'interaction laser matière.

Je remercie aussi Dietmar Kroener et Grégoire Allaire pour avoir accepté de rapporter sur mon travail. Je remercie en particulier M. Allaire pour les nombreuses remarques qu'il m'a faites, qui m'ont permis d'améliorer la qualité et la clarté de ce manuscrit.

Je remercie Frédéric Coquel, qui a accepté de participer au jury, et Thierry Colin, qui a accepté de le présider.

Que ça soit au CELIA ou au MAB, je remercie les personnes avec qui j'ai eu l'occasion de partager des idées, un repas, des discussions ou un bureau: Afeintou, Stéphane, Benoit, Rolands, Mikaël, Samuel, Aubin, Arnaud, PH, Jérôme, Marina, Christophe, Boniface etc... (les trois petits points contiennent toutes les personnes à qui je ne pense pas dans l'immédiat, qu'ils m'en excusent!).

Durant l'été 2006, j'ai eu la chance de participer au CEMRACS. Je remercie les organisateurs, Guillaume Bal, Josselin Garnier, et Didier Lucor ainsi que les autres participants pour la bonne ambiance qui y a régné pendant un mois et demi. Je remercie particulièrement Guillaume et Josselin pour la patience et la disponibilité dont ils ont fait preuve pour me faire découvrir l'homogénéisation stochastique.

Je remercie mes parents, grand-parents ainsi que mes frères pour le soutien et les encouragements qu'ils m'ont apportés pendant mes études.

Enfin, je remercie tous mes amis, de Reims, Lyon, Paris ou d'ailleurs.

Une mention spéciale pour mes camarades de la section Rugby du B.E.C. avec qui j'ai passé pas mal de temps ces dernières années, dans la boue et dans les bars.

Introduction

This PhD deals mainly with the approximation of compressible multiphase flows with or without phase transition. The numerical approximation of such problems is of direct industrial applications, and we will first give some context in which such flows may be encountered.

High energetic materials

In a simple material, the energetic properties, i.e. its performance in detonation and its stability, are limited by the properties induced by their molecular structure. In a multimaterial medium, the properties of the different materials can be combined. For example, in an alloy, one of the material can be more malleable, and the other one more combustible: then the alloy will be very combustible, but also few sensitive to mechanical stress. Nevertheless, the interaction between the different materials: relaxation, capillarity, chemical reactions leads to much more numerical difficulties. The main difficulties are due to high pressures, all these materials can be considered as compressible flows. A deep study of the numerical problems and their solution for the simulation of high energetic multimaterials can be found in [24].

Oil extraction [8]

When petroleum is extracted offshore, the pipeline that drive the fuel to earth contains a mixture of water, gas and liquid oil. Due to the ground topography, the flows in the pipelines can be very different: annular, stratified, dispersed... The simulation of such flows can prevent slugging, help in dimensioning the pipes.

Nuclear safety [16]

A well known phenomenon that can be encountered in nuclear engines is the boiling crisis. In a nuclear reactor, the cooling is made with high pressure water. If the temperature becomes high enough, the water may be vaporized. Nevertheless, the thermal conduction of the vapour is lower than the one of the liquid water. Therefore, if a thin of vapour appears, the heat is no more dissipated, and the engine is no more cooled, see Figure 1.

Inertial Confinement Fusion (ICF)

The aim of inertial confinement fusion is to produce energy with thermonuclear fusion. The conditions of fusion are very hard to reach, because the material must be at a high density and a high temperature. In ICF, a laser

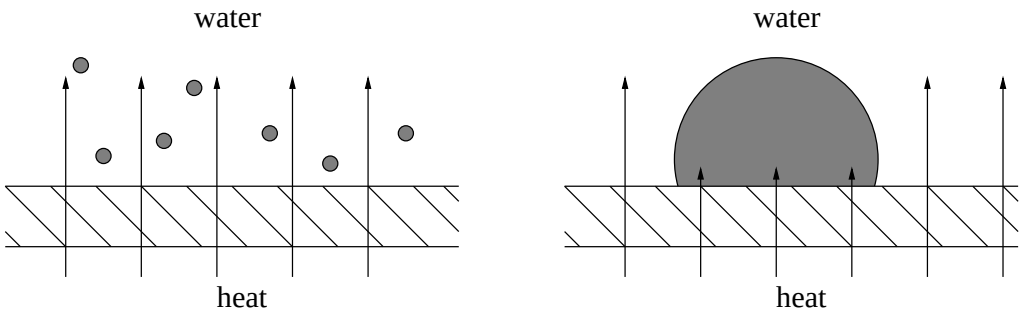

Figure 1: On the left, the heat can be transmitted to the water. Some vapour bubbles appear (in grey). On the right, a boiling crisis occurs: a big bubble of vapour grows and remains on the wall;the heat is fewer transmitted to the water, because the vapour has a lower thermal conduction than the liquid. In that case, the engine is no more cooled.

is used to make implode a target, in order to increase its density, and to enlighten it, in order to increase its temperature. The target is initially composed of gaseous Deuterium inside a Deuterium-Tritium solid shell. When the shell is enlightened, it implodes, and the solid is transformed into a gas. In the thermodynamic conditions, the solid can be considered as compressible. Modelling phase transition for compressible flows becomes crucial in this context.

Multiphase flows can be encountered in many other contexts such as reentry of objects [46], fuel engines [39]... These last applications may also include phase transition.

The modelling of one phase flow, without viscosity nor thermal conductivity is modelled by the Euler system

$$\begin{cases} \dfrac{\partial \rho}{\partial t} + \nabla \cdot (\rho \mathbf{u}) = 0 \\ \dfrac{\partial (\rho \mathbf{u})}{\partial t} + \nabla \cdot (\rho \mathbf{u} \otimes \mathbf{u} + P) = 0 \\ \dfrac{\partial (\rho E)}{\partial t} + \nabla \cdot ((\rho E + P)\mathbf{u}) = 0 \end{cases} \tag{1}$$

where ρ is the density of the fluid, P its pressure and $\mathbf{u}$ its velocity. E is the total specific energy, which is equal to

$$E = \varepsilon + \frac{|\mathbf{u}|^2}{2}$$

where ε is the specific internal energy. The pressure P, specific energy ε and density ρ are linked with an equation of state

$$\varepsilon = \varepsilon(P, \rho).$$

(1) holds only for regular solutions. The weak solutions must ensure another equation

$$\frac{\partial(\rho s)}{\partial t} + \nabla \cdot (\rho s \mathbf{u}) \geq 0$$

where s is the entropy of the fluid.

However there remains difficulties, as for free surface, or when vacuum appears, or when the equation of state is strongly nonlinear, the numerical approximation for (1) is well known in normal conditions.

For multiphase flows, things become more complex, because even the system of partial derivative equations is not clear. In some cases, when the size of the bubbles or droplets is larger than the typical size of the mesh, a Lagrangian approximation can be used, in order to keep separate phases. Nevertheless, Lagrangian methods can become very costly and inaccurate when the mesh becomes very distorted. Moreover, these approximations hold only when the two fluids are very well separated, and when the scale of the inclusions remains large. If one of the fluids is very dispersed, then the carrier phase is approximated with the Eulerian system, and the particles are modelled with their Lagrangian equations.

In many cases, the exact description of bubbles, droplets and interfaces is too costly to describe, and then homogenised models are preferred. The system of governing equations is obtained by volume and time averaging of the single phases equations [20]. Most of these systems include equations on mass, momentum, and energy for each phase. As we will see in Chapter 1, the averaging does not solve all the problems, because additional fluctuations terms appear, that must be modelled.

In all these models, combustion and phase transition can be taken into account by source terms. Nevertheless, their compatibility with the second principle of thermodynamic is not always ensured.

This PhD is divided into three parts

1. Approximation of compressible multiphase flows.
2. Modelling and numerical simulation of phase transition in multiphase flows.
3. Stochastic homogenization.

and we give more details on the content of each part in the following.

1. Approximation of compressible multiphase flows

In this first part, we present a numerical scheme for the simulation of compressible multiphase flows.

In Chapter 1, we use the derivation of [20] to obtain an homogenised model of two phase flows. This model reads

$$\begin{cases} \dfrac{\partial \alpha^{(k)}}{\partial t} + \mathbf{u}_I \cdot \nabla \alpha^{(k)} = FV^{(k)} \\ \dfrac{\partial \left(\alpha^{(k)} \rho^{(k)}\right)}{\partial t} + \nabla \cdot \left(\alpha^{(k)} \rho^{(k)} \mathbf{u}^{(k)}\right) = \Gamma^{(k)} \\ \dfrac{\partial \left(\alpha^{(k)} \rho^{(k)} \mathbf{u}^{(k)}\right)}{\partial t} + \nabla \cdot \left(\alpha^{(k)} \left(\rho^{(k)} \mathbf{u}^{(k)} \otimes \mathbf{u}^{(k)} + P^{(k)} \mathbf{I}\right)\right) = P_I \nabla \alpha^{(k)} + \mathbf{u}_\Gamma^{(k)} \Gamma^{(k)} \\ \qquad\qquad + \mathbf{M}^{(k)} \\ \dfrac{\partial \left(\alpha^{(k)} \rho^{(k)} E^{(k)}\right)}{\partial t} + \nabla \cdot \left(\alpha^{(k)} \left(\rho^{(k)} E^{(k)} + P^{(k)}\right) \mathbf{u}^{(k)}\right) = -P_I \dfrac{\partial \alpha^{(k)}}{\partial t} + \Gamma^{(k)} h_\Gamma^{(k)} \\ \qquad\qquad + \mathbf{u}_I \cdot \mathbf{M}^{(k)} + Q^{(k)} \end{cases} \tag{2}$$

where $FV^{(k)}$, $\Gamma^{(k)}$, $\mathbf{u}_\Gamma^{(k)}$, $\mathbf{M}^{(k)}$, $h_\Gamma^{(k)}$ and $Q^{(k)}$ are fluctuations terms that appear in the homogenisation of the equations. $\mathbf{u}_I$ and P_I are the velocity and the pressure at the interface. The interface variables and the fluctuations terms are not known and therefore must be modelled. Based on entropy considerations, we give some example of closure of the above system. We show why it is natural to model the fluctuation terms by relaxation terms. They physically mean that the phases tend to return to thermodynamic and mechanical equilibrium. The system that is of interest in the following of this part is

$$\begin{array}{lll} \dfrac{\partial \alpha^{(k)}}{\partial t} + \mathbf{u}_I \cdot \nabla \alpha^{(k)} & = & \mu (P^{(k)} - P^{(\bar{k})}) \\ \dfrac{\partial \left(\alpha^{(k)} \rho^{(k)}\right)}{\partial t} + \operatorname{div}\left(\alpha^{(k)} \rho^{(k)} \mathbf{u}^{(k)}\right) & = & 0 \\ \dfrac{\partial \left(\alpha^{(k)} \rho^{(k)} \mathbf{u}^{(k)}\right)}{\partial t} + \operatorname{div}\left(\alpha^{(k)} \rho^{(k)} \mathbf{u}^{(k)} \otimes \mathbf{u}^{(k)}\right) + \nabla (\alpha^{(k)} P^{(k)}) & = & P_I \nabla \alpha^{(k)} \\ & & + \lambda (\mathbf{u}^{(\bar{k})} - \mathbf{u}^{(k)}) \\ \dfrac{\partial \left(\alpha^{(k)} \rho^{(k)} E^{(k)}\right)}{\partial t} + \operatorname{div}\left(\alpha^{(k)} (\rho^{(k)} E^{(k)} + P^{(k)}) \mathbf{u}^{(k)}\right) & = & P_I \mathbf{u}_I \cdot \nabla \alpha^{(k)} \\ & & - \mu P_I (P^{(k)} - P^{(\bar{k})}) \\ & & + \lambda \mathbf{u}_I (\mathbf{u}^{(\bar{k})} - \mathbf{u}^{(k)}) \end{array} \tag{3}$$

The numerical approximation of (3) is difficult, at least for two reasons: first, even with the closure derived with entropy considerations, there remains to model the interfacial variables P_I and $\mathbf{u}_I$, and the time relaxations λ and

μ. The second reason is that (2) involves terms that are not in divergence form: nonconservative products. This is a deep problem in the context of hyperbolic problems. Indeed, it is well known that even in the scalar case

$$\frac{\partial u}{\partial t} + \frac{\partial (f(u))}{\partial x} = 0$$

the solutions become irregular in general, and we have to define shocks for such a system. For conservative systems as

$$\frac{\partial \mathbf{U}}{\partial t} + \frac{\partial (F(\mathbf{U}))}{\partial x} = 0$$

the shocks are defined by the jump condition $[F(\mathbf{U}) - \sigma \mathbf{U}] = 0$. For nonconservative problems, the shocks cannot be defined in general. Note that the problem of nonconservativity is a mathematical problem, and a numerical problem, because for example, in the Godunov' method, we need to solve a Riemann problem, which cannot be done in general without a clear definition of shocks [19].

In some contexts, the time relaxation can be very small, so that the system is like

$$\frac{\partial \mathbf{U}}{\partial t} + A(\mathbf{U}) \frac{\partial \mathbf{U}}{\partial x} = \frac{R(\mathbf{U})}{\varepsilon} \tag{4}$$

where $\varepsilon \to 0$. In Chapter 2, we show how to derive a reduced system from the system (4). We then apply this method to the seven equations model when the time relaxation in pressure and velocity tends to 0. In that case, if N_φ is the number of phases, and N the space dimension, then the number of equations decrease from $N_\varphi(3+3N)-1$ to $2N_\varphi + N$. For two phases flow, the reduced system is

$$\begin{cases} \dfrac{\partial \alpha^{(k)}}{\partial t} + u \dfrac{\partial \alpha^{(k)}}{\partial x} = \alpha^{(k)} \alpha^{(\bar{k})} \dfrac{\rho^{(\bar{k})} \, {c^{(\bar{k})}}^2 - \rho^{(k)} \, {c^{(k)}}^2}{\alpha^{(2)} \rho^{(1)} {c^{(1)}}^2 + \alpha^{(1)} \rho^{(2)} {c^{(2)}}^2} \dfrac{\partial u}{\partial x} \\ \dfrac{\partial (\alpha^{(k)} \rho^{(k)})}{\partial t} + \dfrac{\partial}{\partial x} \left(\alpha^{(k)} \rho^{(k)} u^{(k)} \right) = 0 \\ \dfrac{\partial (\rho u)}{\partial t} + \dfrac{\partial}{\partial x} \left(\rho u \otimes u + P \right) = 0 \\ \dfrac{\partial (\rho E)}{\partial t} + \dfrac{\partial}{\partial x} \left((\rho E + P) u \right) = 0 \end{cases} \tag{5}$$

We remark that this system does not suffer from any modelling problem. Nevertheless, a nonconservative product appears again, in the volume fraction equation. In the acoustic approximation of (5), we make a formal link with the system found by homogenising the acoustic approximation of the

Euler equations. This proves that, at least for small perturbations around an equilibrium, the modelling with relaxation terms, and then the asymptotic expansion are not fully wrong.

In Chapter 3, we propose an approximation of the system (5). For that, we start from the scheme developed in [2], which gives a numerical approximation of (3), and in which terms appear that can be seen as relaxation terms. The scheme of [2] is based on an averaging of Riemann problems between pure fluids. The problem is that the relaxation terms depend on the solver used for the pure fluids Riemann problems. In Chapter 3, we prove that even if the terms depend on the solver, the equilibrium variety of these terms is equivalent to equilibrium of pressure and velocity. We prove also that their first order asymptotic expansion can be led independently from the solver. We thus can make an asymptotic expansion of the seven equations scheme to obtain a numerical scheme for the five equations model. Eventually, several numerical tests are presented in order to demonstrate the potential of this technique.

Chapter 3 was published in [4]:

- Rémi Abgrall and Vincent Perrier. Asymptotic expansion of a multiscale numerical scheme for compressible multiphase flows. *Multiscale Model. Simul.*, 5, 2006.

This chapter was also presented in the ICCFD 2004 [3]

- Rémi Abgrall and Vincent Perrier. Numerical approximation of multiphase flows. In *Third International Conference on Computational Fluid Dynamics*, Lecture Notes in Physics. Springer-Verlag, 2004.

2. Modelling and numerical simulation of phase transition in compressible flows

This is the largest part of this PhD. Chapter 4 is devoted to thermodynamic of phase transition. We begin by giving the usual definition of stability: a state is said to be stable provided its (physical) entropy is at a local maximum. It is necessary to suppose that the entropy is locally convave in order to ensure the existence of such an maximum. Given two equations of state, we build a mixture equation of state by maximising the mixture entropy. If the two fluids are here, then the optimisation gives the equality of pressures, temperature and chemical potential. Under some assumptions on the chemical potentials, this is equivalent to the fact that the pressure is a function of the temperature: $P = P_{\text{sat}}(T)$.

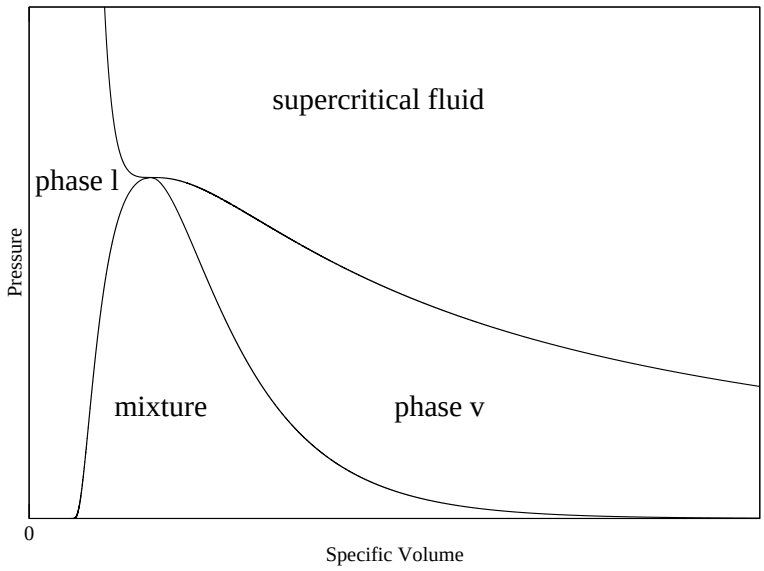

Figure 2: Above a given temperature and pressure, the vapour and liquid phases are the same, and the fluid is said to be supercritical. Otherwise, for low specific volume, the liquid is the most stable, for high specific volume, the vapour is the most stable, and between them, an area exists in which the most stable is the mixture.

For a given τ and P, there exists a state, liquid, gas or mixture, that is the most stable. The usually observed repartition of this state is shown on Figure 2. Above given temperature and pressure, the two phases are the same, and then the fluid is said to be supercritical. Otherwise, either the vapour is the most stable, or the liquid is the most stable, or it is the mixture. In some conditions, it may happen that a liquid or a gas exists for thermodynamic variables for which the mixture is stable: in that case, the state is said to be metastable.

Then we prove that the mixture entropy is concave provided

$$\frac{\mathrm{d}P_{\mathrm{sat}}}{\mathrm{d}T} > 0$$

To finish this chapter, we compare two types of phase transition modelling: the Van-der-Waals one, and a modelling with two stiffened gas equations of state. We show that the situation described in Figure 2 can be obtained with this modelling, but we prove also that we cannot model arbitrary metastable states. Modelling with two stiffened gas leads to the contrary: we cannot model supercritical fluid, and all the more, there may exist a pressure above

which the mixture equation of state is no more convex, even if the equation of state of the pure fluids are always convex. For the other chapters, we chose the model with two stiffened gas, because one of our aim is to model phase transition with metastable states.

In Chapter 5, we recall the classical way to solve the Riemann problem for a system of conservation laws.

$$\frac{\partial \mathbf{u}}{\partial t} + \frac{\partial (\mathbf{F}(\mathbf{u}))}{\partial x} = 0$$
$$\mathbf{u}(x,0) = \begin{cases} \mathbf{u}_L & \text{if} \quad x < 0 \\ \mathbf{u}_R & \text{if} \quad x > 0 \end{cases}$$

We emphasise the importance of the supposition of the genuinely nonlinearity of the linearly degeneracy to ensure the simplicity of the solution of the Riemann problem. We apply this way of solving the Riemann problem to the Eulerian system. We prove that the genuinely nonlinearity of the fields is linked with the sign of the fundamental derivative

$$\mathscr{G} = -\frac{\tau}{2} \frac{\left(\dfrac{\partial^3 \varepsilon}{\partial \tau^3}\right)_s}{\left(\dfrac{\partial^2 \varepsilon}{\partial \tau^2}\right)_s}$$

The problem in the equations of state built by entropy optimisation (and actually all the equation of states modelling first order phase transition) is that the first order coefficients are discontinuous across the saturation curve. This induces that the genuinely nonlinearity fails (the very definition of the genuinely nonlinearity relies on these first order thermodynamic parameters). In that case, a wave splitting may appear, and as an example, we remind the Liu solution, which is a split shock of liquefaction.

Chapter 6 deals with the application of the Chapman-Jouguet theory for solving the Riemann problem with vaporisation. In [56], it was observed that a vaporisation wave can be a self-similar discontinuity, between on one side a metastable liquid, and on the other side a mixture at thermodynamic equilibrium. Across this wave, the Rankine-Hugoniot relations hold. But as the equation of state of the mixture and the liquid are very different, the situation is slightly different from the classical shocks: as for a given pressure and specific volume we have

$$\varepsilon_{\text{mixture}}(P,\tau) - \varepsilon_{\text{liquid}}(P,\tau) = Q < 0$$

the Chapman-Jouguet theory shall be used. We recall the main assumptions of this theory: overheat, and positivity of the fundamental derivative, that

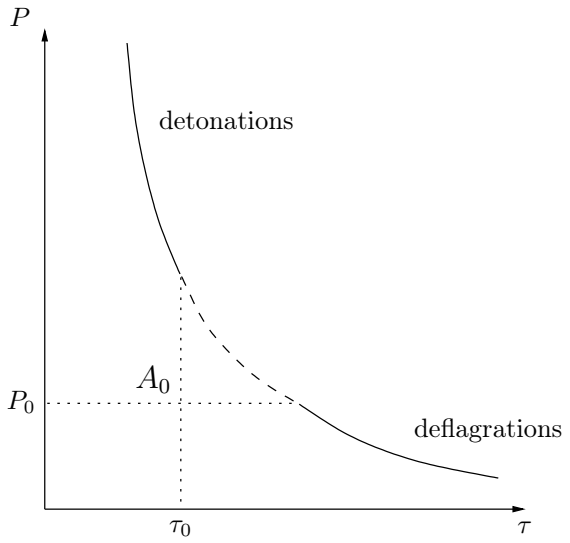

Figure 3: The Crussard curve related to an initial point (τ_0, P_0). Under the assumption of overheat, the set of the downstream states is over the initial point. If the fundamental derivative is positive, then the set of the downstream states is convex. This set is cut into three parts: if $\tau < \tau_0$ and $P > P_0$, then the wave is called a detonation, if $\tau > \tau_0$ but $P > P_0$, the states cannot be reached (we will explain in Chapter 6 why), and if $\tau > \tau_0$ and $P < P_0$, the wave is a deflagration.

can lead to the situation of Figure 3. We check in which condition these assumptions hold in our context. As the vaporisation is a wave in which the specific volume increases, it is necessary a deflagration. We then give a necessary condition under which the entropy growth criterion holds. As the deflagration waves are subsonic, the Lax criterion does not hold, so that a supplementary relation is needed to solve the Riemann problem: the kinetic closure. In [56], the vaporisation wave velocity was measured as being the Chapman-Jouguet velocity. This closure was extended in [39] to total vaporization front. Nevertheless, we prove that if the Chapman-Jouguet closure is used for both partial and total vaporisation front, then the resulting solution does not depend continuously in L^1 sense on its initial data. In a particular case (two perfect gas equation of state), we propose another relevant kinetic closure, that overcome this difficulty.

The part on phase transition ends with Chapter 7, which deals with the numerical simulation of compressible flows involving phase transition. We begin by recalling the discrete equations method for inert flows [2]. Actually, the main idea is to make an average of Riemann problems with pure phases on each side. The extension is straightforward in the case of total vaporisation [39]: actually, the contacts are replaced by the vaporisation fronts, and the Lagrangian fluxes are replaced by reactive fluxes. We also show how to integrate the fluxes when the vaporisation is only partial. Finally, we give some numerical examples, and an application in the context of laser interaction with matter.

Part of the Chapter 4 and of Chapter 6, are submitted in

- Vincent Perrier. The Chapman-Jouguet closure for the Riemann problem with vaporization. *SIAM Journal on Appl. Math.*, 2006. In revision.

Some parts were presented in [49, 50, 30]

- Vincent Perrier, Rémi Abgrall, and Ludovic Hallo. A numerical scheme for the modelling of condensation and flash vaporization in compressible multi-phase flows. In *Numerical Mathematics and Advanced Applications (ENUMATH 2005)*. Springer, 2005.

and a similar talk was made in the "Workshop on Numerical methods for multi–material fluid flows", in Oxford from 5 to 8 September 2005, and in the "first Workshop on Micro-Macro Modelling and simulation of liquid-vapour flows" (DGF-CNRS group), in Kirchzarten from 16 to 18 November 2005.

The laser interaction with matter simulations were presented in

- Vincent Perrier, Ludovic Hallo, and Rémi Abgrall. A several waves solver for phase transition in laser-matter interaction. In *28th European Conference on laser interaction with matter*, 2004.

- Ludovic Hallo, Vincent Perrier, and Rémi Abgrall. Application of a multiwave solver to ICF like problems. 46th APS, 2004.

and in an article that has not been submitted yet.

3. Stochastic homogenisation

This part of the PhD was made during the Cemracs 2006. As stated in Chapter 1, stochastic homogenization is the origin of the multiphase flow model used in this PhD. Nevertheless, the derivation led in this chapter was only formal, and the Cemracs gave me the opportunity to discover rigorously stochastic homogenization. The potential links with multiphase flows are exposed in Chapter 3 and in the conclusion.

The initial problem was posed by EADS. The aim is similar as what was exposed for high energetic materials in the beginning of this introduction. We have two materials: the material (A), which has some required physical properties, but that is too soft for being used in the industry, and another material, (B) that is very rigid. The idea is to mix them in order to build pieces that have the physical properties of (A), but that also have the rigidity of (B).

Some traction experiments are led to test this building process: we start with a material composed with pure (A), and more and more needles of (B) are put inside. We expect that, when the fraction of (B) becomes uniform, the material tends to an homogenised material. This is indeed what is observed, but the dispersion of the results is very large, typically not in $1/\sqrt{\varepsilon}$ (ε is the correlation length of heterogeneities), as it can be expected usually for stochastic homogenisation.

The traction experiments can be modelled with the linear elasticity system. In Chapter 8, we are interested in a simplified one dimensional problem: we consider the problem

$$\left\{ \begin{array}{l} -\dfrac{d}{dx}\Big(a\Big(\dfrac{x}{\varepsilon},\omega\Big)\dfrac{d}{dx}u^\varepsilon\Big) = f(x), \qquad 0 \leq x \leq 1, \quad \omega \in \Omega, \\ u^\varepsilon(0,\omega) = 0, \qquad u^\varepsilon(1,\omega) = q. \end{array} \right.$$

where a is a stationary ergodic random process such that $0 < a_0 \leq a(x,\omega) \leq 1/a_0$ for $(x,\omega) \in (0,1) \times \Omega$ where $(\Omega, \mathcal{F}, \mathcal{P})$ is an abstract probability space.

Then with classical assumptions on f, u^ε converges $\mathcal{P}$ - a.s. weakly in $H^1(0,1)$ to the deterministic solution $\bar{u}$ of

$$\begin{array}{l} -\dfrac{d}{dx}\Big(a^*\dfrac{d}{dx}\bar{u}\Big) = f(x), \qquad 0 \le x \le 1, \\ \bar{u}(0) = 0, \qquad \bar{u}(1) = q. \end{array} \tag{6}$$

where the effective diffusion coefficient is given by $a^* = \big(\mathscr{E}\{a^{-1}(0,\cdot)\}\big)^{-1}$.

We are interested here in the derivation of corrector for the convergence of the heterogeneous solution to the homogeneous solution, i.e. we look for the equivalent of $u^\varepsilon - \bar{u}$. We make the hypothesis that the process $1/a$ is the image of a Gaussian process g_x:

$$\frac{1}{a} = \frac{1}{a^\star} + \Phi(g_x) \tag{7}$$

where Φ is a bounded function such that

$$\int_{-\infty}^{+\infty} \Phi(g)\mathrm{e}^{-g^2/2}\, dg = 0.$$

We denote by R the autocorrelation function $R(\tau) = \mathscr{E}\left(a(x+\tau,\omega)a(x,\omega)\right)$. We prove that if g_x has an heavy tail, typically $R(\tau) \sim \kappa/\tau^\alpha$ with $0 \le \alpha \le 1$, then the process a has also an heavy tail. In [37, 13], if R is L^1, and under some mixing conditions on a, it is proved the following convergence in distribution

$$\frac{u^\varepsilon - \bar{u}}{\sqrt{\varepsilon}} \to \left(2\int_0^\infty R(\tau)\, d\tau\right)^{1/2} \mathcal{U}(x)$$

where

$$\mathcal{U}(x) = \int K(x,t) dW_t$$

where dW_t is a classical Wiener process. When a is defined by (7), the we proved the following convergence in distribution

$$\frac{u^\varepsilon - \bar{u}}{\varepsilon^{\alpha/2}} \to \sqrt{\frac{\kappa}{H(2H-1)}}\mathcal{U}^H(x)$$

where

$$\mathcal{U}(x) = \int K(x,t) dW_t^H$$

where dW_t^H is a fractional Brownian motion with Hurst parameter $H = 1 - \dfrac{\alpha}{2}$. This part ends with numerical simulations which confirm the theoretical asymptotic behaviour of the error $u^\varepsilon - \bar{u}$.

Chapter 8 is submitted in

- Guillaume Bal, Josselin Garnier, Sébastien Motsch, and Vincent Perrier. Random integrals and correctors in homogenization. *Asymptotic Analysis*, 2007. Submitted.

Part I

Simulation of compressible multiphase flows

Table of Contents

[1] $\tilde{x} := \frac{\sqrt{\rho_L}x_L + \sqrt{\rho_R}x_R}{\sqrt{\rho_L} + \sqrt{\rho_R}}$.

Chapter 1

Derivation of a continuous multiphase model

In this chapter, we expose how to obtain a continuous model for describing the multiphase flows. Multiphase flows that are encountered can be very different depending on the phase materials, flow configuration, scale of interaction. Basically, their modelling can be divided into two categories

- Either we describe explicitly the interfaces. Then the equations are the Euler or Navier-Stokes equations with free surface, on which additional equations are required to describe the interface. This allows for example to make a computation with very different fluids (compressible and incompressible). Even if the flows are very well separated, this way of describing the flow can become very hard in some extreme situations for example when there are strong interface deformations (computation of instabilities).

- Or the exact position of interfaces is not necessary, or not known or too hard to compute. Then the better alternative are the *homogenized models*.

The way of describing the flows is crucial for the numerical approximation of the problem. Indeed, if the domain on which we want to compute a flow is meshed then if we want to use an explicit description of the flow, the mesh must move with the flow, and the most tiny elements of the mesh must be smaller than the smallest inclusions. Then for very small inclusions, the cost of the computation might become huge.

In this part, we are concerned only with homogenized models. In this chapter, we shortly recall how to begin deriving a continuous model with

the homogenisation theory of Drew and Passman [20]. The problem of this method is that it is not able to derive a complete set of equations, so that closures are necessary. We thus give some closures that are commonly used [26, 47, 16] to ensure some usual criteria.

1.1 Homogenisation theory of Drew and Passman

In this section, we sum up the main ideas of [20] that can lead to a modelling of averaged equations for multiphase flows.

1.1.1 The rules for averaging

In the context of multicomponent flows, we suppose that we can predict neither the exact location of each flows, interface, nor micro-scale phenomena. As remarked in [20], it can also be not desirable to know them in term of repeatability. Indeed, as the flow might depend on many parameters, it is likely that different experimentation or realization will lead to different results. We therefore aim only at describing the flow as an *ensemble average*. One realization will be a member of the ensemble see Figure 1.1.

The derivation we will do is purposely done in a non strict framework, and is in some sense only formal. In the derivation, we will need to know the value of functions on the boundary of the bubbles. For that, we use

Theorem 1.1. *if Ω^x is a bounded open subset, if $\partial\Omega^x$ is $\mathscr{C}^{1+[s]}$ ($s > \frac{1}{2}$), and if Ω^x is in one side of its boundary, then there exist a unique $\gamma \in \mathscr{L}(H^s(\Omega^x), H^{s-1/2}(\partial\Omega^x))$ such that for all $u \in \mathscr{D}(\mathbb{R}^n)$*

$$\gamma(u_{|\Omega^x}) = u_{|\partial\Omega^x}$$

so that we suppose that the following assumption holds

Assumption 1.1. *In a given realization, the interface is sufficiently regular (i.e. at least $\mathscr{C}^{3/2}$) compared with the regularity of the functions considered, to define the trace of all these functions.*

We parameterize the realizations by a random parameter ω, and we make the following assumption for a given realization

Assumption 1.2. *We suppose that for a given realization, the fluids can be isolated. Then we denote by χ_k the characteristic function of the fluid k:*

$$\begin{cases} \chi_k(\mathbf{x}, t, \omega) = 1 & \text{if } \mathbf{x} \text{ lies on the fluid } k \text{ for the realization } \omega, \\ \qquad\quad = 0 & \text{otherwise.} \end{cases}$$

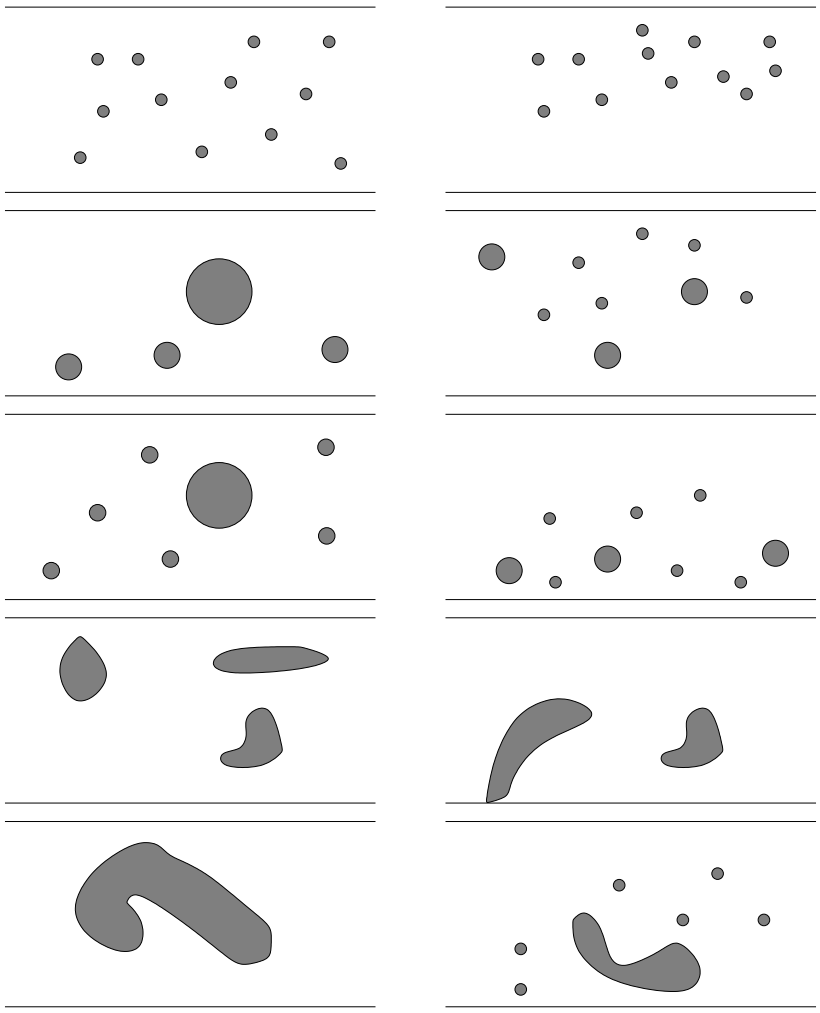

Figure 1.1: What we aim at computing is only the ensemble average of many different situations. All theses ten flows will be considered as different realizations of the same ensemble, because the black flow has more or less always the same volume.

When we will homogenise the equations, we will need an expression of the topological equation. It is given by the

Proposition 1.1 (Topological equation)**.** *The following equation holds (in the sense of distribution)*

$$\frac{\partial \chi_k}{\partial t} + \mathbf{v}_i \cdot \nabla \chi_k = 0 \tag{1.1}$$

Proof. We denote by ϕ a function in $\mathscr{D}(\Omega^x \times \mathbb{R})$. Then we have

$$\begin{aligned}\int_{\Omega^x} \phi \left(\frac{\partial \chi_k}{\partial t} + \mathbf{v}_i \cdot \nabla \chi_k \right) dv\, dt &= -\int_{\Omega^x} \chi_k \left(\frac{\partial \phi}{\partial t} + \nabla(\phi \mathbf{v}_i) \right) dv\, dt \\ &= \int_{-\infty}^{+\infty} \frac{\mathrm{d}}{\mathrm{d}t} \left(\int_{V_k(t)} \phi\, dv \right) dt \\ &= \left[\int_{V_k(t)} \phi\, dv \right]_{-\infty}^{\infty} \\ &= 0\end{aligned}$$

because $\phi \in \mathscr{D}(\Omega^x \times \mathbb{R})$. □

We denote by $\mathscr{E}(\cdot)$ the mathematical expectancy over all the realization considered. We remark that, again, the rigorous mathematical framework is left unclear: for example, the σ algebra is such that Assumption 1.1 holds for any realization. As we supposed that the boundaries are $\mathscr{C}^{3/2}$, we also suppose that this regularity is conserved by the topological equation. We suppose moreover that we have the following property,

Assumption 1.3. *We suppose that the derivation with respect to time and to space commute with the mathematical expectancy.*

For a given realization ω, the following set of equations holds

$$\frac{\partial W_k}{\partial t} + \frac{\partial}{\partial x} \left(F_k(W_k) \right) = 0$$

for all $\mathbf{x}$ and t such that $\chi_k(\mathbf{x}, t, \omega) = 1$, so actually, the following system holds

$$\chi_k \left(\frac{\partial W_k}{\partial t} + \frac{\partial}{\partial x} \left(F_k(W_k) \right) \right) = 0$$

As what we want to compute are the averaged variables, we are only interested in

$$\mathscr{E} \left(\chi_k \left(\frac{\partial W_k}{\partial t} + \frac{\partial}{\partial x} \left(F_k(W_k) \right) \right) \right) = 0 \tag{1.2}$$

Given this set of equations, we need to transform (1.2) in order to separate the mean values from the fluctuations. For that, we have two rules : the Gauss' and the Leibniz' ones.

Proposition 1.2 (Gauss rule)**.** *We denote by* $\mathbf{f}$ *a function that is regular in* Ω_k^x*. Then we have*

$$\mathscr{E}\left(\chi_k \nabla \mathbf{f}\right) = \nabla \mathscr{E}\left(\chi_k \mathbf{f}\right) - \mathscr{E}\left(\mathbf{f}_{ki} \nabla \chi_k\right)$$

where $\mathbf{f}_{ki}$ *is the value of the function evaluated on the component* k *side of the interface.*

Proof. We denote by ϕ a function in $\mathscr{D}(\Omega^x \times \mathbb{R})$. Then we have

$$\begin{aligned}\int_{\Omega^x} \phi \nabla(\chi_k \mathbf{f})\, dv\, dt &= -\int_{\Omega^x} \chi_k \mathbf{f} \nabla\phi\, dv\, dt \\ &= -\int_{\Omega_k^x} \mathbf{f} \nabla\phi\, dv\, dt \\ &= -\oint_{\partial\Omega_k^x} \phi \mathbf{f}_{ki} \cdot d\mathbf{S}\, dt + \int_{\Omega_k^x} \phi \nabla f\, dv\, dt\end{aligned}$$

Now, we need to express the integral on $\partial\Omega_k^x$ as an integral on Ω^x. We know that for any function g that is regular, with a compact support

$$\begin{aligned}\int_{\Omega^x} \mathbf{g} \nabla\chi_k\, dv\, dt &= -\int_{\Omega^x} \chi_k \nabla \mathbf{g}\, dv\, dt \\ &= -\int_{\Omega_k^x} \nabla \mathbf{g}\, dv\, dt \\ &= -\oint_{\partial\Omega_k^x} \mathbf{g}_{ki} \cdot d\mathbf{S}\, dt\end{aligned}$$

so that we eventually find

$$\int_{\Omega^x} \phi \nabla(\chi_k \mathbf{f})\, dv\, dt = \int_{\Omega^x} \phi \mathbf{f}_{ki} \nabla\chi_k\, dv\, dt + \int_{\Omega_k^x} \phi \nabla \mathbf{f}\, dv\, dt$$

which means that

$$\nabla(\chi_k \mathbf{f}) = \mathbf{f}_{ki} \nabla\chi_k + \chi_k \nabla \mathbf{f}$$

in the sense of distributions. Last, taking the mathematical expectancy $\mathscr{E}()$ gives the result.

□

Proposition 1.3 (Leibniz'rule)**.** *If we keep the same notations as in the Proposition 1.2 we have*

$$\mathscr{E}\left(\chi_k \frac{\partial \mathbf{f}}{\partial t}\right) = \frac{\partial}{\partial t} \mathscr{E}\left(\chi_k \mathbf{f}\right) - \mathscr{E}\left(\mathbf{f}_{ki} \frac{\partial \chi_k}{\partial t}\right)$$

where $\mathbf{f}_{ki}$ *was defined at the Proposition 1.2.*

As the proof is exactly the same as for Gauss' rule, we do not detail it here.

Thanks for Gauss' and Leibniz'rules, we can transform the system (1.2) to make appear equations on averaged quantities, as described in the following proposition

Proposition 1.4. *The system* (1.2) *can be put in the following form*

$$\frac{\partial}{\partial t}\left(\mathscr{E}\left(\chi_k W\right)\right) + \nabla \cdot \left(\mathscr{E}\left(\chi_k F(W)\right)\right) = \mathscr{E}\left(\left(F(W)_{ki} - \mathbf{v}_i W_{ki}\right)\nabla\chi_k\right) \tag{1.3}$$

Proof. The Gauss' and Leibniz' rules respectly give

$$\begin{aligned}\mathscr{E}\left(\chi_k \frac{\partial W}{\partial t}\right) &= \frac{\partial}{\partial t}\left(\mathscr{E}\left(\chi_k W\right)\right) - \mathscr{E}\left(W_{ki}\frac{\partial \chi_k}{\partial t}\right)\\ \mathscr{E}\left(\chi_k \nabla \cdot F(W)\right) &= \nabla \cdot \left(\mathscr{E}\left(\chi_k W\right)\right) - \mathscr{E}\left(W_{ki}\nabla\chi_k\right)\end{aligned}$$

and if we apply them, we get

$$\frac{\partial}{\partial t}\left(\mathscr{E}\left(\chi_k W\right)\right) + \nabla \cdot \left(\mathscr{E}\left(\chi_k F(W)\right)\right) = \mathscr{E}\left(W_{ki}\frac{\partial \chi_k}{\partial t}\right) + \mathscr{E}\left(F(W)_{ki}\nabla\chi_k\right)$$

Last, using the transport equation on χ_k gives

$$\frac{\partial}{\partial t}\left(\mathscr{E}\left(\chi_k W\right)\right) + \nabla \cdot \left(\mathscr{E}\left(\chi_k F(W)\right)\right) = \mathscr{E}\left(\left(F(W)_{ki} - \mathbf{v}_i W_{ki}\right)\nabla\chi_k\right)$$

□

1.1.2 Averaging of the Eulerian system

From now on, we suppose that the set of equations verified by the fluids is the Eulerian one, without viscosity nor thermal conductivity:

$$W = (\rho, \rho\mathbf{u}, \rho E)$$

$$F(W) = (\rho\mathbf{u}, \rho\mathbf{u}\otimes\mathbf{u} + \boldsymbol{\tau}, (\rho E + \boldsymbol{\tau})\cdot\mathbf{u})$$

where ρ denotes the density of the fluid, $\mathbf{u}$ its velocity. E is the specific total energy, and is the addition of the kinetic energy and the specific internal energy ε

$$E = \varepsilon + \frac{\mathbf{u}^2}{2}$$

$\boldsymbol{\tau}$ is the strain tensor, which is often taken equal to $P\mathbf{I}$, where P is the pressure. The system must be closed by an equation linking the thermodynamical parameters ρ, P and ε.

Definition 1.1 (Definition of the averaged variables)**.** *The mathematical expectancy of χ_k is the volume fraction of the fluid k.*

$$\alpha^{(k)} = \mathscr{E}(\chi_k)$$

The other variables are defined as Fabre average

$$\begin{aligned} \bar{\rho}^{(k)} &= \frac{\mathscr{E}\left(\chi_k \rho^{(k)}\right)}{\alpha^{(k)}} & \bar{\mathbf{u}}^{(k)} &= \frac{\mathscr{E}\left(\chi_k \rho^{(k)} \mathbf{u}^{(k)}\right)}{\alpha^{(k)} \bar{\rho}^{(k)}} \\ \bar{\boldsymbol{\tau}}^{(k)} &= \frac{\mathscr{E}\left(\chi_k \boldsymbol{\tau}^{(k)}\right)}{\alpha^{(k)}} & \bar{\varepsilon}^{(k)} &= \frac{\mathscr{E}\left(\chi_k \rho^{(k)} \varepsilon^{(k)}\right)}{\alpha^{(k)} \bar{\rho}^{(k)}} \end{aligned} \tag{1.4}$$

when there is no ambiguity, we will omit the bars over the variables.

Now, we aim at finding a system of PDE verified by the average variables that we have just defined. For a given variable a, we will consider that its fluctuations $a - \mathscr{E}(a)$ are small, and we will put all the fluctuations in the right hand side.

Proposition 1.5 (Mass equation)**.** *With the definitions of* (1.4)*, the equation on the mass is*

$$\frac{\partial(\alpha^{(k)} \rho^{(k)})}{\partial t} + \nabla \cdot \left(\alpha^{(k)} \rho^{(k)} \mathbf{u}^{(k)}\right) = \Gamma^{(k)} \tag{1.5}$$

with

$$\Gamma^{(k)} = \mathscr{E}\left(\rho_{ki} \left(\mathbf{u}_{ki} - \mathbf{v}_i\right) \cdot \nabla \chi_k\right)$$

Proof. This is just the consequence of (1.3) applied to the mass conservation equation of the Eulerian system, with the definitions of (1.4). □

Now, we compute an equation on the momentum. It is given by

Proposition 1.6 (Momentum equation)**.** *We suppose that the averaged strain tensor $\bar{\boldsymbol{\tau}}$ is equal to $P^{(k)}\mathbf{I}$. We suppose moreover that*

$$\forall k \qquad \mathscr{E}\left(P_i^{(k)}\right) = P_I$$

then the following equation on momentum holds

$$\frac{\partial(\alpha_k \rho_k \mathbf{u}_k)}{\partial t} + \nabla \cdot \left(\alpha^{(k)} \left(\rho^{(k)} \mathbf{u}^{(k)} \otimes \mathbf{u}^{(k)} + P^{(k)} \mathbf{I}\right)\right) = P_I \nabla \alpha^{(k)} + \mathbf{u}_\Gamma^{(k)} \Gamma^{(k)} + \mathbf{M}^{(k)} \tag{1.6}$$

with

$$\begin{aligned} \mathbf{u}_\Gamma^{(k)} &= \frac{\mathscr{E}\left(\rho_{ki} \mathbf{u}_{ki} \otimes \left(\mathbf{u}_{ki} - \mathbf{v}_i\right) \nabla \chi_k\right)}{\mathscr{E}\left(\rho_{ki} \left(\mathbf{u}_{ki} - \mathbf{v}_i\right) \cdot \nabla \chi_k\right)} \\ \mathbf{M}^{(k)} &= \mathscr{E}\left(\left(P_i^{(k)} - P_I\right) \nabla \chi_k\right) - \nabla \mathscr{E}\left(\chi_k \rho^{(k)} \left(\mathbf{u}^{(k)} - \bar{\mathbf{u}}^{(k)}\right) \otimes \left(\mathbf{u}^{(k)} - \bar{\mathbf{u}}^{(k)}\right)\right) \end{aligned}$$

Proof. Thanks for the definition of $\bar{\mathbf{u}}^{(k)}$, we have

$$\frac{\partial}{\partial t}\left(\mathscr{E}\left(\chi_k\rho^{(k)}\mathbf{u}^{(k)}\right)\right) = \frac{\partial(\alpha^{(k)}\rho^{(k)}\mathbf{u}^{(k)})}{\partial t}$$

We remark that, also with the definition of $\bar{\mathbf{u}}^{(k)}$

$$\begin{aligned}\mathscr{E}\left(\chi_k\rho^{(k)}\left(\mathbf{u}^{(k)}-\bar{\mathbf{u}}^{(k)}\right)\otimes\left(\mathbf{u}^{(k)}-\bar{\mathbf{u}}^{(k)}\right)\right) = \mathscr{E}\left(\chi_k\rho^{(k)}\mathbf{u}^{(k)}\otimes\mathbf{u}^{(k)}\right)\\ -\alpha^{(k)}\rho^{(k)}\bar{\mathbf{u}}^{(k)}\otimes\bar{\mathbf{u}}^{(k)}\end{aligned}$$

so that if we use the definition of the pressure, and of $\mathbf{u}_\Gamma^{(k)}$ the averaging (1.3) applied to the momentum equation becomes

$$\begin{aligned}&\frac{\partial(\alpha_k\rho_k\mathbf{u}_k)}{\partial t}+\nabla\cdot\left(\alpha^{(k)}\left(\rho^{(k)}\mathbf{u}^{(k)}\otimes\mathbf{u}^{(k)}+P^{(k)}\mathbf{I}\right)\right)\\ &= -\nabla\mathscr{E}\left(\chi_k\rho^{(k)}\left(\mathbf{u}^{(k)}-\bar{\mathbf{u}}^{(k)}\right)\otimes\left(\mathbf{u}^{(k)}-\bar{\mathbf{u}}^{(k)}\right)\right)\\ &\quad +\mathbf{u}_\Gamma^{(k)}\Gamma^{(k)}+\mathscr{E}\left(P_i^{(k)}\mathbf{I}\cdot\nabla\chi_k\right)\end{aligned}$$

By writing

$$\mathscr{E}\left(P_i^{(k)}\nabla\chi_k\right) = P_I\mathscr{E}\left(\nabla\chi_k\right)+\mathscr{E}\left(\left(P_i^{(k)}-P_I\right)\nabla\chi_k\right)$$

we remark that the last term is a fluctuation, so that

$$\begin{aligned}&\frac{\partial(\alpha_k\rho_k\mathbf{u}_k)}{\partial t}+\nabla\cdot\left(\alpha^{(k)}\left(\rho^{(k)}\mathbf{u}^{(k)}\otimes\mathbf{u}^{(k)}+P^{(k)}\mathbf{I}\right)\right)\\ &\qquad = \mathbf{M}^{(k)}+\mathbf{u}_\Gamma^{(k)}\Gamma^{(k)}+P_I\cdot\nabla\alpha^{(k)}\end{aligned}$$

with

$$\mathbf{M}^{(k)} = \mathscr{E}\left(\left(P_i^{(k)}-P_I\right)\nabla\chi_k\right)-\nabla\mathscr{E}\left(\chi_k\rho^{(k)}\left(\mathbf{u}^{(k)}-\bar{\mathbf{u}}^{(k)}\right)\otimes\left(\mathbf{u}^{(k)}-\bar{\mathbf{u}}^{(k)}\right)\right)$$

□

Remark 1.1 (Pressure)**.** We note that if the strain tensor before homogenization $\boldsymbol{\tau}$ is equal to $P\mathbf{I}$, and if we have an equation of state

$$P = P(\rho,\varepsilon)$$

then, given an averaged density and specific internal energy, the thermodynamical consistent pressure is equal to $P(\mathscr{E}(\rho),\mathscr{E}(\varepsilon))$ whereas the homogenized tensor $\bar{\boldsymbol{\tau}}$ is equal to $\mathscr{E}(P(\rho,\varepsilon))$ so that except for when the equation of state is linear in (ρ,ε), either the initial tensor is not equal to $P\mathbf{I}$ or we loose the thermodynamical consistency (i.e. the link between ρ,ε,P is not the same after homogenization).

Proposition 1.7 (Energy equation)**.** *As in Proposition 1.6, we suppose that*

$$\forall k \qquad \mathbf{u}_I = \mathscr{E}\left(u_i^{(k)}\right)$$

then we have

$$\begin{aligned}\frac{\partial\left(\alpha^{(k)}\rho^{(k)}E^{(k)}\right)}{\partial t} + \nabla\cdot\left(\alpha^{(k)}\left(\rho^{(k)}E^{(k)}+P^{(k)}\right)\mathbf{u}^{(k)}\right) = & -P_I\frac{\partial\alpha^{(k)}}{\partial t} + \Gamma^{(k)}h_\Gamma^{(k)} \\ & +\mathbf{u}_I\cdot\mathbf{M}^{(k)} + Q^{(k)}\end{aligned}$$

where $Q^{(k)}$ will be detailed in the proof.

Proof. If we use the result (1.3) for the energy equation of the Eulerian system, we have

$$\begin{aligned}&\frac{\partial}{\partial t}\left(\mathscr{E}\left(\chi_k\rho^{(k)}E^{(k)}\right)\right) + \nabla\cdot\left(\mathscr{E}\left(\chi_k\left(\rho^{(k)}E^{(k)}+P^{(k)}\right)\mathbf{u}^{(k)}\right)\right) \\ &\quad = \mathscr{E}\left(\rho_i^{(k)}E_i^{(k)}\left(\mathbf{u}_i^{(k)}-\mathbf{v}_i\right)\cdot\nabla\chi_k\right) + \mathscr{E}\left(P_i^{(k)}\mathbf{u}_i^{(k)}\nabla\chi_k\right)\end{aligned}$$

The first thing we want is to replace $\mathscr{E}\left(\chi_k\rho^{(k)}E^{(k)}\right)$ to recover the total energy:

$$\begin{aligned}\mathscr{E}\left(\chi_k\rho^{(k)}E^{(k)}\right) &= \mathscr{E}\left(\chi_k\rho^{(k)}\left(\varepsilon^{(k)}+\frac{\mathbf{u}^{(k)^2}}{2}\right)\right) \\ &= \alpha^{(k)}\rho^{(k)}\left(\varepsilon^{(k)}+\frac{\mathbf{u}^{(k)^2}}{2}\right) + \frac{1}{2}\mathscr{E}\left(\chi_k\rho^{(k)}\left(\mathbf{u}^{(k)}-\bar{\mathbf{u}}^{(k)}\right)^2\right) \\ &= \alpha^{(k)}\rho^{(k)}E^{(k)} + \frac{1}{2}\mathscr{E}\left(\chi_k\rho^{(k)}\left(\mathbf{u}^{(k)}-\bar{\mathbf{u}}^{(k)}\right)^2\right)\end{aligned}$$

Using the same ideas, we have

$$\mathscr{E}\left(\chi_k\rho^{(k)}\varepsilon^{(k)}\right) = \alpha^{(k)}\rho^{(k)}\varepsilon^{(k)} + \mathscr{E}\left(\chi_k\rho^{(k)}\left(\mathbf{u}^{(k)}-\bar{\mathbf{u}}^{(k)}\right)\left(\varepsilon^{(k)}-\bar{\varepsilon}^{(k)}\right)\right),$$

$$\begin{aligned}\mathscr{E}\left(\chi_k\rho^{(k)}\mathbf{u}^{(k)^3}\right) = & \ \alpha^{(k)}\rho^{(k)}\mathbf{u}^{(k)^3} + 3\mathbf{u}^{(k)}\mathscr{E}\left(\chi_k\rho^{(k)}\left(\mathbf{u}^{(k)}-\bar{\mathbf{u}}^{(k)}\right)^2\right) \\ & +\mathscr{E}\left(\chi_k\rho^{(k)}\left(\mathbf{u}^{(k)}-\bar{\mathbf{u}}^{(k)}\right)^3\right),\end{aligned}$$

and

$$\mathscr{E}\left(\chi_k P^{(k)}\mathbf{u}^{(k)}\right) = \alpha^{(k)}P^{(k)}\mathbf{u}^{(k)} + \mathscr{E}\left(\chi_k P^{(k)}(\mathbf{u}^{(k)}-\bar{\mathbf{u}}^{(k)})\right)$$

so that the equation on energy becomes

$$\begin{aligned}
&\frac{\partial\left(\alpha^{(k)}\rho^{(k)}E^{(k)}\right)}{\partial t}+\nabla\cdot\left(\alpha_k\left(\rho_k E_k+P_k\right)\mathbf{u}_k\right)\\
&\quad=\mathscr{E}\left(\left(\rho_i^{(k)}E_i^{(k)}\left(\mathbf{u}_i^{(k)}-\mathbf{v}_i\right)+P_i^{(k)}\mathbf{u}_i^{(k)}\right)\cdot\nabla\chi_k\right)\\
&\qquad-\frac{\partial}{\partial t}\left(\frac{1}{2}\mathscr{E}\left(\chi_k\rho^{(k)}\left(\mathbf{u}^{(k)}-\bar{\mathbf{u}}^{(k)}\right)^2\right)\right)\\
&\qquad-\nabla\cdot\mathscr{E}\left(\chi_k\rho^{(k)}\left(\mathbf{u}^{(k)}-\bar{\mathbf{u}}^{(k)}\right)\left(\varepsilon^{(k)}-\bar{\varepsilon}^{(k)}\right)\right)\\
&\qquad-\frac{3}{2}\nabla\cdot\left(\mathbf{u}^{(k)}\mathscr{E}\left(\chi_k\rho^{(k)}\left(\mathbf{u}^{(k)}-\bar{\mathbf{u}}^{(k)}\right)^2\right)\right)\\
&\qquad-\frac{1}{2}\nabla\cdot\mathscr{E}\left(\chi_k\rho^{(k)}\left(\mathbf{u}^{(k)}-\bar{\mathbf{u}}^{(k)}\right)^3\right)\\
&\qquad-\nabla\cdot\mathscr{E}\left(\chi_k P^{(k)}(\mathbf{u}^{(k)}-\bar{\mathbf{u}}^{(k)})\right)
\end{aligned}$$

The five last lines will be a part of $Q^{(k)}$. Eventually, we need to simplify the first line of the right hand side to make appear fluctuations

$$\begin{aligned}
&\mathscr{E}\left((\rho_i^{(k)}E_i^{(k)}(\mathbf{u}_i^{(k)}-\mathbf{v}_i)+P_i^{(k)}\mathbf{u}_i^{(k)})\cdot\nabla\chi_k\right)\\
&\quad=\mathscr{E}\left((\rho_i^{(k)}E_i^{(k)}(\mathbf{u}_i^{(k)}-\mathbf{v}_i)+P_i^{(k)}(\mathbf{u}_i^{(k)}-\mathbf{v}_i)+P_i^{(k)}\mathbf{v}_i)\cdot\nabla\chi_k\right)\\
&\quad=\mathscr{E}\left(\left(\rho_i^{(k)}h_i^{(k)}(\mathbf{u}_i^{(k)}-\mathbf{v}_i)+P_i^{(k)}\mathbf{v}_i\right)\cdot\nabla\chi_k\right)
\end{aligned}$$

where $h_i^{(k)}=E_i^{(k)}+\dfrac{P_i^{(k)}}{\rho_i^{(k)}}$. In the same manner as we defined $u_\Gamma^{(k)}$, we denote by $h_\Gamma^{(k)}$

$$h_\Gamma^{(k)}=\frac{\mathscr{E}\left(\rho_i^{(k)}h_i^{(k)}\left(\mathbf{u}_i^{(k)}-\mathbf{v}_i\right)\nabla\chi_k\right)}{\mathscr{E}\left(\rho_i^{(k)}\left(\mathbf{u}_i^{(k)}-\mathbf{v}_i\right)\cdot\nabla\chi_k\right)}$$

so that

$$\mathscr{E}\left((\rho_i^{(k)}E_i^{(k)}(\mathbf{u}_i^{(k)}-\mathbf{v}_i)+P_i^{(k)}\mathbf{u}_i^{(k)})\cdot\nabla\chi_k\right)=h_\Gamma^{(k)}\Gamma_k+\mathscr{E}\left(P_i^{(k)}\mathbf{v}_i\cdot\nabla\chi_k\right)$$

As $\mathbf{u}_I$ is defined as $\mathbf{u}_I = \mathscr{E}\left(u_i^{(k)}\right)$, we can finish to simplify the last term:

$$\begin{aligned}
\mathscr{E}\left(P_i^{(k)}\mathbf{v}_i\cdot\nabla\chi_k\right) &= \mathscr{E}\left(P_I\mathbf{v}_i\cdot\nabla\chi_k\right) + \mathscr{E}\left((P_i^{(k)}-P_I)\mathbf{v}_i\cdot\nabla\chi_k\right)\\
&= P_I\mathscr{E}\left(\mathbf{v}_i\cdot\nabla\chi_k\right) + \mathscr{E}\left((P_i^{(k)}-P_I)\mathbf{u}_I\cdot\nabla\chi_k\right)\\
&\quad +\mathscr{E}\left((P_i^{(k)}-P_I)(\mathbf{v}_i-\mathbf{u}_I)\cdot\nabla\chi_k\right)\\
&= P_I\mathscr{E}\left(\mathbf{v}_i\cdot\nabla\chi_k\right) + \mathbf{u}_I\cdot\mathscr{E}\left((P_i^{(k)}-P_I)\nabla\chi_k\right)\\
&\quad +\mathscr{E}\left((P_i^{(k)}-P_I)(\mathbf{v}_i-\mathbf{u}_I)\cdot\nabla\chi_k\right)\\
&= P_I\mathscr{E}\left(\mathbf{v}_i\cdot\nabla\chi_k\right) + \mathbf{u}_I\cdot\mathbf{M}^{(k)}\\
&\quad +\mathbf{u}_I\cdot\mathscr{E}\left(\chi_k\rho^{(k)}(\mathbf{u}^{(k)}-\bar{\mathbf{u}}^{(k)})\otimes(\mathbf{u}^{(k)}-\bar{\mathbf{u}}^{(k)})\right)\\
&\quad +\mathscr{E}\left((P_i^{(k)}-P_I)(\mathbf{v}_i-\mathbf{u}_I)\cdot\nabla\chi_k\right)
\end{aligned}$$

According to the volume fraction equation

$$\frac{\partial\alpha^{(k)}}{\partial t} + \mathscr{E}\left(\mathbf{v}_i\nabla\chi_k\right) = 0$$

so that $P_I\mathscr{E}\left(\mathbf{v}_i\cdot\nabla\chi_k\right) = -P_I\dfrac{\partial\alpha_k}{\partial t}$ Eventually, if we denote by $Q^{(k)}$ all the fluctuations, the following equation holds for energy

$$\frac{\partial\left(\alpha_k\rho_k E_k\right)}{\partial t} + \nabla\cdot\left(\alpha_k\left(\rho_k E_k + P_k\right)\mathbf{u}_k\right) = -P_I\frac{\partial\alpha_k}{\partial t} + \Gamma^{(k)}h_\Gamma^{(k)} + \mathbf{u}_I\cdot\mathbf{M}^{(k)} + Q^{(k)}$$

□

More than the equations on the phasic mass, momentum and energy, we need an equation on the volume fraction. to close the system. It is given by averaging the equation

$$\frac{\partial\chi_k}{\partial t} + \mathbf{v}_i\cdot\nabla\chi_k = 0$$

By definition, we have $\mathscr{E}\left(\chi_k\right) = \alpha^{(k)}$, and as for the other equations, we can rewrite the remaining term as

$$\mathscr{E}\left(\mathbf{v}_i\cdot\nabla\chi_k\right) = \mathbf{u}_I\cdot\nabla\chi_k + \mathscr{E}\left(\left(\mathbf{v}_i - \mathscr{E}\left(\mathbf{u}_i^{(k)}\right)\right)\cdot\nabla\chi_k\right)$$

and we assume that this last term is a fluctuation. Finally, we proved that

after homogenization, the following system holds

$$\begin{cases} \dfrac{\partial \alpha^{(k)}}{\partial t} + \mathbf{u}_I \cdot \nabla \alpha^{(k)} = FV^{(k)} \\ \dfrac{\partial (\alpha^{(k)} \rho^{(k)})}{\partial t} + \nabla \cdot \left(\alpha^{(k)} \rho^{(k)} \mathbf{u}^{(k)} \right) = \Gamma^{(k)} \\ \dfrac{\partial (\alpha^{(k)} \rho^{(k)} \mathbf{u}^{(k)})}{\partial t} + \nabla \cdot \left(\alpha^{(k)} \left(\rho^{(k)} \mathbf{u}^{(k)} \otimes \mathbf{u}^{(k)} + P^{(k)} \mathbf{I} \right) \right) = P_I \nabla \alpha^{(k)} + \mathbf{u}_\Gamma^{(k)} \Gamma^{(k)} \\ \qquad\qquad + \mathbf{M}^{(k)} \\ \dfrac{\partial \left(\alpha^{(k)} \rho^{(k)} E^{(k)} \right)}{\partial t} + \nabla \cdot \left(\alpha^{(k)} \left(\rho^{(k)} E^{(k)} + P^{(k)} \right) \mathbf{u}^{(k)} \right) = -P_I \dfrac{\partial \alpha^{(k)}}{\partial t} + \Gamma^{(k)} h_\Gamma^{(k)} \\ \qquad\qquad + \mathbf{u}_I \cdot \mathbf{M}^{(k)} + Q^{(k)} \end{cases} \tag{1.7}$$

where $\mathbf{u}_\Gamma^{(k)}$, $FV^{(k)}$ $h_\Gamma^{(k)}$, $\mathbf{M}^{(k)}$ and $Q^{(k)}$ contains only fluctuation terms. We could develop the computation further (as long as the courage stays), but we see that we already have managed our first aim: giving equations for the mean values of the flow. As it is usually done, we will now try to model the fluctuations with the other variables so as to ensure some common criteria.

1.2 Closure of the model and entropy

To close the system (1.7) we need to give an expression to the fluctuations terms: $\mathbf{u}_\Gamma^{(k)}$, $h_\Gamma^{(k)}$, $\mathbf{M}^{(k)}$ and $Q^{(k)}$, and to the interface terms: $\mathbf{u}_I$ and P_I. We remind that the initial system is hyperbolic and admits an entropy. So that we want that the convective part of (1.7)

- is hyperbolic.
- is entropy dissipative.
- verifies other criteria on hyperbolic systems.

The fact that the system is (weakly) hyperbolic is well known [26, 46, 53], provided the eigenvalues of the Jacobian which are $\mathbf{u}_I$, $\mathbf{u}^{(k)}$ and $\mathbf{u}^{(k)} \pm c^{(k)}$ are not equal. One of the key point of the closure is to ensure the entropy growth criterion. The entropy equation is given by

Theorem 1.2. *If the continuous model is given by* (1.7)*, then the following*

equation holds for the entropy of each phase

$$\begin{aligned}&\frac{\partial(\alpha^{(k)}\rho^{(k)}s^{(k)})}{\partial t}+\nabla\cdot\left(\alpha^{(k)}\rho^{(k)}s^{(k)}\mathbf{u}^{(k)}\right)\\&=\\&\frac{1}{T^{(k)}}\Bigg\{(P^{(k)}-P_I)\frac{D_k\alpha^{(k)}}{Dt}+h_\Gamma^{(k)}\Gamma^{(k)}-\Gamma^{(k)}\mathbf{u}^{(k)}\cdot\mathbf{u}_\Gamma^{(k)}\\&\quad+(\mathbf{u}_I-\mathbf{u}^{(k)})\cdot\mathbf{M}^{(k)}+\Gamma^{(k)}\frac{{\mathbf{u}^{(k)}}^2}{2}+Q^{(k)}-\Gamma^{(k)}g^{(k)}\Bigg\}\end{aligned}\tag{1.8}$$

where

$$\frac{D_k\alpha^{(k)}}{Dt}=\frac{\partial\alpha^{(k)}}{\partial t}+\mathbf{u}^{(k)}\cdot\nabla\alpha^{(k)}$$

Proof. The proof relies on the following equation, given by the first and second law of thermodynamic

$$\mathrm{d}\varepsilon=-P\mathrm{d}\tau+T\mathrm{d}s$$

Thus, we first need to find an equation on the internal energy. For more convenience in the calculations, we denote by $\Gamma^{(k)}$, $SMo^{(k)}$ and $SMe^{(k)}$ the second member of the equations on mass, momentum and energy, put in the following form

$$\begin{cases}\dfrac{\partial(\alpha^{(k)}\rho^{(k)})}{\partial t}+\nabla\cdot\left(\alpha^{(k)}\rho^{(k)}\mathbf{u}^{(k)}\right)=\Gamma^{(k)}\\ \dfrac{\partial(\alpha^{(k)}\rho^{(k)}\mathbf{u}^{(k)})}{\partial t}+\nabla\cdot\left(\alpha^{(k)}\rho^{(k)}\mathbf{u}^{(k)}\otimes\mathbf{u}^{(k)}\right)=SMo^{(k)}\\ \dfrac{\partial(\alpha^{(k)}\rho^{(k)}E^{(k)})}{\partial t}+\nabla\cdot\left(\alpha^{(k)}\rho^{(k)}E^{(k)}\mathbf{u}^{(k)}\right)=SMe^{(k)}\end{cases}$$

We first develop the equation on momentum, and thanks for equation on mass, we get

$$\alpha^{(k)}\rho^{(k)}\frac{\partial\mathbf{u}^{(k)}}{\partial t}+\Gamma^{(k)}\mathbf{u}^{(k)}+(\alpha^{(k)}\rho^{(k)}\mathbf{u}^{(k)}\cdot\nabla)\mathbf{u}^{(k)}=SMo^{(k)}$$

To get an equation on the kinetic energy, we add $\mathbf{u}^{(k)}\cdot\dfrac{\partial(\alpha^{(k)}\rho^{(k)}\mathbf{u}^{(k)})}{\partial t}$ and $\alpha^{(k)}\rho^{(k)}\mathbf{u}^{(k)}\cdot\dfrac{\partial\mathbf{u}^{(k)}}{\partial t}$

$$\begin{aligned}&\mathbf{u}^{(k)}\cdot\frac{\partial(\alpha^{(k)}\rho^{(k)}\mathbf{u}^{(k)})}{\partial t}+\mathbf{u}^{(k)}\cdot\nabla\cdot\left(\alpha^{(k)}\rho^{(k)}\mathbf{u}^{(k)}\otimes\mathbf{u}^{(k)}\right)+\alpha^{(k)}\rho^{(k)}\mathbf{u}^{(k)}\cdot\frac{\partial\mathbf{u}^{(k)}}{\partial t}\\&+\Gamma^{(k)}{\mathbf{u}^{(k)}}^2+\mathbf{u}^{(k)}\cdot\left(\alpha^{(k)}\rho^{(k)}\mathbf{u}^{(k)}\cdot\nabla\right)\mathbf{u}^{(k)}=2\mathbf{u}^{(k)}\cdot SMo^{(k)}\end{aligned}$$

which gives, in a compact form

$$\frac{\partial E_{ck}}{\partial t} + \nabla \cdot \left(E_{ck}\mathbf{u}^{(k)}\right) = \mathbf{u}^{(k)} \cdot SMo^{(k)} - \frac{\Gamma^{(k)}\mathbf{u}^{(k)^2}}{2}$$

where E_{ck} is the kinetic energy, $E_{ck} = \dfrac{\alpha^{(k)}\rho^{(k)}\mathbf{u}^{(k)^2}}{2}$. Withdrawing the equation on the kinetic energy from the equation on total energy gives

$$\frac{\partial(\alpha^{(k)}\rho^{(k)}\varepsilon^{(k)})}{\partial t} + \nabla \cdot \left(\alpha^{(k)}\rho^{(k)}\varepsilon^{(k)}\mathbf{u}^{(k)}\right) = SMe^{(k)} - \mathbf{u}^{(k)} \cdot SMo^{(k)} + \frac{\Gamma^{(k)}\mathbf{u}^{(k)^2}}{2}$$

which can also be written as

$$\varepsilon^{(k)}\Gamma^{(k)} + \alpha^{(k)}\rho^{(k)}\frac{D_k\varepsilon^{(k)}}{Dt} = SMe^{(k)} - \mathbf{u}^{(k)} \cdot SMo^{(k)} + \frac{\Gamma^{(k)}\mathbf{u}^{(k)^2}}{2}$$

Then we need an equation on $\tau^{(k)}$. If we develop the mass equation, we find

$$\alpha^{(k)}\frac{D_k\rho^{(k)}}{Dt} + \rho^{(k)}\frac{D_k\alpha^{(k)}}{Dt} + \alpha^{(k)}\rho^{(k)}\nabla \cdot u = \Gamma^{(k)}$$

which leads to

$$-\alpha^{(k)}\frac{D_k\tau^{(k)}}{Dt} + \tau^{(k)}\frac{D_k\alpha^{(k)}}{Dt} + \alpha^{(k)}\tau^{(k)}\nabla \cdot u = {\tau^{(k)}}^2\Gamma^{(k)}$$

Now, we can calculate the entropy dissipation for each phase

$$\begin{aligned}
&\frac{\partial(\alpha^{(k)}\rho^{(k)}s^{(k)})}{\partial t} + \nabla \cdot \left(\alpha^{(k)}\rho^{(k)}s^{(k)}\mathbf{u}^{(k)}\right) \\
&= \alpha^{(k)}\rho^{(k)}\,\frac{D_k s^{(k)}}{Dt} + s^{(k)}\,\Gamma^{(k)} \\
&= \alpha^{(k)}\rho^{(k)}\left(\frac{1}{T^{(k)}}\,\frac{D_k\varepsilon^{(k)}}{Dt} + \frac{P^{(k)}}{T^{(k)}}\,\frac{D_k\tau^{(k)}}{Dt}\right) + s^{(k)}\,\Gamma^{(k)} \\
&= \frac{1}{T^{(k)}}\Bigg\{ -\nabla \cdot \left(\alpha^{(k)}\rho^{(k)}\mathbf{u}^{(k)}\right) - P_I\frac{\partial\alpha^{(k)}}{\partial t} + h_\Gamma^{(k)}\Gamma^{(k)} + \mathbf{u}_I \cdot \mathbf{M}^{(k)} + Q^{(k)} \\
&\qquad +\mathbf{u}^{(k)} \cdot \nabla\left(\alpha^{(k)}P^{(k)}\right) - P_I\mathbf{u}^{(k)} \cdot \nabla\alpha^{(k)} - P_I\mathbf{u}^{(k)} \cdot \nabla\alpha^{(k)} \\
&\qquad -\Gamma^{(k)}\mathbf{u}^{(k)} \cdot \mathbf{u}_\Gamma^{(k)} - \mathbf{u}^{(k)} \cdot \mathbf{M}^{(k)} + \Gamma^{(k)}\,\frac{\mathbf{u}^{(k)^2}}{2} - g^{(k)}\Gamma^{(k)} \\
&\qquad +P^{(k)}\frac{D_k\alpha^{(k)}}{Dt} + \alpha^{(k)}\rho^{(k)}\nabla \cdot \mathbf{u}^{(k)} \Bigg\} \\
&= \frac{1}{T^{(k)}}\Bigg\{ (P^{(k)} - P_I)\frac{D_k\alpha^{(k)}}{Dt} + h_\Gamma^{(k)}\Gamma^{(k)} - \Gamma^{(k)}\mathbf{u}^{(k)} \cdot \mathbf{u}_\Gamma^{(k)} \\
&\qquad +(\mathbf{u}_I - \mathbf{u}^{(k)}) \cdot \mathbf{M}^{(k)} + \Gamma^{(k)}\,\frac{\mathbf{u}^{(k)^2}}{2} + Q^{(k)} - \Gamma^{(k)}g^{(k)} \Bigg\}
\end{aligned}$$

□

We can then calculate the total entropy dissipation

Theorem 1.3. *Assume that $u_\Gamma^{(k)}$ and $h_\Gamma^{(k)}$ do not depend on k. Then the total entropy is equal to*

$$\begin{aligned}
&\sum_{i=1}^{2}\frac{\partial(\alpha^{(i)}\rho^{(i)}s^{(i)})}{\partial t}+\nabla\cdot(\alpha^{(i)}\rho^{(i)}s^{(i)}\mathbf{u}^{(i)})\\
&=\\
&\frac{P^{(1)}-P_I}{T^{(1)}}\frac{D_1\alpha^{(1)}}{Dt}+\frac{P^{(2)}-P_I}{T^{(2)}}\frac{D_2\alpha_2}{Dt}+h^\lambda\Gamma^{(1)}\left(\frac{1}{T^{(1)}}-\frac{1}{T^{(2)}}\right)\\
&+\Gamma^{(1)}\mathbf{u}^\Gamma\cdot\left(\frac{\mathbf{u}^{(2)}}{T^{(2)}}-\frac{\mathbf{u}^{(1)}}{T^{(1)}}\right)+\left(\frac{\mathbf{u}_I-\mathbf{u}^{(1)}}{T^{(1)}}-\frac{\mathbf{u}_I-\mathbf{u}^{(2)}}{T^{(2)}}\right)\cdot\mathbf{M}^{(1)}\\
&+\Gamma^{(1)}\left(\frac{{\mathbf{u}^{(1)}}^2}{2T^{(1)}}-\frac{{\mathbf{u}^{(2)}}^2}{2T^{(2)}}\right)+Q^{(1)}\left(\frac{1}{T^{(1)}}-\frac{1}{T^{(2)}}\right)+\Gamma^{(1)}\left(\frac{g^{(2)}}{T^{(2)}}-\frac{g^{(1)}}{T^{(1)}}\right)
\end{aligned}\tag{1.9}$$

Proof. We remark that if $u_\Gamma^{(k)}$ and $h_\Gamma^{(k)}$ do not depend on k, then if we want to ensure the total conservation of energy, momentum, then we need that

$$\begin{aligned}\mathbf{M}^{(1)}+\mathbf{M}^{(2)}&=0\\ Q^{(1)}+Q^{(2)}&=0\end{aligned}$$

Last, applying (1.8) gives immediately the result. □

1.3 Some examples of closure

1.3.1 Closure of [26, 29]

In [26, 29] it is proposed to find a closure on P_I and u_I by using a necessary condition to ensure some common criteria on hyperbolic system. The first assumption is that the interface velocity and pressure are convex combination of the velocity and pressure of each phase:

$$\mathbf{u}_I=\beta\mathbf{u}_1+(1-\beta)\mathbf{u}_2 \tag{1.10}$$

where β depends on the thermodynamic state (volume fraction, density and pressures of the fluid). It is proved in [26] that

Theorem 1.4. *If $\mathbf{u}_I$ is given by* (1.10) *and if the field associated to the eigenvalue $\mathbf{u}_I$ is linearly degenerate then*

$$\begin{aligned}
&\textit{either} && \beta=\frac{\alpha^{(k)}\rho^{(k)}}{\alpha^{(k)}\rho^{(k)}+\alpha^{(\bar{k})}\rho^{(\bar{k})}}\\
&\textit{or} && \beta=0\\
&\textit{or} && \beta=1
\end{aligned}$$

The case $\beta = 0$ or $\beta = 1$ corresponds to the famous model of Baer and Nunziato [5] and ensures the global entropy growth criterion. For having a positive entropy dissipation, we assume that all the terms in the second member of (1.9) are positive. For some terms, it is easy to ensure the positivity, for example, if

$$\Gamma^{(1)} = \left(\frac{g^{(2)}}{T^{(2)}} - \frac{g^{(1)}}{T^{(1)}} \right)$$

then

$$\Gamma^{(1)} \times \left(\frac{g^{(2)}}{T^{(2)}} - \frac{g^{(1)}}{T^{(1)}} \right) \geq 0$$

The only term we cannot close in that way is

$$\frac{P^{(1)} - P_I}{T^{(1)}} \frac{D_1 \alpha^{(1)}}{Dt} + \frac{P^{(2)} - P_I}{T^{(2)}} \frac{D_2 \alpha^{(2)}}{Dt}$$

which can be rewritten as ($FV^{(k)}$ was defined in (1.7))

$$\left(\frac{P^{(1)} - P_I}{T^{(1)}} - \frac{P^{(2)} - P_I}{T^{(2)}} \right) FV^{(1)} + \left(\frac{(P^{(1)} - P_I)(\mathbf{u}^{(1)} - \mathbf{u}_I)}{T^{(1)}} - \frac{(P^{(2)} - P_I)(\mathbf{u}^{(2)} - \mathbf{u}_I)}{T^{(2)}} \right) \cdot \nabla \alpha^{(1)}$$

and if we want that the term with $\nabla \alpha$ vanishes, and if we suppose that P_I is a convex combination of the pressures $P^{(k)}$, then [29]

$$P_I = \frac{a^{(1)}(1-\beta)P^{(1)}}{a^{(1)}(1-\beta) + a^{(2)}\beta} + \frac{a^{(2)}\beta P^{(2)}}{a^{(1)}(1-\beta) + a^{(2)}\beta}$$

with $a^{(k)} = (Y^{(k)} T^{(k)})^{-1}$. Last, choosing

$$\frac{D_I \alpha^{(k)}}{Dt} = \frac{P^{(k)} - P^{(\bar{k})}}{\varepsilon_P} \qquad \mathbf{M}^{(k)} = \frac{\mathbf{u}^{(\bar{k})} - P^{(k)}}{\varepsilon_{\mathbf{u}}}$$

$$Q^{(k)} = \frac{T^{(\bar{k})} - T^{(\bar{k})}}{\varepsilon_T} \qquad \Gamma^{(k)} = \frac{1}{\varepsilon_g} \left(\frac{g^{(\bar{k})}}{T^{(\bar{k})}} - \frac{g^{(k)}}{T^{(k)}} \right)$$

and choosing $\mathbf{u}^\Gamma$ and h^Γ such that

$$h^\lambda \Gamma^{(1)} \left(\frac{1}{T^{(1)}} - \frac{1}{T^{(2)}} \right) + \Gamma^{(1)} \mathbf{u}^\Gamma \cdot \left(\frac{\mathbf{u}^{(2)}}{T^{(2)}} - \frac{\mathbf{u}^{(1)}}{T^{(1)}} \right) + \left(\frac{\mathbf{u}^{(1)^2}}{2T^{(1)}} - \frac{\mathbf{u}^{(2)^2}}{2T^{(2)}} \right) = 0$$

the resulting system is entropy dissipative.

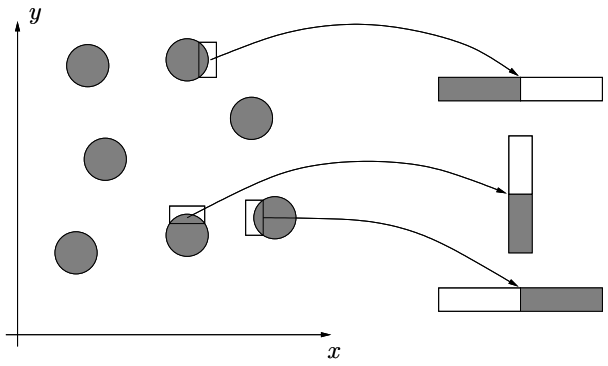

Figure 1.2: As the fluids are locally no mixed (left), and as we supposed that the interfaces are regular, we can rectify the interface in order to transform locally the problem as a Riemann problem (right).

This closure is very satisfactory in a mathematical point of view. Nevertheless, it ensures only the *mixture* entropy growth criterion, but not necessary the *phasic* entropy growth criterion, especially in the case of flows without mass transfer. In the case of flows without mass transfer, we made the assumption that we only have contact surface between the fluids, so that the entropy cannot be transfered from one fluid to the other. It is likely that the physically relevant criterion is the phasic entropy criterion, and we will expose in the next subsection how it can be obtained. .

1.3.2 Closure of [47]

Given an $\mathbf{x}$ where both of the fluids (1) and (2) lies, we wonder how to build an interface pressure and an interface velocity. For a given realization we supposed that the fluids are separated, and that the border of the bubbles are regular. Therefore, for one realization and one given interface, the border can be rectified so that the zoom on the interface is a one dimensional problem (see Figure 1.2) with

- on one side, the fluid 1 with the pressure $P^{(1)}$ and the velocity $\mathbf{u}^{(1)} \cdot \mathbf{n}$ where $\mathbf{n}$ is the normal to the interface
- on one side, the fluid 2 with the pressure $P^{(2)}$ and the velocity $\mathbf{u}^{(2)} \cdot \mathbf{n}$.

Then for these given realization and interface, the interface pressure is the $P^\star$ of the solution of the above Riemann problem (see Figure 1.3). The interfacial velocity is more complicate to evaluate: indeed, if it is natural

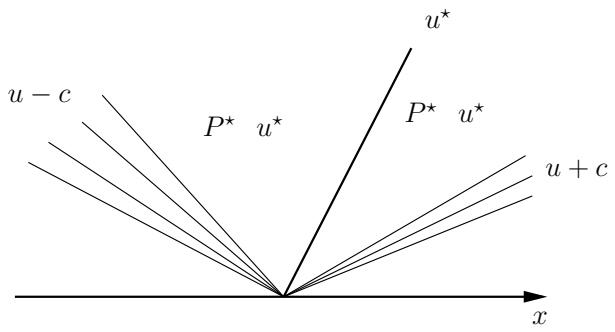

Figure 1.3: At time $t = 0$, we cannot define a interfacial pressure nor an interfacial velocity. But it is well known [28] that the solution of this problem is composed of one acoustic wave on each side, separated by a surface contact, which is the interfacebetwwen both fluids. Thus, if we solve the Riemann problem, the interfacial pressures and velocity are naturally defined as $P^\star$ for the interfacial pressure and $u^\star$ for the interfacial normal velocity.

to use the $u^\star$ of Figure 1.3 for the normal interface velocity, the tangential component of the velocity may be discontinuous across the wave $u^\star$. For a given realization, we remark that the interfacial pressure might be much higher that the initial pressures (if the Riemann problem is a shock–shock interaction). Therefore, it is likely that the average on all the realizations might be higher than both of the pressures.

Now, we suppose that the velocities and pressures are not equal but very close. Then the acoustic approximation holds, and we have, for two given left (L) and right (R) states

$$\left\{\begin{array}{r} P^\star = \dfrac{Z^{(\bar{k})}P^{(k)} + Z^{(k)}P^{(\bar{k})} + Z^{(k)}Z^{(\bar{k})}(\mathbf{u}^{(k)}\cdot\mathbf{n}_{k\bar{k}} - \mathbf{u}^{(\bar{k})}\cdot\mathbf{n}_{k\bar{k}})}{Z^{(\bar{k})}+Z^{(k)}} \\ \mathbf{u}^\star\cdot\mathbf{n}_{k\bar{k}} = \dfrac{Z^{(\bar{k})}\mathbf{u}^{(\bar{k})}\cdot\mathbf{n}_{k\bar{k}} + Z^{(k)}\mathbf{u}^{(k)}\cdot\mathbf{n}_{k\bar{k}} + (P^{(k)} - P^{(\bar{k})})}{Z^{(\bar{k})}+Z^{(k)}} \end{array}\right.$$

where $\mathbf{n}_{k\bar{k}}$ is the local normal vector of the interface, which sense is from k to $\bar{k}$. We denote by

$$\begin{aligned} \delta P^{(k)} &= P^{(k)} - P^{(\bar{k})} \\ \delta\mathbf{u}^{(k)} &= \mathbf{u}^{(k)} - \mathbf{u}^{(\bar{k})} \end{aligned}$$

so that

$$\begin{aligned} P^\star - P^{(k)} &= \frac{Z^{(k)}}{Z^{(k)}+Z^{(\bar{k})}}\left(-\delta P^{(k)} + Z^{(\bar{k})}\delta\mathbf{u}^{(k)}\cdot\mathbf{n}_{k\bar{k}}\right) \\ \left(\mathbf{u}^\star - \mathbf{u}^{(k)}\right)\cdot\mathbf{n}_{k\bar{k}} &= \frac{1}{Z^{(k)}+Z^{(\bar{k})}}\left(\delta P^{(k)} - Z^{(\bar{k})}\delta\mathbf{u}^{(k)}\cdot\mathbf{n}_{k\bar{k}}\right) \end{aligned}$$

if in (1.8), we have $\Gamma^{(k)} = 0$, $h^{(k)} = 0$ and $Q^{(k)} = 0$, the entropy dissipation is equal to

$$(P^{(k)} - P_I)\frac{D_I\alpha^{(k)}}{Dt} + (P^{(k)} - P_I)(\mathbf{u}^{(k)} - \mathbf{u}_I)\cdot\nabla\alpha^{(k)} + (\mathbf{u}_I - \mathbf{u}^{(k)})\cdot\mathbf{M}^{(k)}$$

First, if we assume that $\mathscr{E}(\mathbf{n}_{k\bar{k}}) = -\dfrac{\nabla\alpha^{(k)}}{\|\nabla\alpha^{(k)}\|}$, then

$$\begin{aligned}(P^{(k)} - P_I)(\mathbf{u}^{(k)} - \mathbf{u}_I)\cdot\nabla\alpha^{(k)} &= (P^{(k)} - P_I)(\mathbf{u}^{(k)} - \mathbf{u}_I)\cdot\frac{\nabla\alpha^{(k)}}{\|\nabla\alpha^{(k)}\|}\|\nabla\alpha^{(k)}\| \\ &= \frac{Z^{(k)}\|\nabla\alpha^{(k)}\|}{(Z^{(k)} + Z^{(\bar{k})})^2}\left(-\delta P^{(k)} + Z^{(\bar{k})}\delta\mathbf{u}^{(k)}\cdot\mathbf{n}_{k\bar{k}}\right)^2 \\ &> 0\end{aligned}$$

and if, as found in the subsection 1.3.1

$$\begin{aligned}\frac{D_I\alpha^{(k)}}{Dt} &= \mu\delta P^{(k)} \\ \mathbf{M}^{(k)} &= -\lambda\left(\delta\mathbf{u}^{(k)}\cdot\mathbf{n}_{k\bar{k}}\right)\mathbf{n}_{k\bar{k}}\end{aligned}$$

then

$$(P^{(k)} - P_I)\delta P^{(k)}\frac{D_I\alpha^{(k)}}{Dt} = \frac{\mu Z^{(k)}\left(\delta P^{(k)}\right)^2}{Z^{(k)} + Z^{(\bar{k})}} + \frac{\mu Z^{(k)}Z^{(\bar{k})}\delta P^{(k)}\delta\mathbf{u}^{(k)}\cdot\mathbf{n}_{k\bar{k}}}{Z^{(k)} + Z^{(\bar{k})}}$$

and

$$(\mathbf{u}_I - \mathbf{u}^{(k)})\cdot\mathbf{M}^{(k)} = -\frac{\lambda\delta P^{(k)}\delta\mathbf{u}^{(k)}\cdot\mathbf{n}_{k\bar{k}}}{Z^{(k)} + Z^{(\bar{k})}} + \frac{\lambda Z^{(k)}\left(\delta\mathbf{u}^{(k)}\cdot\mathbf{n}_{k\bar{k}}\right)^2}{Z^{(k)} + Z^{(\bar{k})}}$$

so that if $\mu Z^{(k)}Z^{(\bar{k})} = \lambda$, then the phasic entropies grow.

In this chapter, we exposed how to obtain a continuous system of PDE able to describe multiphase flows. The convective part of the model is (conditionnaly) hyperbolic, contains nonconservative terms, and the closure of such a system seems very hard. As a consequence, the numerical approximation of such a system seems very difficult. In the next chapter, we will expose how to reduce the difficulty of the system.

Chapter 2

From the seven to the five equations model

As noticed in the previous chapter, the seven equation model deals with a lot of difficulties, and of modelling with the interfacial variables, and with the modelling of fluctuations. In some cases, especially when the fluids are well mixed, it is likely that the velocities and pressures relax quickly, so that they can be considered as equal. Moreover, this case might reduce the difficulty, because part of the modelling problem are solved. Indeed, we saw in the previous chapter that in all the usual closures used, we have

$$P^{(1)} = P^{(2)} \text{ and } \mathbf{u}^{(1)} = \mathbf{u}^{(2)} \implies P_I = P \text{ and } \mathbf{u}_I = \mathbf{u}$$

so that the modelling of the interfacial variables is naturally solved. In this chapter, we derive as in [44, 43] the five equations model for two–phase flows, which is an asymptotic reduction of a general form of the seven equations model found in the previous chapter.

2.1 Chapman–Enskog expansion of an hyperbolic problem

In this section, we consider a formal hyperbolic system with a stiff source term

$$\frac{\partial \mathbf{U}}{\partial t} + A(\mathbf{U})\frac{\partial \mathbf{U}}{\partial x} = \frac{R(\mathbf{U})}{\varepsilon} \tag{2.1}$$

where $\mathbf{U}$ is a vector that belongs to an open subset Ω, $A(\mathbf{U})$ is a $N \times N$ diagonalisable matrix with real eigenvalues for any $\mathbf{U}$, and R is the source

term. We suppose that ε tends to 0, so that when $\varepsilon \to 0$, $\mathbf{U}$ is expected to belong to the set $R(\mathbf{U}) = 0$. We suppose that

Assumption 2.1. *The subset of Ω defined by $R(\mathbf{U}) = 0$ is a smooth manifold of dimension n that can be parameterised by $\mathbf{u}$. The function*

$$M \,:\, \mathbf{u} \in \omega \subset \mathbb{R}^n \mapsto M(\mathbf{u}) = \mathbf{U} \in \Omega \subset \mathbb{R}^N$$

is smooth (i.e. $\mathscr{C}^1$).

Under this hypothesis of smoothness of M, we have

Proposition 2.1. *The zeroth order expansion of* (2.1) *is*

$$\mathrm{d}M_{\mathbf{u}} \frac{\partial \mathbf{u}}{\partial t} + A(M(\mathbf{u}))\mathrm{d}M_{\mathbf{u}} \frac{\partial u}{\partial x} = R'(M(\mathbf{u}))\mathbf{U}_1 + O(\varepsilon) \tag{2.2}$$

Proof. Our aim is to do a formal expansion of (2.1). Thus, we suppose that the vector $\mathbf{U}$ can be written as

$$\mathbf{U} = \sum_0^\infty \varepsilon^k \mathbf{U}^{(k)}$$

As $\varepsilon \to 0$, we can conserve only the two first terms

$$\mathbf{U} = \mathbf{U}_0 + \varepsilon \mathbf{U}_1 + O\left(\varepsilon^2\right)$$

As $\mathbf{U}_0$ belongs to $\mathcal{E}$, it is equal to a $M(\mathbf{u})$. Now, it remains to expand the different terms of (2.1)

$$\begin{aligned}
\frac{\partial \mathbf{U}}{\partial t} &= \frac{\partial}{\partial t}\left(M(\mathbf{u}) + \varepsilon \mathbf{U}_1 + O\left(\varepsilon^2\right)\right) \\
&= \mathrm{d}M_{\mathbf{u}} \frac{\partial \mathbf{u}}{\partial t} + O(\varepsilon) \\
A(\mathbf{U}) \frac{\partial \mathbf{U}}{\partial x} &= A\left(M(\mathbf{u}) + \varepsilon \mathbf{U}_1 + O\left(\varepsilon^2\right)\right) \frac{\partial}{\partial x}\left(M(\mathbf{u}) + \varepsilon \mathbf{U}_1 + O\left(\varepsilon^2\right)\right) \\
&= A(M(\mathbf{u}))\mathrm{d}M_{\mathbf{u}} \frac{\partial \mathbf{u}}{\partial x} + O(\varepsilon) \\
\frac{R(\mathbf{U})}{\varepsilon} &= \frac{R\left(M(\mathbf{u}) + \varepsilon \mathbf{U}_1 O\left(\varepsilon^2\right)\right)}{\varepsilon} \\
&= \frac{R(M(\mathbf{u})) + \varepsilon R'(M(\mathbf{u}))\mathbf{U}_1 + O\left(\varepsilon^2\right)}{\varepsilon} \\
&= R'(M(\mathbf{u}))\mathbf{U}_1 + O(\varepsilon)
\end{aligned}$$

Thus, at the zeroth order, (2.1) becomes

$$\mathrm{d}M_{\mathbf{u}} \frac{\partial \mathbf{u}}{\partial t} + A(M(\mathbf{u}))\mathrm{d}M_{\mathbf{u}} \frac{\partial \mathbf{u}}{\partial x} = R'(M(\mathbf{u}))\mathbf{U}_1$$

□

We aim at describing the relaxed system with the variables $\mathbf{u}$, i.e. we are looking for a system of PDE that is verified by $\mathbf{u}$. Nevertheless, in (2.2), we see that the system has a right hand side that depends on $\mathbf{U}_1$ (the first order fluctuations of $\mathbf{U}$), on which we do not know anything. That is why we will look for a projection that can

- keep as many information as we can: remind that we need n variables to describe the equilibrium set.
- vanishes everything that we do not know.

Here, we see that the best is to find a projection P such that

$$P\mathrm{d}M_{\mathbf{u}} = \mathrm{I}_n \qquad \text{and} \qquad PR'(M(\mathbf{u})) = 0 \tag{2.3}$$

Existence and explicit building of such a projection is the object of the following propositions.

Proposition 2.2. *The columns of* $\mathrm{d}M_{\mathbf{u}}$ *form a basis of* $\mathrm{Ker}(R'(M(\mathbf{u})))$.

Proof. If we differentiate once the equation $R(M(\mathbf{u})) = 0$, then we have $R'(M(\mathbf{u}))\mathrm{d}M_{\mathbf{u}} = 0$. Thus, the columns of $\mathrm{d}M_{\mathbf{u}}$ belong to $\mathrm{Ker}(R'(M(\mathbf{u})))$. As the dimension of the manifold $\mathcal{E}$ is n, the kernel of $R'(M(\mathbf{u}))$ is too of dimension n. Moreover, as M is injective, its derivative is of maximal rank, so that $\mathrm{d}M_{\mathbf{u}}$ is of rank n. This ends the proof. □

Thanks for this proposition, we have $\Im(\mathrm{d}M_{\mathbf{u}}) = \ker R'(M(\mathbf{u}))$, so that the existence of P such that (2.3) holds depends on the crucial following assumption

Assumption 2.2. *We suppose that* M *and* R *are such that for all* $\mathbf{u}$, $\Im(R'(M(\mathbf{u})))$ *and* $\ker(R'(M(\mathbf{u})))$ *have a null intersection.*

With this assumption, we can prove that

Proposition 2.3. *We denote by* $\{\mathrm{d}M^1_{\mathbf{u}}, \mathrm{d}M^2_{\mathbf{u}} \dots \mathrm{d}M^n_{\mathbf{u}}\}$ *the columns of* $\mathrm{d}M_{\mathbf{u}}$, *and by* $\left\{\mathbf{I}^1, \dots, \mathbf{I}^{N-n}\right\}$ *a basis of* $\Im\left(R'(M(\mathbf{u}))\right)$. *We consider the matrix*

$$S = \left[\mathrm{d}M^1_{\mathbf{u}}, \mathrm{d}M^2_{\mathbf{u}} \dots \mathrm{d}M^n_{\mathbf{u}}, \mathbf{I}^1, \dots, \mathbf{I}^{N-n}\right]$$

and we suppose that Assumption 2.2 holds. Then S *is invertible. If we denote by* P *the first* n *rows of* S^{-1}, *and by* Q *the* $N-n$ *last rows of* S^{-1}, *then*

- P *is the projection on* $\ker(R'(M(\mathbf{u})))$ *in the direction of* $\Im(R'(M(\mathbf{u})))$.
- Q *is the projection on* $\Im(R'(M(\mathbf{u})))$ *in the direction of* $\ker(R'(M(\mathbf{u})))$.

Proof. The fact that S is invertible is a simple consequence of Proposition 2.2, combined with Assumption 2.2. Then, for the building of the projection, we use Assumption 2.2 to decompose uniquely any vector V of $\mathbb{R}^N$ as

$$V = V_{(K)} + V_{(I)}$$

where $V_{(K)}$ and $V_{(I)}$ respectly belong to $\Im(\mathrm{d}M_{\mathbf{u}})$ and $\Im(R'(M(\mathbf{u})))$. Thus, there exists $v_{(K)}$ and $v_{(I)}$ such that

$$V = \mathrm{d}M_{\mathbf{u}} v_{(K)} + \mathrm{Rng}(R'(M(\mathbf{u})))v_{(I)}$$

where $\mathrm{Rng}(R'(M(\mathbf{u})))$ is a $N \times (N-n)$ matrix whose image is equal to $\Im R'(M(\mathbf{u}))$. The last equality can be recast into

$$V = \Big[\mathrm{d}M_{\mathbf{u}}, \mathrm{Rng}(R'(M(\mathbf{u})))\Big] \begin{pmatrix} v_{(K)} \\ v_{(I)} \end{pmatrix} = S \begin{pmatrix} v_{(K)} \\ v_{(I)} \end{pmatrix}$$

Last, if we rewrite $S^{-1}S = \mathbf{I}_N$ as

$$S^{-1}\Big[\mathrm{d}M_{\mathbf{u}}, \mathrm{Rng}(R'(M(\mathbf{u})))\Big] = \begin{pmatrix} P\mathrm{d}M_{\mathbf{u}} & PR'(M(\mathbf{u})) \\ Q\mathrm{d}M_{\mathbf{u}} & QR'(M(\mathbf{u})) \end{pmatrix} = \begin{pmatrix} \mathbf{I}_n & 0 \\ 0 & \mathbf{I}_{N-n} \end{pmatrix}$$

which is the required result. □

2.2 Application to the one dimensional seven equations model

We recall that we found the following model with two velocities, two pressure, model

$$\begin{aligned}
&\frac{\partial \alpha^{(k)}}{\partial t} + \mathbf{u}_I \cdot \nabla \alpha^{(k)} = \mu(P^{(k)} - P^{(\bar{k})}) \\
&\frac{\partial \big(\alpha^{(k)}\rho^{(k)}\big)}{\partial t} + \mathrm{div}\big(\alpha^{(k)}\rho^{(k)}\mathbf{u}^{(k)}\big) = 0 \\
&\frac{\partial \big(\alpha^{(k)}\rho^{(k)}\mathbf{u}^{(k)}\big)}{\partial t} + \mathrm{div}\,\big(\alpha^{(k)}\rho^{(k)}\mathbf{u}^{(k)} \otimes \mathbf{u}^{(k)}\alpha^{(k)}P^{(k)}\mathbf{I}_d\big) = P_I \nabla \alpha^{(k)} \\
&\qquad\qquad + \lambda(\mathbf{u}^{(\bar{k})} - \mathbf{u}^{(k)}) \\
&\frac{\partial \big(\alpha^{(k)}\rho^{(k)}E^{(k)}\big)}{\partial t} + \mathrm{div}\,\big(\alpha^{(k)}(\rho^{(k)}E^{(k)} + P^{(k)})\mathbf{u}^{(k)}\big) = P_I \mathbf{u}_I \cdot \nabla \alpha^{(k)} \\
&\qquad\qquad - \mu P_I(P^{(k)} - P^{(\bar{k})}) \\
&\qquad\qquad + \lambda \mathbf{u}_I \cdot (\mathbf{u}^{(\bar{k})} - \mathbf{u}^{(k)})
\end{aligned} \tag{2.4}$$

2.2.1 Asymptotic expansion

We suppose that the pressure and velocities quickly relax to an equilibrium, *i.e.* that μ and λ are large. Then the equilibrium set is equal to

$$\mathcal{E} = \left\{ \begin{array}{l} \left(\alpha^{(1)}, \rho^{(1)}, \mathbf{u}^{(1)}, P^{(1)}, \alpha^{(2)}, \rho^{(2)}, \mathbf{u}^{(2)}, P^{(2)}\right) \\ \text{such that} \quad \mathbf{u}^{(1)} = \mathbf{u}^{(2)} \quad \text{and} \quad P^{(1)} = P^{(2)} \end{array} \right\}$$

Thus $\mathcal{E}$ can be parameterised by $\alpha^{(k)}$, $\rho^{(k)}$, $\rho^{(\bar{k})}$, u and P. Its dimension is 5. For the instance, we do not have chosen any parameterisation of the seven equations model (in (2.4), there remain more than two thermodynamic parameters for each phase). To have the simplest parameterisation of the equilibrium set, we see that the natural variables are the primitive ones. Therefore, we first need to put the seven equations model in primitive variables.

Proposition 2.4. *The primitive variables follow the following system*

$$\left\{ \begin{array}{l} \dfrac{\partial \alpha^{(k)}}{\partial t} + u_I \dfrac{\partial \alpha^{(k)}}{\partial x} = \mu \left(P^{(k)} - P^{(\bar{k})} \right) \\ \dfrac{\partial \rho^{(k)}}{\partial t} + \dfrac{\rho^{(k)} (u^{(k)} - u_I)}{\alpha^{(k)}} \dfrac{\partial \alpha^{(k)}}{\partial x} + u^{(k)} \dfrac{\partial \rho^{(k)}}{\partial x} + \rho^{(k)} \dfrac{\partial u^{(k)}}{\partial x} \\ \qquad\qquad = - \dfrac{\rho^{(k)} \mu (P^{(k)} - P^{(\bar{k})})}{\alpha^{(k)}} \\ \dfrac{\partial u^{(k)}}{\partial t} + u^{(k)} \dfrac{\partial u^{(k)}}{\partial x} + \dfrac{(P^{(k)} - P_I)}{\alpha^{(k)} \rho^{(k)}} \dfrac{\partial \alpha^{(k)}}{\partial x} + \dfrac{1}{\rho^{(k)}} \dfrac{\partial P^{(k)}}{\partial x} \\ \qquad\qquad = \dfrac{\lambda}{\alpha^{(k)} \rho^{(k)}} (u^{(\bar{k})} - u^{(k)}) \\ \dfrac{D_k P^{(k)}}{Dt} + (u^{(k)} - u_I) \dfrac{\rho^{(k)} {c^{(kI)}}^2}{\alpha^{(k)}} \dfrac{\partial \alpha^{(k)}}{\partial x} + \rho^{(k)} {c^{(k)}}^2 \dfrac{\partial u^{(k)}}{\partial x} \\ \qquad = \dfrac{\lambda}{\alpha^{(k)} \rho^{(k)} \beta^{(k)}} (u_I - u^{(k)})(u^{(\bar{k})} - u^{(k)}) - \mu \dfrac{\rho^{(k)} {c^{(kI)}}^2}{\alpha^{(k)}} (P^{(k)} - P^{(\bar{k})}) \end{array} \right. \tag{2.5}$$

Proof. As we did for the proof of Theorem 1.2, we rewrite the system by putting the convective part on one side, and the other terms in the right

hand side.

$$\begin{cases} \dfrac{\partial \alpha^{(k)}}{\partial t} = SVF^{(k)} \\ \dfrac{\partial(\alpha^{(k)}\rho^{(k)})}{\partial t} + \nabla \cdot \left(\alpha^{(k)}\rho^{(k)}\mathbf{u}^{(k)}\right) = 0 \\ \dfrac{\partial(\alpha^{(k)}\rho^{(k)}\mathbf{u}^{(k)})}{\partial t} + \nabla \cdot \left(\alpha^{(k)}\rho^{(k)}\mathbf{u}^{(k)} \otimes \mathbf{u}^{(k)}\right) = SMo^{(k)} \\ \dfrac{\partial(\alpha^{(k)}\rho^{(k)}E^{(k)})}{\partial t} + \nabla \cdot \left(\alpha^{(k)}\rho^{(k)}E^{(k)}\mathbf{u}^{(k)}\right) = SMe^{(k)} \end{cases}$$

First, we develop the equation on mass, to get

$$\rho^{(k)}SFV^{(k)} + \alpha^{(k)}\frac{\partial \rho^{(k)}}{\partial t} + \rho^{(k)}u^{(k)}\frac{\partial \alpha^{(k)}}{\partial x} + \alpha^{(k)}u^{(k)}\frac{\partial \rho^{(k)}}{\partial x} + \alpha^{(k)}\rho^{(k)}\frac{\partial u^{(k)}}{\partial x} = 0$$

If we use the expression of $SFV^{(k)}$, we find

$$\begin{aligned} \alpha^{(k)}\frac{\partial \rho^{(k)}}{\partial t} + \rho^{(k)}(u^{(k)} - u_I)\frac{\partial \alpha^{(k)}}{\partial x} + \alpha^{(k)}u^{(k)}\frac{\partial \rho^{(k)}}{\partial x} + \alpha^{(k)}\rho^{(k)}\frac{\partial u^{(k)}}{\partial x} \\ = -\rho^{(k)}\mu(P^{(k)} - P^{(\bar{k})}) \end{aligned}$$

In the proof of Theorem 1.2 we found that

$$\alpha^{(k)}\rho^{(k)}\frac{\partial u^{(k)}}{\partial t} + \alpha^{(k)}\rho^{(k)}u^{(k)}\frac{\partial u^{(k)}}{\partial x} = SMo^{(k)}$$

so that we directly have the equation on the velocity

$$\alpha^{(k)}\rho^{(k)}\frac{\partial u^{(k)}}{\partial t} + \alpha^{(k)}\rho^{(k)}u^{(k)}\frac{\partial u^{(k)}}{\partial x} + (P^{(k)} - P_I)\frac{\partial \alpha^{(k)}}{\partial x} + \alpha^{(k)}\frac{\partial P^{(k)}}{\partial x} = \lambda(u^{(\bar{k})} - u^{(k)})$$

Still using the proof of Theorem 1.2, we have

$$\alpha^{(k)}\rho^{(k)}\frac{D_k\varepsilon^{(k)}}{Dt} = SMe^{(k)} - u^{(k)}SMo^{(k)}$$

To find an equation on the pressure, we use the differential of the internal specific energy with respect to $(\rho^{(k)}, P^{(k)})$. We denote by

$$\kappa^{(k)} = \left(\frac{\partial \varepsilon^{(k)}}{\partial \rho}\right)_P \qquad \beta^{(k)} = \left(\frac{\partial \varepsilon^{(k)}}{\partial P}\right)_\rho$$

so that we have

$$\mathrm{d}\varepsilon^{(k)} = \kappa^{(k)}\mathrm{d}\rho^{(k)} + \beta^{(k)}\mathrm{d}P$$

Thanks for that, equation on energy becomes

$$\alpha^{(k)}\rho^{(k)}\left(\kappa^{(k)}\frac{D_k\rho^{(k)}}{Dt}+\beta^{(k)}\frac{D_kP^{(k)}}{Dt}\right)=SMe^{(k)}-u^{(k)}SMo^{(k)}$$

therefore, we find for the pressure

$$\alpha^{(k)}\rho^{(k)}\beta^{(k)}\frac{D_kP^{(k)}}{Dt}=SMe^{(k)}-u^{(k)}SMo^{(k)}-\alpha^{(k)}\rho^{(k)}\beta^{(k)}\frac{D_k\rho^{(k)}}{Dt}$$

using the expression of $SMe^{(k)}$, $SMo^{(k)}$ and $\dfrac{D_k\rho^{(k)}}{Dt}$, we find

$$\begin{aligned}\alpha^{(k)}\rho^{(k)}\beta^{(k)}\frac{D_kP^{(k)}}{Dt}=&\ P_I(u_I-u^{(k)})\,\frac{\partial\alpha^{(k)}}{\partial x}+{\rho^{(k)}}^2\kappa^{(k)}(u^{(k)}-u_I)\frac{\partial\alpha^{(k)}}{\partial x}\\&-\alpha^{(k)}(P^{(k)}-{\rho^{(k)}}^2\kappa^{(k)})\frac{\partial u^{(k)}}{\partial x}\\&+\lambda(u_I-u^{(k)})(u^{(\bar{k})}-u^{(k)})\\&-\mu(P_I-{\rho^{(k)}}^2\kappa^{(k)})(P^{(k)}-P^{(\bar{k})})\end{aligned}$$

To simplify the expression, we remark that

$$\mathrm{d}\varepsilon=-P^{(k)}\mathrm{d}\tau+T^{(k)}\mathrm{d}s=\beta^{(k)}\mathrm{d}P+\kappa^{(k)}\mathrm{d}\tau$$

so that if $\mathrm{d}s=0$, we find

$$\beta^{(k)}\mathrm{d}P=\left(\frac{P^{(k)}}{{\rho^{(k)}}^2}-\kappa^{(k)}\right)\mathrm{d}\rho$$

thus, we have

$$\left(\frac{\partial P}{\partial\rho}\right)_s={c^{(k)}}^2=\frac{P^{(k)}-{\rho^{(k)}}^2\kappa^{(k)}}{\rho^2\beta^{(k)}}$$

and we will denote by ${c^{(kI)}}^2$

$${c^{(kI)}}^2=\frac{P_I-{\rho^{(k)}}^2\kappa^{(k)}}{{\rho^{(k)}}^2\beta^{(k)}}$$

Eventually we find

$$\begin{aligned}\alpha^{(k)}\rho^{(k)}\beta^{(k)}\frac{D_kP^{(k)}}{Dt}&+(u^{(k)}-u_I)\,{\rho^{(k)}}^2\beta^{(k)}{c^{(kI)}}^2\,\frac{\partial\alpha^{(k)}}{\partial x}\\&+\alpha^{(k)}{\rho^{(k)}}^2\beta^{(k)}{c^{(k)}}^2\,\frac{\partial u^{(k)}}{\partial x}\\&=\lambda\,(u_I-u^{(k)})(u^{(\bar{k})}-u^{(k)})\\&\quad-\mu\beta^{(k)}{\rho^{(k)}}^2{c^{(kI)}}^2\,(P^{(k)}-P^{(\bar{k})})\end{aligned}$$

□

We are now in the conditions of the theoretical framework of section 2.1, with the system

$$\frac{\partial \mathbf{U}}{\partial t} + A(\mathbf{U})\frac{\partial \mathbf{U}}{\partial x} = \frac{R(\mathbf{U})}{\varepsilon}$$

with

$$\mathbf{U} = (\alpha^{(1)}, \rho^{(1)}, u^{(1)}, P^{(1)}, \rho^{(2)}, u^{(2)}, P^{(2)})$$

The matrix $A(\mathbf{U})$ is equal to

$$\begin{pmatrix}
u_I & 0 & 0 & 0 & 0 & 0 & 0 \\
\frac{\rho^{(1)}(u^{(1)}-u_I)}{\alpha^{(1)}} & u^{(1)} & \rho^{(1)} & 0 & 0 & 0 & 0 \\
\frac{P^{(1)}-P_I}{\alpha^{(1)}\rho^{(1)}} & 0 & u^{(1)} & \frac{1}{\rho^{(1)}} & 0 & 0 & 0 \\
\frac{\rho^{(1)}{c^{(1I)}}^2(P^{(1)}-P_I)}{\alpha^{(1)}\rho^{(1)}} & 0 & \rho^{(1)}{c^{(1)}}^2 & 0 & 0 & 0 & 0 \\
-\frac{\rho^{(2)}(u^{(2)}-u_I)}{\alpha^{(2)}} & 0 & 0 & 0 & u^{(2)} & \rho^{(2)} & 0 \\
-\frac{P^{(2)}-P_I}{\alpha^{(2)}\rho^{(2)}} & 0 & 0 & 0 & 0 & u^{(2)} & \frac{1}{\rho^{(2)}} \\
-\frac{\rho^{(2)}{c^{(2I)}}^2(P^{(2)}-P_I)}{\alpha^{(2)}\rho^{(2)}} & 0 & 0 & 0 & 0 & \rho^{(2)}{c^{(2)}}^2 & 0
\end{pmatrix}$$

$$\frac{R(\mathbf{U})}{\varepsilon} = \begin{pmatrix}
\mu(P^{(1)}-P^{(2)}) \\
-\frac{\mu\rho^{(1)}}{\alpha^{(1)}}(P^{(1)}-P^{(2)}) \\
\frac{\lambda(u^{(1)}-u^{(2)})}{\alpha^{(1)}\rho^{(1)}} \\
\frac{\lambda}{\alpha^{(1)}\rho^{(1)}\beta^{(1)}}(u_I-u^{(1)})(u^{(2)}-u^{(1)}) - \frac{\mu\rho^{(1)}{c^{(1I)}}^2}{\alpha^{(1)}}(P^{(1)}-P^{(2)}) \\
-\frac{\mu\rho^{(2)}}{\alpha^{(2)}}(P^{(2)}-P^{(1)}) \\
\frac{\lambda(u^{(2)}-u^{(1)})}{\alpha^{(2)}\rho^{(2)}} \\
\frac{\lambda}{\alpha^{(2)}\rho^{(2)}\beta^{(2)}}(u_I-u^{(2)})(u^{(1)}-u^{(2)}) - \frac{\mu\rho^{(2)}{c^{(2I)}}^2}{\alpha^{(2)}}(P^{(2)}-P^{(1)})
\end{pmatrix}$$

As we work with primitive variables, and as the equilibrium set is naturally expressed on primitive variables, we have

$$M \,:\, \mathbf{u} = (\alpha^{(1)}, \rho^{(1)}, \rho^{(2)}, u, P) \longmapsto \mathbf{U} = (\alpha^{(1)}, \rho^{(1)}, u, P, \rho^{(2)}, u, P)$$

so that

$$\mathrm{d}M_{\mathbf{u}} = \begin{pmatrix} 1 & 0 & 0 & 0 & 0 \\ 0 & 1 & 0 & 0 & 0 \\ 0 & 0 & 0 & 1 & 0 \\ 0 & 0 & 0 & 0 & 1 \\ 0 & 0 & 1 & 0 & 0 \\ 0 & 0 & 0 & 1 & 0 \\ 0 & 0 & 0 & 0 & 1 \end{pmatrix}$$

and as expected, $\mathrm{d}M_{\mathbf{u}}$ is of rank 5. R can be rewritten as

$$\frac{R(\mathbf{U})}{\varepsilon} = \mu(P^{(1)} - P^{(2)})\mathbf{V}_P + \lambda(u^{(1)} - u^{(2)})\mathbf{V}_u$$

with

$$\mathbf{V}_P = \Big(1,\ -\frac{\rho^{(1)}}{\alpha^{(1)}},\ 0,\ -\frac{\rho^{(1)}{c^{(1I)}}^2}{\alpha^{(1)}},\ \frac{\rho^{(2)}}{\alpha^{(2)}},\ 0,\ \frac{\rho^{(2)}{c^{(2I)}}^2}{\alpha^{(2)}} \Big)$$
$$\mathbf{V}_u = \Big(0,\ 0,\ \frac{1}{\alpha^{(1)}\rho^{(1)}},\ \frac{u^{(1)} - u_I}{\alpha^{(1)}\rho^{(1)}\beta^{(1)}},\ 0,\ -\frac{1}{\alpha^{(2)}\rho^{(2)}},\ -\frac{u^{(2)} - u_I}{\alpha^{(2)}\rho^{(2)}\beta^{(2)}} \Big)$$

Then do differentiate R along the equilibrium set, we immediately have

$$\frac{\partial R}{\partial P^{(1)}} = \mu\mathbf{V}_p \qquad \frac{\partial R}{\partial P^{(2)}} = -\mu\mathbf{V}_p$$
$$\frac{\partial R}{\partial u^{(1)}} = \lambda\mathbf{V}_u \qquad \frac{\partial R}{\partial u^{(2)}} = -\lambda\mathbf{V}_u$$

where $\mathbf{V}_P$ and $\mathbf{V}_u$ are evaluated on the equilibrium set, i.e

$$\mathbf{V}_P = \Big(\ 1, -\frac{\rho^{(1)}}{\alpha^{(1)}},\ 0\ , -\frac{\rho^{(1)}{c^{(1)}}^2}{\alpha^{(1)}}, \frac{\rho^{(2)}}{\alpha^{(2)}},\ 0\ , \frac{\rho^{(2)}{c^{(2)}}^2}{\alpha^{(2)}} \ \Big)$$
$$\mathbf{V}_u = \Big(\ 0,\ \ 0\ , \frac{1}{\alpha^{(1)}\rho^{(1)}}, \ 0\ \ , \ 0\ , -\frac{1}{\alpha^{(2)}\rho^{(2)}}, \ 0\ \ \Big)$$

the derivatives of R with respect to $\alpha^{(1)}, \rho^{(1)}, \rho^{(2)}$ being equal to zero. Then

$$R'(\mathbf{U}) = \begin{pmatrix} 0 & 0 & 0 & 1 & 0 & 0 & -1 \\ 0 & 0 & 0 & -\frac{\rho^{(1)}}{\alpha^{(1)}} & 0 & 0 & \frac{\rho^{(1)}}{\alpha^{(1)}} \\ 0 & 0 & -\frac{1}{\alpha^{(1)}\rho^{(1)}} & 0 & 0 & \frac{1}{\alpha^{(1)}\rho^{(1)}} & 0 \\ 0 & 0 & 0 & -\frac{\rho^{(1)}{c^{(1)}}^2}{\alpha^{(1)}} & 0 & 0 & \frac{\rho^{(1)}{c^{(1)}}^2}{\alpha^{(1)}} \\ 0 & 0 & 0 & \frac{\rho^{(2)}}{\alpha^{(2)}} & 0 & 0 & -\frac{\rho^{(2)}}{\alpha^{(2)}} \\ 0 & 0 & \frac{1}{\alpha^{(2)}\rho^{(2)}} & 0 & 0 & -\frac{1}{\alpha^{(2)}\rho^{(2)}} & 0 \\ 0 & 0 & 0 & \frac{\rho^{(2)}{c^{(2)}}^2}{\alpha^{(2)}} & 0 & 0 & -\frac{\rho^{(2)}{c^{(2)}}^2}{\alpha^{(2)}} \end{pmatrix}$$

The vectors $(\mathbf{V}_P, \mathbf{V}_u)$ form a basis of $\Im R'(\mathbf{U})$. We denote by e_k, $1 \leq k \leq 7$ the vectors of the canonic basis. We immediately see that the kernel of $R'(\mathbf{U})$ is spanned by the vectors e_1, e_2, e_5, e_6+e_3 and e_7+e_4. To see whether $\Im R'(\mathbf{U})$ and $\ker R'(\mathbf{U})$ have a null intersection, we will prove that the space spanned by e_1, e_2, e_5, e_6+e_3, e_7+e_4, $\mathbf{V}_P$ and $\mathbf{V}_u$ is $\mathbb{R}^7$. Straigntforward calculations give

$$\begin{vmatrix} 1 & 0 & 0 & 0 & 0 & 0 & 1 \\ 0 & 1 & 0 & 0 & 0 & 0 & -\frac{\rho^{(1)}}{\alpha^{(1)}} \\ 0 & 0 & 0 & 1 & 0 & -\frac{1}{\alpha^{(1)}\rho^{(1)}} & 0 \\ 0 & 0 & 0 & 0 & 1 & 0 & -\frac{\rho^{(1)}{c^{(1)}}^2}{\alpha^{(1)}} \\ 0 & 0 & 1 & 0 & 0 & 0 & \frac{\rho^{(2)}}{\alpha^{(2)}} \\ 0 & 0 & 0 & 1 & 0 & \frac{1}{\alpha^{(2)}\rho^{(2)}} & 0 \\ 0 & 0 & 0 & 0 & 1 & 0 & \frac{\rho^{(2)}{c^{(2)}}^2}{\alpha^{(2)}} \end{vmatrix}$$
$$= \frac{\rho^{(1)}\rho^{(2)}{\alpha^{(1)}}^2{c^{(2)}}^2 + \alpha^{(1)}\alpha^{(2)}\left(\rho^{(1)}{c^{(1)}}^2 + \rho^{(2)}{c^{(2)}}^2\right) + \rho^{(1)}\rho^{(2)}{\alpha^{(2)}}^2{c^{(1)}}^2}{{\alpha^{(1)}}^2{\alpha^{(2)}}^2\rho^{(1)}\rho^{(2)}} > 0$$

which proves that Assumption 2.2 holds. We can now calculate the matrix

S of Proposition 2.3

$$S = \begin{pmatrix} 1 & 0 & 0 & 0 & 0 & 1 & 0 \\ 0 & 1 & 0 & 0 & 0 & -\frac{\rho^{(1)}}{\alpha^{(1)}} & 0 \\ 0 & 0 & 0 & 1 & 0 & 0 & \frac{1}{\alpha^{(1)}\rho^{(1)}} \\ 0 & 0 & 0 & 0 & 1 & -\frac{\rho^{(1)}{c^{(1)}}^2}{\alpha^{(1)}} & 0 \\ 0 & 0 & 1 & 0 & 0 & \frac{\rho^{(2)}}{\alpha^{(2)}} & 0 \\ 0 & 0 & 0 & 1 & 0 & 0 & -\frac{1}{\alpha^{(2)}\rho^{(2)}} \\ 0 & 0 & 0 & 0 & 1 & \frac{\rho^{(2)}{c^{(2)}}^2}{\alpha^{(2)}} & 0 \end{pmatrix}$$

and its inverse is equal to

$$\begin{pmatrix} 1 & 0 & 0 & \frac{\alpha^{(1)}\alpha^{(2)}}{d} & 0 & 0 & -\frac{\alpha^{(1)}\alpha^{(2)}}{d} \\ 0 & 1 & 0 & -\frac{\alpha^{(2)}\rho^{(1)}}{d} & 0 & 0 & \frac{\alpha^{(2)}\rho^{(1)}}{d} \\ 0 & 0 & 0 & \frac{\alpha^{(1)}\rho^{(2)}}{d} & 1 & 0 & -\frac{\alpha^{(1)}\rho^{(2)}}{d} \\ 0 & 0 & \frac{\alpha^{(1)}\rho^{(1)}}{\rho} & 0 & 0 & \frac{\alpha^{(2)}\rho^{(2)}}{\rho} & 0 \\ 0 & 0 & 0 & \frac{\alpha^{(1)}\rho^{(2)}{c^{(2)}}^2}{d} & 0 & 0 & \frac{\alpha^{(2)}\rho^{(1)}{c^{(1)}}^2}{d} \\ 0 & 0 & 0 & -\frac{\alpha^{(1)}\alpha^{(2)}}{d} & 0 & 0 & \frac{\alpha^{(1)}\alpha^{(2)}}{d} \\ 0 & 0 & \frac{\alpha^{(1)}\alpha^{(2)}\rho^{(1)}\rho^{(2)}}{\rho} & 0 & 0 & -\frac{\alpha^{(1)}\alpha^{(2)}\rho^{(1)}\rho^{(2)}}{\rho} & 0 \end{pmatrix}$$

with

$$\begin{aligned} d &= \alpha^{(1)}\rho^{(2)}{c^{(2)}}^2 + \alpha^{(2)}\rho^{(1)}{c^{(1)}}^2 \\ \rho &= \alpha^{(1)}\rho^{(1)} + \alpha^{(2)}\rho^{(2)} \end{aligned}$$

Keeping the five first lines give the matrix P. It remains to multiply the

matrix P by $A(\mathbf{U})$ to obtain the reduced system in a nonconservative form.

$$\left\{\begin{array}{lllll}
\dfrac{\partial \alpha^{(1)}}{\partial t} + u\dfrac{\partial \alpha^{(1)}}{\partial x} + \alpha^{(1)}\alpha^{(2)}\dfrac{\rho^{(1)}\,{c^{(1)}}^2 - \rho^{(2)}\,{c^{(2)}}^2}{\alpha^{(2)}\rho^{(1)}{c^{(1)}}^2 + \alpha^{(1)}\rho^{(2)}{c^{(2)}}^2}\dfrac{\partial u}{\partial x} = 0 \\
\dfrac{\partial \rho^{(1)}}{\partial t} + u\dfrac{\partial \rho^{(1)}}{\partial x} + \dfrac{\rho^{(1)}\rho^{(2)}\,{c^{(2)}}^2}{\alpha^{(2)}\rho^{(1)}{c^{(1)}}^2 + \alpha^{(1)}\rho^{(2)}{c^{(2)}}^2}\dfrac{\partial u}{\partial x} = 0 \\
\dfrac{\partial \rho^{(2)}}{\partial t} + u\dfrac{\partial \rho^{(2)}}{\partial x} + \dfrac{\rho^{(1)}\rho^{(2)}\,{c^{(1)}}^2}{\alpha^{(2)}\rho^{(1)}{c^{(1)}}^2 + \alpha^{(1)}\rho^{(2)}{c^{(2)}}^2}\dfrac{\partial u}{\partial x} = 0 \\
\dfrac{\partial u}{\partial t} + u\dfrac{\partial u}{\partial x} + \dfrac{1}{\alpha^{(1)}\,\rho^{(1)} + \alpha^{(2)}\,\rho^{(2)}}\dfrac{\partial P}{\partial x} = 0 \\
\dfrac{\partial P}{\partial t} + u\dfrac{\partial P}{\partial x} + \dfrac{\rho^{(1)}\,\rho^{(2)}\,{c^{(2)}}^2\,{c^{(1)}}^2}{\alpha^{(2)}\rho^{(1)}{c^{(1)}}^2 + \alpha^{(1)}\rho^{(2)}{c^{(2)}}^2}\dfrac{\partial u}{\partial x} = 0
\end{array}\right. \tag{2.6}$$

We managed to derive the relaxed system of equations. Nevertheless, this system is in nonconservative form, so that we cannot define the shocks. Moreover, the Jacobian matrix is still complicated, so we cannot yet know easily its eigenstructure. In the next subsection, we will try to find equations on other variables, so as to avoid these problems. We must keep in mind that to describe the flow, we will need

- the velocity
- two thermodynamic coefficients for each phase. This make actually three coefficients, because these four thermodynamic coefficients are linked by the equation $P^{(1)} = P^{(2)}$.
- One variable describing the mixture: volume fraction, mass fraction, etc...

2.2.2 Other equations

Proposition 2.5. *The four following conservative equations hold*

$$\frac{\partial(\alpha^{(k)}\rho^{(k)})}{\partial t} + \frac{\partial}{\partial x}\left(\alpha^{(k)}\rho^{(k)}u^{(k)}\right) = 0 \tag{2.7a}$$

$$\frac{\partial(\rho u)}{\partial t} + \frac{\partial}{\partial x}\left(\rho u \otimes u + P\right) = 0 \tag{2.7b}$$

$$\frac{\partial(\rho E)}{\partial t} + \frac{\partial}{\partial x}\left((\rho E + P)u\right) = 0 \tag{2.7c}$$

Proof. We remark that if an equation of the initial system does not contain any relaxation term in its right hand side, then this equation holds also for the relaxed system. This proves that the two equations on the partial mass (2.7a) hold. In the same manner, if we add the two equations on partial momentum, then we obtain the equation on total momentum (2.7b), which is conserved in the initial system. This proves that (2.7b) holds. As the total energy is conserved too, (2.7c) holds also. □

Proposition 2.6. *The following equations hold*

$$\frac{Ds^{(k)}}{Dt} = 0 \tag{2.8a}$$

We denote by $Y^{(k)}$ *the mass fraction:* $Y^{(k)} = \alpha^{(k)}\rho^{(k)}/\rho$. *Then*

$$\frac{DY^{(k)}}{Dt} = 0 \tag{2.8b}$$

Proof. We begin by writing the partial mass equation under the form

$$\frac{\partial(\rho Y^{(k)})}{\partial t} + \frac{\partial(\rho Y^{(k)}u)}{\partial x} = 0$$

so that if we develop it, we get

$$\rho\frac{\partial Y^{(k)}}{\partial t} + Y^{(k)}\frac{\partial \rho}{\partial t} + Y^{(k)}\frac{\partial(\rho u)}{\partial x} + \rho u\frac{\partial u}{\partial x} = 0$$

because the total mass is conserved, we actually have

$$\frac{\partial Y^{(k)}}{\partial t} + u\frac{\partial Y^{(k)}}{\partial x} = 0$$

which is (2.8b). For the entropy, we use the classical thermodynamic relation

$$\mathrm{d}s^{(k)} = \frac{\beta^{(k)}}{T^{(k)}}\left(\mathrm{d}P - {c^{(k)}}^2\mathrm{d}\rho^{(k)}\right)$$

so that

$$\frac{Ds^{(k)}}{Dt} = \frac{\beta^{(k)}}{T^{(k)}}\left(\frac{DP}{Dt} - {c^{(k)}}^2\frac{D\rho^{(k)}}{Dt}\right)$$

and according to the system (2.6), we find $\dfrac{Ds^{(k)}}{Dt} = 0$. This ends the proof. □

We remark that the system composed of the conservative equations (2.7) is not able to describe totally the flow. The problem is that this four equation system cannot be supplemented of a fifth conservative equation: *the five equations model is essentially nonconservative*. The "most conservative" form of the system can be the following

$$\begin{cases} \dfrac{\partial \alpha^{(k)}}{\partial t} + u\dfrac{\partial \alpha^{(k)}}{\partial x} = \alpha^{(k)}\alpha^{(\bar{k})}\dfrac{\rho^{(\bar{k})}\,{c^{(\bar{k})}}^2 - \rho^{(k)}\,{c^{(k)}}^2}{\alpha^{(2)}\rho^{(1)}{c^{(1)}}^2 + \alpha^{(1)}\rho^{(2)}{c^{(2)}}^2}\dfrac{\partial u}{\partial x} \\ \dfrac{\partial(\alpha^{(k)}\rho^{(k)})}{\partial t} + \dfrac{\partial}{\partial x}\left(\alpha^{(k)}\rho^{(k)}u^{(k)}\right) = 0 \\ \dfrac{\partial(\rho u)}{\partial t} + \dfrac{\partial}{\partial x}\left(\rho u \otimes u + P\right) = 0 \\ \dfrac{\partial(\rho E)}{\partial t} + \dfrac{\partial}{\partial x}\left((\rho E + P)u\right) = 0 \end{cases} \tag{2.9}$$

In this last system, if we know $\alpha^{(k)}$, $\alpha^{(k)}\rho^{(k)}$, ρu and ρE, then:

- we naturally have the description of the mixture with $\alpha^{(k)}$
- the densities are calculated by dividing $\alpha^{(k)}\rho^{(k)}$ by $\alpha^{(k)}$.
- the velocity u is obtained by dividing ρu by $\alpha^{(1)}\rho^{(1)} + \alpha^{(2)}\rho^{(2)}$.
- the pressure is calculated by solving the implicit nonmlinear equation

$$\alpha^{(1)}\rho^{(1)}\varepsilon^{(1)}(\rho^{(1)}, P) + \alpha^{(2)}\rho^{(2)}\varepsilon^{(2)}(\rho^{(2)}, P) + \rho\,\frac{u^2}{2} = \rho E$$

  where $\varepsilon^{(k)}$ denotes the internal specific energy of the fluid k.

2.3 Properties of the model

2.3.1 Eigenvalues and Hyperbolicity

For the study of eigenvalues, we need to study the eigenstructure of the Jacobian matrix. Thus we choose the variables such that the Jacobian matrix is the simplest. As we saw in the previous section, the phasic entropy and the mass fraction follow an advection equation. Therefore we choose as variables $(Y^{(1)}, s^{(1)}, s^{(2)}, u, P)$. With these variables, the Jacobian matrix is equal to

$$\begin{pmatrix} u & 0 & 0 & 0 & 0 \\ 0 & u & 0 & 0 & 0 \\ 0 & 0 & u & 0 & 0 \\ 0 & 0 & 0 & u & \frac{1}{\rho} \\ 0 & 0 & 0 & \frac{\rho^{(1)}\,\rho^{(2)}\,{c^{(2)}}^2\,{c^{(1)}}^2}{\alpha^{(2)}\rho^{(1)}{c^{(1)}}^2+\alpha^{(1)}\rho^{(2)}{c^{(2)}}^2} & u \end{pmatrix} \tag{2.10}$$

Proposition 2.7. *The system* (2.6) *is hyperbolic.*

Proof. The characteristic polynomial of the matrix (2.10)is equal to

$$(X-u)^3\left((X-u)^2-\frac{\rho^{(1)}\,\rho^{(2)}\,{c^{(2)}}^2\,{c^{(1)}}^2}{\rho(\alpha^{(2)}\rho^{(1)}{c^{(1)}}^2+\alpha^{(1)}\rho^{(2)}{c^{(2)}}^2)}\right)$$

We conclude that u is a third order eigenvalue. The three eigenvectors are $(1,0,0,0,0)$, $(0,1,0,0,0)$ and $(0,0,1,0,0)$. The Jacobian matrix has two other eigenvalues: $u \pm \tilde{c}$ with

$$\tilde{c}^2=\frac{\rho^{(1)}\,\rho^{(2)}\,{c^{(2)}}^2\,{c^{(1)}}^2}{\rho(\alpha^{(2)}\rho^{(1)}{c^{(1)}}^2+\alpha^{(1)}\rho^{(2)}{c^{(2)}}^2)}$$

Actually, the relation between the mixture sound velocity and the phasic sound velocity can be cast into

$$\frac{1}{\rho\tilde{c}^2}=\frac{\alpha^{(1)}}{\rho^{(1)}{c^{(1)}}^2}+\frac{\alpha^{(2)}}{\rho^{(2)}{c^{(2)}}^2}$$

Some algebra give these two eigenvectors

$$\begin{array}{ll} u-\tilde{c} & (0,0,0,1,-\rho\tilde{c}) \\ u+\tilde{c} & (0,0,0,1,\rho\tilde{c}) \end{array}$$

□

2.3.2 Entropy

Theorem 2.1. *The total entropy*

$$S=\frac{\alpha^{(1)}\rho^{(1)}s^{(1)}+\alpha^{(2)}\rho^{(2)}s^{(2)}}{\rho}$$

verifies the following conservation law

$$\frac{\partial(\rho S)}{\partial t}+\frac{\partial(\rho S u)}{\partial x}=0$$

Proof. Actually we prove that for regular solutions, the phasic entropies follow

$$\frac{\partial(\alpha^{(k)}\rho^{(k)}s^{(k)})}{\partial t}+\frac{\partial(\alpha^{(k)}\rho^{(k)}s^{(k)}u)}{\partial x}=0$$

We first put the equation in its nonconservative form

$$\begin{aligned}\frac{\partial(\alpha^{(k)}\rho^{(k)}s^{(k)})}{\partial t}+\frac{\partial(\alpha^{(k)}\rho^{(k)}s^{(k)}u)}{\partial x} =& \; s^{(k)}\left(\frac{\partial(\alpha^{(k)}\rho^{(k)})}{\partial t}+\frac{\partial(\alpha^{(k)}\rho^{(k)}u)}{\partial x}\right)\\ &+\alpha^{(k)}\rho^{(k)}\frac{Ds^{(k)}}{Dt}\\ =& \; \alpha^{(k)}\rho^{(k)}\frac{Ds^{(k)}}{Dt}\end{aligned}$$

Last, Proposition 2.6 gives the result for the phasic entropy. The total entropy follows immediately. □

2.3.3 Fields and Riemann invariants

Proposition 2.8. *The field u is linearly degenerate*

Proof. Here, we are interested in the field u which gradient is equal to $(0,0,0,1,0)$. It is clearly orthogonal to the three eigenvectors found in the previous subsection. Therefore the field u is linearly degenerate. □

Proposition 2.9. *If the equations of state of each fluid is such that*

$$1+\rho^{(k)}c^{(k)}\left(\frac{\partial c}{\partial P}\right)_s$$

has the same sign for each k, and never vanishes. Then the fields $u\pm\tilde{c}$ are genuinely nonlinear.

Proof. We prove this proposition only for the right eigenvalues $u+\tilde{c}$. The gradient of the field $u+\tilde{c}$ is equal to

$$\nabla\left(u+\tilde{c}\right)=\left(\frac{\partial\tilde{c}}{\partial\alpha^{(1)}},\frac{\partial\tilde{c}}{\partial\rho^{(1)}},\frac{\partial\tilde{c}}{\partial\rho^{(1)}},1,\frac{\partial\tilde{c}}{\partial P}\right)$$

so that its dot product with the associated eigenvector is equal to $1+\rho\tilde{c}\left(\frac{\partial\tilde{c}}{\partial P}\right)_{(s^{(1)},s^{(2)},Y^{(1)})}$. We need to calculate this last derivative. For that, we rewrite

$$\begin{aligned}\rho=&\;\alpha^{(1)}\rho^{(1)}+\alpha^{(2)}\rho^{(2)}\\ =&\;\frac{1}{\frac{Y^{(1)}}{\rho^{(1)}}+\frac{Y^{(2)}}{\rho^{(2)}}}\end{aligned}$$

so that we have

$$\begin{aligned}-\frac{1}{\rho^2}\left(\frac{\partial\rho}{\partial P}\right)_{(s^{(1)},s^{(2)},Y^{(1)})} &= -\sum_{k=1}^{2}\frac{Y^{(k)}}{{\rho^{(k)}}^2}\left(\frac{\partial\rho^{(k)}}{\partial P}\right)_{(s^{(1)},s^{(2)},Y^{(1)})}\\ &= -\frac{Y^{(1)}}{{\rho^{(1)}}^2{c^{(1)}}^2}-\frac{Y^{(2)}}{{\rho^{(2)}}^2{c^{(2)}}^2}\\ &= -\frac{\alpha^{(1)}\rho^{(1)}}{\rho{\rho^{(1)}}^2{c^{(1)}}^2}-\frac{\alpha^{(2)}\rho^{(2)}}{\rho{\rho^{(2)}}^2{c^{(2)}}^2}\end{aligned}$$

eventually

$$\left(\frac{\partial\rho}{\partial P}\right)_{(s^{(1)},s^{(2)},Y^{(1)})}=\frac{1}{\tilde{c}^2}$$

The equality defining $\tilde{c}$ can be rewritten as

$$\frac{1}{\tilde{c}^2}=\rho^2\left(\frac{Y^{(1)}}{{\rho^{(1)}}^2{c^{(1)}}^2}+\frac{Y^{(2)}}{{\rho^{(2)}}^2{c^{(2)}}^2}\right)$$

so that if we differentiate once

$$\begin{aligned}\frac{-2\left(\frac{\partial\tilde{c}}{\partial P}\right)_{(s^{(1)},s^{(2)},Y^{(1)})}}{\tilde{c}^3} = {}& 2\rho\left(\frac{\partial\rho}{\partial P}\right)_{(s^{(1)},s^{(2)},Y^{(1)})}\left(\frac{Y^{(1)}}{{\rho^{(1)}}^2{c^{(1)}}^2}+\frac{Y^{(2)}}{{\rho^{(2)}}^2{c^{(2)}}^2}\right)\\ & -2\rho^2\left(\sum_{k=1}^{2}\frac{Y^{(k)}\left(\frac{\partial(\rho^{(k)}c^{(k)})}{\partial P}\right)_{(s^{(1)},s^{(2)},Y^{(1)})}}{{\rho^{(k)}}^2{c^{(k)}}^2}\right)\end{aligned}$$

and

$$\left(\frac{\partial(\rho^{(1)}c^{(1)})}{\partial P}\right)_{(s^{(1)},s^{(2)},Y^{(1)})}=\frac{1+\rho^{(1)}c^{(1)}\left(\frac{\partial c^{(1)}}{\partial P}\right)_{s^{(1)}}}{{c^{(1)}}^2}$$

so that

$$1+\rho\tilde{c}\left(\frac{\partial\tilde{c}}{\partial P}\right)_{(Y^{(1)},s^{(1)},s^{(2)})}=\rho\tilde{c}^2\left(\sum_{k=1}^{2}\frac{1+\rho^{(k)}c^{(k)}\left(\frac{\partial c^{(k)}}{\partial P}\right)_{s^{(k)}}}{{\rho^{(k)}}^2{c^{(k)}}^2}\right)$$

Therefore, if the

$$1+\rho^{(k)}c^{(k)}\left(\frac{\partial c}{\partial P}\right)_s$$

have the same sign and never vanish, then

$$1+\rho\tilde{c}\left(\frac{\partial\tilde{c}}{\partial P}\right)_{(Y^{(1)},s^{(1)},s^{(2)})}\neq 0$$

which ends the proof. □

Remark 2.1. 1. We remind that for the classical Eulerian system, the Jacobian matrix with (s,u,P) as variables is equal to

$$\begin{pmatrix} u & 0 & 0 \\ 0 & u & \frac{1}{\rho} \\ 0 & \rho c^2 & u \end{pmatrix}$$

and that its eigenvalues are u and $u\pm c$. The eigenvector associated to $u+c$ is equal to $(0,1,\rho c)$, and the genuinely nonlinearity of this field is equivalent to

$$1+\rho c\left(\frac{\partial c}{\partial P}\right)_s\neq 0$$

so that what we supposed for Proposition 2.9 is a bit stronger than what is usually supposed to ensure the genuinely nonlinearity of the Eulerian system.

2. The effect of the sign of

$$1+\rho c\left(\frac{\partial c}{\partial P}\right)_s\neq 0$$

on the solution of the Riemann problem for the Eulerian system will be discussed in Chapter 5.

2.3.4 Formal link with stochastic homogenization

We perform a comparison with the theory of linear waves propagation in a random medium. Given an hyperbolic system

$$\frac{\partial\mathbf{U}}{\partial t}+A(\mathbf{U})\frac{\partial\mathbf{U}}{\partial x}=0$$

we recall that the small perturbations $\hat{\mathbf{U}}$ near a constant state $\overline{\mathbf{U}}$ are given by expanding formally $\mathbf{U}$ as

$$\mathbf{U}=\overline{\mathbf{U}}+\varepsilon\hat{\mathbf{U}}+O\left(\varepsilon^2\right)$$

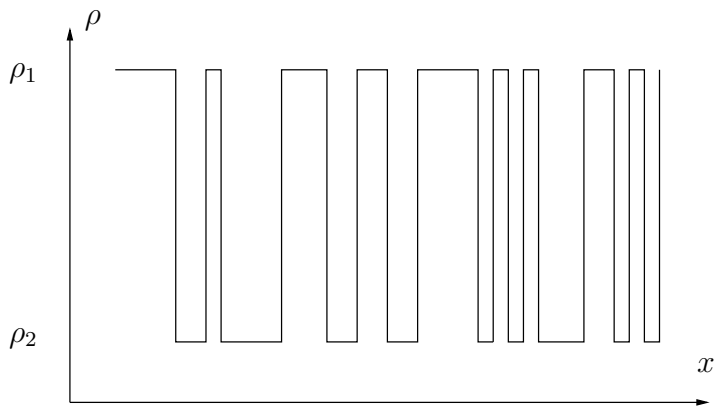

Figure 2.1: A random medium composed of a material of density $\rho^{(1)}$ and $\rho^{(2)}$. We study the propagation of acoustic wave in such a medium, and we especially want to compute the limite of the propagation velocity when the two materials are very well mixed.

and by keeping the first order terms in the original system, which leads to

$$\frac{\partial \hat{\mathbf{U}}}{\partial t} + A(\overline{\mathbf{U}})\frac{\partial \hat{\mathbf{U}}}{\partial x} = 0$$

For the Eulerian system, the system in variables (ρ, u, P) reads

$$\left\{ \begin{array}{l} \dfrac{\partial \hat{\rho}}{\partial t} + \overline{u}\,\dfrac{\partial \hat{\rho}}{\partial x} + \overline{\rho}\,\dfrac{\partial \hat{u}}{\partial x} = 0 \\ \dfrac{\partial \hat{P}}{\partial t} + \overline{u}\,\dfrac{\partial \hat{P}}{\partial x} + \overline{\rho}\,\overline{c}^2\,\dfrac{\partial \hat{u}}{\partial x} = 0 \\ \dfrac{\partial \hat{u}}{\partial t} + \overline{u}\,\dfrac{\partial \hat{u}}{\partial x} + \dfrac{1}{\overline{\rho}}\,\dfrac{\partial \hat{P}}{\partial x} = 0 \end{array} \right.$$

we suppose that $\overline{u} = 0$ (which is equivalent to change to a reference frame moving at the velocity $\overline{u}$), so that the system becomes

$$\left\{ \begin{array}{l} \dfrac{\partial \hat{\rho}}{\partial t} + \overline{\rho}\,\dfrac{\partial \hat{u}}{\partial x} = 0 \\ \dfrac{\partial \hat{P}}{\partial t} + \overline{\rho}\,\overline{c}^2\,\dfrac{\partial \hat{u}}{\partial x} = 0 \\ \dfrac{\partial \hat{u}}{\partial t} + \dfrac{1}{\overline{\rho}}\,\dfrac{\partial \hat{P}}{\partial x} = 0 \end{array} \right.$$

In this last system, we see that if we know $\hat{u}$, the density follows by a simple time integration. We thus are interested in the system (omitting the bars

and the hats)

$$\left\{ \begin{array}{l} \rho \dfrac{\partial u}{\partial t} + \dfrac{\partial P}{\partial x} = 0 \\ \dfrac{\partial P}{\partial t} + \kappa \dfrac{\partial u}{\partial x} = 0 \end{array} \right.$$

where ρ is the material density and κ is the bulk modulus of the medium.

$$\kappa = \bar{\rho}\bar{c}^2$$

The medium variables are assumed to be function of x/ε, and are stationnary process (see Figure 2.1). This means that the medium oscillates between two different media, each of them being characterized by a density $\rho^{(k)}$ and a bulk modulus $\kappa^{(k)}$. We perform a Fourier transform with respect to t, so that the system becomes

$$\frac{\mathrm{d}X^\varepsilon}{\mathrm{d}x} = F\left(\frac{x}{\varepsilon}, X^\varepsilon\right)$$

where

$$X^\varepsilon = \begin{pmatrix} \hat{P} \\ \hat{u} \end{pmatrix} \qquad F(x, X) = -\mathrm{i}\xi \begin{pmatrix} 0 & \rho(x) \\ \dfrac{1}{\kappa(x)} & 0 \end{pmatrix} X$$

Following the theorem of effective medium [23, 35], X^ε converges to $\bar{X}$ (in probability), where $\bar{X}$ is solution of

$$\frac{\mathrm{d}\bar{X}}{\mathrm{d}x} = -\mathrm{i}\xi \begin{pmatrix} 0 & \mathscr{E}(\rho) \\ \mathscr{E}\left(\dfrac{1}{\kappa}\right) & 0 \end{pmatrix} \bar{X}$$

If the random medium is composed of a fluid 1 with probability $\alpha^{(1)}$, and a fluid 2 with probability $\alpha^{(2)}$, then

$$\left\{ \begin{array}{l} \mathscr{E}(\rho) = \alpha^{(1)}\rho^{(1)} + \alpha^{(2)}\rho^{(2)} \\ \mathscr{E}\left(\dfrac{1}{\kappa}\right) = \dfrac{\alpha^{(1)}}{\kappa^{(1)}} + \dfrac{\alpha^{(2)}}{\kappa^{(2)}} \end{array} \right.$$

so that the wave propagation in the random medium is equal to $\tilde{\bar{c}}^2 = \bar{\kappa}/\bar{\rho}$, which means that

$$\frac{1}{\bar{\rho}\tilde{\bar{c}}^2} = \frac{\alpha^{(1)}}{\kappa^{(1)}} + \frac{\alpha^{(2)}}{\kappa^{(2)}} = \frac{\alpha^{(1)}}{\rho^{(1)}{c^{(1)}}^2} + \frac{\alpha^{(2)}}{\rho^{(2)}{c^{(2)}}^2}$$

which is the same result as if we compute the velocity of the acoustic wave of the five equations model (2.6). This gives a rigorous framework on the derivation led in this chapter, at least in the acoustic approximation.

In this chapter, we derived a continuous system modelling two phase flow, in the limit of zero-relaxation of pressure and velocity. This system is unconditionnaly hyperbolic. Nevertheless, there remains a problem in this system: a nonconservative product. This is a mathematical problem because there are product of distribution, that may not be defined, and numerical problem, because we cannot define a whole set of jump relations across a shock, so that the Riemann problem cannot be solved. Last, even if we had jump relations, we would not have a Lax–Wendroff theorem for a Godunov' type scheme, because the Lax–Wendroff theorem applies only in the conservative framework. The numerical approximation of the five equations model is the object of the next chapter.

Chapter 3

Numerical approximation of the five equations model

In Chapter 1, the following system was considered for compressible multi-phase flows

$$\begin{array}{lll}
\dfrac{\partial \alpha^{(k)}}{\partial t} + \mathbf{u}_I \cdot \nabla \alpha^{(k)} & = & \mu(P^{(k)} - P^{(\bar{k})}) \\
\dfrac{\partial \big(\alpha^{(k)}\rho^{(k)}\big)}{\partial t} + \mathrm{div}\big(\alpha^{(k)}\rho^{(k)}\mathbf{u}^{(k)}\big) & = & 0 \\
\dfrac{\partial \big(\alpha^{(k)}\rho^{(k)}\mathbf{u}^{(k)}\big)}{\partial t} + \mathrm{div}\,\big(\alpha^{(k)}\rho^{(k)}\mathbf{u}^{(k)} \otimes \mathbf{u}^{(k)}\big) + \nabla(\alpha^{(k)}P^{(k)}) & = & P_I \nabla \alpha^{(k)} \\
 & & +\lambda(\mathbf{u}^{(\bar{k})} - \mathbf{u}^{(k)}) \\
\dfrac{\partial \big(\alpha^{(k)}\rho^{(k)}E^{(k)}\big)}{\partial t} + \mathrm{div}\,\big(\alpha^{(k)}(\rho^{(k)}E^{(k)} + P^{(k)})\mathbf{u}^{(k)}\big) & = & P_I \mathbf{u}_I \cdot \nabla \alpha^{(k)} \\
 & & -\mu P_I (P^{(k)} - P^{(\bar{k})}) \\
 & & +\lambda \mathbf{u}_I (\mathbf{u}^{(\bar{k})} - \mathbf{u}^{(k)})
\end{array} \tag{3.1}$$

In (3.1), $P^{(k)}$ is the pressure of phase Σ_k, the total energy is related to the pressure by $E^{(k)} = \varepsilon^{(k)}(P^{(k)}, \rho^{(k)}) + \frac{1}{2}{\mathbf{u}^{(k)}}^2$ where the internal energy is a concave function of its arguments. We define $\bar{k} = 1$ (resp. $= 2$) when $k = 2$ (resp. $k = 1$). The interface velocity and pressure $\mathbf{u}_I$ and P_I are modelled, this is one of the difficult points, as we saw in the end of Chapter 1. The variables μ and λ are relaxation parameters that depend on the inter-facial area.

With respect to standard approaches, the seven equation model (3.1) has several original features and properties. First, (3.1) is hyperbolic whatever the choice of the interface parameters. This in contrast with models that are only conditionally hyperbolic such as in [63, 22]. From the numerical point of view, the interesting consequence is that one may adapt the now-days

standard techniques for the approximation of hyperbolic problems. Another interesting feature is the occurrence of the relaxation parameters μ and λ that can be interpreted as a way to introduce the local flow topology.

However, the model (3.1) leads to several difficult issues such as

- *a modelling problem :* how can we define the interface velocity and pressure ? From a rigorous point of view, the situation is rather clear only when $\lambda \to +\infty$ and $\mu \to +\infty$, in which case we have pressure and velocity equilibrium. This corresponds to interface problems or problems where the phases are intimately mixed.

- *a mathematical problem :* the system cannot be cast into conservative form, which induces difficulties for the definition of a shock and for the derivation of a numerical scheme. This point is in contradiction with the initial goal, the use of standard hyperbolic techniques for the simulation of multiphase flow problems.

In the limit $\lambda, \mu \to +\infty$, while μ/λ remains bounded, we obtained in the previous chapter the following model by asymptotic expansion:

$$\begin{array}{rcl}
\dfrac{\partial \alpha^{(k)}}{\partial t} + \mathbf{u}\cdot\nabla\alpha^{(k)} & = & \dfrac{\rho^{(\bar{k})}c^{(\bar{k})^2} - \rho^{(k)}c^{(k)^2}}{\frac{\rho^{(k)}c^{(k)^2}}{\alpha^{(k)}} + \frac{\rho^{(\bar{k})}c^{(\bar{k})^2}}{\alpha^{(\bar{k})}}}\text{div } \mathbf{u} \\
\dfrac{\partial\big(\alpha^{(k)}\rho^{(k)}\big)}{\partial t} + \text{div }\big(\alpha^{(k)}\rho^{(k)}\mathbf{u}\big) & = & 0 \\
\dfrac{\partial\big(\rho\mathbf{u}\big)}{\partial t} + \text{div }\big(\rho\mathbf{u}\otimes\mathbf{u}\big) + \nabla P & = & 0 \\
\dfrac{\partial\big(\rho E\big)}{\partial t} + \text{div }\big((\rho E + P)\mathbf{u}\big) & = & 0,
\end{array} \tag{3.2}$$

where ρ and E are the mixture density and the mixture energy defined by

$$\rho = \alpha^{(1)}\rho^{(1)} + \alpha^{(2)}\rho^{(2)}$$

$$E = \frac{\alpha^{(1)}\rho^{(1)}E^{(1)} + \alpha^{(2)}\rho^{(2)}E^{(2)}}{\rho}$$

and $c^{(k)}$ are the isentropic sound velocity of each phase defined by

$$c^{(k)^2} = \left(\frac{\partial P^{(k)}}{\partial \rho^{(k)}}\right)_{s^{(k)}}$$

This system was obtained by developing the different pressures and velocities of (3.1) around the equilibrium variables P and $\mathbf{u}$. In the sequel, we often denote this model as the "five equations model".

This system can be shown to be unconditionally hyperbolic. Unfortunately, a non–conservative product appears one more time in the volume of

fluid equation. This term can be interpreted as follows : when a shock enters a mixture zone, the volume fraction must change because the shock speed is different in the two phases. This term is proportional to the divergence of the velocity, and does not play any role in pure interface problems. In contrast, this term does not vanish in general across a shock wave, and induces a change in volume. However, the difficulty, from a mathematical point of view, is that this term has no precise meaning in the case where $\mathbf{u}$ and $\frac{\rho^{(\bar{k})}c^{(\bar{k})^2}-\rho^{(k)}c^{(k)^2}}{\frac{\rho^{(k)}c^{(k)^2}}{\alpha^{(k)}}+\frac{\rho^{(\bar{k})}c^{(\bar{k})^2}}{\alpha^{(\bar{k})}}}$ are simultaneously discontinuous. In that case, it is difficult to derive a numerical scheme.

In the present contribution, we propose to answer this problem by starting with the scheme of [2] and then to derive an asymptotic expansion from the discrete scheme, instead of the system of PDE (3.1). The scheme of [2] which is well adapted to approximate multiphase problems, relies on a multi-scale representation of the flow. We recall the fact that (3.1) is obtained from an ensemble average of realization ; for any realization we have well localised interfaces between phases, with possibly different scales for bubbles. From the numerical point of view, we write a scheme for each realization, using standard assumptions in the finite volume context. This scheme makes use of ones favourite Riemann solver. Here, we consider several solvers : Godunov', HLL type, acoustic, and a relaxation solver. We take into account the various scales by dividing cells into sub-cells being filled by any of the two phases. Then we make an ensemble average of the different schemes. This avoids to define precisely interface variables (even-though a limit model can be derived), this also solve the problem of non conservative products (since the scheme for each realization is obtained from conservation principles). We can identify terms that correspond to relaxation terms as in (3.1), they are consequence of acoustic effects. The last step, write scheme for (3.2), is obtained by doing an asymptotic expansion of the scheme of [2].

This chapter is organised as follows. We first recall in details the results of [2] with a particular emphasis on the relaxation terms. This is the topic of section 3.1. The structure of the equilibrium variety for several numerical schemes is studied in section 3.2. section 3.3 is devoted to the derivation of the asymptotic scheme of (3.2). Numerical illustrations are provided in section 3.4.

This chapter has been published in [4, 3].

3.1 A numerical scheme for the seven equations model

The derivation of the scheme uses the ensemble averaging ideas of Drew and Passman [20] combined with the discretisation principle introduced by Godunov. In [20], the non–conservative and the modelling terms appear after a ensemble average. The idea of [2] is to begin the derivation of the numerical scheme *before* the averaging procedure. We describe the scheme in the case of the Godunov solver. All this can easily be adapted to other solvers. We also note that the different terms of (3.5) can be approximated with different solvers, the only constraint is conservation.

At each time step, the flow is described in each computational cell by the average

$$W_j = (\alpha_j^{(1)}, \alpha_j^{(1)}\rho_j^{(1)}, \alpha_j^{(1)}\rho_j^{(1)}u_j^{(1)}, \alpha_j^{(1)}\rho_j^{(1)}E_j^{(1)}, \alpha_j^{(2)}, \alpha_j^{(2)}\rho_j^{(2)}, \alpha_j^{(2)}\rho_j^{(2)}u_j^{(2)}, \alpha_j^{(2)}\rho_j^{(2)}E_j^{(2)}).$$

We consider a family of random subdivision of the cell

$$\mathcal{C}_j = [x_{j-1/2}, x_{j+1/2}] = \cup_k [\xi_k, \xi_{k+1}].$$

In each of the sub-cells $]\xi_k, \xi_{k+1}[$, we randomly set the flow variables (see Figure 3.1)

$$U_j^{(1)} = (\rho_j^{(1)}, \rho_j^{(1)}u_j^{(1)}, \rho_j^{(1)}E_j^{(1)}) \quad \text{or} \quad U_j^{(2)} = (\rho_j^{(2)}, \rho_j^{(2)}u_j^{(2)}, \rho_j^{(2)}E_j^{(2)})$$

The only constraint on the random subdivision is that it must be consistent with the volume fraction of each phase. Therefore, if X is the indicator function of Σ_1, the average $\mathscr{E}\left(\int_{x_{j-1/2}}^{x_{j+1/2}} X dx\right)$ must precisely be $\alpha_1^{(j)}(x_{j+1/2} - x_{j-1/2})$.

In the cell $\mathcal{C}_i$, the phase Σ_1 satisfies

$$\int_{\mathcal{C}_i} X \left(\frac{\partial \mathbf{U}}{\partial t} + \frac{\partial \mathbf{F}}{\partial x}\right) \mathrm{d}x\, \mathrm{d}t = 0$$

Then

$$\sum_{j=0}^{N(\omega)-1} \int_{\xi_j}^{\xi_{j+1}} X \frac{\partial \mathbf{U}}{\partial t}\, \mathrm{d}x + \sum_{j=0}^{N(\omega)-1} \int_{\xi_j}^{\xi_{j+1}} X \frac{\partial \mathbf{F}}{\partial x}\, \mathrm{d}x = 0 \tag{3.3}$$

and the characteristic function X obeys

$$\sum_{j=0}^{N(\omega)-1} \int_t^{t+s} \frac{\partial X}{\partial t}\, \mathrm{d}x\, \mathrm{d}t + \sum_{j=0}^{N(\omega)-1} \int_t^{t+s} \int_{\xi_j}^{\xi_{j+1}} \sigma \frac{\partial X}{\partial x}\, \mathrm{d}x\, \mathrm{d}t = 0$$

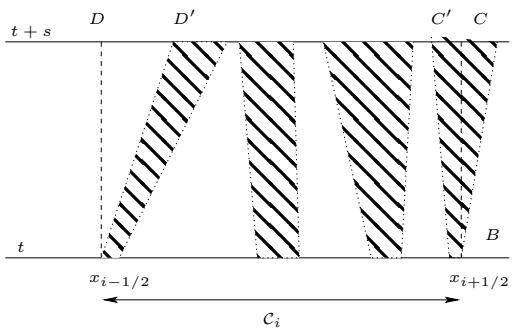

Figure 3.1: Evolution of each phase after a random subdivision of the cell $\mathcal{C}_i$ between time t and $t+s$

where σ is the local interface velocity. The derivative of X is to be taken in the sense of distribution. We denote by $\lambda_{\max}$ the maximum wave speed in the internal Riemann problems. Under the CFL condition

$$|\lambda_{\max}| \frac{s}{\Delta\xi} \leq \frac{1}{2},$$

we can integrate (3.3) to get

$$\sum_{l=1}^{N(\omega)-1} \int_t^{t+s} \int_{\xi_l}^{\xi_{l+1}} X \frac{\partial \mathbf{U}}{\partial t} \mathrm{d}x\, \mathrm{d}t + \sum_{l=1}^{N(\omega)-1} \int_t^{t+s} \int_{\xi_l}^{\xi_{l+1}} X \frac{\partial \mathbf{F}}{\partial x} \mathrm{d}x\, \mathrm{d}t = 0 \tag{3.4}$$

The equation (3.4) can be split into three parts: interaction with the left cell (3.5a), interaction with the right cell (3.5c) and internal interactions (3.5b)

$$\int_{AD'D} X \left(\frac{\partial \mathbf{U}}{\partial t} + \frac{\partial \mathbf{F}}{\partial x} \right) \mathrm{d}x\, \mathrm{d}t \tag{3.5a}$$

$$+ \sum_{l=2}^{N(\omega)-1} \int_t^{t+s} \int_{\xi_l + s'\sigma\left(\mathbf{U}_i^{l-1}, \mathbf{U}_i^{l}\right)}^{\xi_{l+1} + s'\sigma\left(\mathbf{U}_i^{l}, \mathbf{U}_i^{l+1}\right)} X \left(\frac{\partial \mathbf{U}}{\partial t} + \frac{\partial \mathbf{F}}{\partial x} \right) \mathrm{d}x\, \mathrm{d}s' \tag{3.5b}$$

$$+ \int_{CBB'} X \left(\frac{\partial \mathbf{U}}{\partial t} + \frac{\partial \mathbf{F}}{\partial x} \right) \mathrm{d}x\, \mathrm{d}t = 0 \tag{3.5c}$$

We study the three terms of (3.5).

- Boundary terms. For the term (3.5a), a straightforward calculation

provides :

$$\begin{aligned}\int_{AD'D} X\left(\frac{\partial \mathbf{U}}{\partial t}+\frac{\partial \mathbf{F}}{\partial x}\right)\mathrm{d}x\,\mathrm{d}t = & \int_{AD'D}\left(\frac{\partial X\mathbf{U}}{\partial t}+\frac{\partial X\mathbf{F}}{\partial x}\right)\mathrm{d}x\,\mathrm{d}t \\ & -\int_{AD'D}\left(\mathbf{U}\frac{\partial X}{\partial t}+\mathbf{F}\left(\mathbf{U}\right)\frac{\partial X}{\partial x}\right)\mathrm{d}x\,\mathrm{d}t \\ = & \int_{x_{i-\frac{1}{2}}}^{x_{i-\frac{1}{2}}+s\sigma^{+}\left(\mathbf{U}_{i-1}^{+},\mathbf{U}_{i}^{-}\right)} X\left(x,t+s\right)\mathbf{U}(x,t+s)\mathrm{d}x \\ & -sX\left(x_{i-\frac{1}{2}},t^{+}\right)\mathbf{F}\left(\mathbf{U}_{i-\frac{1}{2}}^{\star}\right) \\ & +s\mathbf{F}^{lag}\left(\mathbf{U}_{i-1}^{+},\mathbf{U}_{i}^{-}\right)[X]_{j=0}\end{aligned}$$

Doing the same for the right term (3.5c), we find

$$\begin{aligned}\int_{BCC'} X\left(\frac{\partial \mathbf{U}}{\partial t}+\frac{\partial \mathbf{F}}{\partial x}\right)\mathrm{d}x\,\mathrm{d}t = & \int_{x_{i+\frac{1}{2}}}^{x_{i+\frac{1}{2}}+s\sigma^{-}\left(\mathbf{U}_{i}^{+},\mathbf{U}_{i+1}^{-}\right)} X(x,t+s)\mathbf{U}(x,t+s)\mathrm{d}x \\ & -sX\left(x_{i+\frac{1}{2}},t^{+}\right)\mathbf{F}\left(\mathbf{U}_{i+\frac{1}{2}}^{\star}\right) \\ & +s\mathbf{F}^{lag}\left(\mathbf{U}_{i}^{+},\mathbf{U}_{i+1}^{-}\right)[X]_{j=N(\omega)}\end{aligned}$$

- Internal terms (3.5b). A similar algebra provides

$$\begin{aligned}\int_{t}^{t+s}\int_{\xi_l+s'\sigma\left(\mathbf{U}_i^l,\mathbf{U}_i^{l+1}\right)}^{\xi_{l+1}+s'\sigma\left(\mathbf{U}_i^l,\mathbf{U}_i^{l+1}\right)} X\left(\frac{\partial \mathbf{U}}{\partial t}+\frac{\partial \mathbf{F}}{\partial x}\right)\mathrm{d}x\,\mathrm{d}s' & \\ = s\left([X]_j\,\mathbf{F}^{lag}\left(\mathbf{U}_i^j,\mathbf{U}_i^{j+1}\right)+[X]_{j-1}\,\mathbf{F}^{lag}\left(\mathbf{U}_i^{j-1},\mathbf{U}_i^j\right)\right) & \\ +\int_{\xi_j+s\sigma\left(\mathbf{U}_i^{j-1},\mathbf{U}_i^j\right)}^{\xi_{j+1}+s\sigma\left(\mathbf{U}_i^j,\mathbf{U}_i^{j+1}\right)} X\left(x,t+s\right)\mathbf{U}(x,t+s)\mathrm{d}x & \\ -\int_{\xi_j}^{\xi_{j+1}} X(x,t)\mathbf{U}(x,t)\mathrm{d}x & \end{aligned}$$

By summing the different terms and taking the limit when $s \to 0$, we obtain

the semi–discrete scheme

$$\begin{aligned}
&\frac{\partial}{\partial t}\left(\frac{1}{\Delta x}\int_{x_{i-\frac{1}{2}}}^{x_{i+\frac{1}{2}}} X(x,t)\mathbf{U}(x,t)\mathrm{d}x\right)\\
&\qquad+\frac{1}{\Delta x}\left(X\left(x_{i+\frac{1}{2}},t^{+}\right)\mathbf{F}\left(\mathbf{U}^{\star}_{i+\frac{1}{2}}\right)-X\left(x_{i-\frac{1}{2}},t^{+}\right)\mathbf{F}\left(\mathbf{U}^{\star}_{i-\frac{1}{2}}\right)\right)\\
&=\frac{1}{\Delta x}\sum_{j=1}^{N(\omega)}\left([X]_j\,\mathbf{F}^{lag}\left(\mathbf{U}_i^{j},\mathbf{U}_i^{j-1}\right)-[X]_{j-1}\,\mathbf{F}^{lag}\left(\mathbf{U}_i^{j-1},\mathbf{U}_i^{j-2}\right)\right)\\
&\qquad+\frac{1}{\Delta x}\left([X]_0\,\mathbf{F}^{lag}\left(\mathbf{U}_{i-1}^{+},\mathbf{U}_i^{-}\right)+[X]_{N(\omega)}\,\mathbf{F}^{lag}\left(\mathbf{U}_i^{+},\mathbf{U}_{i+1}^{-}\right)\right)
\end{aligned}\tag{3.6}$$

We may assume that two adjacent sub-cells contains different phases[1], so that the sum in (3.6) can be rewritten as

$$\begin{aligned}
&\sum_{j=1}^{N(\omega)-1}\left([X]_j\,\mathbf{F}^{lag}\left(\mathbf{U}_i^{j},\mathbf{U}_i^{j-1}\right)-[X]_{j-1}\,\mathbf{F}^{lag}\left(\mathbf{U}_i^{j-1},\mathbf{U}_i^{j-2}\right)\right)\\
&\qquad=\pm N(\omega)_i\left(\mathbf{F}^{lag}\left(\mathbf{U}_i^{(2)},\mathbf{U}_i^{(1)}\right)-\mathbf{F}^{lag}\left(\mathbf{U}_i^{(1)},\mathbf{U}_i^{(2)}\right)\right)
\end{aligned}$$

3.1.1 Averaging procedure

It remains to take the mathematical expectancy of the semi-discrete scheme (3.6). For the first term, we have

$$\mathcal{E}\left(\frac{\partial}{\partial t}\left(\frac{1}{\Delta x}\int_{x_{i-\frac{1}{2}}}^{x_{i+\frac{1}{2}}} X(x,t)\mathbf{U}(x,t)\mathrm{d}x\right)\right)=\frac{\partial(\alpha_i^{(1)}\mathbf{U}_i^{(1)})}{\partial t}$$

Then the scheme can be rewritten as

$$\begin{aligned}
&\frac{\partial(\alpha_i^{(1)}\mathbf{U}_i^{(1)})}{\partial t}\\
&\quad+\frac{1}{\Delta x}\left(\mathcal{E}\left(X\left(x_{i+\frac{1}{2}},t^{+}\right)\mathbf{F}\left(\mathbf{U}^{\star}_{i+\frac{1}{2}}\right)\right)-\mathcal{E}\left(X\left(x_{i-\frac{1}{2}},t^{+}\right)\mathbf{F}\left(\mathbf{U}^{\star}_{i-\frac{1}{2}}\right)\right)\right)\\
&=\lambda_i\left(\mathbf{F}^{\ell ag}\left(\mathbf{U}_i^{(2)},\mathbf{U}_i^{(1)}\right)-\mathbf{F}^{\ell ag}\left(\mathbf{U}_i^{(1)},\mathbf{U}_i^{(2)}\right)\right)\\
&\qquad+\frac{1}{\Delta x}\left(\mathcal{E}\left([X]_0\right)\mathbf{F}^{\ell ag}\left(\mathbf{U}_{i-1}^{+},\mathbf{U}_i^{-}\right)+\mathcal{E}\left([X]_{N(\omega)}\right)\mathbf{F}^{\ell ag}\left(\mathbf{U}_i^{+},\mathbf{U}_{i+1}^{-}\right)\right)
\end{aligned}\tag{3.7}$$

[1] otherwise, if two neighbouring cells contain the same phase, we gather them : this is not an extra assumption.

Here, we have introduced the notation

$$\lambda_i = \mathcal{E}\left(\frac{N(\omega)_i}{\Delta x}\right)$$

which can be interpreted as the number of interface per cell [2]

Similarly we get, for Σ_2,

$$\begin{aligned}
&\frac{\partial(\alpha_i^{(2)}\mathbf{U}_i^{(2)})}{\partial t} \\
&\quad + \frac{1}{\Delta x}\left(\mathcal{E}\left(X\left(x_{i+\frac{1}{2}},t^+\right)\mathbf{F}\left(\mathbf{U}^\star_{i+\frac{1}{2}}\right)\right) - \mathcal{E}\left(X\left(x_{i-\frac{1}{2}},t^+\right)\mathbf{F}\left(\mathbf{U}^\star_{i-\frac{1}{2}}\right)\right)\right) \\
&\quad = -\lambda_i\left(\mathbf{F}^{\ell ag}\left(\mathbf{U}_i^{(2)},\mathbf{U}_i^{(1)}\right) - \mathbf{F}^{\ell ag}\left(\mathbf{U}_i^{(1)},\mathbf{U}_i^{(2)}\right)\right) \\
&\qquad -\frac{1}{\Delta x}\left(\mathcal{E}\left([X]_0\right)\mathbf{F}^{\ell ag}\left(\mathbf{U}^+_{i-1},\mathbf{U}^-_i\right) + \mathcal{E}\left([X]_{N(\omega)}\right)\mathbf{F}^{\ell ag}\left(\mathbf{U}^+_i,\mathbf{U}^-_{i+1}\right)\right)
\end{aligned} \tag{3.8}$$

In (3.7) and (3.8), the expected fluxes

$$\begin{aligned}
&\mathcal{E}\left(X\left(x_{i\pm\frac{1}{2}},t^+\right)\mathbf{F}\left(\mathbf{U}^\star_{i+\frac{1}{2}}\right)\right), \\
&\mathcal{E}\left([X]_0\right)\mathbf{F}^{\ell ag}\left(\mathbf{U}^+_{i-1},\mathbf{U}^-_i\right), \\
&\mathcal{E}\left([X]_{N(\omega)}\right)\mathbf{F}^{\ell ag}\left(\mathbf{U}^+_i,\mathbf{U}^-_{i+1}\right)
\end{aligned}$$

are evaluated by a close examination of each possible case.

In the case of $\mathcal{E}\left(X\left(x_{i\pm\frac{1}{2}},t^+\right)\mathbf{F}\left(\mathbf{U}^\star_{i+\frac{1}{2}}\right)\right)$, and specialising on the right interface of the cell $\mathcal{C}_i$, four cases may happen:

- either fluid Σ_1 is on the left and fluid Σ_1 is on the right
- or fluid Σ_1 is on the left and fluid Σ_2 is on the right
- or fluid Σ_2 is on the left and fluid Σ_2 is on the right
- or fluid Σ_2 is on the left and fluid Σ_1 is on the right.

Depending on which case occurs, we may or may not take into account the fluxes. Four fluxes are evaluated (and summarised in table 3.1); they are flagged when needed following the procedure we describe now. Of course, a similar situation happens on the left interface. Then if we define

[2] In the multidimensional case, more than one relaxation parameter can be introduced. Typically, the same arguments show that there is one relaxation parameter associated to the pressure, and two for the velocity in 2D, three in 3D. These relaxation parameters depend on thermodynamical parameters, such as the acoustic impedance, but also on the inter-facial area between the faces. More details can be found in [1].

Table 3.1: Flux indicator for the Eulerian Flux where we denote $\beta_{i+\frac{1}{2}}^{(l,p)} = \text{sign}\left(\sigma\left(U_i^l, U_{i+1}^p\right)\right)$

flow patterns	left and right states	flux indicator
$\Sigma_1 - \Sigma_2$	$U_i^{(1)}, U_{i+1}^{(2)}$	$\left(\beta_{i+\frac{1}{2}}^{(1,2)}\right)^+$
$\Sigma_1 - \Sigma_1$	$U_i^{(1)}, U_{i+1}^{(1)}$	1
$\Sigma_2 - \Sigma_1$	$U_i^{(2)}, U_{i+1}^{(1)}$	$\left(-\beta_{i+\frac{1}{2}}^{(2,1)}\right)^+$
$\Sigma_2 - \Sigma_2$	$U_i^{(2)}, U_{i+1}^{(2)}$	0

$$\mathcal{P}_{i+\frac{1}{2}}\left(\Sigma_1, \Sigma_1\right) = \mathcal{P}\left(X\left(x_{i+\frac{1}{2}}^-\right) = 1 \text{ and } X\left(x_{i+\frac{1}{2}}^+\right) = 1\right)$$

$$\mathcal{P}_{i+\frac{1}{2}}\left(\Sigma_2, \Sigma_2\right) = \mathcal{P}\left(X\left(x_{i+\frac{1}{2}}^-\right) = 0 \text{ and } X\left(x_{i+\frac{1}{2}}^+\right) = 0\right)$$

$$\mathcal{P}_{i+\frac{1}{2}}\left(\Sigma_1, \Sigma_2\right) = \mathcal{P}\left(X\left(x_{i+\frac{1}{2}}^-\right) = 1 \text{ and } X\left(x_{i+\frac{1}{2}}^+\right) = 0\right)$$

$$\mathcal{P}_{i+\frac{1}{2}}\left(\Sigma_2, \Sigma_1\right) = \mathcal{P}\left(X\left(x_{i+\frac{1}{2}}^-\right) = 0 \text{ and } X\left(x_{i+\frac{1}{2}}^+\right) = 1\right)$$

we get

$$\begin{aligned}\mathcal{E}\left(X\left(x_{i+\frac{1}{2}}, t_n^+\right)\mathbf{F}\left(U_{i+\frac{1}{2}}^\star\right)\right) = {} & \mathcal{P}_{i+\frac{1}{2}}\left(\Sigma_1, \Sigma_1\right)\mathbf{F}\left(\mathbf{U}_i^{(1)}, \mathbf{U}_{i+1}^{(1)}\right) \\ & + \mathcal{P}_{i+\frac{1}{2}}\left(\Sigma_1, \Sigma_2\right)\left(\beta_{i+\frac{1}{2}}^{(1,2)}\right)^+ \mathbf{F}\left(\mathbf{U}_i^{(1)}, \mathbf{U}_{i+1}^{(2)}\right) \\ & + \mathcal{P}_{i+\frac{1}{2}}\left(\Sigma_2, \Sigma_1\right)\left(-\beta_{i+\frac{1}{2}}^{(2,1)}\right)^+ \mathbf{F}\left(\mathbf{U}_i^{(2)}, \mathbf{U}_{i+1}^{(1)}\right)\end{aligned}$$

Similarly, in the case of the Lagrangian term of the right interface, the four cases are summarised in the table 3.2, a similar situation occurs at the left interface. We get for the right interface

$$\begin{aligned}\mathcal{E}\left(\left[X\right]_{N(\omega)}\right)\mathbf{F}^{\ell ag}\left(\mathbf{U}_i^{N(\omega)}, \mathbf{U}_{i+1}^-\right) = {} & \mathcal{P}_{i+\frac{1}{2}}\left(\Sigma_1, \Sigma_2\right)\left(\beta_{i+\frac{1}{2}}^{(1,2)}\right)^- \mathbf{F}^{\ell ag}\left(\mathbf{U}_i^{(1)}, \mathbf{U}_{i+1}^{(2)}\right) \\ & - \mathcal{P}_{i+\frac{1}{2}}\left(\Sigma_2, \Sigma_1\right)\left(\beta_{i+\frac{1}{2}}^{(2,1)}\right)^- \mathbf{F}^{\ell ag}\left(\mathbf{U}_i^{(2)}, \mathbf{U}_{i+1}^{(1)}\right)\end{aligned}$$

and for the left one

$$\begin{aligned}\mathcal{E}\left(\left[X\right]_0\right)\mathbf{F}^{\ell ag}\left(\mathbf{U}_{i-1}^+, \mathbf{U}_i^0\right) = {} & -\mathcal{P}_{i-\frac{1}{2}}\left(\Sigma_1, \Sigma_2\right)\left(\beta_{i-\frac{1}{2}}^{(1,2)}\right)^+ \mathbf{F}^{\ell ag}\left(\mathbf{U}_i^{(1)}, \mathbf{U}_{i+1}^{(2)}\right) \\ & + \mathcal{P}_{i-\frac{1}{2}}\left(\Sigma_2, \Sigma_1\right)\left(\beta_{i-\frac{1}{2}}^{(2,1)}\right)^+ \mathbf{F}^{\ell ag}\left(\mathbf{U}_{i-1}^{(2)}, \mathbf{U}_i^{(1)}\right)\end{aligned}$$

Table 3.2: Flux indicator for the Lagrangian Flux where we denote $\beta_{i+\frac{1}{2}}^{(l,p)} = \text{sign}\left(\sigma\left(U_i^l, U_{i+1}^p\right)\right)$

flow patterns	Lagrangian flux	flux indicator
$\Sigma_1 - \Sigma_2$	$F^{\ell ag}\left(U_i^{(1)}, U_{i+1}^{(2)}\right)$	$\left(\beta_{i+\frac{1}{2}}^{(1,2)}\right)^-$
$\Sigma_1 - \Sigma_1$	$F^{\ell ag}\left(U_i^{(1)}, U_{i+1}^{(1)}\right)$	0
$\Sigma_2 - \Sigma_1$	$F^{\ell ag}\left(U_i^{(2)}, U_{i+1}^{(1)}\right)$	$-\left(-\beta_{i+\frac{1}{2}}^{(2,1)}\right)^-$
$\Sigma_2 - \Sigma_2$	$F^{\ell ag}\left(U_i^{(2)}, U_{i+1}^{(2)}\right)$	0

These expressions are given for the phase Σ_1. Similar expressions can be given for Σ_2 : the variable X is changed into $1 - X$, the phase index for Σ_1 (resp. Σ_2) is changed into the one for Σ_2 (resp. Σ_1).

3.1.2 A numerical scheme

As detailed in [2], a natural choice for the probability is

$$\begin{aligned}
\mathcal{P}_{i+\frac{1}{2}}\left(\Sigma_1, \Sigma_1\right) &= \min\left(\alpha_i^{(1)}, \alpha_{i+1}^{(1)}\right) \\
\mathcal{P}_{i+\frac{1}{2}}\left(\Sigma_2, \Sigma_2\right) &= \min\left(\alpha_i^{(2)}, \alpha_{i+1}^{(2)}\right) \\
\mathcal{P}_{i+\frac{1}{2}}\left(\Sigma_1, \Sigma_2\right) &= \max\left(\alpha_i^{(1)} - \alpha_{i+1}^{(1)}, 0\right) \\
\mathcal{P}_{i+\frac{1}{2}}\left(\Sigma_2, \Sigma_1\right) &= \max\left(\alpha_i^{(2)} - \alpha_{i+1}^{(2)}, 0\right)
\end{aligned}$$

This leads to the following numerical scheme

$$\begin{aligned}
&\frac{\partial\left(\alpha^{(1)}\mathbf{U}^{(1)}\right)}{\partial t} + \frac{\mathcal{E}\left(X\mathbf{F}\right)_{i+\frac{1}{2}} - \mathcal{E}\left(X\mathbf{F}\right)_{i-\frac{1}{2}}}{\Delta x} \\
&\qquad = \frac{1}{\Delta x}\mathcal{E}\left(\mathbf{F}^{\ell ag}\frac{\partial X}{\partial x}\right)_{i,\text{bound}} + \mathcal{E}\left(\mathbf{F}^{\ell ag}\frac{\partial X}{\partial x}\right)_{i,\text{relax}}
\end{aligned} \tag{3.9}$$

with

$$\begin{aligned}
\mathcal{E}\left(X\mathbf{F}\right)_{i+\frac{1}{2}} =& \max\left(\alpha_i^{(1)} - \alpha_{i+1}^{(1)}, 0\right)\left(\beta_{i+\frac{1}{2}}^{(1,2)}\right)^+ \mathbf{F}\left(\mathbf{U}_i^{(1)}, \mathbf{U}_{i+1}^{(2)}\right) \\
&+ \min\left(\alpha_i^{(1)}, \alpha_{i+1}^{(1)}\right)\mathbf{F}\left(\mathbf{U}_i^{(1)}, \mathbf{U}_{i+1}^{(1)}\right) \\
&- \max\left(\alpha_i^{(2)} - \alpha_{i+1}^{(2)}, 0\right)\left(\beta_{i+\frac{1}{2}}^{(2,1)}\right)^- \mathbf{F}\left(\mathbf{U}_i^{(2)}, \mathbf{U}_{i+1}^{(1)}\right),
\end{aligned}$$

$$\begin{aligned}\mathcal{E}\left(\mathbf{F}^{\ell ag}\frac{\partial X}{\partial x}\right)_{i,\text{bound}} =& \max\left(\alpha_i^{(1)}-\alpha_{i+1}^{(1)},0\right)\left(\beta_{i+\frac{1}{2}}^{(1,2)}\right)^{-}\mathbf{F}^{\ell ag}\left(\mathbf{U}_i^{(1)},\mathbf{U}_{i+1}^{(2)}\right)\\ &-\max\left(\alpha_i^{(2)}-\alpha_{i+1}^{(2)},0\right)\left(\beta_{i+\frac{1}{2}}^{(2,1)}\right)^{-}\mathbf{F}^{\ell ag}\left(\mathbf{U}_i^{(2)},\mathbf{U}_{i+1}^{(1)}\right)\\ &-\max\left(\alpha_{i-1}^{(1)}-\alpha_i^{(1)},0\right)\left(\beta_{i-\frac{1}{2}}^{(1,2)}\right)^{+}\mathbf{F}^{\ell ag}\left(\mathbf{U}_{i-1}^{(1)},\mathbf{U}_i^{(2)}\right)\\ &+\max\left(\alpha_{i-1}^{(2)}-\alpha_i^{(2)},0\right)\left(\beta_{i-\frac{1}{2}}^{(2,1)}\right)^{+}\mathbf{F}^{\ell ag}\left(\mathbf{U}_{i-1}^{(2)},\mathbf{U}_i^{(1)}\right)\end{aligned}$$

and

$$\mathcal{E}\left(\mathbf{F}^{\ell ag}\frac{\partial X}{\partial x}\right)_{i,\text{relax}} = \lambda_i\left(\mathbf{F}^{\ell ag}\left(\mathbf{U}_i^{(2)},\mathbf{U}_i^{(1)}\right)-\mathbf{F}^{\ell ag}\left(\mathbf{U}_i^{(1)},\mathbf{U}_i^{(2)}\right)\right)$$

Setting $F=0$ and $U=1$ leads to the following numerical semi–discrete scheme for the volume fraction

$$\begin{aligned}\frac{\mathrm{d}\alpha_i^{(1)}}{\mathrm{d}t} =& \frac{1}{\Delta x}\Bigg[\max\left(\alpha_i^{(1)}-\alpha_{i+1}^{(1)},0\right)\left(\beta_{i+\frac{1}{2}}^{(1,2)}\right)^{-}u^{\star}\left(\mathbf{U}_i^{(1)},\mathbf{U}_{i+1}^{(2)}\right)\\ &-\max\left(\alpha_i^{(2)}-\alpha_{i+1}^{(2)},0\right)\left(\beta_{i+\frac{1}{2}}^{(2,1)}\right)^{-}u^{\star}\left(\mathbf{U}_i^{(2)},\mathbf{U}_{i+1}^{(1)}\right)\\ &-\max\left(\alpha_{i-1}^{(1)}-\alpha_i^{(1)},0\right)\left(\beta_{i-\frac{1}{2}}^{(1,2)}\right)^{+}u^{\star}\left(\mathbf{U}_{i-1}^{(1)},\mathbf{U}_i^{(2)}\right)\\ &+\max\left(\alpha_{i-1}^{(2)}-\alpha_i^{(2)},0\right)\left(\beta_{i-\frac{1}{2}}^{(2,1)}\right)^{+}u^{\star}\left(\mathbf{U}_{i-1}^{(2)},\mathbf{U}_i^{(1)}\right)\Bigg]\\ &+\lambda_i\left\{u^{\star}\left(\mathbf{U}_i^{(2)},\mathbf{U}_i^{(1)}\right)-u^{\star}\left(\mathbf{U}_i^{(1)},\mathbf{U}_i^{(2)}\right)\right\}\end{aligned} \tag{3.10}$$

In practical applications, the discretisation is achieved via a splitting method. First we integrate (with some abuse of notation [3])

$$\frac{\left(W_i^{(1)}\right)^{n+1/2}-\left(W_i^{(1)}\right)^{n}}{\Delta t}+\frac{\mathscr{E}\left(XF\right)_{i+1/2}-\mathscr{E}\left(XF\right)_{i-1/2}}{\Delta x}=\frac{\mathscr{E}\left(F^{\ell ag}\frac{\partial X}{\partial x}\right)_{i,\text{bound}}}{\Delta x} \tag{3.11}$$

and then a relaxation step

$$\frac{\left(W_i^{(1)}\right)^{n+1}-\left(W_i^{(1)}\right)^{n+1/2}}{\Delta t}=\mathscr{E}\left(F^{\ell ag}\frac{\partial X}{\partial x}\right)_{i,\text{relax}} \tag{3.12}$$

The flux are computed at time t_n. The relaxation step is carried out implicitly.

[3] because (3.10) is not written as a difference of flux plus a relaxation term

3.1.3 Extension to second order

The scheme (3.11)–(3.12) makes use of several terms (the conservative terms, the boundary terms and the relaxation terms) that do not play the same role in the derivation. The "conservative" terms are standard, so that any standard high order extension will do. The "relaxation" and "boundary" terms have the same status : they are agglomeration of fluxes between different phases for which the high order procedure is not immediate.

In order to construct a high order extension of the scheme (3.11)–(3.12), the procedure described in [2] is considered :

1. We extrapolate the physical variables $(\alpha^{(\ell)}, u^{(\ell)}, P^{(\ell)})$, $\ell = 1, 2$ using the MUSCL method. Here, the minmod or van Leer–van Albada limiters are used.

2. We subdivide the cell $\mathcal{C}_i$ into N regular sub-cells (N arbitrary) denoted by $[y_l, y_{l+1}]$ $(1 \leq l \leq N-1)$ and average in each sub–cell the reconstructed variables,

3. Each sub-cell is randomly subdivided as above,

4. Then, we gather the contribution of each sub–sub-cell and let $N \to +\infty$.

In the following, $U^{(\ell)}_{i+1/2,l}$ (resp. $U^{(\ell)}_{i-1/2,r}$) represents the variable $U^{(\ell)}$ at the cell interface $x_{i+1/2}$ (resp. $x_{i-1/2}$) on the left (resp right) after MUSCL extrapolation. If f is any of the extrapolated variables, $\delta_i f$ represents its limited slope in $\mathcal{C}_i$. The jump in $\alpha^{(\ell)}$ at $y_{l+1/2}$ is $\Delta\alpha^{(\ell)}(y_{l+1/2})$.

The non conservative terms

$$\mathscr{E}\left(F^{\ell ag}\frac{\partial X}{\partial x}\right)_i = \mathscr{E}\left(F^{\ell ag}\frac{\partial X}{\partial x}\right)_{i,bound} + \mathscr{E}\left(F^{\ell ag}\frac{\partial X}{\partial x}\right)_{i,relax}$$

sum up to

$$
\begin{aligned}
&-\big(\beta^{(1,2)}_{i+1/2}\big)^{+}\mathcal{P}_{i+1/2}(\Sigma_1,\Sigma_2)\mathbf{F}^{\ell ag}(\mathbf{U}^{(1)}_{i+1/2,l},\mathbf{U}^{(2)}_{i+1/2,r})\\
&\qquad\qquad+\big(\beta^{(2,1)}_{i+1/2}\big)^{+}\mathcal{P}_{i+1/2}(\Sigma_2,\Sigma_1)\mathbf{F}^{\ell ag}(\mathbf{U}^{(2)}_{i+1/2,l},\mathbf{U}^{(1)}_{i+1/2,r})\\
&-\big(\beta^{(1,2)}_{i-1/2}\big)^{-}\mathcal{P}_{i-1/2}(\Sigma_1,\Sigma_2)\mathbf{F}^{\ell ag}(\mathbf{U}^{(1)}_{i-1/2,l},\mathbf{U}^{(2)}_{i-1/2,r})\\
&\qquad\qquad+\big(\beta^{(2,1)}_{i-1/2}\big)^{-}\mathcal{P}_{i-1/2}(\Sigma_2,\Sigma_1)\mathbf{F}^{\ell ag}(\mathbf{U}^{(2)}_{i-1/2,l},\mathbf{U}^{(1)}_{i-1/2,r})\\
&+\sum_{l=1}^{N-1}\max\Big(0,\Delta\alpha^{(1)}(y_{l+1/2})\Big)\mathbf{F}^{\ell ag}(\mathbf{U}^{(2)}_2(y_{l+1/2}),\mathbf{U}^{(1)}_1(y_{l+1/2}))\\
&-\sum_{l=1}^{N-1}\max\Big(0,\Delta\alpha^{(2)}(y_{l+1/2}))\Big)\mathbf{F}^{\ell ag}(\mathbf{U}^{(2)}_2(y_{l+1/2}),\mathbf{U}^{(1)}_1(y_{l+1/2}))\\
&+\sum_{l=1}^{N-1}\lambda(y_{l+1/2})\Big(\mathbf{F}^{\ell ag}(\mathbf{U}^{(2)}_2(y_{l+1/2}),\mathbf{U}^{(1)}_1(y_{l+1/2}))\\
&\qquad\qquad-\sum_{l=1}^{N-1}\mathbf{F}^{\ell ag}(\mathbf{U}^{(1)}_1(y_{l+1/2}),\mathbf{U}^{(2)}_2(y_{l+1/2}))\Big)
\end{aligned}
\tag{3.13}
$$

where

$$\Delta\alpha^{(1)}(y_{l+1/2})=\big(\delta_i\alpha^{(1)}\big)(y_{l+1}-y_l).$$

We do not need any additional β terms because we account for all the internal cells in $]x_{i-1/2},x_{i+1/2}[$.

The third and fourth terms of the above formula converge, when $N\to+\infty$, to

$$
\begin{aligned}
&\Big(\int_{x_{i-1/2}}^{x_{i+1/2}}\mathbf{F}^{\ell ag}(\mathbf{U}^{(2)}(y),\mathbf{U}^{(1)}(y))dy\Big)\max\Big(0,\delta_i\alpha^{(1)}\Big)\\
&\qquad\qquad-\\
&\Big(\int_{x_{i-1/2}}^{x_{i+1/2}}\mathbf{F}^{\ell ag}(\mathbf{U}^{(1)}(y),\mathbf{U}^{(2)}(y))dy\Big)\max\Big(0,\delta_i\alpha^{(2)}\Big).
\end{aligned}
\tag{3.14}
$$

A similar formula is obtained for the phase Σ_2. The integrals in (3.14) are evaluated via the mid point formula (since second order accuracy is sought for).

Similarly, the relaxation terms corresponding to a linear reconstruction of the data can be approximated, thanks to the same interpretation in terms of Riemann sums and to the mid point rule by

$$\lambda_i\ \Big(\mathbf{F}^{\ell ag}(\mathbf{U}^{(2)}_i,\mathbf{U}^{(1)}_i)-\mathbf{F}^{\ell ag}(\mathbf{U}^{(1)}_i,\mathbf{U}^{(2)}_i)\Big)\,. \tag{3.15}$$

We finally obtain a second order approximation of the non conservative terms by

$$
\begin{aligned}
\Delta x \, \mathscr{E}\left(\mathbf{F}^{\ell ag}\frac{\partial X}{\partial x}\right) = & -\left(\beta^{(1,2)}_{i+1/2}\right)^{+}\mathcal{P}_{i+1/2}(\Sigma_1,\Sigma_2)\mathbf{F}^{\ell ag}(\mathbf{U}^{(1)}_{i+1/2,l},\mathbf{U}^{(2)}_{i+1/2,r}) \\
& +\left(\beta^{(2,1)}_{i+1/2}\right)^{+}\mathcal{P}_{i+1/2}(\Sigma_2,\Sigma_1)\mathbf{F}^{\ell ag}(\mathbf{U}^{(2)}_{i+1/2,l},\mathbf{U}^{(1)}_{i+1/2,r}) \\
& -\left(\beta^{(1,2)}_{i-1/2}\right)^{-}\mathcal{P}_{i-1/2}(\Sigma_1,\Sigma_2)\mathbf{F}^{\ell ag}(\mathbf{U}^{(1)}_{i-1/2,l},\mathbf{U}^{(2)}_{i-1/2,r}) \\
& +\left(\beta^{(2,1)}_{i-1/2}\right)^{-}\mathcal{P}_{i-1/2}(\Sigma_2,\Sigma_1)\mathbf{F}^{\ell ag}(\mathbf{U}^{(2)}_{i-1/2,l},\mathbf{U}^{(1)}_{i-1/2,r}) \\
& +\lambda_i\ \left(\mathbf{F}^{\ell ag}(\mathbf{U}^{(2)}_i,\mathbf{U}^{(1)}_i)-\mathbf{F}^{\ell ag}(\mathbf{U}^{(1)}_i,\mathbf{U}^{(2)}_i)\right) \\
& +\max\left(0,\delta\alpha^{(1)}_i\right)\mathbf{F}^{\ell ag}(\mathbf{U}^{(2)}_i,\mathbf{U}^{(1)}_i) \\
& -\max\left(0,\delta\alpha^{(2)}_i\right)\mathbf{F}^{\ell ag}(\mathbf{U}^{(1)}_i,\mathbf{U}^{(2)}_i)
\end{aligned}
\tag{3.16}
$$

where $\delta\alpha^{(1)}_i = \alpha^{(1)}_{i+1/2,l} - \alpha^{(1)}_{i-1/2,r}$ and $\delta\alpha^{(2)}_i = \alpha^{(2)}_{i+1/2,l} - \alpha^{(2)}_{i-1/2,r}$ are the limited slope of $\alpha^{(1)}$ and $\alpha^{(2)}$ in the cell C_i.

Hence, the second order extension of the scheme can be geometrically interpreted by adding an additional interface inside the cell $\mathcal{C}_i$, this is the meaning of last two terms of (3.16).

3.1.4 Extension to other solvers

In (3.9), the numerical flux F that we use at the microscopic level is obtained thanks to an approximate Riemann solver for which it is possible to define a contact speed. The contact speed between the left state U_L and the right state U_R is denoted by $\sigma(U_L,U_R)$. We also denote by $U^{\pm}_{LR}$ the left and right states surrounding the approximate contact discontinuity, similarly as in Figure 3.2 for the Godunov solver. This permits to define the Lagrangian flux $F^{\ell ag}(U_L,U_R) = F(U^{+}_{LR}) - \sigma(U_L,U_R)U^{+}_{LR} = F(U^{-}_{LR}) - \sigma(U_L,U_R)U^{-}_{LR}$. Last, we define $\beta^{(p,q)}_{i+1/2} = \text{sign}(\sigma(U^{(p)}_i,U^{(q)}_{i+1}))$.

All the calculations have been performed for the Godunov scheme, but can be extended to more general fluxes The key ingredient of the derivation are, besides the randomisation, average procedures and estimation of the various coefficients, the use of a Riemann solver for which it is possible to define a contact discontinuity speed $\sigma(U,V)$. This property is needed because we must define a Lagrangian flux, $F^{\ell ag}(U,V) = F(U,V) - \sigma(U,V)U^{\star}$. This Lagrangian flux has to be consistent, as well as the base flux $F(U,V)$.

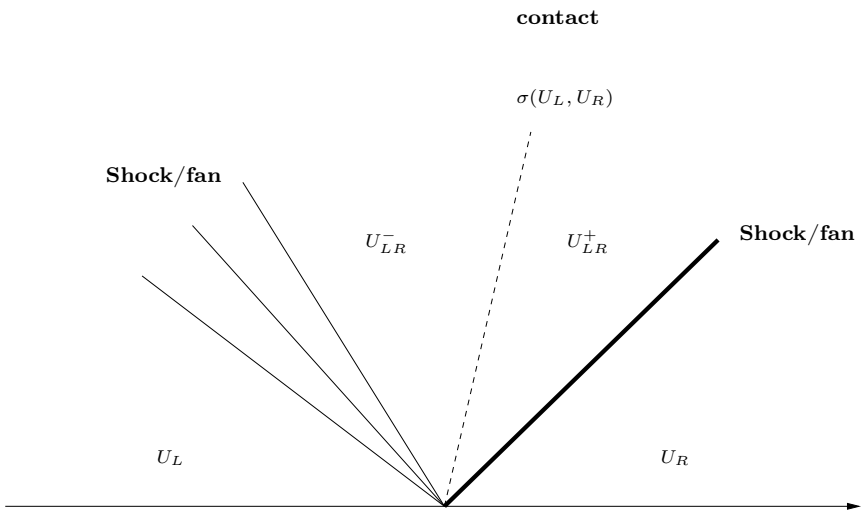

Figure 3.2: Structure of the Riemann problem.

Even more, the choice of the base flux F and the Lagrangian flux $F^{\ell ag}$ may be independent : we do not really need a relation of the type $F^{\ell ag} = F^* - \sigma U^\star$, see [2] for more details.

3.2 Asymptotic model for the numerical scheme

To get the numerical scheme for the five equations model (3.2), we propose to follow a similar technique as in [44], where the continuous model was derived via an asymptotic expansion of (3.1). The very difference is that we will do it at a *discrete* level. If we set $\varepsilon_i = \frac{1}{\lambda_i}$, the discrete scheme for the seven equations model can be formally rewritten as

$$\frac{\partial W}{\partial t} + \frac{G}{\Delta x} = \frac{R(W)}{\varepsilon_i} \tag{3.17}$$

and we assume that ε_i is large.

The first step to get the asymptotic scheme is to determine the equilibrium set

$$\{W \text{ such that } R(W) = 0\}.$$

From the previous section, this set is defined as

$$\begin{aligned} \mathcal{V} = \big\{ W = (\alpha^{(1)}, \alpha^{(1)}\mathbf{U}^{(1)}, \alpha^{(2)}, \alpha^{(2)}\mathbf{U}^{(2)}) \\ \text{such that } F^{\ell ag}(W_1, W_2) = F^{\ell ag}(W_2, W_1) \big\} \end{aligned} \tag{3.18}$$

Then, as proved in Chapter 2 the limit model is obtained by developing the variables around the equilibrium set. We assume that $\mathcal{V}$ can be parameterised by a mapping $M : \mathbf{u} \mapsto M(\mathbf{u})$ (we prove this fact later), and that $R(W)$ has an expansion of the form

$$R(W) = R(M(u)) + \varepsilon R'(M(u))V + o(\varepsilon).$$

Thus equation (3.17) becomes

$$\mathrm{d}M_{\mathbf{u}} \frac{\partial u}{\partial t} + \frac{G}{\Delta x} = R'(M(\mathbf{u}))V + o(1).$$

To get the reduced model, it remains to multiply by the projection P onto the kernel of $R'(M(\mathbf{u}))$ in the direction of $\mathrm{d}M_{\mathbf{u}},$. This gives the model

$$P\ \mathrm{d}M_{\mathbf{u}} \frac{\partial u}{\partial t} + P\ \frac{G}{\Delta x} = 0. \tag{3.19}$$

The aim of this section is to show that for several classical solvers, P does not depend on the solver. We have to prove two properties :

1. $\mathcal{V}$ is equal to

$$\{(\alpha^{(1)}, \alpha^{(1)}\mathbf{U}^{(1)}, \alpha^{(2)}, \alpha^{(2)}\mathbf{U}^{(2)}) \text{ such that } u_1 = u_2 \ \text{ and } \ P_1 = P_2\} \tag{3.20}$$

   as in the continuous case.

2. The Jacobian matrix of $F^{\ell ag}(\mathbf{U}^{(1)}, \mathbf{U}^{(2)}) - F^{\ell ag}(\mathbf{U}^{(2)}, \mathbf{U}^{(1)})$ in primitive variables is

$$\mathrm{D}R(M(u)) = \begin{pmatrix} 0 & 0 & 0 & -\lambda' & 0 & 0 & 0 & \lambda' \\ 0 & 0 & 0 & 0 & 0 & 0 & 0 & 0 \\ 0 & 0 & \mu' & 0 & 0 & 0 & -\mu' & 0 \\ 0 & 0 & \mu' u & \lambda' P & 0 & 0 & -\mu' u & -\lambda' P \\ 0 & 0 & 0 & \lambda' & 0 & 0 & 0 & -\lambda' \\ 0 & 0 & 0 & 0 & 0 & 0 & 0 & 0 \\ 0 & 0 & -\mu' & 0 & 0 & 0 & \mu' & 0 \\ 0 & 0 & -\mu' u & -\lambda' P & 0 & 0 & \mu' u & \lambda' P \end{pmatrix} \tag{3.21}$$

   as in the continuous case.

In the following, we denote by a subscript 12 (resp. 21) the intermediate states obtained by solving an elementary Riemann problem *before averaging* with left and right states given by the phase Σ_1 (resp. Σ_2) on the left and Σ_2 (resp. Σ_1) on the right.

3.2.1 Case of the acoustic solver

Given two states, left and right, described by the physical variables, ρ_L, u_L, P_L for the left state and ρ_R,u_R,P_R for the right state, the Lagrangian flux for the acoustic solver is defined as $(0, P^\star, P^\star u^\star)$ with the pressure and the velocity of the intermediate state($\star$) are given by (see e.g. [52]):

$$\begin{aligned} P^\star &= \frac{Z_R P_L + Z_L P_R + Z_L Z_R \left(u_L - u_R\right)}{Z_R + Z_L} \\ u^\star &= \frac{Z_R u_R + Z_L u_L + P_L - P_R}{Z_R + Z_L}. \end{aligned} \tag{3.22}$$

In (3.22), $Z_{L,R} = \rho_{L,R} c_{L,R}$ is the acoustic impedance. Therefore, using the above mentioned conventions, and using the fact that within the cell we consider, the left/right states are defined from the conservative variables $U^{(1)}$ for Σ_1 and $U^{(2)}$ for Σ_2, we have

$$P_{12}^\star = \frac{Z_1 P_1 + Z_2 P_2 + Z_1 Z_2 \left(u_2 - u_1\right)}{Z_2 + Z_1} \quad P_{21}^\star = \frac{Z_1 P_1 + Z_2 P_2 + Z_1 Z_2 \left(u_1 - u_2\right)}{Z_1 + Z_2}$$

$$u_{12}^\star = \frac{Z_1 u_1 + Z_2 u_2 + P_2 - P_1}{Z_1 + Z_2} \qquad u_{21}^\star = \frac{Z_1 u_1 + Z_2 u_2 + P_1 - P_2}{Z_1 + Z_2}$$

so that

$$u_{12}^\star - u_{21}^\star = \frac{2}{Z_1 + Z_2} \left(P_1 - P_2\right)$$

$$P_{12}^\star - P_{21}^\star = \frac{2 Z_1 Z_2}{Z_1 + Z_2} \left(u_1 - u_2\right)$$

We immediately see that if $u_{12}^\star - u_{21}^\star = 0$ and $P_{12}^\star - P_{21}^\star = 0$, we have $u_1 = u_2$ and $P_1 = P_2$.

Let us evaluate now the Jacobian matrix of $\mathbf{F}^{\ell ag}(U^{(1)}, U^{(2)}) - \mathbf{F}^{\ell ag}(U^{(2)}, U^{(1)})$ with respect to the primitive variable on $\mathcal{V}$. We have

$$\mathbf{F}^{\ell ag}(U^{(1)}, U^{(2)}) - \mathbf{F}^{\ell ag}(U^{(2)}, U^{(1)}) = (0, P_{12}^\star - P_{21}^\star, P_{12}^\star u_{12}^\star - P_{21}^\star u_{21}^\star)$$

and we have to evaluate the partial derivative of this vector with respect to $v = \rho$, u and P. Using the fact that the considered state lies in $\mathcal{V}$, a straightforward calculation gives (with $u = u_1 = u_2$ and $P = P_1 = P_2$)

$$\frac{\partial \left(P_{12}^\star - P_{21}^\star\right)}{\partial v} = \frac{2}{Z_1 + Z_2} \left(\frac{\partial P_1}{\partial v} - \frac{\partial P_2}{\partial v} \right)$$

$$\begin{aligned} \frac{\partial \left(P_{12}^\star u_{12}^\star - P_{21}^\star u_{21}^\star\right)}{\partial v} = {} & \frac{2 Z_1 Z_2}{Z_1 + Z_2} \, u \left(\frac{\partial P_1}{\partial v} - \frac{\partial P_2}{\partial v} \right) \\ & + \frac{2}{Z_1 + Z_2} \, P \left(\frac{\partial u_1}{\partial v} - \frac{\partial u_2}{\partial v} \right) \end{aligned}$$

so that we get (3.21) with

$$\lambda = \frac{2}{Z_1 + Z_2} \qquad \text{and} \qquad \mu = \frac{2Z_1Z_2}{Z_1 + Z_2}$$

.

3.2.2 Case of the exact solver

For the exact solver, the Lagrangian flux can be written as $(0, P^\star, P^\star u^\star)$, where $P^\star$ and $u^\star$ are the intermediate velocity and pressure when the Riemann problem is solved exactly. The equation (3.20) can be rewritten as

$$(0, P^\star_{12}, P^\star_{12}u^\star_{12}) = (0, P^\star_{21}, P^\star_{21}u^\star_{21})$$

so that

$$u^\star = u^\star_{21} = u^\star_{12} \text{ and } P^\star = P^\star_{21} = P^\star_{12}.$$

Thus in the (u, P) variables, the point $(u^\star, P^\star)$ lies on the 1–wave curve coming from the state (u_1, P_1) and on the 3–wave curve coming from the state (u_1, P_1). Therefore $u^\star = u_1$ and $P^\star = P_1$, because the 1–wave curve is decreasing and the 3–wave curve is increasing : this is a consequence of the convexity of the equation of state [42], page 89. The same argument holds for the state 2, so that $u^\star = u_2$ and $P^\star = P_2$ so that $u_1 = u_2$ and $P_1 = P_2$.

Now we estimate the Jacobian matrix. Indeed, we find exactly the same Jacobian matrix as for the acoustic solver because the relations (3.22) are obtained by a linearization in the (u, P) variables of the true Riemann invariants at $(u = u_1 = u_2, P = P_1 = P_2)$.

3.2.3 Case of the HLLC solver

The HLLC solver is based on the choice of two wave velocities S^L and S^R. The intermediate states are calculated by writing the Rankine-Hugoniot relations across these waves, see [62] pp. 293 for more details. With this solver, the intermediates states are given by

$$\mathbf{U}^\star_K = \rho_K \frac{S^K - u_K}{S^K - u^\star} \begin{pmatrix} 1 \\ u^\star \\ E_K + (u^\star - u_K)\left(u^\star + \dfrac{P_K}{\rho_K\,(S^K - u_K)}\right) \end{pmatrix}$$

with $K = L$ or R. The Lagrangian flux is then

$$\mathbf{F}^{\ell ag} = \begin{pmatrix} 0 \\ \rho_K\,(u^\star - u_K)\left(S^L - u_L\right) + P_L \\ \left(\rho_K\,(u^\star - u_K)\left(S^L - u_L\right) + P_L\right) u^\star \end{pmatrix}$$

Thus $\mathbf{F}_{12}^{\ell ag}$ and $\mathbf{F}_{21}^{\ell ag}$ are given by the following expressions

$$\mathbf{F}_{12}^{\ell ag} = \begin{pmatrix} 0 \\ \rho_1 \left(u_{12}^\star - u_1\right)\left(S_{12}^L - u_1\right) + P_1 \\ \left(\rho_1 \left(u_{12}^\star - u_1\right)\left(S_{12}^L - u_1\right) + P_1\right) u_{12}^\star \end{pmatrix} \tag{3.23a}$$

$$= \begin{pmatrix} 0 \\ \rho_2 \left(u_{12}^\star - u_2\right)\left(S_{12}^R - u_2\right) + P_2 \\ \left(\rho_2 \left(u_{12}^\star - u_2\right)\left(S_{12}^R - u_2\right) + P_2\right) u_{12}^\star \end{pmatrix} \tag{3.23b}$$

$$\mathbf{F}_{21}^{\ell ag} = \begin{pmatrix} 0 \\ \rho_1 \left(u_{21}^\star - u_1\right)\left(S_{21}^R - u_1\right) + P_1 \\ \left(\rho_1 \left(u_{21}^\star - u_1\right)\left(S_{21}^R - u_1\right) + P_1\right) u_{21}^\star \end{pmatrix} \tag{3.23c}$$

$$= \begin{pmatrix} 0 \\ \rho_2 \left(u_{21}^\star - u_2\right)\left(S_{21}^L - u_2\right) + P_2 \\ \left(\rho_2 \left(u_{21}^\star - u_2\right)\left(S_{21}^L - u_2\right) + P_2\right) u_{21}^\star \end{pmatrix} \tag{3.23d}$$

The intermediate velocity is given by

$$u^\star = \frac{P_R - P_L + \rho_L u_L (S^L - u_L) - \rho_R u_R (S^R - u_R)}{\rho_L (S^L - u_L) - \rho_R (S^R - u_R)} \tag{3.24}$$

For more convenience, we denote by

$$\begin{cases} Z^L = \rho_L (u_L - S^L) \\ Z^R = \rho_R (S^R - u_R) \end{cases}$$

Then (3.24) becomes

$$u^\star = \frac{P_L - P_R + Z^R u_R + Z^L u_L}{Z^R + Z^L}.$$

Here, we have used the same notation convention as in subsection 3.2.1 for the velocity and pressure. The subscripts 1 and 2 in Z are intended to highlight the fact that the definition of Z depends on the left and right state through ρ and u, but also on the ordering of the waves through the speed S. For example, Z_1^{12} is evaluated with $U^{(1)}$ on the left, $U^{(2)}$ on the right and

corresponds to the most left wave S. Thus we have

$$\begin{aligned} u^\star_{12} - u^\star_{21} &= \frac{P_2 - P_1 + Z_1^{21}u_1 + Z_2^{21}u_2}{Z_1^{21} + Z_2^{21}} - \frac{P_1 - P_2 + Z_1^{12}u_1 + Z_2^{12}u_2}{Z_1^{12} + Z_2^{12}} \\ &= \frac{Z_1^{21} + Z_2^{21} + Z_1^{12} + Z_2^{12}}{(Z_1^{21} + Z_2^{21})(Z_1^{12} + Z_2^{12})}(P_2 - P_1) \\ &\quad + \frac{Z_1^{21}Z_2^{12} - Z_2^{21}Z_1^{12}}{(Z_1^{21} + Z_2^{21})(Z_1^{12} + Z_2^{12})}u_1 \\ &\quad - \frac{Z_1^{21}Z_2^{12} - Z_2^{21}Z_1^{12}}{(Z_1^{21} + Z_2^{21})(Z_1^{12} + Z_2^{12})}u_2 \\ &= A(u_1 - u_2) + B(P_2 - P_1) \end{aligned}$$

with

$$A = \frac{Z_1^{21}Z_2^{12} - Z_2^{21}Z_1^{12}}{(Z_1^{21} + Z_2^{21})(Z_1^{12} + Z_2^{12})} \tag{3.25a}$$

$$B = \frac{Z_1^{21} + Z_2^{21} + Z_1^{12} + Z_2^{12}}{(Z_1^{21} + Z_2^{21})(Z_1^{12} + Z_2^{12})} \tag{3.25b}$$

Let us examine the difference between the second component of (3.23a) and (3.23c), i.e $P^\star_{12} - P^\star_{21}$. We need to evaluate $u^\star - u_L$ and $u^\star - u_R$. From (3.24), we have

$$\begin{aligned} u^\star - u_R &= \frac{P_L - P_R + Z^L(u_L - u_R)}{Z^R + Z^L} \\ u^\star - u_L &= \frac{P_L - P_R + Z^R(u_R - u_L)}{Z^R + Z^L}. \end{aligned}$$

This leads to

$$\begin{aligned} P^\star_{12} - P^\star_{21} &= Z_2^{12}(u^\star_{12} - u_2) + Z_2^{21}(u^\star_{21} - u_2) \\ &= Z_2^{12}\frac{P_1 - P_2 + Z_1^{12}(u_1 - u_2)}{Z_1^{12} + Z_2^{12}} + Z_2^{21}\frac{P_2 - P_1 + Z_1^{21}(u_1 - u_2)}{Z_1^{21} + Z_2^{21}} \\ &= \frac{Z_1^{21}Z_2^{12} - Z_2^{21}Z_1^{12}}{(Z_1^{21} + Z_2^{21})(Z_1^{12} + Z_2^{12})}(P_1 - P_2) \\ &\quad + \left(\frac{Z_2^{12}Z_1^{12}}{Z_1^{12} + Z_2^{12}} + \frac{Z_2^{21}Z_1^{21}}{Z_1^{21} + Z_2^{21}}\right)(u_1 - u_2) \\ &= C(u_1 - u_2) - A(P_2 - P_1) \end{aligned}$$

with

$$C = \frac{Z_2^{12}Z_1^{12}}{Z_1^{12} + Z_2^{12}} + \frac{Z_2^{21}Z_1^{21}}{Z_1^{21} + Z_2^{21}} \tag{3.26}$$

Clearly, the system

$$\begin{cases} u_{12}^\star - u_{21}^\star = 0 \\ P_{12}^\star - P_{21}^\star = 0 \end{cases}$$

is equivalent to

$$\begin{cases} A(u_1 - u_2) + B(P_2 - P_1) = 0 \\ C(u_1 - u_2) - A(P_2 - P_1) = 0 \end{cases}$$

which determinant is $-A^2 - BC$.

For the system to be invertible, it is sufficient that B and C be strictly positive. This is true in particular if all the Z are strictly positive. We show later in this section, and for several choices of speeds $S_{L,R}$ that $Z > 0$, and thus the system is invertible.

Assume the system is invertible : the equilibrium set is (3.20).

It remains to evaluate the Jacobian matrix along the equilibrium set $\mathcal{V}$. This is done as in subsection 3.2.1. For example, if we compute the derivative of $P_{12}^\star - P_{21}^\star$ with respect to $v = \rho$, u or P, we have

$$\frac{\partial(P_{12}^\star - P_{21}^\star)}{\partial v} = \frac{\partial A}{\partial v}(P_1 - P_2) + \frac{\partial B}{\partial v}(u_1 - u_2) + A\frac{\partial(P_1 - P_2)}{\partial v} + B\frac{\partial(u_1 - u_2)}{\partial v}$$

If the variables belongs to $\mathcal{V}$, we have

$$\frac{\partial(P_{12}^\star - P_{21}^\star)}{\partial v} = A\frac{\partial(P_1 - P_2)}{\partial v} + B\frac{\partial(u_1 - u_2)}{\partial v}$$

Therefore, if $A = 0$ in the equilibrium set, we get the result for $P_{12}^\star - P_{21}^\star$. The same result holds for $u_{12}^\star - u_{21}^\star$. Thus, the only thing left is to show that A is zero along (3.20).

The remaining of this section is devoted to showing, for several classical choices of speeds S [62], that

1. $Z > 0$,
2. A defined in (3.25b) satisfies $A = 0$ along $\mathcal{V}$.

Case where $S^L = u_L - c_L$ and $S^R = u_R + c_R$

We have

$$\begin{aligned} Z_1^{12} &= \rho_1 c_1 \\ Z_2^{12} &= \rho_2 c_2 \\ Z_1^{21} &= \rho_1 c_1 \\ Z_2^{21} &= \rho_2 c_2 \end{aligned}$$

and we see immediately that the Z are all strictly positive and that, directly from (3.25b), $A = 0$ along $\mathcal{V}$.

Case where $S^L = \min(u_L - c_L, u_R - c_R)$ and $S^R = \max(u_R + c_R, u_L + c_L)$

In this case, it is obvious that the Zs are strictly positive so that the equilibrium set is (3.20). Along this equilibrium set, we denote by $\bar{c}$ the maximum sound speed and u the velocity of each fluid. We have

$$\begin{aligned} Z_1^{12} &= \rho_1 \bar{c} \\ Z_2^{12} &= \rho_2 \bar{c} \\ Z_1^{21} &= \rho_1 \bar{c} \\ Z_2^{21} &= \rho_2 \bar{c} \end{aligned}$$

therefore, $A = 0$ along the equilibrium set.

Case where $S^L = \tilde{u} - \tilde{c}$ and $S^R = \tilde{u} + \tilde{c}$ where $\tilde{x}$ is the Roe–average [4] of x

The equation which gives the intermediate velocity does not hold any more because we are not sure that the denominator is nonzero. Nevertheless we still can use the equations (3.23). The equality of the second and third component of (3.23a) and (3.23b) gives immediately

$$u_{12}^\star = u_{21}^\star$$

and we denote by $u^\star$ this velocity. Moreover, by abstracting the second component of (3.23c) and the second component of (3.23a), and by doing the same algebra with (3.23b) and (3.23d), we get

$$\left\{ \begin{array}{l} (u^\star - u_2)\left(S_{12}^L - S_{21}^R\right) = 0 \\ (u^\star - u_1)\left(S_{21}^L - S_{12}^R\right) = 0 \end{array} \right. \tag{3.27}$$

Here, the wave velocities are symmetric in u_1 and u_2, so that $S_{12}^L = S_{21}^L = S^L$ and $S_{21}^R = S_{12}^R = S^R$. We have $S^L - S^R = -2\tilde{c} \neq 0$ which leads to

$$u_1 = u_2 = u^\star.$$

Last, the equality of the second component of (3.23a) and (3.23b) provides $P_1 = P_2$. Thus, the equilibrium set is once more (3.20). Along the equilibrium set, we have

$$\begin{aligned} Z_1^{12} &= \rho_1 \tilde{c} \\ Z_2^{12} &= \rho_2 \tilde{c} \\ Z_1^{21} &= \rho_1 \tilde{c} \\ Z_2^{21} &= \rho_2 \tilde{c} \end{aligned}$$

where a is the Roe–average of c_1 and c_2, so that Zs are strictly positive, and we can use the formula (3.25a) for A which gives immediately $A = 0$ on $\mathcal{V}$.

[4] $\tilde{x} := \frac{\sqrt{\rho_L} x_L + \sqrt{\rho_R} x_R}{\sqrt{\rho_L} + \sqrt{\rho_R}}$.

Case of pressure-velocity based wave speed estimates

A different approach, that works for perfect gases only, consists in first estimating the pressure $P^\star$ and $u^\star$ and then derivating the estimates of S^L and S^R. If we suppose that we have estimated $P^\star$ and $u^\star$, then we choose the following wave speeds

$$S^L = u_L - c_L q_L \qquad S^R = u_R + c_R q_R$$

where

$$q_K = \begin{cases} 1 & \text{if} \quad P^\star \leq P_K \\ \left(1 + \dfrac{\gamma+1}{2\gamma}\left(\dfrac{P^\star}{P_K} - 1\right)\right)^{\frac{1}{2}} & \text{if} \quad P^\star > P_K \end{cases} \tag{3.28}$$

Then we find

$$\begin{aligned} Z_1^{12} &= \rho_1 c_1 q_L^{12} \\ Z_2^{12} &= \rho_2 c_2 q_R^{12} \\ Z_1^{21} &= \rho_1 c_1 q_R^{21} \\ Z_2^{21} &= \rho_2 c_2 q_L^{21} \end{aligned}$$

These Z are all strictly non–negative, so that the equilibrium set is (3.20). On the equilibrium set $P_{12}^\star = P_{21}^\star$ so that with (3.28), we have

$$q_L^{12} = q_R^{21} \qquad \text{and} \qquad q_R^{12} = q_L^{21}$$

and A is null on the equilibrium set.

3.2.4 Case of the relaxation solver of [17]

We approximate the solutions of the Euler equations with those of the following relaxation system

$$\begin{cases} \dfrac{\partial \rho}{\partial t} + \dfrac{\partial (\rho u)}{\partial x} = 0 \\ \dfrac{\partial (\rho u)}{\partial t} + \dfrac{\partial (\rho u^2 + \pi)}{\partial x} = 0 \\ \dfrac{\partial (\rho E)}{\partial t} + \dfrac{\partial ((\rho E + \pi) u)}{\partial x} = 0 \\ \dfrac{\partial \pi}{\partial t} + u \dfrac{\partial \pi}{\partial x} + \dfrac{a^2}{\rho} \dfrac{\partial u}{\partial x} = \dfrac{P - \pi}{\eta} \end{cases} \tag{3.29}$$

where a is a parameter chosen to ensure the system is dissipative when the relaxation time $\eta \to \infty$ ($a > \max(\rho c)$). The solution of the Riemann problem for (3.29) can easily be computed because all the fields are linearly degenerate. In particular, we find the following formulas for the intermediate

pressure and velocity

$$\pi^\star = \frac{\pi_R + \pi_L}{2} + \frac{a}{2}(u_L - u_R)$$
$$u^\star = \frac{\pi_L - \pi_R}{2a} + \frac{u_L + u_R}{2}.$$

Thus we immediately get

$$P_{12}^\star - P_{21}^\star = \frac{a_{12} + a_{21}}{2}(u_1 - u_2)$$
$$u_{12}^\star - u_{21}^\star = \frac{1}{2}\left(\frac{1}{a_{12}} + \frac{1}{a_{21}}\right)(P_1 - P_2)$$

As in the case of the acoustic solver, we see immediately that the equilibrium set is (3.20). Last the study of the Jacobian matrix with the same method as before shows that (3.21) is true with

$$\lambda = \frac{1}{2}\left(\frac{1}{a_{12}} + \frac{1}{a_{21}}\right) \qquad \text{and} \qquad \mu = \frac{a_{12} + a_{21}}{2}.$$

3.3 Derivation of the numerical scheme for the five equations model

In the previous section, we have shown that, for several classical solvers, the equilibrium variety is the same as the one in the continuous case, namely

$$\mathcal{V} = \Big\{ u_1 = u_2 \quad \text{and} \quad P_1 = P_2 \Big\} \tag{3.30}$$

Therefore, $\mathcal{V}$ is of dimension 6 and can be parametrised by the mapping M

$$M : \begin{pmatrix} \alpha_1 \\ \rho_1 \\ u \\ P \\ \alpha_2 \\ \rho_2 \end{pmatrix} \mapsto \begin{pmatrix} \alpha_1 \\ \rho_1 \\ u \\ P \\ \alpha_2 \\ \rho_2 \\ u \\ P \end{pmatrix}$$

Since this parametrisation is naturally written in primitive variables and not in conservative variables, the first thing to do is to provide the form of the numerical scheme for the seven equations model in primitive variables which is equivalent to the form in conserved variables.

The next step is to compute the projector P onto the kernel of $R'(M(\mathbf{u}))$ in the direction of $\mathrm{d}M_{\mathbf{u}}$, and then to evaluate (3.19).

3.3.1 Transformation into primitive form

In order to simplify the algebra, we rewrite (3.17) as

$$\begin{aligned}
&\frac{\partial \alpha_i^{(k)}}{\partial t} = V F_i^{(k)} \\
&\frac{\partial \left(\alpha_i^{(k)} \rho_i^{(k)}\right)}{\partial t} = M_a F_i^{(k)} \\
&\frac{\partial \left(\alpha_i^{(k)} \rho_i^{(k)} u_i^{(k)}\right)}{\partial t} = M_o F_i^{(k)} \\
&\frac{\partial \left(\alpha_i^{(k)} \rho_i^{(k)} E_i^{(k)}\right)}{\partial t} = E F_i^{(k)}
\end{aligned} \tag{3.31}$$

Since

$$\alpha_i^{(k)} \rho_i^{(k)} \frac{\partial u_i^{(k)}}{\partial t} = M_o F_i^{(k)} - u_i^{(k)} M_a F_i^{(k)} \tag{3.32}$$

we have

$$\begin{aligned}
\frac{1}{2}\frac{\partial \left(\alpha_i^{(k)} \rho_i^{(k)} {u_i^{(k)}}^2\right)}{\partial t} &= \frac{u_i^{(k)}}{2}\frac{\partial \left(\alpha_i^{(k)} \rho_i^{(k)} u_i^{(k)}\right)}{\partial t} + \frac{\alpha_i^{(k)} \rho_i^{(k)} u_i^{(k)}}{2}\frac{\partial u_i^{(k)}}{\partial t} \\
&= \frac{1}{2} u_i^{(k)} M_o F_i^{(k)} + \frac{1}{2} u_i^{(k)} \left(M_o F_i^{(k)} - u_i^{(k)} M_a F_i^{(k)}\right) \\
&= \frac{1}{2} u_i^{(k)} M_o F_i^{(k)} + \frac{1}{2} u_i^{(k)} M_o F_i^{(k)} - \frac{{u_i^{(k)}}^2}{2} M_a F_i^{(k)} \\
&= u_i^{(k)} M_o F_i^{(k)} - \frac{\left(u_i^{(k)}\right)^2}{2} M_a F_i^{(k)}
\end{aligned}$$

Similarly,

$$E F_i^{(k)} = \frac{\partial \left(\alpha_i^{(k)} \rho_i^{(k)} E_i^{(k)}\right)}{\partial t} = \frac{\partial \left(\alpha_i^{(k)} \rho_i^{(k)} \varepsilon_i^{(k)}\right)}{\partial t} + \frac{1}{2}\frac{\partial \left(\alpha_i^{(k)} \rho_i^{(k)} \left(u_i^{(k)}\right)^2\right)}{\partial t}$$

and

$$\frac{\partial \left(\alpha_i^{(k)} \rho_i^{(k)} \varepsilon_i^{(k)}\right)}{\partial t} = E F_i^{(k)} - u_i^{(k)} M_o F_i^{(k)} + \frac{\left(u_i^{(k)}\right)^2}{2} M_a F_i^{(k)}$$

We develop the energy equation to get an equation on the pressure

$$\begin{aligned}
\frac{\partial \left(\alpha_i^{(k)} \rho_i^{(k)} \varepsilon_i^{(k)}\right)}{\partial t} &= \varepsilon_i^{(k)} \frac{\partial \left(\alpha_i^{(k)} \rho_i^{(k)}\right)}{\partial t} + \alpha_i^{(k)} \rho_i^{(k)} \frac{\partial \varepsilon_i^{(k)}}{\partial t} \\
&= \varepsilon_i^{(k)} M_a F_i^{(k)} + \alpha_i^{(k)} \rho_i^{(k)} \beta_i^{(k)} \frac{\partial P_i^{(k)}}{\partial t} + \alpha_i^{(k)} \rho_i^{(k)} \kappa_i^{(k)} \frac{\partial \rho_i^{(k)}}{\partial t}
\end{aligned}$$

where

$$\beta_i^{(k)} = \left(\frac{\partial \varepsilon_i^{(k)}}{\partial P_i^{(k)}}\right)_{\rho_i^{(k)}} \qquad \text{and} \qquad \kappa_i^{(k)} = \left(\frac{\partial \varepsilon_i^{(k)}}{\partial \rho_i^{(k)}}\right)_{P_i^{(k)}}$$

When we combine the mass and the volume fraction equations, we obtain

$$\alpha_i^{(k)} \frac{\partial \rho_i^{(k)}}{\partial t} = M_a F_i^{(k)} - \rho_i^{(k)} V F_i^{(k)}. \tag{3.33}$$

Then we have

$$\begin{aligned}
\alpha_i^{(k)} \rho_i^{(k)} \beta_i^{(k)} \frac{\partial P_i^{(k)}}{\partial t} &= E F_i^{(k)} - u_i^{(k)} M_o F_i^{(k)} + \frac{{u_i^{(k)}}^2}{2} M_a F_i^{(k)} - \varepsilon_i^{(k)} M_a F_i^{(k)} \\
&\quad - \alpha_i^{(k)} \rho_i^{(k)} \kappa_i^{(k)} \frac{\partial \rho_i^{(k)}}{\partial t} \\
&= E F_i^{(k)} - u_i^{(k)} M_o F_i^{(k)} + \frac{{u_i^{(k)}}^2}{2} M_a F_i^{(k)} - \varepsilon_i^{(k)} M_a F_i^{(k)} \\
&\quad - \rho_i^{(k)} \kappa_i^{(k)} \left(M_a F_i^{(k)} - \rho_i^{(k)} V F_i^{(k)} \right),
\end{aligned}$$

that is

$$\begin{aligned}
\frac{\partial P_i^{(k)}}{\partial t} &= \frac{E F_i^{(k)}}{\alpha_i^{(k)} \rho_i^{(k)} \beta_i^{(k)}} - \frac{u_i^{(k)} M_o F_i^{(k)}}{\alpha_i^{(k)} \rho_i^{(k)} \beta_i^{(k)}} \\
&\quad + \frac{\left(\dfrac{{u_i^{(k)}}^2}{2} - \varepsilon_i^{(k)} - \rho_i^{(k)} \kappa_i^{(k)} \right)}{\alpha_i^{(k)} \rho_i^{(k)} \beta_i^{(k)}} M_a F_i^{(k)} + \frac{{\rho_i^{(k)}}^2 \kappa_i^{(k)} V F_i^{(k)}}{\alpha_i^{(k)} \rho_i^{(k)} \beta_i^{(k)}}
\end{aligned} \tag{3.34}$$

The scheme (3.9) is equivalent to (3.33), (3.32) and (3.34).

3.3.2 The projection

Formally, the seven equations numerical scheme in primitive variables is

$$\frac{\partial \mathbf{U}'}{\partial t} + \frac{G'}{\Delta x} = T \frac{R(\mathbf{U}')}{\varepsilon_j}$$

where T is the linear transformation between primitive and conservative variables

$$T = \begin{pmatrix} T_1 & 0 \\ 0 & T_2 \end{pmatrix}$$

with

$$T_i = \begin{pmatrix} 1 & 0 & 0 & 0 \\ -\dfrac{\rho_i}{\alpha_i} & \dfrac{1}{\alpha_i} & 0 & 0 \\ 0 & -\dfrac{u_i}{\alpha_i} & \dfrac{1}{\alpha_i \rho_i} & 0 \\ \dfrac{\kappa_i {\rho_i}^2}{\alpha_i \rho_i \beta_i} & \dfrac{\frac{u_i^2}{2} - \varepsilon_i - \rho_i \kappa_i}{\alpha_i \rho_i \beta_i} & -\dfrac{u}{\alpha_i \rho_i \beta_i} & \dfrac{1}{\alpha_i \rho_i \beta_i} \end{pmatrix} \tag{3.35}$$

The range of D$R(M(u))$ is spanned by

$$\mathbf{V}_1 = (1, 0, 0, -P, -1, 0, 0, P) \qquad \text{and} \qquad \mathbf{V}_2 = (0, 0, 1, u, 0, 0, -1, -u).$$

and we want to project in the direction of[5]

$$T\,\mathbf{V}_1 = \begin{pmatrix} 0 \\ 0 \\ \alpha_2\rho_2 \\ 0 \\ 0 \\ -\alpha_1\rho_1 \\ 0 \end{pmatrix} \qquad \text{and} \qquad T\,\mathbf{V}_2 = \begin{pmatrix} 1 \\ -\dfrac{\rho_1}{\alpha_1} \\ 0 \\ -\dfrac{\rho_1 {c_1}^2}{\alpha_1} \\ \dfrac{\rho_2}{\alpha_2} \\ 0 \\ \dfrac{\rho_2 {c_2}^2}{\alpha_2} \end{pmatrix}$$

A tedious but straightforward calculation shows that the matrix of the projector is

$$\Pi = \begin{pmatrix} 1 & 0 & 0 & \dfrac{\alpha_1\alpha_2}{d} & 0 & 0 & -\dfrac{\alpha_1\alpha_2}{d} \\ 0 & 1 & 0 & -\dfrac{\rho_1\alpha_2}{d} & 0 & 0 & \dfrac{\rho_1\alpha_2}{d} \\ 0 & 0 & \dfrac{\rho_1\alpha_1}{\alpha_1\rho_1 + \alpha_2\rho_2} & 0 & 0 & \dfrac{\rho_2\alpha_2}{\alpha_1\rho_1 + \alpha_2\rho_2} & 0 \\ 0 & 0 & 0 & \dfrac{\alpha_1\rho_2 {c_2}^2}{d} & 0 & 0 & \dfrac{\alpha_2\rho_1 {c_1}^2}{d} \\ 0 & 0 & 0 & \dfrac{\alpha_1\rho_2}{d} & 1 & 0 & -\dfrac{\alpha\rho_2}{d} \end{pmatrix} \tag{3.36}$$

with

$$d = \alpha_1\rho_2(c_2)^2 + \alpha_2\rho_1(c_1)^2$$

By putting back the system into the reduced conservative variables

$$(\alpha_i, \alpha_i\rho_i, \rho u, \rho E),$$

[5]Note that $\dfrac{P_k - \kappa_k {\rho_k}^2}{\beta_k {\rho_k}^2} = {c_k}^2$.

the evaluation of (3.19) provides the following scheme for the five equations model

$$\begin{aligned}
\frac{\partial \alpha_2}{\partial t} &= FV_2 + \\
&\frac{\alpha_1\alpha_2}{\alpha_2\rho_1c_1^2+\alpha_1\rho_2c_2^2}\left(\frac{SE_2}{\alpha_2\rho_2\beta_2}-\frac{u_2SU_2}{\alpha_2\rho_2\beta_2}+\frac{\left(\frac{u_2^2}{2}-\varepsilon_2-\rho_2\kappa_2\right)}{\alpha_2\rho_2\beta_2}M_2\right. \\
&\left.+\frac{\rho_2^2\kappa_2FV_2}{\alpha_2\rho_2\beta_2}-\frac{SE_1}{\alpha_1\rho_1\beta_1}+\frac{u_1SU_1}{\alpha_1\rho_1\beta_1}-\frac{\left(\frac{u_1^2}{2}-\varepsilon_1-\rho_1\kappa_1\right)}{\alpha_1\rho_1\beta_1}M_1\right. \\
&\left.-\frac{\rho_1^2\kappa_1FV_1}{\alpha_1\rho_1\beta_1}\right) \\
\frac{\partial\left(\alpha_k\rho_k\right)}{\partial t} &= M_k \\
\frac{\partial\left(\rho u\right)}{\partial t} &= SU_1+SU_2 \\
\frac{\partial\left(\rho E\right)}{\partial t} &= SE_1+SE_2
\end{aligned}$$

where we have used the notations of (3.31).

We conclude this section by noting that this applies to the first order as well as the second order scheme.

3.4 Numerical results

In the numerical tests, all the fluids were described by the Stiffened–gas equation of state:

$$\varepsilon_k(P,\rho)=\frac{P+\gamma_kP_k^\infty}{(\gamma_k-1)\rho}$$

where γ and P^∞ are constant that depend on the phase under consideration. In this paper, the fluids used in the numerical tests are the water and the air which coefficients γ and P^∞ are given in the Tables 3.3 and 3.6. In some cases, one side of the tube will be filled with pure fluids, in which case the volume fraction of the fluid that is not here will be initialised with $\alpha_\epsilon = 10^{-8}$. All

Table 3.3: EOS coefficients for water and air

air	water
$\gamma = 1.4$	$\gamma = 4.4$
$P^\infty = 0\,\text{Pa}$	$P^\infty = 6.10^8\,\text{Pa}$

examples are run with a CFL number of 0.6. The CFL number is computed on the largest wave speed in the flow.

The test cases are chosen so that one can see the influence of the div $\mathbf{u}$ terms and ordered by increasing difficulty. The last case is a comparison with experimental data.

We have chosen to use different solvers in the experiments. Several considerations have motivated our choices : the best possible accuracy and the most possible robustness. In interface–like problems, we need to initialise one of the fluids with a very small volume fraction, typically of the order of 10^{-8}. In that case, the solver "sees" the fluid as vacuum, and might be very sensitive to any numerical error especially in the case of complex and stiff wave systems. Because of that, some solvers are not suited to some cases. In the following, we have chosen to use the acoustic solver in the tests of subsection 3.4.2 (in fact all the solvers are working fine on this case) and the relaxation solver on the other ones. This choice seems to be the best compromise.

3.4.1 Single fluid test

In that case, the shock–tube is filled with water only. At time $t = 0$, the left part of the tube is at rest, with a pressure of $10^9\,\text{Pa}$ and the right side is at rest too, but with a pressure of $10^5\,\text{Pa}$. The separation between both sides is at $x = 0.5\text{m}$, and the profiles are shown at $t = 150\,\mu\text{s}$. The approximated solution is computed with a 1000 points grid mesh, and is compared with the analytical solution on Figure 3.3. The second order scheme has been run. The exact solution and the numerical one are in good agreement.

3.4.2 Pure interface advection

A one meter long tube is filled on the right with air and on the left with water. The pressure is uniform, equal to $10^5\,\text{Pa}$, and the velocity is uniform too, equal to $1000\,\text{m.s}^{-1}$. At time $t = 0$, the discontinuity is localised at $x = 0.5\text{m}$. The exact solution consists in the advection of mass at $1000\,\text{m.s}^{-1}$, the pressure and the velocity remain uniform. The results are shown at time

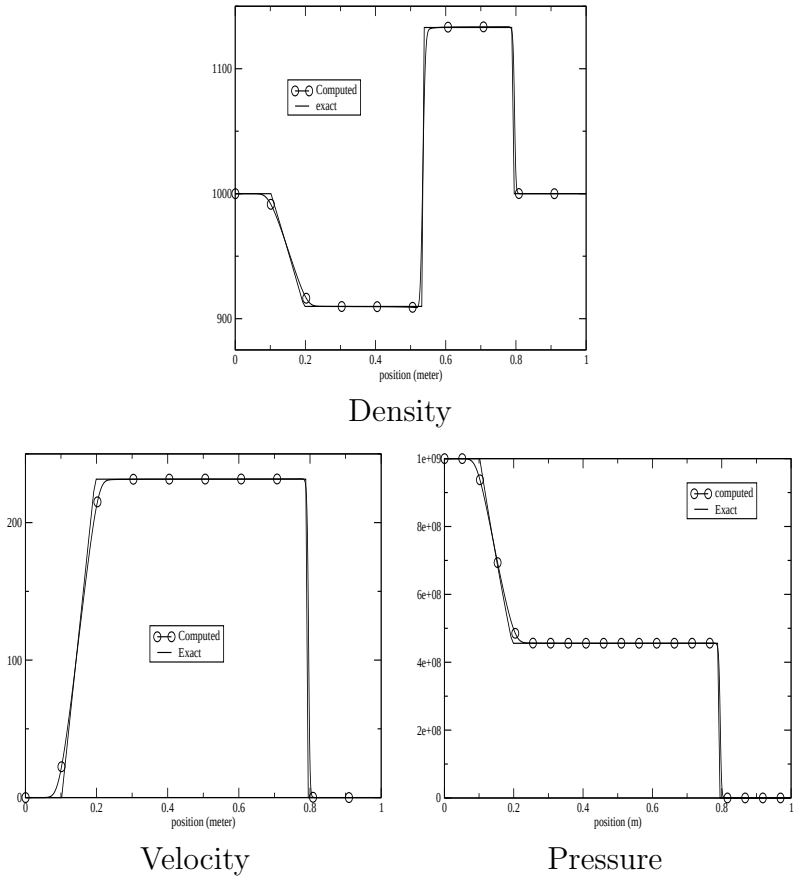

Figure 3.3: Single fluid problem : approximated solution (circles) and exact solution (solid).

$t = 200\,\mu$s when the exact discontinuity is located at $x = 0.7\,$m. The solution is computed with a 1000 cells mesh and is shown on Figure 3.4. The results show that the velocity and the pressure remain uniform, and the density and volume of fluids are simply advected, as expected.

3.4.3 Liquid-gas shock tube

Here we study the evolution of a tube filled on the left with high–pressure water ($10^9\,$Pa) and on the right with atmospheric pressure air ($10^5\,$Pa). The discontinuity is initially at $x = 0,7\,$m. The details of the initial conditions are given in Table 3.4. Computed solution of the present scheme and of [2] are compared on Figure 3.5.

Note that these solutions are computed with the second order scheme. In

Figure 3.6, we display the first and second order accurate solutions for this problem. Clearly, the second order results are much more accurate than the first order ones as expected.

3.4.4 Two phase flow problem

In that case, the left and the right part of the shock–tube are filled with water and air at the same volume fraction of 0.5. The pressure is of 10^9 Pa on the left and of 10^5 Pa on the right. The discontinuity is initially at $x = 0.5$ m. The details of the initial conditions are given in Table 3.5. Computed solution of the present scheme and of [2] are compared on Figure 3.7. The results are in good agreement, but we note some discrepancies. The main difference between the present schemes and that of [2], as it can be seen on Figure 3.7 consists in the density levels between the contact and the shock wave. The location of the discontinuities as well as the extreme points of the fan coincide exactly, up to numerical errors of course. Note however that the average densities almost coincide between the contact and the shock and do coincide elsewhere. The pressure and velocity plots superimpose up to numerical errors. In our opinion, the fact that the discontinuities move at the same speed is a good indication that we are computing the same system : our experience indicates that in the case of non conservative systems, as here, a small modification in the approximation of non conservative terms implies a large modification of the numerical wave speeds. These are certainly consequence of the different techniques in time integration : in the original scheme, the relaxation terms are integrated by a splitting technique, but one has to remember that the relaxation terms originate from fluxes. On the contrary, in the present technique, no splitting technique is used. The asymptotic expansion we use has some features of a direct integration of the relaxation terms inside the solver, which is probably better in principle. These algorithmic differences seem here to have a large impact on the volume fraction, but we have no clear explanation why. In Figure3.8, we have represented a zoom of the average density between the contact discontinuity and the shock wave for the first and second order versions of the present scheme and the original one. We clearly see the (small) differences. The most interesting phenomenon is that : first, the two first order solutions are very close, second the second order solution for the present scheme is much closer from the first order ones than is the second order version of the original scheme. From the algorithmic point of view, the original second order scheme uses a predictor corrector method, and the predicted quantities are projected onto the equilibrium manifold after the predictor and the corrector steps. In the present scheme, this is translated into the choice of the states that are needed

in the computation of the projector Π defined in (3.36). In the second order version of the present scheme, Π is evaluated after each substep. Hence, there is no reason why the two sets of results should coincide exactly. It appears however that the present technique, based on an asymptotic expansion, is a more stable technique that a simple fractional step method. The lack of exact solution does not enable more accurate comments.

3.4.5 Comparison with experiment

We make a simulation on an alloy made of epoxy and spinel for which experimental data exist. The tube is impacted with a piston, so that a shock propagates. The experimental setup is sketched in Figure 3.9. There exists a linear relation between the shock speed u_c and the impact velocity u_i : $u_c = a_0 + su_i$. Epoxy and spinel are described by the stiffened–gas equation of state with the coefficient of the Table 3.6.

Initially, both of the solids are at atmospheric pressure and their densities are $\rho_1 = 1185\,\mathrm{kg.m^{-3}}$ and $\rho_2 = 3622\,\mathrm{kg.m^{-3}}$ Their respective volume fraction are $\alpha_1 = 0.595$ and $\alpha_2 = 0,405$. We measure the different variables in $x = 0.1\,\mathrm{m}$ and in $x = 0.6\,\mathrm{m}$. Thanks for these measures (shown on Figure 3.10) we can compute the shock speed. On Figure 3.11, we compare our results with the experimental measures taken from [41], those of [44], those obtained by the original scheme and the present scheme.

We see that our results are very close to those of the original scheme, and in good agreement with the experimental results. In particular, we see that there is an excellent agreement between the results of the seven equation model with instantaneous relaxation and the present scheme. The agreement is much better than with Guillard and Murrone scheme for which the div $\mathbf{u}$ terms are discretized independently because

- our results are closer from the experimental ones,
- there is very few difference between the results with the complete seven equation model and the reduced five equations one discretized with our technique.

We have presented a numerical scheme able to compute compressible multiphase schemes that relies on a multi–scale description of the flow. Three types of terms can be identified in the scheme in addition to the temporal terms. One is a conservative terms, the second one plays the role of a non

conservative term that is related to inter-facial quantities, and the last one is a relaxation term that is associated to acoustic phenomena. The key feature of the scheme is that it is *locally* conservative, contrarily to many other schemes devoted to compressible multiphase problems. The scheme is developed for several Riemann solvers. A second order extension is also described.

In many physical situations, it is reasonable to assume that the relaxation is instantaneous : either the bubbles are very small, more generally the inter-facial area between phase is large. We present an asymptotic expansion of the scheme that keeps the local conservation properties of the original scheme. The asymptotic expansion relies on the understanding of an equilibrium variety. Its structure depends, in principle, on the Riemann solver. We show that for several standard solvers that this is not the case, and hence this variety is characterised by the local pressure and velocity of the flow. Several numerical test cases are presented in order to demonstrate the potential of this technique.

A possible remaining problem (that was not encountered in the simulations whatever stiff the tests are), is that the positivity of the volume fraction is not ensured. Another problem is the use of a nonconservative variable in the projection: an usual way to approximate a nonconservative hyperbolic system is to perform the first step with an exact Riemann solver (then the genuinely nonlinear wave are computed by adding regularising viscous terms to the system), and the second step with a nonlinear projection [10]. Here, the method we exposed avoids the first step, but could be improved by replacing the linear projection by a nonlinear projection.

The computation of an exact solution for multiphase shocks, which would be the best accuracy test for the computation of multiphase flows is still an open question. Up to us, the following solutions are explored

- In [54], Saurel & al. derived shock jumps relations that can fit with a lot of experimental data. Nevertheless, the linked numerical method, which includes a nonlinear projection cannot handle with strong shocks.

- In [43], the five equations model is expanded to the ε order so that viscous terms appear in the right hand side. A possible way to compute shocks relations is to study travelling waves for this system. This work is in progress with Hervé Guillard (INRIA Sophia–Antipolis) in the case of isothermal flows.

- A rigorous, but very costly way would be to model a multiphase flow as a stochastic stationary random process, and to use a Monte-Carlo method to answer to

1. Does the random medium converge or not to a one pressure, one velocity medium?
2. If it does, in which sense does the limit depend on the random process (especially the variance and the behaviour of the self-correlation function in the case of zero variance process)?
3. If results are positive, can shock jumps be heuristically derived form this experiment?

Nevertheless, this way would be fully numeric, because stochastic homogenization for nonlinear hyperbolic problems is not very advanced on the theoretical point of view.

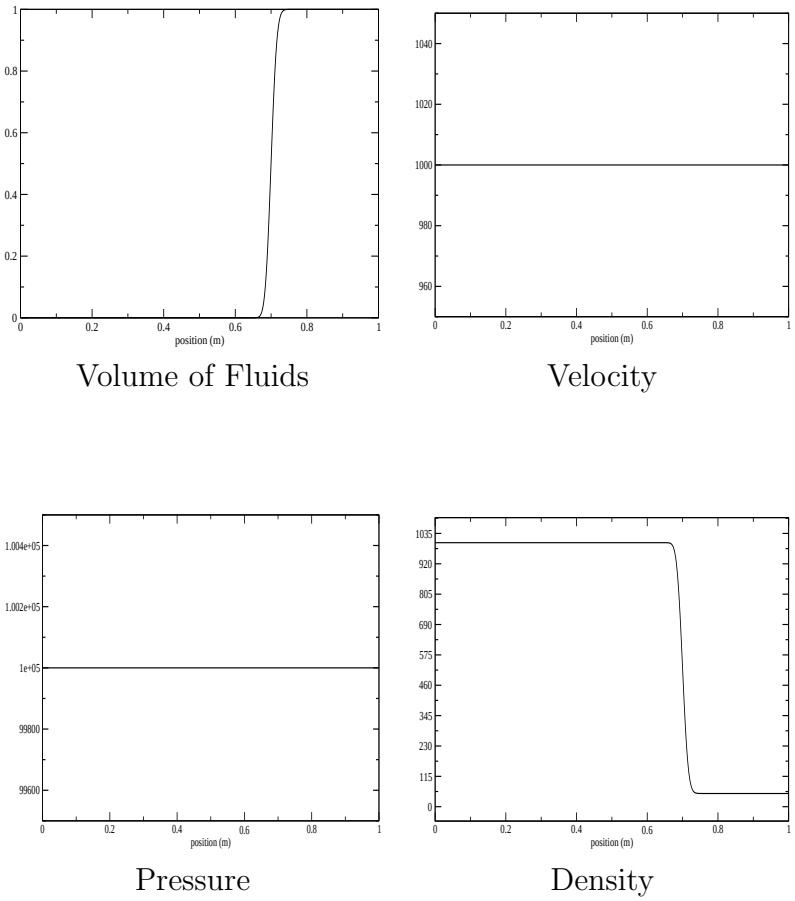

Volume of Fluids Velocity

Pressure Density

Figure 3.4: Pure fluid advection : the interface is diffused and centred around $x = 0.7m$. The pressure and velocity are left unchanged.

Table 3.4: Details of the conditions for the liquid–gas shock tube of subsection 3.4.3.

fluid 1 : air	
$\alpha_1 = \alpha_\epsilon$ $\rho_1 = 50\,\text{kg.m}^{-3}$	$\alpha_1 = 1 - \alpha_\epsilon$ $\rho_1 = 50\,\text{kg.m}^{-3}$
fluid 2 : water	
$\alpha_2 = 1 - \alpha_\epsilon$ $\rho_2 = 1000\,\text{kg.m}^{-3}$	$\alpha_2 = \alpha_\epsilon$ $\rho_2 = 1000\,\text{kg.m}^{-3}$
Global variables	
$P = 10^9\,\text{Pa}$ $u = 0\,\text{m.s}^{-1}$	$P = 10^5\,\text{Pa}$ $u = 0\,\text{m.s}^{-1}$

Table 3.5: Details of the conditions for the two phase flow problem of section 3.4.4.

Fluid 1 : air	
$\alpha_1 = 0.5$ $\rho_1 = 50\,\text{kg.m}^{-3}$	$\alpha_1 = 0.5$ $\rho_1 = 50\,\text{kg.m}^{-3}$
Fluid 2 : water	
$\alpha_2 = 0.5$ $\rho_2 = 1000\,\text{kg.m}^{-3}$	$\alpha_2 = 0.5$ $\rho_2 = 1000\,\text{kg.m}^{-3}$
Global variables	
$P = 10^9\,\text{Pa}$ $u = 0\,\text{m.s}^{-1}$	$P = 10^5\,\text{Pa}$ $u = 0\,\text{m.s}^{-1}$

Table 3.6: EOS coefficients for epoxy and spinel

epoxy	spinel
$\gamma = 2.94$ $P^\infty = 3.2 \times 10^9\text{Pa}\,\text{Pa}$	$\gamma = 1.62$ $P^\infty = 141 \times 10^8\,\text{Pa}$

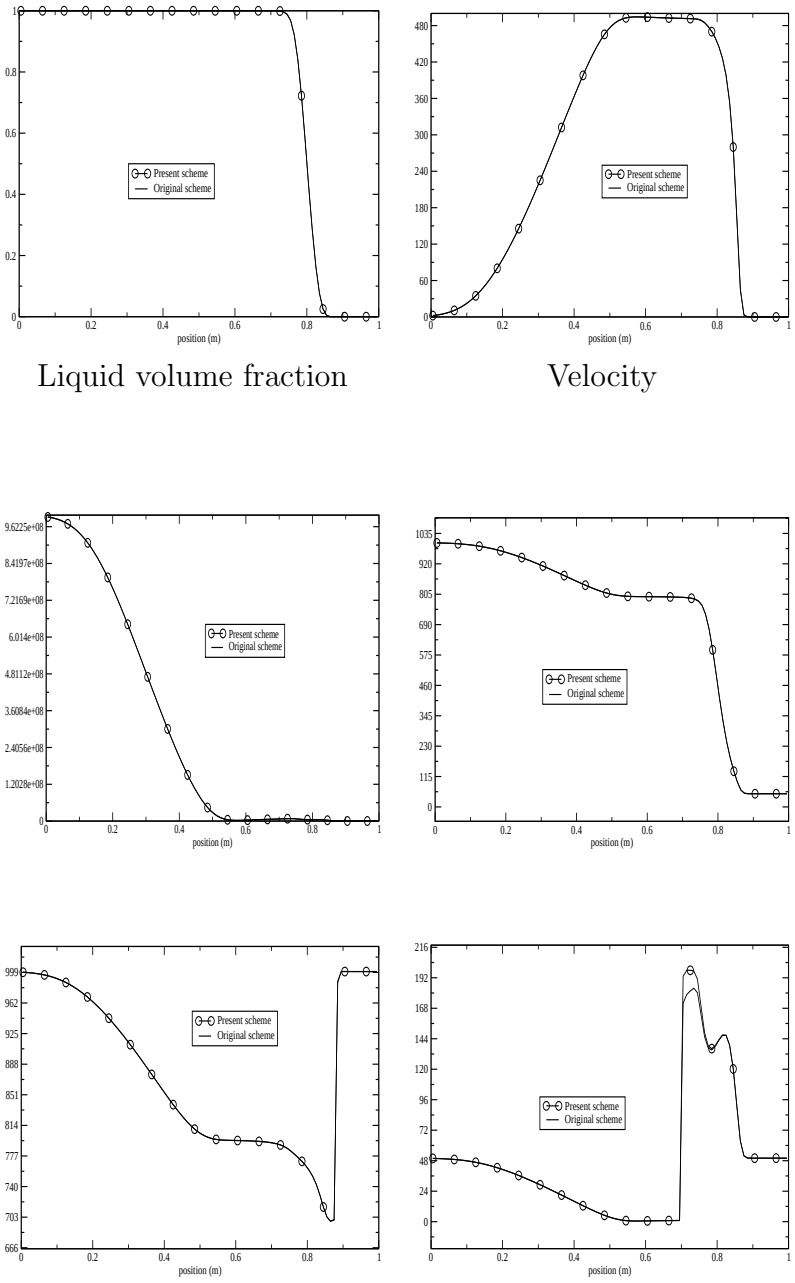

Figure 3.5: Liquid-gas shock tube: Comparison between the solutions obtained by the original scheme of [2] (circles) and the present scheme (solid). Both solutions differs only on the densities, in zones where they have few meaning because the corresponding volume fraction are nearly zero

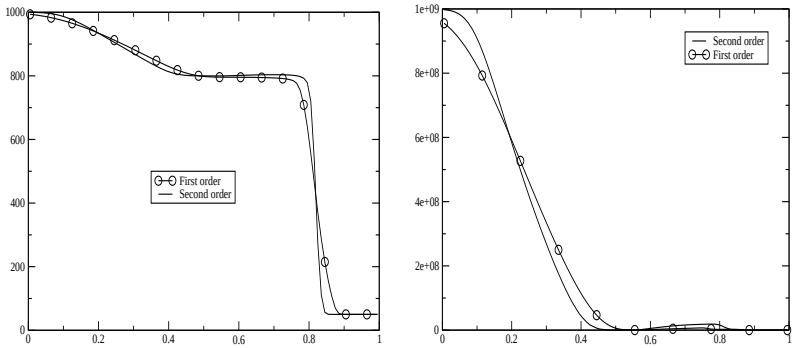

Density profile Pressure profile

Figure 3.6: Comparison between the first and second order accurate schemes.

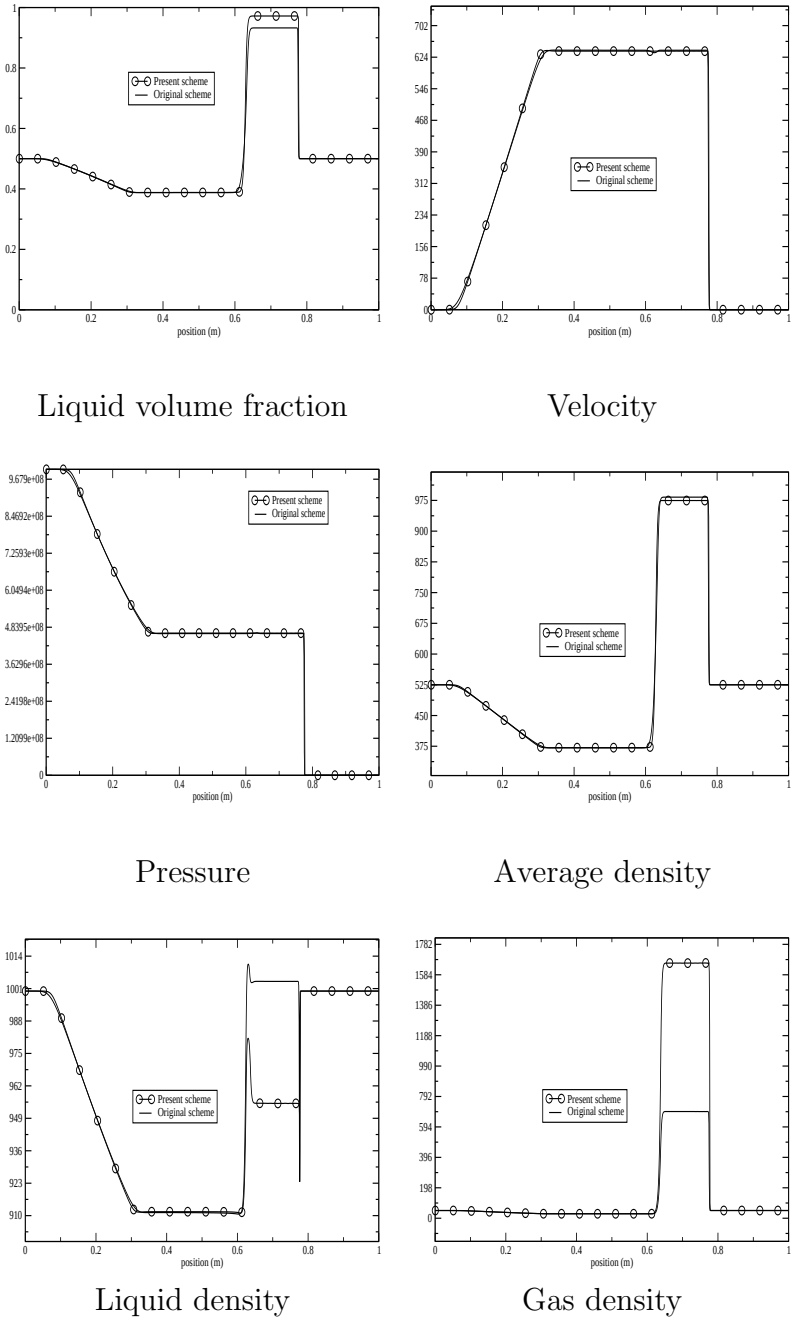

Figure 3.7: Two phase flow problem : the present scheme (circles) is compared with the original scheme of [2] (solid lines).

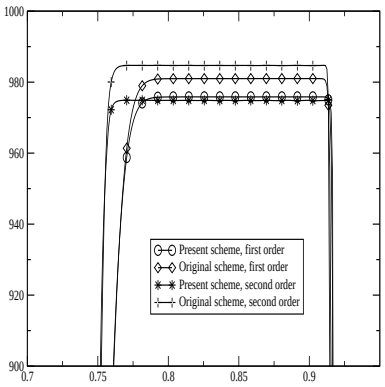

Figure 3.8: Comparison of the first and second order version of the original scheme and the present one for the averaged density. Zoom between the contact discontinuity and the shock wave for the data of Table 3.5.

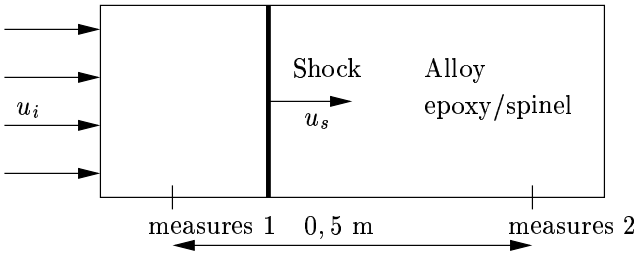

Figure 3.9: Experimental setup.

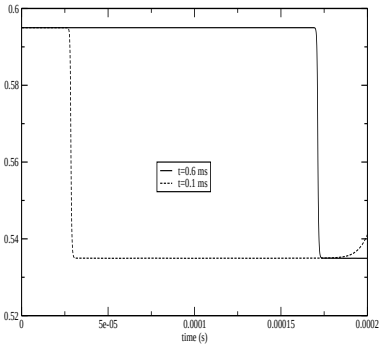

Volume fraction

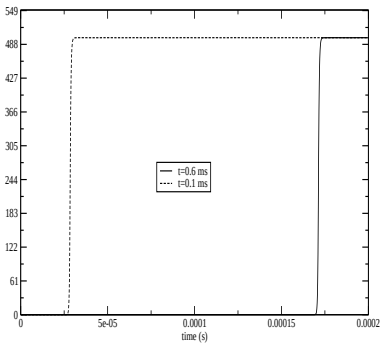

Velocity

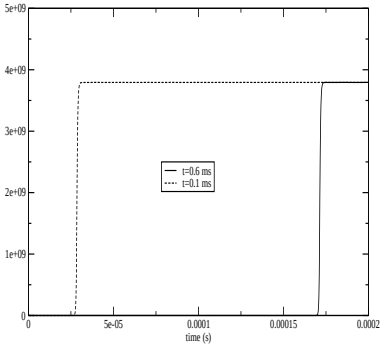

Pressure

Figure 3.10: : Evolution of the variables at $x = 0.1\,\mathrm{m}$ and $x = 0.6\,\mathrm{m}$ between the initial time and $t = 2.\ 10^{-4}$ s.

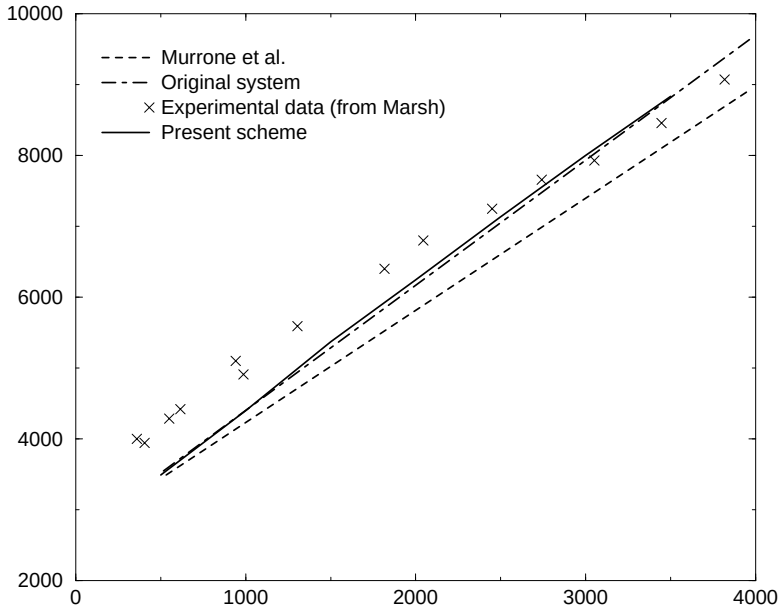

Figure 3.11: Shock velocity, comparison between several approaches.

Part II

Phase transition in compressible flows

Table of Contents

Chapter 4

Thermodynamic of phase transition

In this chapter, we introduce the main thermodynamic features that are necessary to model phase transition. A good understanding of phase transition is a necessary step before our very aim: trying to solve the Riemann problem with equations of state modelling phase transition.

What we aim at modelling is presented in Figure 4.1: we denote by a subscript l and v two phases of the same fluid. l is for the liquid phase and v for the vapor phase in general, but actually, we can model by this way any interaction of two compressible phases of the same fluid, in which case l is the heaviest phase, and v the lightest. Above a given temperature T_{crit} and pressure P_{crit}, the phases cannot be distinguished. Under these critical values, we have

- either a mixture of the two phases
- or a pure phase of l
- or a pure phase of v.

The first thing we want is to give a meaning of the thermodynamical stability of a mixture, and to specify in which sense a thermodynamic state is more or less *stable* than another one. Then we study the main properties of the mixture equation of state. In particular, we find a sufficient condition under which the mixture equation of state is convex. Finally, we evaluate the potentiality of two models: the Van-der-Waals' one, and a model with two convex equations of state.

section 4.2 and section 4.5 are a part of an article in revision [48].

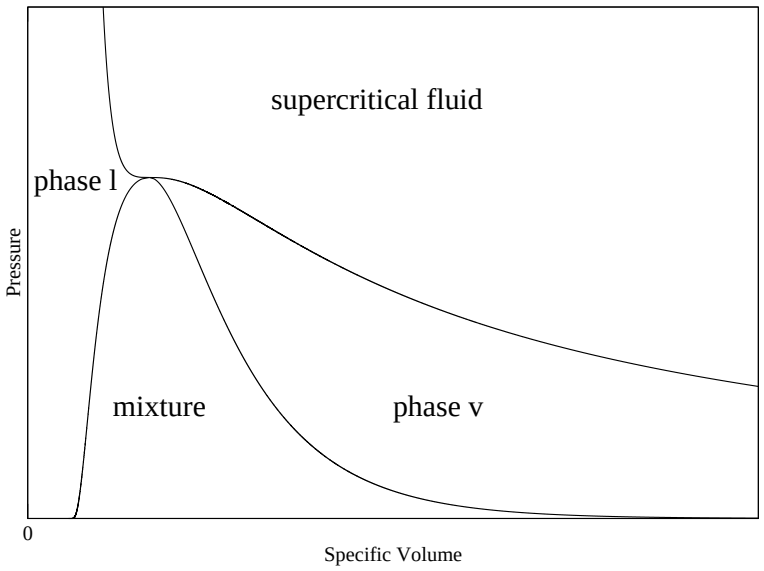

Figure 4.1: What we aim at simulating is the following: we have two phases of the same fluid that cannot be distinguished above a given temperature T_{crit} and pressure P_{crit}. Under these critical values, we have either a mixture of the two fluids, or one pure phase.

4.1 Stability in thermodynamic

Given a system with an entropy, the system is said to be at *equilibrium* if it is an maximum of the entropy (see [15]). This induces the fact that the entropy of a given state must always ensure the following criterion: $\mathrm{d}^2 s < 0$. Thus, for a given system with one concave entropy, no stability issue may occur because a maximum is always an absolute maximum.

For a mixture, the things are more difficult. The entropy of a mixture of two non miscible fluids is given by

$$s(\tau, \varepsilon) = y_l s_l(\varepsilon_l, \tau_l) + y_v s_v(\varepsilon_v, \tau_v) \tag{4.1a}$$

where y_k denotes the mass fraction of each fluid, ε_k is the specific energy of the fluid k, and τ_k is the specific volume of the fluid k. The total specific energy and specific volume are equal to

$$\tau = y_l \tau_l + y_v \tau_v \tag{4.1b}$$

$$\varepsilon = y_l \varepsilon_l + y_v \varepsilon_v \tag{4.1c}$$

Therefore we see that even if the entropy of both of the fluids are concave,

the mixture entropy might not be concave: local maximum may not be an absolute maximum. We thus define different degrees in stability:

Definition 4.1. *A thermodynamic state is said to be*

- **stable** *if the point* (τ, ε) *is an absolute maximum of the entropy*
- **metastable** *if the point* (τ, ε) *is a relative maximum of the entropy*
- **unstable** *if the point* (τ, ε) *is not a maximum of the entropy.*

In the same manner as in [42], we define the following adimensioned parameters

$$\Gamma = -\frac{\tau}{T}\left(\frac{\partial T}{\partial \tau}\right)_s, \qquad \gamma = -\frac{\tau}{P}\left(\frac{\partial P}{\partial \tau}\right)_s, \qquad g = \frac{P\tau}{T^2}\left(\frac{\partial T}{\partial s}\right)_\tau. \tag{4.2}$$

These coefficients are the ones of the Hessian of ε. With these notations, the following identities hold

$$\mathrm{d}s = \frac{P\tau}{T^2}\frac{1}{g}\,\mathrm{d}T + \frac{P}{T}\frac{\Gamma}{g}\,\mathrm{d}\tau \tag{4.3a}$$

$$\mathrm{d}s = -\frac{\tau}{T}\frac{\Gamma}{\gamma g - \Gamma^2}\,\mathrm{d}P + \frac{P\tau}{T^2}\frac{\gamma}{\gamma g - \Gamma^2}\,\mathrm{d}T \tag{4.3b}$$

$$\mathrm{d}s = \frac{\tau}{T}\frac{1}{\Gamma}\,\mathrm{d}P + \frac{P}{T}\frac{\gamma}{\Gamma}\,\mathrm{d}\tau \tag{4.3c}$$

$$\mathrm{d}\tau = -\frac{\tau}{P}\frac{g}{\gamma g - \Gamma^2}\,\mathrm{d}P + \frac{\tau}{T}\frac{\Gamma}{\gamma g - \Gamma^2}\,\mathrm{d}T \tag{4.3d}$$

$$\mathrm{d}h = \tau\frac{\Gamma + 1}{\Gamma}\,\mathrm{d}P + P\frac{\gamma}{\Gamma}\mathrm{d}\tau \tag{4.3e}$$

$$\mathrm{d}\varepsilon = \tau\frac{1}{\Gamma}\,\mathrm{d}P + P\frac{(\gamma - \Gamma)}{\Gamma}\,\mathrm{d}\tau \tag{4.3f}$$

The Hessian of the entropy is then given by

Proposition 4.1. *With the notations* (4.2)*, the Hessian of* $s(\tau, \varepsilon)$ *is equal to*

$$\mathrm{d}^2 s = -\begin{pmatrix} \dfrac{g}{TP\tau} & \dfrac{g-\Gamma}{\tau T} \\ \dfrac{g-\Gamma}{\tau T} & \dfrac{P}{\tau T}\,(\gamma + g - 2\Gamma) \end{pmatrix}$$

Proof. The first and second principles of thermodynamic give

$$\mathrm{d}s = \frac{1}{T}\,\mathrm{d}\varepsilon + \frac{P}{T}\,\mathrm{d}\tau$$

so that

$$\left(\frac{\partial^2 s}{\partial \varepsilon^2}\right)_\tau = \left(\frac{\partial}{\partial \varepsilon}\left(\frac{1}{T}\right)\right)_\tau$$
$$\frac{\partial^2 s}{\partial \varepsilon \partial \tau} = \left(\frac{\partial}{\partial \tau}\left(\frac{1}{T}\right)\right)_\varepsilon$$

Combining the principles of thermodynamic with (4.3a) gives

$$\mathrm{d}T = \frac{Tg}{P\tau}\,\mathrm{d}\varepsilon + \frac{T(g-\Gamma)}{\tau}\,\mathrm{d}\tau$$

so that we get the two first coefficients of the Hessian

$$\left(\frac{\partial^2 s}{\partial \varepsilon^2}\right)_\tau = -\frac{g}{P\tau T}$$
$$\frac{\partial^2 s}{\partial \varepsilon \partial \tau} = -\frac{g-\Gamma}{T\tau}$$

It remains to compute

$$\left(\frac{\partial^2 s}{\partial \tau^2}\right)_\varepsilon = \left(\frac{\partial}{\partial \tau}\left(\frac{P}{T}\right)\right)_\varepsilon = \frac{1}{T}\left(\frac{\partial P}{\partial \tau}\right)_\varepsilon + P\left(\frac{\partial}{\partial \tau}\left(\frac{1}{T}\right)\right)_\varepsilon = \frac{1}{T}\left(\frac{\partial P}{\partial \tau}\right)_\varepsilon - \frac{P(g-\Gamma)}{\tau T}.$$

Thanks to the identity (4.3f), we have

$$\left(\frac{\partial P}{\partial \tau}\right)_\varepsilon = -\frac{P(\gamma-\Gamma)}{\tau}$$

so that we get the last coefficient of the Hessian of s

$$\left(\frac{\partial^2 s}{\partial \tau^2}\right)_\varepsilon = -\frac{P(g+\gamma-2\Gamma)}{\tau T}.$$

□

Then the positivity of the Hessian of s and ε are linked by

Proposition 4.2. *The Hessian of ε is positive (resp. strictly positive) if and only if the Hessian of s is negative (resp. strictly negative).*

Proof. If the Hessian of ε is positive then

$$\gamma, g \geq 0 \qquad \text{and} \qquad \gamma g - \Gamma^2 \geq 0$$

then the first coefficient of the diagonal is positive. The second one,

$$g + \gamma - 2\Gamma = (\sqrt{\gamma} - \sqrt{g})^2 + 2\sqrt{\gamma g} - 2\Gamma,$$

is also positive. The determinant of the Hessian of s is proportional to the one of the Hessian of ε, so that it is also positive.

If the Hessian of s is positive, then $\gamma \geq 0$, and

$$\gamma = \frac{\gamma g}{g} = \frac{\gamma g - \Gamma^2}{g} + \frac{\Gamma^2}{g},$$

is also positive. This ends the proof. □

The Definition 4.1 and Proposition 4.2 imply that the following inequalities are necessary for a stable or a metastable state (they correspond to the diagonal and the determinant of the Hessian of ε)

$$\gamma, g \geq 0 \qquad \text{and} \qquad \gamma g - \Gamma^2 \geq 0 \tag{4.4}$$

4.2 Mixture equation of state

4.2.1 Entropy optimization

In order to find which of the mixtures is the most stable, the total mixture entropy (4.1a) must be optimized. Of course, the optimization must be consistent with the following constraints:

$$\text{conservation of total energy} \qquad y_l \varepsilon_l + y_v \varepsilon_v = cste \tag{4.5a}$$

$$\text{conservation of mass} \qquad y_l + y_v = 1 \tag{4.5b}$$

Moreover, as we supposed that the phases are not miscible, we have

$$y_l \tau_l + y_v \tau_v = cste \tag{4.5c}$$

Then under these constraints, the optimum is characterized by

Proposition 4.3. *If the mixture entropy is at a local optimum, and if the mass fraction of the constituents are neither equal to* 1 *nor to* 0*, then the two phases have the same pressure, temperature and chemical potential.*

Proof. We choose to optimize (4.1a) with the variables τ, ε, y for each phase. The first and second principle of thermodynamic impose that for each phase

$$\mathrm{d}s = \frac{\mathrm{d}\varepsilon}{T} + \frac{P}{T}\,\mathrm{d}\tau$$

Then the differential of s_{tot} must belong to the set spanned by the gradients of the constraints; if we denote by $\lambda_1, \lambda_2, \lambda_3$ the Lagrange multipliers associated to the constraints (4.5a), (4.5b),(4.5c), we find (with the notations of 4.1)

T	temperature
τ	specific volume
ρ	density
s	specific entropy
μ	chemical potential
h	specific enthalpy
f	specific free energy
P	pressure
ε	specific internal energy
y	mass fraction
α	volume fraction

Table 4.1: Thermodynamic notations

$$
\begin{aligned}
s_l &= \lambda_1\varepsilon_l + \lambda_2 + \lambda_3\tau_l && \text{(4.6a)}\\
\frac{y_l}{T_l} &= \lambda_1 y_l && \text{(4.6b)}\\
\frac{y_l P_l}{T_l} &= \lambda_3 y_l && \text{(4.6c)}\\
s_v &= \lambda_1\varepsilon_v + \lambda_2 + \lambda_3\tau_v && \text{(4.6d)}\\
\frac{y_v}{T_v} &= \lambda_1 y_v && \text{(4.6e)}\\
\frac{y_v P_v}{T_v} &= \lambda_3 y_v && \text{(4.6f)}
\end{aligned}
$$

If we suppose that both of the phases coexist, then equations (4.6b) and (4.6e) give

$$T_l = T_v =: T$$

equations (4.6c) and (4.6f) give

$$P_l = P_v =: P$$

and finally, (4.6a) and (4.6d) lead to

$$\mu_l = \mu_v$$

□

Proposition 4.4. *The set*

$$\{(P,T) \qquad \mu_l(P,T) = \mu_v(P,T)\} \tag{4.7}$$

is a one dimensional variety in the set of the non supercritical states.

Proof. We know that

$$\nabla_{(P,T)}(\mu_l - \mu_v) = (\tau_l(P,T) - \tau_v(P,T))\ \mathrm{d}P - (s_l(P,T) - s_v(P,T))\ \mathrm{d}T$$

if this differential vanishes, then we have simultaneously

$$\tau_l(P,T) = \tau_v(P,T) \qquad \text{and} \qquad s_l(P,T) = s_v(P,T)$$

With the previous constraints, we have equality of the pressure, temperature, entropy, and specific volume. This means actually that the states are thermodynamically the sames, which is in contradiction with the fact that the fluid is not supercritical. □

Assumption 4.1. *From now on, we suppose that $\tau_v > \tau_l$ and $s_v > s_l$.*

Remark 4.1. Assumption 4.1 is physically true because

- the liquid is heavier than the vapor
- as the entropy describes how disordered is the medium, then the vapor is more disordered than the liquid.

A simple differentiation of the equality of the thermodynamic potential gives the *Clausius-Clapeyron* relation

$$\frac{\mathrm{d}P_{\mathrm{sat}}}{\mathrm{d}T} = \frac{s_l(P,T) - s_v(P,T)}{\tau_l(P,T) - \tau_v(P,T)} \tag{4.8}$$

Thus, we see that Assumption 4.1 induces

$$\frac{\mathrm{d}P_{\mathrm{sat}}}{\mathrm{d}T} > 0$$

Moreover, Assumption 4.1, combined with the implicit function theorem gives the existence of two local $\mathscr{C}^1$ diffeomorphisms $T \mapsto P_{\mathrm{sat}}(T)$ and $P \mapsto T_{\mathrm{sat}}(P)$ that parameterize the set (4.7).

Thanks for

Definition 4.2 (Saturation dome in the (τ, P) plane)**.** *The saturation dome is the set defined by*

- *in the (τ, P) plane*

$$\Big\{(P,\tau) \qquad \exists y \in [0;1] \qquad \tau = y\tau_l(P, T_{\mathrm{sat}}(P)) + (1-y)\tau_v(P, T_{\mathrm{sat}}(P))\Big\}$$

- *in the (T, S) plane*

$$\Big\{(T,s) \qquad \exists y \in [0;1] \qquad s = ys_l(P_{\mathrm{sat}}(T), T) + (1-y)s_v(P_{\mathrm{sat}}(T), T)\Big\}$$

4.2.2 Parameterization

In the following, we will denote with a subscript m all the variables relative to the mixture equation of state. The mixture equation of state is naturally parameterized by y, the mass fraction of the vapor, and T, the temperature. Nevertheless, in the next sections, the parameters that will be used are mostly τ and s. They are linked by the transformation

$$\Phi : \begin{pmatrix} y \\ T \end{pmatrix} \mapsto \begin{pmatrix} y\tau_v(T) + (1-y)\tau_l(T) \\ ys_v(T) + (1-y)s_l(T) \end{pmatrix} = \begin{pmatrix} \tau \\ s \end{pmatrix}. \tag{4.9}$$

Proposition 4.5. *For all points in the saturation dome, Φ is a local diffeomorphism provided the equations of state of the liquid and of the vapor are both convex.*

Proof. To prove that Φ is a local diffeomorphism, it is sufficient to show that its Jacobian does not vanish. Differentiation of (4.9) and using the Clausius–Clapeyron relation leads to

$$\det(\mathrm{D}\Phi) = (\tau_v - \tau_l)\left(y\left(\frac{\mathrm{d}s_v}{\mathrm{d}T} - \frac{\mathrm{d}P_{\mathrm{sat}}}{\mathrm{d}T}\frac{\mathrm{d}\tau_v}{\mathrm{d}T}\right) + (1-y)\left(\frac{\mathrm{d}s_l}{\mathrm{d}T} - \frac{\mathrm{d}P_{\mathrm{sat}}}{\mathrm{d}T}\frac{\mathrm{d}\tau_l}{\mathrm{d}T}\right)\right). \tag{4.10}$$

We supposed that $\tau_v - \tau_l > 0$ (except at the critical point), so that there remains to show that

$$y\left(\frac{\mathrm{d}s_v}{\mathrm{d}T} - \frac{\mathrm{d}P_{\mathrm{sat}}}{\mathrm{d}T}\frac{\mathrm{d}\tau_v}{\mathrm{d}T}\right) + (1-y)\left(\frac{\mathrm{d}s_l}{\mathrm{d}T} - \frac{\mathrm{d}P_{\mathrm{sat}}}{\mathrm{d}T}\frac{\mathrm{d}\tau_l}{\mathrm{d}T}\right), \tag{4.11}$$

never vanishes. The term (4.11) is a convex combination of

$$\frac{\mathrm{d}s_v}{\mathrm{d}T} - \frac{\mathrm{d}P_{\mathrm{sat}}}{\mathrm{d}T}\frac{\mathrm{d}\tau_v}{\mathrm{d}T} \qquad \text{and} \qquad \frac{\mathrm{d}s_l}{\mathrm{d}T} - \frac{\mathrm{d}P_{\mathrm{sat}}}{\mathrm{d}T}\frac{\mathrm{d}\tau_l}{\mathrm{d}T}. \tag{4.12}$$

Using the equations (4.6a),(4.6b) for $P = P_{\mathrm{sat}}(T)$ leads to

$$\frac{\mathrm{d}s_b}{\mathrm{d}T} - \frac{\mathrm{d}P_{\mathrm{sat}}}{\mathrm{d}T}\frac{\mathrm{d}\tau_b}{\mathrm{d}T} = \frac{\gamma g - \Gamma^2}{g}\frac{P}{\tau}\left(\frac{\mathrm{d}\tau_b}{\mathrm{d}T}\right)^2 + \frac{P\tau}{T^2}\frac{1}{g} > 0, \tag{4.13}$$

for $b = v$ or l, which is positive provided each pure phase equation of state is convex.

Therefore (4.11) is positive, because it is a convex combination of two terms like (4.13). As a consequence, $\det(\mathrm{D}\Phi) > 0$. □

4.2.3 Convexity

Thanks to the parameterization (4.9), we can calculate the adimensioned coefficients defined by (4.2), to prove that

Proposition 4.6. *If both equation of state are convex, and if* $\dfrac{\mathrm{d}P_{\mathrm{sat}}}{\mathrm{d}T} > 0$ *then the mixture equation of state is convex too, i.e. inequalities* (4.4) *hold.*

Proof. We denote by a subscript m the thermodynamic parameters relative to the mixture equation of state.

- **Calculation of** Γ_m. To calculate Γ_m, we first use the chain rule

$$\left(\frac{\partial \tau}{\partial T}\right)_s = \left(\frac{\partial y}{\partial T}\right)_s \left(\frac{\partial \tau}{\partial y}\right)_T + \left(\frac{\partial \tau}{\partial T}\right)_y.$$

  Then the differentiation of the definition of mixture entropy shows that

$$\left(\frac{\partial y}{\partial T}\right)_s = \frac{y\dfrac{\mathrm{d}s_v}{\mathrm{d}T} + (1-y)\dfrac{\mathrm{d}s_l}{\mathrm{d}T}}{s_l - s_v},$$

  which leads to

$$\left(\frac{\partial \tau}{\partial T}\right)_s = -\frac{y\dfrac{\mathrm{d}s_v}{\mathrm{d}T} + (1-y)\dfrac{\mathrm{d}s_l}{\mathrm{d}T}}{s_l - s_v}(\tau_l - \tau_v) + y\frac{\mathrm{d}\tau_v}{\mathrm{d}T} + (1-y)\frac{\mathrm{d}\tau_l}{\mathrm{d}T}.$$

  Thanks for the Clausius–Clapeyron relation we find

$$\left(\frac{\partial \tau}{\partial T}\right)_s = y\left(\frac{\mathrm{d}\tau_v}{\mathrm{d}T} - \frac{\mathrm{d}T}{\mathrm{d}P}\frac{\mathrm{d}s_v}{\mathrm{d}T}\right) + (1-y)\left(\frac{\mathrm{d}\tau_v}{\mathrm{d}T} - \frac{\mathrm{d}T}{\mathrm{d}P}\frac{\mathrm{d}s_l}{\mathrm{d}T}\right),$$

  which is negative according to what we did for the Jacobian of Φ. Therefore

$$\Gamma_m = -\frac{T}{\tau}\left(\frac{\partial \tau}{\partial T}\right)_s \geq 0.$$

- **Calculation of** γ_m. As $P = P_{\mathrm{sat}}(T)$ in the saturation area, we have

$$\left(\frac{\partial \tau}{\partial P}\right)_s = \frac{\mathrm{d}T_{\mathrm{sat}}}{\mathrm{d}P}\left(\frac{\partial \tau}{\partial T}\right)_s.$$

  Thus $\gamma_m = \Gamma_m \dfrac{T}{P}\left(\dfrac{\mathrm{d}P}{\mathrm{d}T}\right)_{sat} \geq 0.$

- **Calculation of g_m.** By using the identity

$$\left(\frac{\partial T}{\partial s}\right)_\tau \left(\frac{\partial s}{\partial \tau}\right)_T \left(\frac{\partial \tau}{\partial T}\right)_s = -1,$$

we have

$$\left(\frac{\partial T}{\partial s}\right)_\tau = -\frac{1}{\left(\frac{\partial s}{\partial \tau}\right)_T \left(\frac{\partial \tau}{\partial T}\right)_s}.$$

Along an isotherm we have $\mathrm{d}s = (s_v - s_l)\mathrm{d}y$, and $\mathrm{d}\tau = (\tau_v - \tau_l)\mathrm{d}y$, so that

$$\left(\frac{\partial s}{\partial \tau}\right)_T = \left(\frac{\mathrm{d}P}{\mathrm{d}T}\right)_{sat}.$$

Therefore, we find

$$\left(\frac{\partial T}{\partial s}\right)_\tau = \left(\frac{\mathrm{d}T}{\mathrm{d}P}\right)_{sat} \frac{\Gamma_m T}{\tau},$$

which induces $\gamma_m g_m = \Gamma_m^2$. As $\gamma_m \geq 0$, this means that $g_m \geq 0$.

Therefore, we proved that $g_m \geq 0$, $\gamma \geq 0$, and that $\gamma_m g_m - \Gamma_m^2 = 0$, so that the convexity of energy is ensured. □

4.3 Behavior near a phase transition boundary

4.3.1 Adimensioned coefficients

In that section, we keep on denoting by the subscript m the thermodynamic coefficients of the mixture equation of state, the coefficients with no subscript being the one of the pure phase.

In [42] (p.121), the following identity is proved

$$\frac{\gamma - \gamma_m}{\gamma_m} = (\gamma g - \Gamma^2)\left(\frac{T}{\tau}\left(\frac{\mathrm{d}s_b}{\mathrm{d}P}\right)_{sat}\right)^2 > 0, \tag{4.14}$$

with $b = v$ or l. This identity proves that isentropes are stiffer in the pure phases than in the mixture. In the same manner it is proved that

$$\frac{\Gamma_m}{\Gamma} = \frac{\gamma_m - \xi}{\gamma - \xi}, \tag{4.15}$$

with $\xi = -\frac{\tau}{P}\left(\frac{\mathrm{d}P}{\mathrm{d}\tau}\right)_{sat}$. As in [42], we suppose that the isentropes can be parameterized by τ, so that

$$\frac{\gamma_m - \xi}{\gamma - \xi} > 0, \tag{4.16}$$

so that Γ is positive too, because $\Gamma_m > 0$.

4.3.2 Retrograde and Regular behavior

In [60], the retrogradicity r was introduced, to study the behavior of isentropes near a phase transition boundary

$$r = \left(\frac{\partial T}{\partial \tau}\right)_P \left(\frac{\mathrm{d}s_b}{\mathrm{d}P}\right).$$

Thanks for (4.3d) and as Γ is positive near a phase transition boundary, $\left(\frac{\partial T}{\partial \tau}\right)_P$ is positive, so that the sign of r is the same as the sign of $\frac{\mathrm{d}s_b}{\mathrm{d}P}$.

We suppose now that a fluid undergoes a rarefaction isentrope : this is the only regular transformation that a fluid can undergo. In the (S,T) plane, this transformation is drawn as a vertical line. As the transformation is undercompressive, the temperature decreases (at least near the phase transition boundary, because $\Gamma > 0$ and $\Gamma_m > 0$). If $r > 0$ then the isentrope crosses the saturation curve from the pure phase to to the mixture phase (as on both of the sides of the left Figure of Figure 4.2 and of the Liquid side of the right Figure of Figure 4.2). In that case, the fluid is said to be *regular*. If r is negative, then the isentrope crosses the saturation curve from the mixture to the pure phase, as on the vapor side of the right Figure of Figure 4.2.

In [42] (p.121), others expressions of r are given

$$r = \frac{\Gamma_m}{\Gamma}\frac{\gamma g - \Gamma^2}{\gamma_m}\frac{\mathrm{d}s_b}{\mathrm{d}T} = \frac{\gamma - \gamma_m}{\gamma_m}\frac{\xi}{\xi - \gamma}.$$

Experiments show that the liquid saturation curve is always regular. The vapor saturation curve can be either regular or retrograde.

4.4 The Van-der-Waals equation of state

A widely used model is the Van-der-Waals one. Its non adimensioned form is

$$\left(P + \frac{an^2}{V^2}\right)(V - nb) = nRT$$

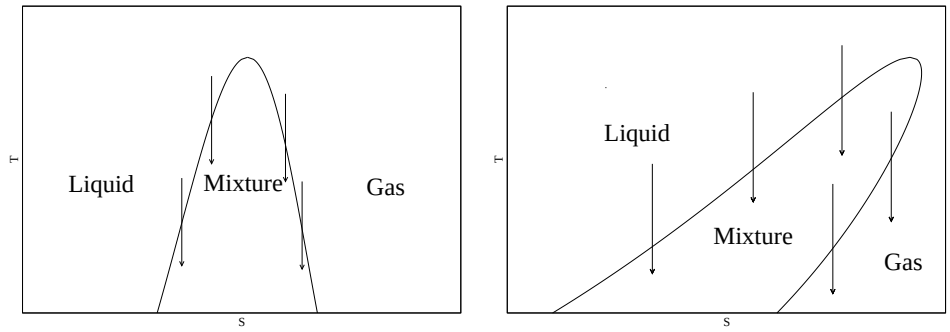

Regular Retrograde

Figure 4.2: The saturation dome in the (S, T) plane. On the left, the fluid is regular: all the isentropes (drawn as arrows) cross the saturation dome from the pure phase to the mixture. On the right, the fluid is retrograde: the isentropes are crossing the liquid saturation curve from the pure phase to the mixture, whereas it is the contrary on the vapor side.

where V is the volume, a and b are given coefficients, and n is the number of atoms. For this model, isotherm are cubic curves that admit either one or three roots. At the limit between these two cases, the cubic has one third order root, the *critical point*. By writing that this cubic is equal to $\lambda(V-V_c)^3$, we find the coordinates of this critical point

$$V_c = 3Nb \qquad P_c = \frac{a}{27b^2} \qquad k_B T_c = \frac{8a}{27b}$$

where the subscribes c are for the thermodynamic variables at the critical point. So that we can adimension the equation of state, and find

$$\left(p + \frac{3}{v^2}\right)(3v - 1) = 8t \tag{4.17}$$

with $p = \dfrac{P}{P_c}$, $v = \dfrac{V}{V_c}$, $t = \dfrac{T}{T_c}$. As we deal with adimensioned variables, we can divide V and V_c by the molar mass, so that we can replace v by τ, the adimensioned specific volume, which gives

$$\left(p + \frac{3}{\tau^2}\right)(3\tau - 1) = 8t \tag{4.18}$$

To ensure the positivity of the temperture, we need that $\tau > 1/3$, what we will suppose in the following. Last, the Van-der-Waals equation of state must

be supplemented with an equation on the entropy to be complete

$$s = c_v \log t + \frac{8}{3} \log\left(\tau - \frac{1}{3}\right)$$

(the 8/3 is for being consistent with the Clapeyron relations).

4.4.1 Convexity domain of Van-der-Waals

Some calculations give the following results for the coefficients (4.2)

$$\begin{aligned} g &= \frac{p\tau}{c_v t} \\ \Gamma &= \frac{8\tau}{c_v(3\tau - 1)} \\ \gamma g - \Gamma^2 &= \frac{\tau^2\left(\frac{2}{\tau^3} + p - \frac{3}{\tau^2}\right)}{c_v t\left(\tau - \frac{1}{3}\right)} \end{aligned}$$

we see that g is always positive. If we suppose that $\gamma g - \Gamma^2$ is positive, then rewriting γ as

$$\gamma = \frac{(\gamma g - \Gamma^2) + \Gamma^2}{g}$$

we see that it implies that $\gamma > 0$. Thus, the only inequality that may fail for ensuring the convexity of the Van-der-Waals equation of state is the positivity of $\gamma g - \Gamma^2$, *i.e.* the positivity of $\left(\frac{\partial P}{\partial \tau}\right)_T$ (thanks for (4.3d)). Actually, we will prove that

Proposition 4.7. *The convexity domain of the Van-der-Waals equation is given by the following alternative*

- *If $t \geq 1$, then $\gamma g - \Gamma^2 \geq 0$ for any τ.*
- *If $t \leq 1$, then $\gamma g - \Gamma^2$ has two roots between which it is negative.*

Proof. For a given case, we suppose that the temperature is positive, so that we rewrite $\gamma g - \Gamma^2$ by eliminating the pressure for the temperature. Then it has the same sign as

$$k_t(\tau) = 4t\tau^3 - 9\tau^2 + 6\tau - 1$$

- If we suppose first that $t \geq 1$, then

$$k_t(\tau) \geq k_1(\tau) = 4\tau^3 - 9\tau^2 + 6\tau - 1$$

and

$$k_1'(\tau) = 12\,(\tau - 1)\left(\tau - \frac{1}{2}\right)$$

moreover, $k_1(1) = 0$, $k_1(1/2) > 0$, and $k_1(1/3) > 0$ so that

$$\forall \tau \geq \frac{1}{3} \qquad k_t(\tau) \geq 0$$

as a consequence,

$$\forall t \geq 1 \quad \forall \tau \geq \frac{1}{3} \qquad k_t(\tau) \geq 0$$

which is the first point we wanted to prove.

- We suppose now that $t < 1$. Then $k_t(1) = 4(t-1) < 0$. As $k_t(1/3) > 0$, and as $\lim_{\tau \to \infty} k_t(\tau) > 0$, and as k_t is a cubic, it has exactly two roots.

□

The two situations are illustrated on Figure 4.3.

4.4.2 Convexification / Maxwell area law

If we look precisely at the Van-der-Waals equation of state, it is hard to understand how it can itself model phase transition: indeed as we saw in section 4.1, the description of phase transition necessitates two equations of state. Actually, the Van-der-Waals equation of state describes

- the heavy phase for high density
- the lightest phase for low density
- *the interaction* of the two phases for intermediate densities.

In the case of the Van-der-Waals equation of state, the optimization theory applied to the interaction of the phases can be interpreted as follows

Proposition 4.8 (Maxwell area law)**.** *For a given temperature, the saturation pressure follows*

$$p_{\text{sat}}(t)(\tau_l - \tau_v) = \int_{\tau_v}^{\tau_l} p(\tau, t)\,\mathrm{d}\tau$$

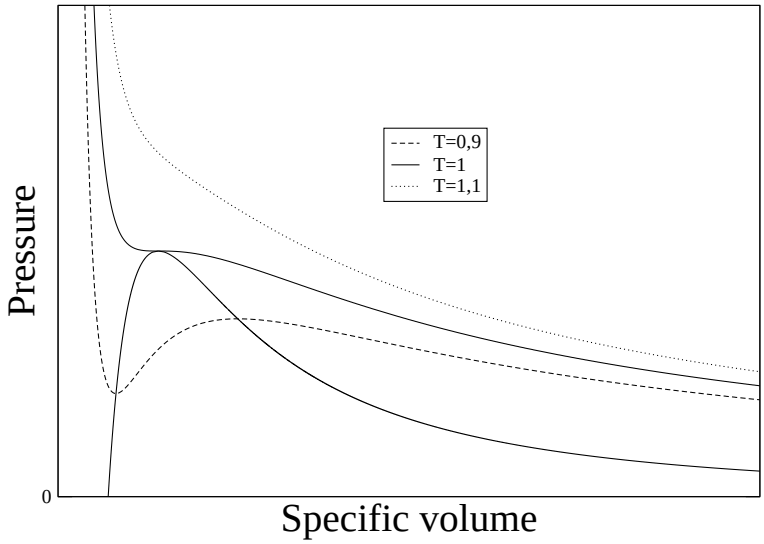

Figure 4.3: Three isotherm: for $t > 1$, the isotherm strictly decresases, whereas for $t < 1$, the isotherm has an increasing part. The set of all the specific volumes for which $\left(\frac{\partial P}{\partial \tau}\right)_t$ vanishes. Between these curves, a fluid described by the Van-der-Waals equation of state is not stable.

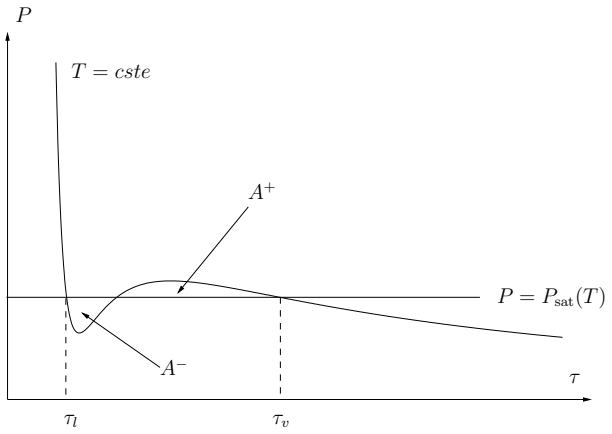

Figure 4.4: The Maxwell' area law proved in Proposition 4.8 means that the line $p = p_{\text{sat}}$ is such that the area under the curve (A^-) and above the curve (A^+) are equal.

Proof. Across an isothermic transformation, we have

$$\mathrm{d}g = \tau \mathrm{d}p = \mathrm{d}(p\tau) - p\mathrm{d}\tau$$

so that if we integrate this equation between a point 1 and a point 2, we find

$$g_2(p_2, t) - g_1(p_1, t) = \int_{\tau_1}^{\tau_2} (\mathrm{d}(p\tau) - p(\tau, t)\,\mathrm{d}\tau) = p_2\tau_2 - p_1\tau_1 - \int_{\tau_1}^{\tau_2} p(\tau, t)\,\mathrm{d}\tau$$

Now, if we suppose that $p_1 = p_2 = p_{\text{sat}}(t)$, then $g_1 = g_2$, so that

$$0 = p_{\text{sat}}(t)\tau_2 - p_{\text{sat}}(t)\tau_1 - \int_{\tau_1}^{\tau_2} p(\tau, t)\,\mathrm{d}\tau$$

τ_2 and τ_1 are equal to τ_v and τ_l, because they are respectively high and low density state that have t as a temperature, and $p_{\text{sat}}(t)$ as a pressure. This gives thus

$$p_{\text{sat}}(t)(\tau_l - \tau_v) = \int_{\tau_v}^{\tau_l} p(\tau, t)\,\mathrm{d}\tau$$

□

On Figure 4.4 the geometric interpretation of the Maxwell'area law is shown. To ensure the convexity of the resulting mixture equation of state, we draw the function $T \mapsto P_{\text{sat}}(T)$ on Figure 4.5. As it is always increasing, the mixture equation of state is always convex. The resulting diagram for the convexified Van-der-Waals equation of state is shown on Figure 4.6. The (τ, P) plane is divided into four areas:

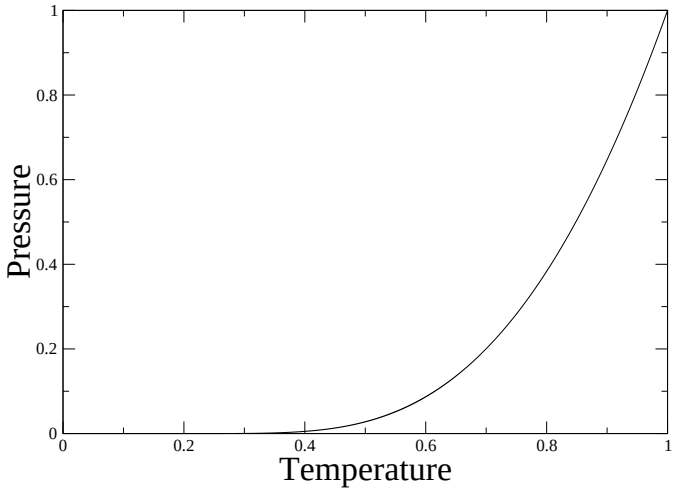

Figure 4.5: The function $t \mapsto p_{\text{sat}}(t)$ is drawn for $0 \leq t \leq 1$. We see that it always increases, so that the resulting mixture equation of state is convex.

- Above the supercritical isotherm, the Van-der-Waals equation of state describes a supercritical fluid.

- Under the supercritical isotherm, outside of the binodal, the equation of state describes a pure phase (liquid on the left, and vapor on the right).

- Under the supercritical isotherm, between the binodal and the spinodal, the pure phase is stable, but the mixture is more stable.

- Inside the spinodal: only the mixture is stable.

Thus, the Van-der-Waals equation of state describes well what we wanted on Figure 4.1. Nevertheless, it is unable to describe arbitrary metastable states. That is why we will not use this model: we will see indeed in the Chapter 6 that we need arbitrary metastable states to solve the Riemann problem. Moreover, as it is stated in [60], the shock structure found for the Euler equations with Van-der-Waals equation of state in [57] does not match with any experiment.

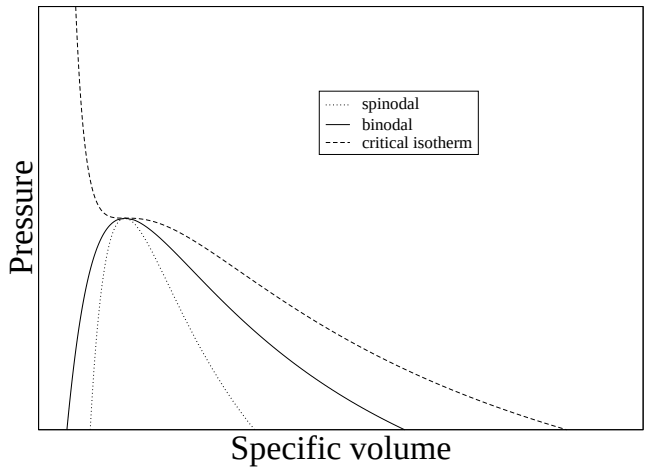

Figure 4.6: Eventually, the (P, τ) plane, under the supercritical part, is divided into 3 parts: one in which the pure phase is stable, one in which the equation of state is stable, but in which the most stable is the mixture (between the binodal and the spinodal curve), and one in which only the mixture is stable (inside the spinodal).

4.5 Two equations of state model

4.5.1 Validity domain of an equation of state

To compute quickly a solution of the Riemann Problem for fluid flows, simplified equation of state (perfect gas of stiffened gas for example) are often preferred to tabulated ones. Nevertheless such equations of state have often only a narrow range of validity, out of which they do not have a physical behavior (negative energy, non convexity).

If we want to use a simplified EOS for both liquid and vapor, we have to care not only about the physical behavior of the two EOS, but also about the mixture EOS computed. If we look at the properties needed in section 4.1, we see that the property $\frac{\mathrm{d}P_{\mathrm{sat}}}{\mathrm{d}T} > 0$ is fundamental to ensure the local convexity of energy. Nevertheless, it is not always true as we show now on examples.

4.5.2 Two perfect gas

This model was proposed by [33, 31]. The two phases are modeled with a perfect gas equation of state. To complete the equation of state, we suppose moreover that $C_v = 1$ for each fluid. We denote by $\overline{\Gamma}_i$ the Grüneisen coefficient of the phase i. Then we have

$$\varepsilon_i(P,\tau) = \frac{P\tau}{\overline{\Gamma}_i}, \tag{4.19a}$$

$$s_i(P,T) = \log\left(T\left(\frac{\overline{\Gamma}_i T}{P}\right)^{\overline{\Gamma}_i}\right), \tag{4.19b}$$

$$\mu_i(P,T) = (\overline{\Gamma}_i + 1)T - T\log\left(T\left(\frac{\overline{\Gamma}_i T}{P}\right)^{\overline{\Gamma}_i}\right). \tag{4.19c}$$

The equation $\mu_1(P,T) = \mu_2(P,T)$ can be explicitly solved to get $P = \beta T$, with $\beta = \exp(1)\left(\frac{\Gamma_2^{\Gamma_2}}{\Gamma_1^{\Gamma_1}}\right)^{\frac{1}{\Gamma_1-\Gamma_2}}$. We see here that the condition $\frac{\mathrm{d}P_{\mathrm{sat}}}{\mathrm{d}T} > 0$ always holds. The limits of the saturation dome are given by the equations

$$T = \varepsilon = \frac{P_{\mathrm{sat}}(T)\tau_i(T)}{\Gamma_i}$$

which gives $\tau_i(T) = \frac{\Gamma_i}{\beta}$. Thus, $T \mapsto \tau_i(T)$ is a constant function. In particular, the critical point does not exist. If we decide for example that $\Gamma_1 < \Gamma_2$

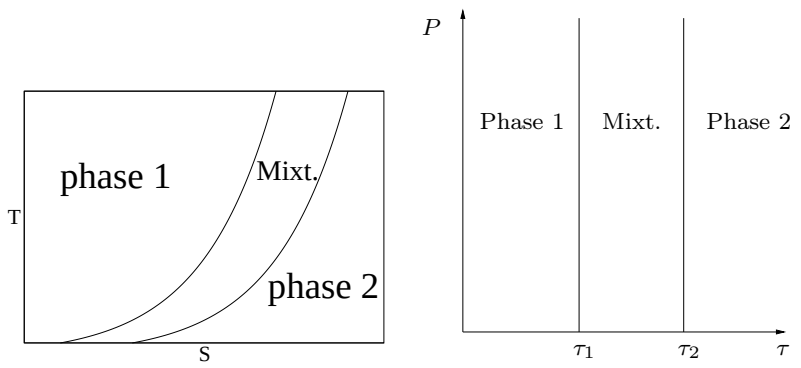

Figure 4.7: Shape of the saturation dome for two perfect gas. We note that the fluid is always retrograde.

then we get the projections of the phase diagram in the (P, τ) plane and in the (S, T) plane that is drawn on Figure 4.7. The mixture equation of state can be explicitly calculated:

$$\begin{cases} P(\tau,\varepsilon) = \Gamma_2 \dfrac{\varepsilon}{\tau} & \text{if} \quad \tau \leq \tau_2 \\ P(\tau,\varepsilon) = \Gamma_2 \dfrac{\varepsilon}{\tau_2} = \Gamma_1 \dfrac{\varepsilon}{\tau_1} & \text{if} \quad \tau_2 \leq \tau \leq \tau_1 \\ P(\tau,\varepsilon) = \Gamma_1 \dfrac{\varepsilon}{\tau} & \text{if} \quad \tau_1 \leq \tau \end{cases}$$

Nevertheless, we remark that the most heavy phase is described by the lowest adiabatic coefficient, which is in contradiction with what is described for example in [67] (chapter XI). Thus, the model with two perfect gas is a good mathematical model because the mixture equation of state can be explicitly calculated, but it cannot give a good account for the physic.

4.5.3 Two stiffened gas

We model the two phases of a fluid with the Stiffened gas equation of state, for which we have (see [38])

$$\varepsilon(P,\tau) = \frac{P + \overline{\gamma} P^{\infty}}{\overline{\gamma} - 1} \tau + q \tag{4.20a}$$

$$s(P,T) = C_v \log\left(\frac{T^{\overline{\gamma}}}{(P + P^{\infty})^{\overline{\gamma}-1}} \right) + q' \tag{4.20b}$$

$$G(P,T) = (\overline{\gamma} C_v - q')T - C_v T \log\left(\frac{T^{\overline{\gamma}}}{(P + P^{\infty})^{\overline{\gamma}-1}} \right) + q \tag{4.20c}$$

Phase	$\overline{\gamma}$	P^∞	C_v	q	q'
Vapor	1.025	0	1956.45	$-237547.$	-24485.
Liquid	2.35	4.10^8 Pa	1077.7	-755269	0.

Table 4.2: Thermodynamic coefficients for the liquid and vapor phase of dodecane.

For this equation of state, the adimensioned coefficients are given by

$$\gamma = \overline{\gamma}\left(1 + \frac{P^\infty}{P}\right) \qquad \Gamma = \overline{\gamma} - 1 \qquad g = \frac{(\overline{\gamma} - 1)P}{P + P^\infty}$$

$\gamma > 0$ and $g > 0$ are ensured if $\overline{\gamma} > 1$. In [38], the coefficients $q, q', C_v, \overline{\gamma}, P^\infty$ were calculated for the vapor and liquid phases to fit with the saturation curves near $T = 298$K. These coefficients are in Table 4.2. The function $P_{\text{sat}}(T)$ was computed by equaling (4.20c) with the liquid and vapour coefficients of Table 4.2. The resulting $P_{\text{sat}}(T)$ was drawn in Figure 4.8. For the two stiffened gas model, we cannot be sure that the functions $T \mapsto s_v(T) - s_l(T)$ and $T \mapsto \tau_v(T) - \tau_l(T)$ simultaneously vanish. Therefore, the critical point does not really exist. As we saw in the section 4.2, we need that $\dfrac{\mathrm{d}P_{\text{sat}}}{\mathrm{d}T} > 0$ to ensure the convexity of the mixture equation of state. Thus, the model is valid only when $\tau_v(T) - \tau_l(T)$ and $s_v(T) - s_l(T)$ are both positive. In our example, with the coefficients of Table 4.2, the function $T \mapsto P_{\text{sat}}(T)$ are drawn on Figure 4.8. We can see that the limit is near $T = 970\,\mathrm{K}$, for which $\dfrac{\mathrm{d}P_{\text{sat}}}{\mathrm{d}T}$ vanishes.

In this chapter, we presented the main thermodynamic features that are needed to model phase transition. We first gave some definitions to understand why the thermodynamic of phase transition is much more complicated than the thermodynamic of a single phase: this is due to the fact that the two phases might appear simultaneously, in which case the mixture is described by a mixture equation of state, obtained by an entropy optimization criterion. We then emphasized how important is the condition

$$\frac{\mathrm{d}P_{\text{sat}}}{\mathrm{d}T} > 0$$

to ensure the convexity of this mixture equation of state. Finally, we gave two examples: first, the Van-der-Waals equation of state, and then a model

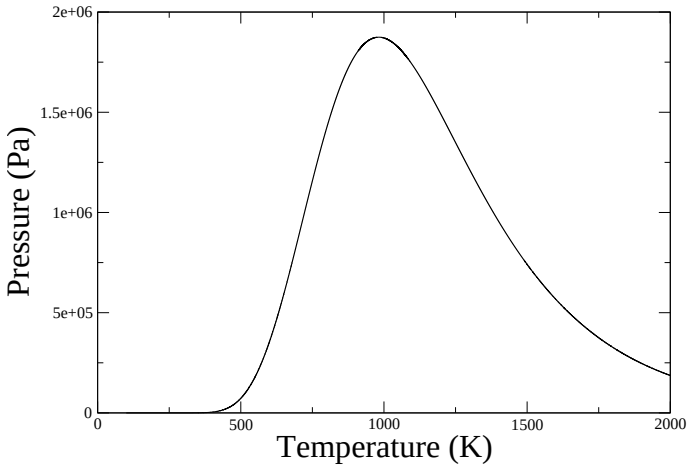

Figure 4.8: Numerical computation of the behavior of $P_{\text{sat}}(T)$ for two phases of stiffened–gas with the coefficients of Table 4.2. For temperatures below 970 K, $T \mapsto P_{\text{sat}}(T)$ increases. For $T \approx 970\,\text{K}$, the function $T \mapsto s_v(T) - s_l(T)$ vanishes and its sign changes, whereas the function $T \mapsto \tau_v(T) - \tau_l(T)$ does not vanish. As a consequence, $T \mapsto P_{\text{sat}}(T)$ does not increase any more and the equation of state is no more valid.

with two equations of state. The properties of these model are sum up in Table 4.3. In the solution of the Riemann problem, we will need arbitrary metastable states, so that in the following, we will choose to use the model with two equations of state.

EOS	supercritical	convexity	Mixture EOS
Van der Waals	Yes	limited	Yes
two EOS	No	Yes	Yes

Table 4.3: Comparison of what can be modelized by Van-der-Waals and two EOS model. It appears that both of them allow to build a convex mixture equation of state. The Van-der-Waals EOS can also model a supercritical fluid, but cannot model arbitrary metastable states, whereas the model with two EOS has the opposite property.

Chapter 5

The Riemann problem for the Eulerian system

In this chapter, we give some foundations and problems that occur when the Riemann problem is solved for the Eulerian system.

A good knowledge of the solution of the Riemann problem for an hyperbolic system is important at least for two reasons. The first is that it is the simplest Cauchy problem that can be posed. The second is for the numerical approximation of such a system with a Godunov' method. Indeed, a fundamental property of the hyperbolic systems is the finite velocity propagation of informations. Therefore, for a given discrete solution Figure 5.1, one may solve the Riemann problem at each interface. Under the CFL condition

$$\frac{\Delta x}{\Delta t} \leq \frac{\max(\sigma_i^+, \sigma_i^-)}{2}$$

the solutions of each of the Riemann problems do not interact (see Figure 5.2). The solution is then projected on the mesh, and this finish one time step. The following time steps are computed in the same way.

This chapter is organised as follows: in section 5.1, we give the general method for solving the Riemann problem for an hyperbolic system of conservation laws, in the case when the fields are genuinely nonlinear or linearly degenerate. Then in section 5.2, we expose how this method can be applied for the Eulerian system, and discuss the hypothesis to ensure the genuinely nonlinearity of the fields $u \pm c$. We eventually expose one well known case in section 5.3, in which the genuinely nonlinearity fail, and we explain how to overcome the difficulty.

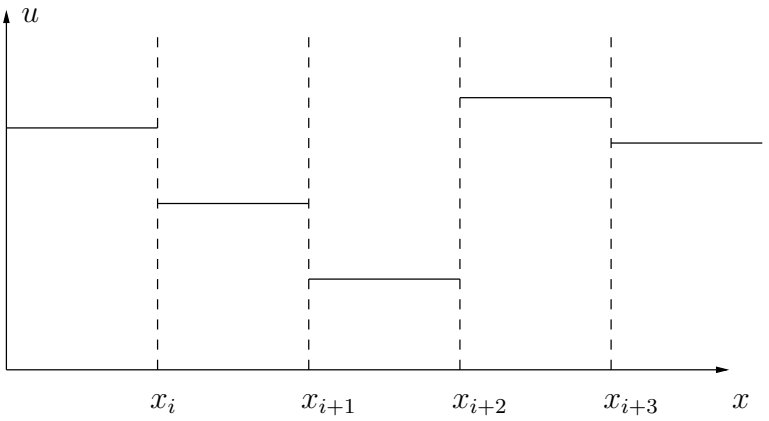

Figure 5.1: A variable u is discretized on a given mesh. On each interface x_i, the Riemann problem can be solved

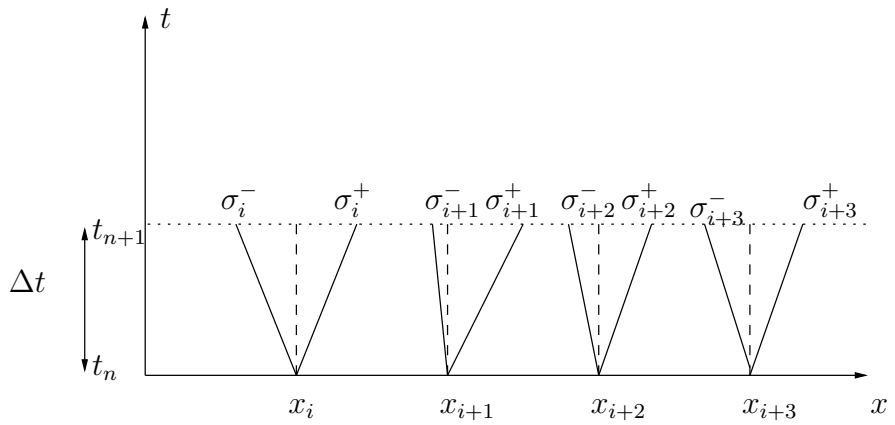

Figure 5.2: On each interface, the Riemann problem is solved. As the system is hyperbolic, the information propagates at a finite velocity. Therefore, the discontinuity on x_i has an effect in the (x,t) plane only in the cone $x_i+\lambda\sigma_i^- t+(1-\lambda)\sigma_i^+ t$, $t \geq 0$, $\lambda \in [0,1]$. Therefore, under the CFL condition, the Riemann problems do not interact.

5.1 The Riemann problem for a system of conservation law

In this section, we aim at giving the basis of the resolution of the Riemann problem for a system of conservation law. We only summarise some definitions and usual theorem of [28], so that all the proofs will be omitted.

We are interested in the solution of the Riemann problem for a given system of conservation law

$$\frac{\partial \mathbf{u}}{\partial t} + \frac{\partial (\mathbf{f}(\mathbf{u}))}{\partial x} = 0 \tag{5.1a}$$

$$\mathbf{u}(x,0) = \begin{cases} \mathbf{u}_L & \text{if} \quad x < 0 \\ \mathbf{u}_R & \text{if} \quad x > 0 \end{cases} \tag{5.1b}$$

where $\mathbf{f}$ is a $\mathbb{R}^p \to \mathbb{R}^p$ regular map. The unknown $\mathbf{u}$ belongs to an open Ω. We recall that the definition of hyperbolicity is

Definition 5.1 (Hyperbolicity)**.** *The system* (5.1a) *is* hyperbolic *provided the Jacobian matrix of* $\mathbf{f}$ *is diagonalisable with real eigenvalues.*

The hyperbolicity is a necessary condition to ensure the well-posedness of the Cauchy problem, at least for a first order linear system [55]. Moreover, it is well known that the hyperbolic systems do not have a unique weak solution: the weak solutions must be selected with an entropy

Definition 5.2 (Entropy)**.** *Assume that* Ω *is convex. Then a convex function* $U : \Omega \mapsto \mathbb{R}$ *is called an* entropy *for the system* (5.1a) *if there exists a function* F*, called the entropy flux such that*

$$U'(\mathbf{u})\mathbf{f}'(\mathbf{u}) = F'(\mathbf{u}).$$

A weak solution $\mathbf{u}$ *of* (5.1a) *is called an entropy solution if* $\mathbf{u}$ *satisfies, for all entropy functions* U *of* (5.1a) *(with an initial condition* $\mathbf{u}_0$*) and for all test functions* $\varphi \in \mathscr{C}^1(\mathbb{R} \times [0, \infty[,\ \varphi \geq 0$

$$\int_0^\infty \int_{\mathbb{R}} \left(U(\mathbf{u}) \frac{\partial \varphi}{\partial t} + F(\mathbf{u}) \frac{\partial \varphi}{\partial x} \right) dx\, dt + \int_{\mathbb{R}} U(\mathbf{u}_0(x)) \varphi(x,0)\, dx \geq 0 \tag{5.2}$$

We denote by λ_k the eigenvalues of $\mathbf{f}'$, and by $\mathbf{r}_k$ and $\mathbf{l}_k$ the right and left eigenvectors of $\mathbf{f}'$. An eigenvalue λ_k is often called, in that context, a *field*.

Definition 5.3. *The field* λ_k *is said to be*

- linearly degenerate *if* $\nabla \lambda_k \cdot \mathbf{r}_k(\mathbf{u}) = 0$ *for all* $\mathbf{u} \in \Omega$,

- genuinely nonlinear *if* $\nabla\lambda_k \cdot \mathbf{r}_k(\mathbf{u}) \neq 0$ *for all* $\mathbf{u} \in \Omega$.

If the field is genuinely nonlinear, then the vector $\mathbf{r}_k(\mathbf{u})$ can be chosen such that

$$\nabla\lambda_k \cdot \mathbf{r}_k(\mathbf{u}) = 1 \tag{5.3}$$

5.1.1 Regular waves

In this subsection, we look for the regular, self-similar solutions of (5.1a), i.e. the solutions $\mathbf{u}(x,t)$ such that there exists $\mathbf{v}$ such that

$$\mathbf{u}(x,t) = \mathbf{v}\left(\frac{x}{t}\right).$$

In that case, we have

$$-\frac{x}{t^2}\mathbf{v}'\left(\frac{x}{t}\right) + \frac{1}{t}\,\mathbf{f}'\left(\mathbf{v}\left(\frac{x}{t}\right)\right)\mathbf{v}'\left(\frac{x}{t}\right) = 0,$$

so that by setting $\xi = \dfrac{x}{t}$

$$(A(\mathbf{v}(\xi)) - \xi\mathbf{I})\,\mathbf{v}'(\xi) = 0.$$

Therefore,

- either
$$\mathbf{v}'(\xi) = 0$$
- or there exists $k \in 1..p$ such that
$$\mathbf{v}'(\xi) = \alpha(\xi)\mathbf{r}_k(\mathbf{v}(\xi)) \qquad \text{and} \qquad \lambda_k(\mathbf{v}(\xi)) = \xi \tag{5.4}$$
If we differentiate the second equation with respect to ξ, we get
$$\nabla\lambda_k(\mathbf{v}(\xi))\mathbf{v}'(\xi) = 1$$
so that
$$\alpha(\xi)\nabla\lambda_k(\mathbf{v}(\xi)) \cdot \mathbf{r}_k(\mathbf{v}(\xi)) = 1$$
this last equation has no solution if the field is linearly degenerate. Contrarily, if it is genuinely nonlinear, we get, thanks to (5.3), $\alpha(\xi) = 1$.

Hence we find either $\mathbf{v}'(\xi) = 0$ or

$$\begin{cases} \mathbf{v}'(\xi) = \mathbf{r}_k(\mathbf{v}(\xi)), \\ \lambda_k(\mathbf{v}(\xi)) = \xi \end{cases}$$

Thus, if we assume that the field is genuinely nonlinear, then if $\mathbf{u}_L$ and $\mathbf{u}_R$ are two states such that

$$\mathbf{v}(\lambda_k(\mathbf{u}_L)) = \mathbf{u}_L \qquad \text{and} \qquad \mathbf{v}(\lambda_k(\mathbf{u}_R)) = \mathbf{u}_R$$

then the function

$$u(x,t) = \begin{cases} \mathbf{u}_L & \text{if } \dfrac{x}{t} < \lambda_k(\mathbf{u}_L) \\ \mathbf{v}\left(\dfrac{x}{t}\right) & \text{if } \lambda_k(\mathbf{u}_L) < \dfrac{x}{t} < \lambda_k(\mathbf{u}_R) \\ \mathbf{u}_R & \text{if } \dfrac{x}{t} > \lambda_k(\mathbf{u}_R) \end{cases}$$

is a regular self similar weak solution of (5.1). The set of all the states that can be linked to a given state $\mathbf{u}_L$ via such a solution is given by

Theorem 5.1 (Theorem 3.1 of [28], p.51)**.** *Assume that the k^{th} field is genuinely nonlinear. Given a state $\mathbf{u}_L \in \Omega$, there exists a curve $\mathcal{R}_k(\mathbf{u}_L)$ of states of Ω that can be connected to $\mathbf{u}_L$ on the right by a k simple wave. Moreover, there exists a parameterisation of $\mathcal{R}_k(\mathbf{u}_L) : \varepsilon \mapsto \Phi_k(\varepsilon)$ defined for $0 \leq \varepsilon \leq \varepsilon_0$, ε_0 small enough, such that*

$$\Phi_k(\varepsilon) = \mathbf{u}_L + \varepsilon \mathbf{r}_k(\mathbf{u}_L) + \frac{\varepsilon^2}{2} D\mathbf{r}_k(\mathbf{u}_L) \cdot \mathbf{r}_k(\mathbf{u}_L) + O\left(\varepsilon^3\right) \tag{5.5}$$

5.1.2 Shock curves

In this subsection, we look for the discontinuous solutions that are piecewise constant. We recall that for a discontinuity that moves at the velocity σ, we have

$$[\mathbf{f}(\mathbf{u})] = \sigma [\mathbf{u}]$$

where the brackets of $[u]$ denotes the jump of u across the discontinuity. So that for a given state $\mathbf{u}_0$, we define the set of all the states that can be connected with a discontinuity by

Definition 5.4 (Rankine-Hugoniot set)**.** *The Rankine-Hugoniot set is the set of all the states $\mathbf{u} \in \Omega$ such that there exists $\sigma(\mathbf{u}_0, \mathbf{u}) \in \mathbb{R}$ with*

$$\sigma(\mathbf{u}_0, \mathbf{u})(\mathbf{u} - \mathbf{u}_0) = \mathbf{f}(\mathbf{u}) - \mathbf{f}(\mathbf{u}_0)$$

The structure of the Rankine-Hugoniot set is given by

Theorem 5.2 (Theorem 4.1 of [28] p.61)**.** *Let $\mathbf{u}_0$ be in Ω. The Rankine-Hugoniot set of $\mathbf{u}_0$ is locally made of p smooth curves $\mathcal{S}_k(\mathbf{u}_0)$, $1 \leq k \leq p$. Moreover, for all k^{th}, there exists a parameterisation of $\mathcal{S}_k(\mathbf{u}_0) : \varepsilon \mapsto \Psi_k(\varepsilon)$, defined for $|\varepsilon| \leq \varepsilon_1$, ε_1 small enough, such that*

$$\Psi_k(\varepsilon) = \mathbf{u}_0 + \varepsilon \mathbf{r}_k(\mathbf{u}_0) + \frac{\varepsilon^2}{2} D\mathbf{r}_k(\mathbf{u}_0) \cdot \mathbf{r}_k(\mathbf{u}_0) + O\left(\varepsilon^3\right) \tag{5.6}$$

Remark 5.1. According to (5.6) and (5.5), if the k^{th} field is genuinely nonlinear, then the Rankine-Hugoniot set and the set of the k simple waves have the same third order development.

The application of the entropy condition (5.2) implies that, for a discontinuity

$$\sigma(\mathbf{u}_L, \mathbf{u}) \left(U(\mathbf{u}) - U(\mathbf{u}_L)\right) \geq F(\mathbf{u}) - F(\mathbf{u}_L)$$

When the field is genuinely nonlinear, only a part of the curve $\mathcal{S}_k$ of Theorem 5.2 satisfies this criterion

Theorem 5.3 (Theorem 5.3 of [28] p.77)**.** *Let (U, F) be an entropy pair. If the k^{th} characteristic field is genuinely nonlinear and if U is strictly convex, then the inequality*

$$\sigma(\mathbf{u}_L, \Psi_k(\varepsilon)) \left(U(\Psi_k(\varepsilon)) - U(\mathbf{u}_L)\right) \geq F(\psi_k(\varepsilon)) - F(\mathbf{u}_L)$$

holds for $|varepsilon|$ small enough, if and only if $\varepsilon \leq 0$.

If the k^{th} characteristic field is linearly degenerate, then

$$\forall \mathbf{u} \in \mathcal{S}_k(\mathbf{u}_L) \qquad \sigma(\mathbf{u}_L, \mathbf{u}) \left(U(\mathbf{u}) - U(\mathbf{u}_L)\right) = F(\mathbf{u}) - F(\mathbf{u}_L)$$

5.1.3 Wave curves

If we summarize the results of the previous subsections, given a state $\mathbf{u}_L$,

- either the field k is linearly degenerate, then no regular k wave exists from $\mathbf{u}_L$, but the whole Rankine-Hugoniot set is composed of states that ensure the entropy condition,
- or the field is genuinely nonlinear, then the states that can be reached with a regular wave or an admissible shock is a curve, tangent to $\mathbf{r}_k(\mathbf{u}_0)$, composed on one side of the regular waves, and on the other of the admissible Rankine Hugoniot states.

that is why we define

Definition 5.5 (Wave curve)**.** *We define the locally the k* wave curve χ_k *by*

- *if k is genuinely nonlinear,*

$$\chi_k(\varepsilon, \mathbf{u}_L) = \begin{cases} \Phi_k(\varepsilon) & \text{if} \quad \varepsilon \geq 0 \\ \Psi_k(\varepsilon) & \text{if} \quad \varepsilon \leq 0 \end{cases}$$

- *if the field k is linearly degenerate*

$$\chi_k(\varepsilon, \mathbf{u}_L) = \Psi_k(\varepsilon)$$

Remark 5.2. The wave curves are often globally defined, not only for a neighbourhood of $\mathbf{u}_0$ as it is done in Definition 5.5. Nevertheless, their global definition (for example the fact that they do not have double point), is deeply linked with the global behaviour of the eigenvalues of λ_k and their derivative, see [42] for the exact conditions in the case of the Eulerian system.

Once the wave curves are identified, the existence of a solution for the Riemann problem is proved in

Theorem 5.4 (Theorem 6.1 of [28] p.84)**.** *Assume that for all $k = 1 \dots p$ the k^{th} field is either genuinely nonlinear or linearly degenerate. Then for all $\mathbf{u}_L \in \Omega$, there exists a neighbourhood $\mathscr{O}$ of $\mathbf{u}_L$ in Ω such that: if $\mathbf{u}_R$ belongs to $\mathscr{O}$, the Riemann problem has a weak solution that consists of at most $p+1$ constant states separated by a regular wave or a entropy admissible discontinuity. Moreover, a weak solution of this kind is unique.*

The different results exposed in this section thus give a way of solving the Riemann problem for an hyperbolic system of conservation law:

1. Identify and order the eigenvalues of $\mathbf{f}'$
2. Compute the left and right eigenvectors for each eigenvalues
3. Identify for each field whether it is genuinely nonlinear or linearly degenerate
4. Calculate an entropy for the system.
5. For each field, compute the wave curve χ_k (in particular, exclude the discontinuities for which the entropy growth criterion fails).
6. Finally, look for a solution of the form

$$\mathbf{u}_R = \chi_p(\varepsilon_p, \chi_{p-1}(\varepsilon_{p-1}, \dots \chi_1(\varepsilon_1, \mathbf{u}_L) \dots))$$

where the ε_k are to be determined.

5.2 Application to the Eulerian system

5.2.1 Eigenvalues

In this section, we apply the results of the previous section to the one dimensional Eulerian system

$$\begin{cases} \dfrac{\partial \rho}{\partial t} + \dfrac{\partial (\rho u)}{\partial x} = 0 \\ \dfrac{\partial (\rho u)}{\partial t} + \dfrac{\partial (\rho u^2 + P)}{\partial x} = 0 \\ \dfrac{\partial (\rho E)}{\partial t} + \dfrac{\partial ((\rho E + P)u)}{\partial x} = 0 \end{cases}$$

where ρ is the density, u the velocity, P the pressure, and E is the total energy $E = \dfrac{u^2}{2} + \varepsilon$ where ε is the specific internal energy. ε, P and ρ are linked by a thermodynamic relation: the equation of state (see Chapter 4 for the usual properties of this equation of state). As we have already seen in Chapter 1 and Chapter 2, the Eulerian system can be put into the following nonconservative form

$$\frac{\partial}{\partial t} \begin{pmatrix} s \\ u \\ P \end{pmatrix} + \begin{pmatrix} u & 0 & 0 \\ 0 & u & \dfrac{1}{\rho} \\ 0 & \rho c^2 & u \end{pmatrix} \frac{\partial}{\partial x} \begin{pmatrix} s \\ u \\ P \end{pmatrix} = 0$$

where $c^2 = \left(\dfrac{\partial P}{\partial \rho} \right)_s$. In this form, the eigenvalues are evident: the characteristic polynomial is equal to

$$(X - u)((X - u)^2 - c^2)$$

and the eigenvalues are u, $u - c$ and $u + c$.

Proposition 5.1. *If the equation of state is strictly convex, then the Euler system is strictly convex.*

If the equation of state is a mixture equation of state as built in Chapter 4 and if $\dfrac{\mathrm{d}P_{\mathrm{sat}}}{\mathrm{d}T} > 0$ *then the Euler system is strictly hyperbolic.*

Proof. To prove that the system is strictly hyperbolic, we just need to prove that $c > 0$. The first point is straightforward because if the equation of state is strictly convex, then $\gamma > 0$, so that

$$c^2 = \frac{\gamma P}{\rho} > 0$$

As seen in the proof of Proposition 4.6, γ of the mixture is proportional to $\frac{\mathrm{d}P_{\mathrm{sat}}}{\mathrm{d}T} > 0$. Therefore c^2 is strictly positive, so that the system is strictly hyperbolic. □

5.2.2 Eigenvectors

The eigenvectors can be chosen as

$$\begin{array}{lll} \text{for the eigenvalue} & u-c & \mathbf{r}_1 = (0, 1, -\rho c) \\ \text{for the eigenvalue} & u & \mathbf{r}_2 = (1, 0, 0) \\ \text{for the eigenvalue} & u+c & \mathbf{r}_3 = (0, 1, \rho c) \end{array}$$

By inverting the matrix $(\mathbf{r}_1, \mathbf{r}_2, \mathbf{r}_3)$, we find the left eigenvectors

$$\begin{array}{lll} \text{for the eigenvalue} & u-c & \mathbf{l}_1 = \left(0, \dfrac{1}{1+c^2}, -\dfrac{c}{\rho(1+c^2)}\right) \\ \text{for the eigenvalue} & u & \mathbf{l}_2 = (1, 0, 0) \\ \text{for the eigenvalue} & u+c & \mathbf{l}_3 = \left(0, \dfrac{1}{1+c^2}, \dfrac{c}{\rho(1+c^2)}\right) \end{array}$$

5.2.3 Genuinely nonlinearity and linearly degeneracy

In Chapter 4, we only used first order thermodynamic parameters. In [59], the following second order thermodynamic parameter is introduced

Definition 5.6 (Fundamental derivative)**.** *The fundamental derivative is defined as*

$$\mathscr{G} = -\frac{\tau}{2} \frac{\left(\dfrac{\partial^3 \varepsilon}{\partial \tau^3}\right)_s}{\left(\dfrac{\partial^2 \varepsilon}{\partial \tau^2}\right)_s} \tag{5.7}$$

We remark that it is defined if $\left(\dfrac{\partial^2 \varepsilon}{\partial \tau^2}\right)_s$ does not vanish, but as we supposed that the equation of state is strictly convex, there is not matter. Moreover, as the denominator of (5.7) is positive, and as $P = -\left(\dfrac{\partial \varepsilon}{\partial \tau}\right)_s$, the sign of the fundamental derivative is the same as the one of $\left(\dfrac{\partial^2 P}{\partial \tau^2}\right)_s$.

The nature of the fields is given by

Theorem 5.5. *The field u is always linearly degenerate. The fields $u \pm c$ are genuinely nonlinear provided*

$$\left(\frac{\partial^2 P}{\partial \tau^2}\right)_s \neq 0. \tag{5.8}$$

Proof. The first point is straightforward. To prove the second point, we translate (5.8) in the variables ρ, s: we differentiate once $P(1/\rho, s)$ to get

$$c^2 = -\frac{1}{\rho^2}\left(\frac{\partial P}{\partial \tau}\right)_s \left(\frac{1}{\rho}, s\right)$$

we then differentiate with respect to ρ the above expression of $-\rho^2 c^2$, to find

$$-2\rho c\left(c + \rho\left(\frac{\partial c}{\partial \rho}\right)_s\right) = -\frac{1}{\rho^2}\left(\frac{\partial^2 P}{\partial \tau^2}\right)_s$$

Last, using $\left(\frac{\partial c}{\partial P}\right)_s = \left(\frac{\partial c}{\partial \rho}\right)_s \left(\frac{\partial \rho}{\partial P}\right)_s$ gives

$$1 + \rho c\left(\frac{\partial c}{\partial P}\right)_s = \frac{1}{\rho^3 c^2}\left(\frac{\partial^2 P}{\partial \tau^2}\right)_s$$

Now, if we compute the dot product of $\mathbf{r}_1$ by $\nabla(u-c)$, we get

$$\mathbf{r}_1 \cdot \nabla(u-c) = (0, 1, -\rho c) \cdot \left(-\left(\frac{\partial c}{\partial s}\right)_P, 1, -\left(\frac{\partial c}{\partial P}\right)_s\right) = 1 + \rho c\left(\frac{\partial c}{\partial P}\right)_s$$

so that

$$\mathbf{r}_1 \cdot \nabla(u-c) = \frac{1}{\rho^3 c^2}\left(\frac{\partial^2 P}{\partial \tau^2}\right)_s$$

which ends the proof. The proof for the field $u + c$ is the similar. □

Thus, the genuinely nonlinearity of the fields $u \pm c$ is equivalent to the fact that the fundamental derivative does not vanish. The effect of the sign of the fundamental derivative will be studied in the next subsection.

5.2.4 Some numerical examples of fundamental derivative

Stiffened gas

We recall that for the stiffened gas equation of state, we found in Chapter 4

$$\begin{cases} \gamma = \overline{\gamma}\left(1 + \dfrac{P^\infty}{P}\right) \\ \Gamma = \overline{\gamma} - 1 \\ g = \dfrac{(\overline{\gamma} - 1)P}{P + P^\infty} \end{cases}$$

this means that $\left(\frac{\partial^2 \varepsilon}{\partial \tau^2}\right)_s = \frac{\overline{\gamma}(P+P^\infty)}{\tau}$. If we derive again, we have

$$\left(\frac{\partial^3 \varepsilon}{\partial \tau^3}\right)_s = \overline{\gamma}\,\frac{\left(\frac{\partial P}{\partial \tau}\right)_s \tau - (P+P^\infty)\left(\frac{\partial \tau}{\partial \tau}\right)_s}{\tau^2} = -\frac{\overline{\gamma}(\overline{\gamma}+1)(P+P^\infty)}{\tau^2}$$

Eventually, we find

$$\mathscr{G} = \frac{\overline{\gamma}+1}{2}$$

In particular, $\mathscr{G}$ is positive.

Mixture equation of state

Here, we compute the fundamental derivative of the mixture equation of state given by optimization of Table 4.2. It is computed only in the area we are interested in, i.e. for $y \in [0;1]$, and for temperature corresponding to a convex equation of state. For such states, the equation of state is parameterized by the mass fraction of the vapor y and the temperature T.

$$\begin{cases} s = y s_v(T, P_{\text{sat}}(T)) + (1-y) s_l(T, P_{\text{sat}}(T)) \\ \tau = y \tau_v(T, P_{\text{sat}}(T)) + (1-y) \tau_l(T, P_{\text{sat}}(T)) \end{cases}$$

For a given perturbation $\mathrm{d}T$, we have

$$\begin{cases} \mathrm{d}s = \left(s_v(T, P_{\text{sat}}(T)) - s_l(T, P_{\text{sat}}(T))\right)\mathrm{d}y + y\dfrac{\mathrm{d}s_v}{\mathrm{d}T}(T, P_{\text{sat}}(T))\,\mathrm{d}T \\ \qquad\qquad + (1-y)\dfrac{\mathrm{d}s_l}{\mathrm{d}T}(T, P_{\text{sat}}(T))\,\mathrm{d}T \\ \mathrm{d}\tau = \left(\tau_v(T, P_{\text{sat}}(T)) - \tau_l(T, P_{\text{sat}}(T))\right)\mathrm{d}y + y\dfrac{\mathrm{d}\tau_v}{\mathrm{d}T}(T, P_{\text{sat}}(T))\,\mathrm{d}T \\ \qquad\qquad + (1-y)\dfrac{\mathrm{d}\tau_l}{\mathrm{d}T}(T, P_{\text{sat}}(T))\,\mathrm{d}T \end{cases}$$

If the entropy is constant then

$$\mathrm{d}y = \frac{y\dfrac{\mathrm{d}s_v}{\mathrm{d}T}(T, P_{\text{sat}}(T)) + (1-y)\dfrac{\mathrm{d}s_l}{\mathrm{d}T}(T, P_{\text{sat}}(T))}{s_v(T, P_{\text{sat}}(T)) - s_l(T, P_{\text{sat}}(T))}\,\mathrm{d}T$$

and the corresponding $\mathrm{d}\tau$ can be computed. The fundamental derivative is then computed with the classical finite difference approximation

$$\left(\frac{\partial^2 P}{\partial \tau^2}\right)_s \approx \frac{P(\tau+\mathrm{d}\tau) + P(\tau-\mathrm{d}\tau) - 2P(\tau)}{2(\mathrm{d}\tau)^2}$$

The results are shown on Figure 5.3. They prove that even if $\mathscr{G}$ is positive for both equation of state, the mixture equation of state might have a negative fundamental derivative.

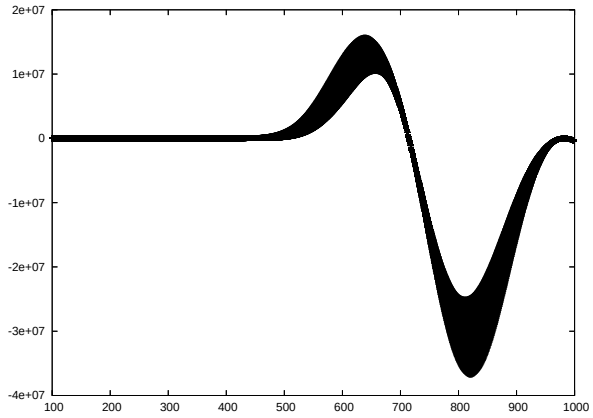

Figure 5.3: For all y, we compute $T \mapsto \mathscr{G}(T)$. We remark that even if $\mathscr{G}$ is positive for both equation of state, the mixture equation of state might have a negative fundamental derivative.

5.2.5 Wave curves

The sign of $\mathscr{G}$ determines whether the Hugoniot curve and the isentropes are convex or not in the (τ, P) plane. We will suppose in the following that $\mathscr{G}$ is positive, so that no undercompressive discontinuity nor expansion fans can exist (see [59, 64, 65]).

Regular waves

The computation of the regular wave in the phase space (ρ, u, P) can be led thanks to

Theorem 5.6. *We define ℓ as*

$$\ell = \int \frac{c}{\rho}\, d\rho$$

Then s and $u \pm \ell$ are Riemann invariants for the wave $u \mp c$, i.e. they are constant through the regular waves.

Proof. Applying (5.4), we have, across a regular wave of the field $u - c$

$$\begin{aligned} \frac{\mathrm{d}s}{\mathrm{d}\xi} &= 0 \\ \frac{\mathrm{d}u}{\mathrm{d}\xi} &= \alpha(\xi) \\ \frac{\mathrm{d}P}{\mathrm{d}\xi} &= -\rho c \alpha(\xi) \end{aligned} \tag{5.9}$$

We see that the entropy is indeed constant across the regular waves of the field $u - c$. We have too

$$\begin{aligned}
\frac{\mathrm{d}(u+\ell)}{\mathrm{d}\xi} &= \frac{\mathrm{d}u}{\mathrm{d}\xi} + \frac{\mathrm{d}\ell}{\mathrm{d}\xi} \\
&= \frac{\mathrm{d}u}{\mathrm{d}\xi} + \left(\frac{\partial \ell}{\partial s}\right)_\rho \frac{\mathrm{d}s}{\mathrm{d}\xi} + \left(\frac{\partial \ell}{\partial \rho}\right)_s \frac{\mathrm{d}\rho}{\mathrm{d}\xi} \\
&= \frac{\mathrm{d}u}{\mathrm{d}\xi} + \left(\frac{\partial \ell}{\partial s}\right)_\rho \frac{\mathrm{d}s}{\mathrm{d}\xi} + \left(\frac{\partial \ell}{\partial \rho}\right)_s \left(\frac{\partial \rho}{\partial P}\right)_s \frac{\mathrm{d}P}{\mathrm{d}\xi} \\
&= \alpha(\xi) - \rho c \frac{c}{\rho}\frac{1}{c^2}\alpha(\xi) \\
\frac{\mathrm{d}(u+\ell)}{\mathrm{d}\xi} &= 0
\end{aligned}$$

so that $u+\ell$ is constant across the regular waves of the field $u-c$. The proof for the field $u + c$ follows the same arguments. □

With this last theorem, we have a natural parameterisation of the regular waves in the phase plane. Indeed, if we choose for example P as a parameter, we have immediately a second thermodynamic parameter, s because it is constant, and then the velocity is computed with the Riemann invariant $u \pm \ell$.

The direction in the phase space of the regular waves is specified by the following

Theorem 5.7. *If the fundamental derivative is positive, then*

- *the pressure and the density decrease across a regular wave,*
- *the velocity increases for the left field, whereas it increases for the right field.*

If the fundamental derivative is negative, then all the monotonies are inverted.

Proof. We first prove the properties for the left wave. We know that for such a wave, $\lambda_k(\mathbf{v}(\xi)) = \xi$, so that λ_k increases across a regular wave. Applying that to the field $u - c$, we find

$$\frac{\mathrm{d}(u-c)}{\mathrm{d}\xi} = \alpha(\xi)\left(1 + \rho c\left(\frac{\partial c}{\partial P}\right)_s\right) = \alpha(\xi)\left(\frac{\partial^2 P}{\partial \tau^2}\right)_s$$

so that α has the same sign as $\mathscr{G}$. Therefore, thanks to (5.9), we see that if $\mathscr{G}$ is positive, then u increases and P decreases. Moreover, (4.3c) proves that ρ has the same monotony as P. Contrarily, if $\mathscr{G}$ is negative, then ρ and P increase, and u decreases.

The proof can be adapted to the case of the right field $u + c$. □

Rankine-Hugoniot relations

For the Eulerian system, the Rankine-Hugoniot relations reads

$$\begin{cases} \sigma\left[\rho\right] = \left[\rho u\right] \\ \sigma\left[\rho u\right] = \left[\rho u^2 + P\right] \\ \sigma\left[\rho E\right] = \left[(\rho E + P)u\right] \end{cases} \tag{5.10}$$

so that if we are interested in the jump relations for the field u, which is linearly degenerate, u is constant across the discontinuity, so that $\sigma = u$. The other relation give the equality of pressures. Therefore

Theorem 5.8. *The jump relations across the linearly degenerate field u give*

$$u_1 = u_2 \qquad P_1 = P_2$$

As we aim at calculating the wave curve, the best is to parameterise it with a thermodynamic variable. We thus need to eliminate σ from (5.10). In some cases, the Rankine-Hugoniot relations can be put in the following form

Theorem 5.9. *We denote by $M = \rho(u - \sigma)$ (according to* (5.10)*, M is constant across the discontinuity). If $M \neq 0$, then the system* (5.10) *is equivalent to*

$$M = \frac{u_1 - u_0}{\tau_1 - \tau_0} \tag{5.11a}$$

$$M^2 = -\frac{P_1 - P_0}{\tau_1 - \tau_0} \tag{5.11b}$$

$$\varepsilon_1 - \varepsilon_0 + \frac{1}{2}\left(P_1 + P_0\right)\left(\tau_1 - \tau_0\right) = 0 \tag{5.11c}$$

We remark that (5.11b) and (5.11c) are purely thermodynamic. In the plane (τ, P), (5.11b) is the equation of a straight line, *the Rayleigh line*, and (5.11c) is the equation of the *Hugoniot curve*. Satisfying equations (5.11b) and (5.11c) is equivalent to intersecting the Rayleigh line with the Hugoniot curve (see Figure 5.4). The system (5.11) gives a natural parameterisation of the wave curve in variable (τ, u, P): indeed, given a pressure P_1, one can calculate thanks to (5.11c) the corresponding density. Then M is computed thanks to (5.11b), which allows to calculate u with (5.11a). We remain to determinate which branch of the shocks is to be used. For that, we need to know the behaviour of s along the Hugoniot curve.

Theorem 5.10. *If the fundamental derivative is positive, then s locally increases for increasing P, whereas if the fundamental derivative is negative, s locally increases for decreasing P*

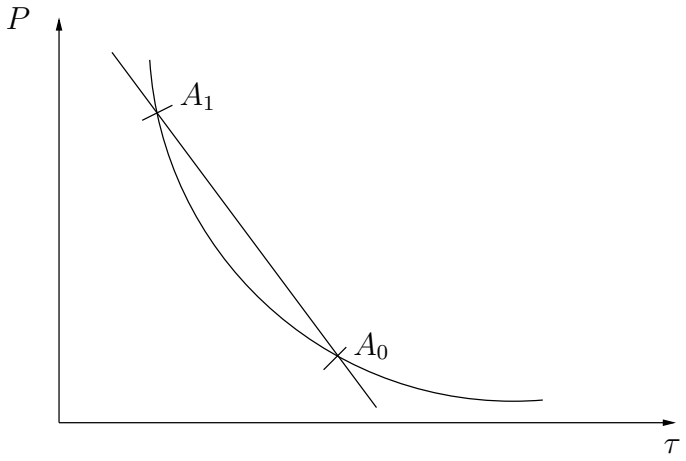

Figure 5.4: Solving (5.11) is equivalent in the thermodynamic plane, to intersecting a line (5.11b) with a curve (5.11c).

Proof. We begin by deriving (5.11c) with respect to a curvilinear abscissa. We find, using the first and second law of thermodynamic

$$Ts' = \frac{1}{2}\left(\tau'(P-P_0) - P'(\tau-\tau_0)\right) \tag{5.12}$$

so that $s'(\tau_0, P_0) = 0$. We differentiate again, to find

$$(Ts')' = \frac{1}{2}\left(\tau''(P-P_0) - P''(\tau-\tau_0)\right)$$

the right hand side vanishes in (τ_0, P_0). If we develop the left hand side, we have

$$T's'(\tau_0, P_0) + Ts''(\tau_0, P_0) = 0$$

so that $s''(\tau_0, P_0) = 0$. We differentiate once more $(Ts')'$ to find

$$(Ts')'' = \frac{1}{2}\left(P'\tau'' + (P-P_0)\tau''' - \tau'P'' - (\tau-\tau_0)P'''\right)$$

if we simplify as for the previous derivatives, we find

$$Ts''' = \frac{1}{2}\left(P'\tau'' - \tau'P''\right)$$

It remains to simplify the right hand side. As P is a function of τ and s, and as $s'(\tau_0, P_0) = 0$ and $s''(\tau_0, P_0) = 0$, we have

$$\begin{aligned} P'(\tau_0, P_0) &= \left(\frac{\partial P}{\partial \tau}\right)_s (P_0, \tau_0)\tau'(\tau_0, P_0) \\ P''(\tau_0, P_0) &= \left(\frac{\partial P}{\partial \tau}\right)_s (P_0, \tau_0)\tau''(\tau_0, P_0) + \left(\frac{\partial^2 P}{\partial \tau^2}\right)_s (\tau_0, P_0)\left(\tau'(\tau_0, P_0)\right)^2 \end{aligned}$$

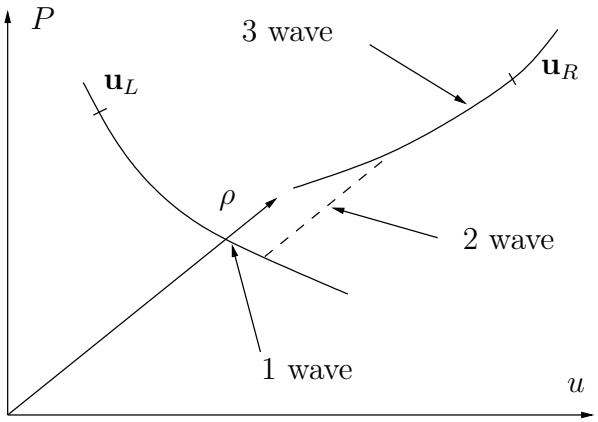

Figure 5.5: The solution of a Riemann problem for the Eulerian system in the phase space (ρ, u, P).

Eventually we find

$$Ts''' = -\frac{1}{2}\left(\frac{\partial^2 P}{\partial \tau^2}\right)_s (\tau_0, P_0)\left(\tau'(\tau_0, P_0)\right)^3$$

We want that $s''' > 0$, i.e. $-\mathscr{G}\tau' > 0$. Thanks to (4.3c), and as $s'(\tau_0, P_0) = 0$, τ' and P' have an opposite sign near A_0. Therefore

- If $\mathscr{G} > 0$, then the entropy increases in the sense of the increasing P.
- If $\mathscr{G} < 0$, then the entropy increases in the sense of the decreasing P.

This ends the proof. □

Projection in the (u, P) plane

We are now able to solve the Riemann problem by following the framework of section 5.1: starting from one point $\mathbf{u}_L$, we compute the curve of all the downstream state that can be linked with $\mathbf{u}_L$ by a 1 wave. Then, starting from one point of this curve, the set of all the states that can be linked with a 2 wave is a straight line $P = cste$, $u = cste$. Last, we compute the states that can be linked with a 3 wave, to the reached point, and we hope that this point is $\mathbf{u}_R$. Such a configuration is shown on Figure 5.5. As the 2 wave is a straight line in the phase space (ρ, u, P), we see that solving the Riemann problem is equivalent to intersecting the 1 wave curve from $\mathbf{u}_L$ and the 3 wave curve from $\mathbf{u}_R$ in the plane (P, u).

5.2.6 Conclusion

In this section, we have shown how to compute the wave curves for the Eulerian system. The solution has a simple structure because we supposed that the fundamental derivative does not vanish. When the fundamental derivative vanishes, the Riemann problem can still be solved, but the structure becomes more complicated [64, 65] or [42, pp.105-108]: for a given field, there are successive composite waves that are built as simple wave or as shock, depending if the fundamental derivative is positive or negative. This is actually the same problem as when one wants to solve the Riemann problem for a scalar hyperbolic equation

$$\frac{\partial u}{\partial t} + \frac{\partial (f(u))}{\partial x} = 0$$

if f supposed to be convex-concave. We thus see that in a usual context, the genuinely nonlinearity of the fields is a necessary condition for keeping a simple structure to the solution of the Riemann problem.

In the context of phase transition, when a wave curve crosses the saturation dome, the first order parameters are discontinuous (as seen in Chapter 4). Thus, $\nabla\lambda$ has no meaning, so that we cannot use the concept of genuinely nonlinearity, and a new wave, connecting one phase to a mixture or another phase, may appear. In the next section, we show some problems that might appear in the context of phase transition, induced by the kinks of the equation of state.

5.3 Shocks and the Liu solution

In this section, we suppose that the fundamental derivative $\mathscr{G}$ is positive.

We saw in section 5.1 that the solution of the Riemann problem is unique in the class of the solutions with simple waves, at least when the states $\mathbf{u}_R$ and $\mathbf{u}_L$ are close enough.

For example, it is natural to ask why a shock cannot be decomposed into two shocks. We denote by $\mathcal{H}_{(\tau_0,P_0)}(\tau, P)$ the Hugoniot curve of the point (τ_0, P_0). To reach a point with a pressure P_2 from a point P_0, we can

- either follow $\mathcal{H}_{(\tau_0,P_0)}$ until P_2.
- or for example, follow $\mathcal{H}_{(\tau_0,P_0)}$ until a point P_1 such that $P_0 < P_1 < P_2$, and then follow $\mathcal{H}_{(\tau_1,P_1)}$ until P_2.

Actually, such a decomposition of a shock might not be stable

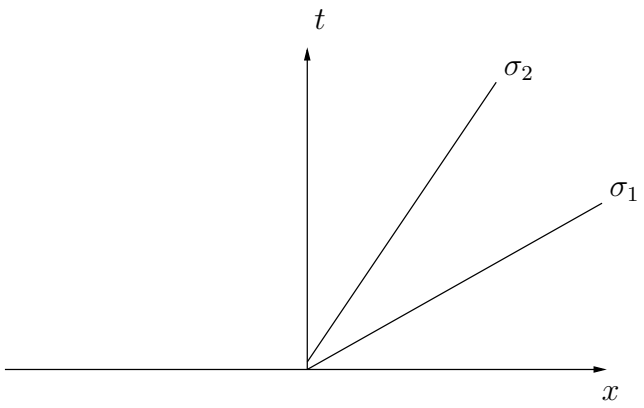

Figure 5.6: The shock decomposition in the (x,t) plane. The second shock (velocity σ_2) must move slower than the precursor shock (velocity σ_1) for the decomposition to be stable.

Theorem 5.11. *We denote by M_1 and M_2 the flux mass of each of the shocks of the previous described shock decomposition. This decomposition is stable provided*

$$M_2^2 < M_1^2$$

Proof. As M is constant across a shock, and as the two shocks have a common point, we have

$$\begin{cases} M_1 = \rho_1(u_1 - \sigma_1) \\ M_2 = \rho_1(u_1 - \sigma_2) \end{cases}$$

If we suppose that the shocks are a 3 wave, then $M < 0$. As stated in the Figure 5.6, the shock decomposition is stable provided $\sigma_1 < \sigma_2$. This induces that $M_1 < M_2$, and as M_1 and M_2 are negative, we find

$$M_1^2 > M_2^2$$

The proof for a left wave is the same. □

Actually, in the usual case of the resolution of the Riemann problem with one equation of state with a positive fundamental derivative, the case stated in Theorem 5.11 cannot happen

Theorem 5.12. *If the entropy increases with the shock strength and if $\Gamma < 2\gamma$, then a shock decomposition is not stable.*

Proof. If we use the theorem 5.4 of [42, p. 102], then we have

$$-\frac{\Delta P}{\Delta \tau} < -\left(\frac{\partial P}{\partial \tau}\right)_s.$$

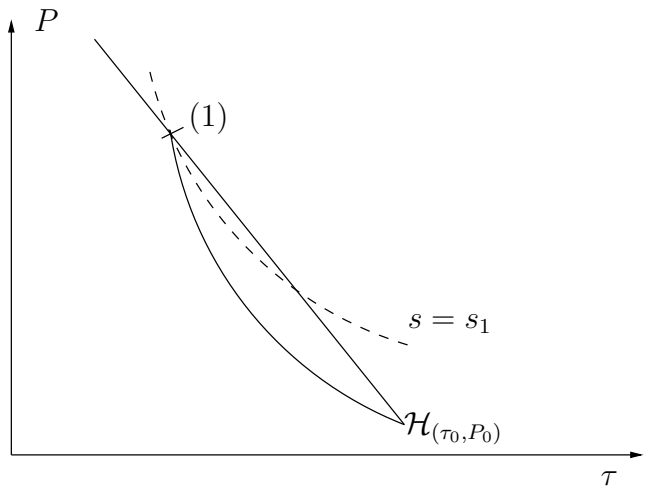

Figure 5.7: The relative behaviour of the Hugoniot curve, the isentrope in the point 1, and the Rayleigh line M_1 in the (τ, P) plane. Thanks to Theorem 5.10 we can state the order of their derivative.

Moreover, as the entropy increases along the Hugoniot curve, the slope of the Hugoniot is less stiff than the isentrope in the point (1) (see Figure 5.7). Therefore the relative slope of the Rayleigh line, the isentrope and the Hugoniot is the one described on Figure 5.7. As the Hugoniot curve $\mathcal{H}_{(\tau_1,P_1)}$ and the isentrope $s = s_1$ are tangent in (1), the Hugoniot curve $\mathcal{H}_{(\tau_1,P_1)}$ is above the Rayleigh line. As a consequence, a Rayleigh line connecting (1) to any point of $\mathcal{H}_{(\tau_1,P_1)}$ is stiffer than the first Rayleigh line. Therefore, the shock decomposition is not stable, according to Theorem 5.11. □

Nevertheless, in the case of phase transition, the case stated in Theorem 5.11 may appear

Theorem 5.13. *We suppose that we are on the gas side of a retrograde boundary mixture-gas. Then for a point (τ_0, P_0) sufficiently close of the gas saturation curve, the Hugoniot crosses the saturation curve. Moreover, the slope of the mixture Hugoniot is smaller than the slope the gaseous Hugoniot. Thus a shock decomposition may be stable.*

Proof. For a retrograde fluid, there exist some thermodynamic states of the gas such that the isentrope comes from the mixture area (see Figure 4.2). As the isentrope and the Hugoniot are tangent, for a point sufficiently close of the saturation curve, the Hugoniot enters too in the mixture zone. Moreover, we know that the slope of the derivative of the mixture isentrope is smaller than the slope of the pure phase isentrope (4.14). Therefore, for a point sufficiently

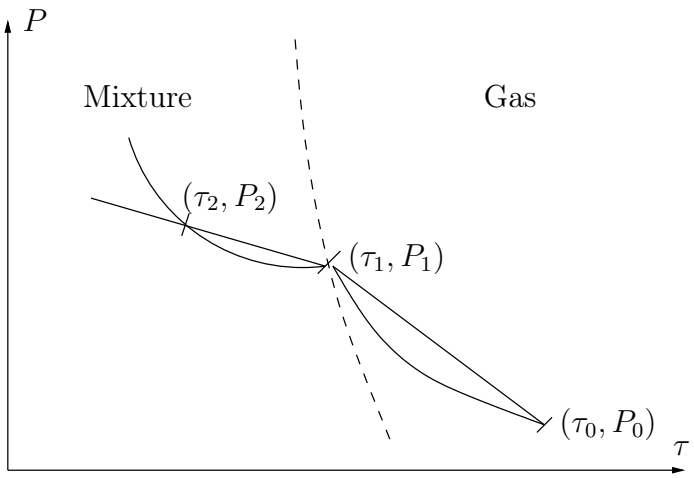

Figure 5.8: For a retrograde fluid, the Hugoniot might enter the mixture zone. The jump in the slopes of the Hugoniot might be negative.

close of the saturation curve, the Hugoniot and the isentrope have nearly the same jump, so that the slope of mixture Hugoniot is smaller than the slope of the gaseous Hugoniot. The situation is shown in Figure 5.8. Therefore, for weak shocks of $\mathcal{H}_{(\tau_0,P_0)}$, the associated Rayleigh line has a smaller slope than the slope of the first Rayleigh line. □

Definition 5.7 (Liu criterion)**.** *A shock solution is said to satisfy the Liu criterion if the slope of the Rayleigh line varies monotonically along the Hugoniot locus for any shock wave.*

If we admit that a solution must satisfy the Liu criterion, then it is clear that the uniqueness is recovered, because the only shock that satisfies the Liu criterion is the one decomposed on point (1) of Figure 5.8.

When the Hugoniot curve is convex, the Liu criterion is equivalent to the classical entropy growth criterion, and when the Hugoniot is no more convex, the Liu criterion gives a unique solution with a shock decomposition. We remark that this criterion always hold in the usual case. Moreover, it has been proven in [40] that the shock decomposition admits a viscosity profile only if the Liu criterion is satisfied.

In this chapter, we gave the basis of the way to solve the Riemann problem for the Eulerian system. We showed that provided the fields $u \pm c$ are

genuinely nonlinear, the solution is very simple. We know that the concept of genuinely nonlinearity has no meaning in the context of phase transition, because the genuinely nonlinearity definition is based on a differential condition, which might not be defined. We showed that the kinks of the equation of state can induce a non-uniqueness of the entropic solution. In the particular context of equilibrium shocks, this non-uniqueness can be overcome with the Liu criterion. In the next section, we will try to solve the Riemann problem, again with phase transition equations of state, but we will moreover try to take into account metastable states.

Chapter 6

The Riemann problem with the Chapman–Jouguet theory

Based on the experiments of [56, 60, 61], we propose to take into account out of thermodynamic equilibrium states for solving the Riemann problem. By "out of equilibrium states" we mean *metastable states*, or *overheated* states, i.e. pure fluids that have a pressure P and a specific volume τ that lie in the saturation dome. Existence of such states is due to some phenomena such as capillarity for example.

In the first section, we recall the main results of the Chapman-Jouguet theory of combustion [28, 18]. Then we apply it in the context of phase transition. In particular, we check whether the model with two equations of state is compatible with the Chapman-Jouguet theory. A condition will be found to ensure the entropy growth criterion. Eventually, we will prove that the closure usually used to close the problem [39], i.e. the CJ closure, leads to a solution that does not depend continuously on its initial data, and this solution will therefore be rejected.

This chapter, except from some details, is a part of [48].

6.1 Reminds on the Chapman–Jouguet theory (see [28, page 142-160])

In [56, 60, 61] it was observed that phase transition waves were self–similar waves, so that Rankine–Hugoniot relations hold across them: $\left[F(U)-\sigma U\right] = 0$, where σ is the velocity of the discontinuity. These relations can be put in

the following form (see [28] for example)

$$\dot{M} = \frac{u_1 - u_0}{\tau_1 - \tau_0}, \tag{6.1a}$$

$$\dot{M}^2 = -\frac{P_1 - P_0}{\tau_1 - \tau_0}, \tag{6.1b}$$

$$\varepsilon_1 - \varepsilon_0 + \frac{1}{2}(P_1 + P_0)(\tau_1 - \tau_0) = 0, \tag{6.1c}$$

where $\dot{M}$ is the flow rate across the wave: $\dot{M} = \rho(u - \sigma)$. The interest of writing the Rankine–Hugoniot relations as in (6.1) is that the two last equations are purely thermodynamic. The equation (6.1b) describes a line in the (τ, P) plane, that is called the Rayleigh line. Equation (6.1c) describes the Crussard curve. The very difference with classical shock relations is that the set of the downstream states is not described with the same equation of state as the upstream one. For that sort of wave, we can use the Chapman–Jouguet theory. Let us remind the main points of that theory (see [28] or [18] for the details and the proofs)

Proposition 6.1 (see [28, p.145])**.** *Suppose that the equation of state $(\tau, s) \mapsto P(\tau, s)$ has the following properties*

$$\left(\frac{\partial P}{\partial \tau}\right)_s < 0 \qquad \textit{and} \qquad \left(\frac{\partial P}{\partial s}\right)_\tau > 0, \tag{6.2a}$$

and that the reaction is exothermic

$$\varepsilon_1(\tau_0, p_0) < \varepsilon_0(\tau_0, p_0); \tag{6.2b}$$

then the point A_0 corresponding to the upstream state is under the Crussard curve.

In this first property, note that (6.2a) is always true provided γ and Γ are both positive (thanks for (4.3c)). We will find in subsection 6.2.1 a condition to ensure the exothermic property (6.2b).

Proposition 6.2 (see [28, p.146])**.** *Suppose moreover that*

$$\left(\frac{\partial^2 P}{\partial \tau^2}\right)_s > 0;$$

then the Crussard curve is convex. Hence, the Rayleigh line (6.1b) *and the Crussard curve are crossing in zero or two points.*

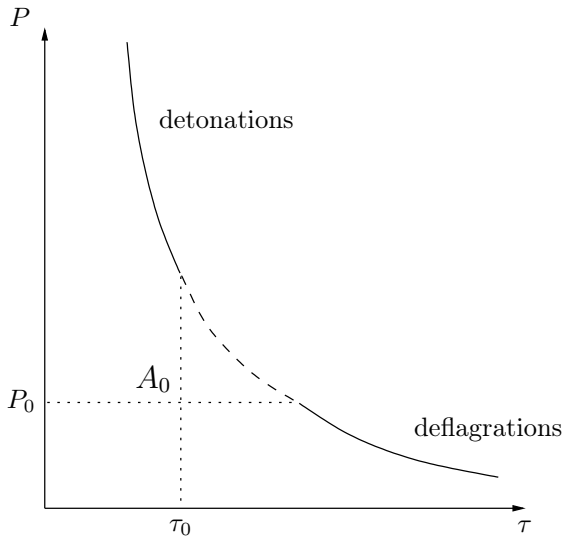

Figure 6.1: The Crussard curve related to an initial point (τ_0, P_0). The curve is cut into three parts : the upper one is the detonation branch, the lower one is the deflagration branch, and the middle part does not match with the negative slope of the Rayleigh line.

Note that the Proposition 6.2 supposes that the pressure can be differentiated twice, which is not the case in our application, because of the local loss of derivative due to phase transition. Nevertheless, if the properties 6.1 and 6.2 hold for the equation of state of the downstream states, then the Crussard curve can be schematically drawn as in Figure 6.1. The Crussard curve is cut into three parts : the uppest part is called the detonation branch, and the lowest one is the deflagration branch. In the middle part of the curve, $\dfrac{P_1 - P_0}{\tau_1 - \tau_0} > 0$. This does not match with the negative slope of the Rayleigh line (6.1b).

The deflagration and the detonation part of the Crussard curve are themselves cut into two parts, separated by the tangential point of the Rayleigh line with the Crussard curve (the existence of such tangential point can be shown under some assumption on the asymptotic behaviour of equation of state). Both branches are schematically drawn on Figure 6.2.

Proposition 6.3. *Along the Crussard curve, the velocity $|v| = |u - \sigma|$ has a local minimum on the CJ-detonation point, and has a local maximum on the CJ-deflagration point. More precisely, we have*

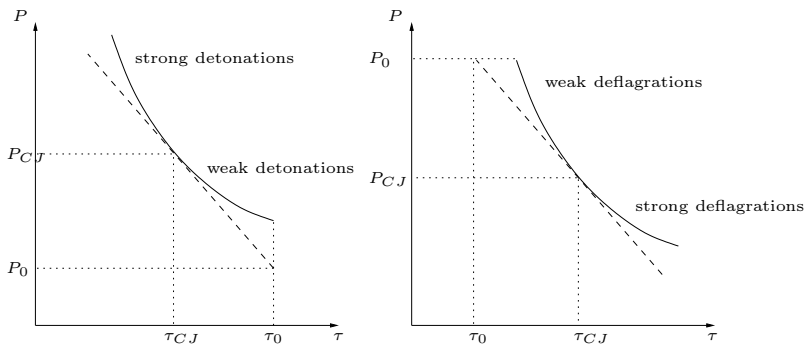

Figure 6.2: Zoom on the Crussard curve; on the left side, the detonation branch ($P \geq P_0$) is cut into two parts by the Chapman–Jouguet point. The upper part is the part of the strong detonations, and the lower part is called the part of the weak detonations. On the right side, the deflagration branch ($P \leq P_0$) is cut into two parts by the Chapman–Jouguet point. The upper part is the part of the weak deflagrations, and the lower part is called the part of the strong deflagrations.

$$\begin{array}{lcll} \textit{for a strong detonation} & : & |v_0| > c_0 & |v_1| < c_1, \\ \textit{for a weak detonation} & : & |v_0| > c_0 & |v_1| > c_1, \\ \textit{for a weak deflagration} & : & |v_0| < c_0 & |v_1| < c_1, \\ \textit{for a strong deflagration} & : & |v_0| < c_0 & |v_1| > c_1. \end{array}$$

This last property is very important because it can allow to know the structure of the half Riemann Problem with a combustion wave provided we know which "family" the combustion wave belongs to. In our case, we are interested in waves which transform a heavy phase into a lighter one. Therefore, we expect that τ will increase, so that we will concentrate only on the deflagration branch of the Crussard curve.

Thanks for the Proposition 6.3, we can give the structure of the Riemann Problem in the case of strong and weak deflagrations. In both cases, from the Property 2, the deflagration wave is always subsonic relative to the liquid; for example, if the liquid is on the left, we have $\dot{M} > 0$, and $u_0 - c_0 < \sigma < u_0$. For the position of the wave relative to the fields of 1, we have

- if the wave is a strong deflagration then $\sigma < u_1 - c_1$
- if the wave is a weak deflagration then $u_1 - c_1 < \sigma < u_1$.

In [18] (p. 230), it is shown that under the assumption that a wave is a deflagration, and that across that wave, the mass fraction of gas always

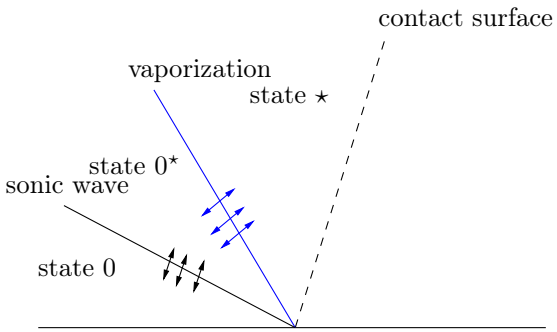

Figure 6.3: Structure of the half Riemann problem : the state 0 is linked with the state $0^\star$ by a forerunner sonic wave (rarefaction wave or shock). Then the state $0^\star$ and the state $\star$ are linked with a deflagration wave. Eventually, there is a contact discontinuity.

increases, then the reaction is a weak deflagration. We will suppose that we are always in that case in the following.

The structure of the Riemann problem with weak deflagrations is drawn on Figure 6.3. The problem for deflagrations is that the Lax characteristic criterion is not satisfied (see [28] p. 154), and the Riemann problem cannot be solved only with the classical relations across the sonic wave and the Rankine–Hugoniot relations across the subsonic wave. There remains one indeterminate. The supplementary relation needed is often called "the kinetic closure".

6.2 Application to the solution of the Riemann problem with vaporization

6.2.1 Useful verifications for the use of CJ theory

In that section, we check whether the inequalities needed for applying the Chapman–Jouguet theory hold.

Theorem 6.1. *1. If both equations of state are convex, and if* $\dfrac{\mathrm{d}P_{sat}}{\mathrm{d}T} > 0$, *then inequalities* (6.2a) *hold.*

2. If (P, τ) *lie in the saturation dome and under the condition*

$$\frac{\gamma}{\Gamma} - \frac{T}{P}\frac{\mathrm{d}P_{sat}}{\mathrm{d}T} > 0 \tag{6.3}$$

the inequality (6.2b) *holds.*

Proof. According to the identity (4.3c), it is sufficient to have γ and $\Gamma > 0$. This is supposed for pure fluids, and this is ensured for mixture equation of state if $\dfrac{\mathrm{d}P_{\mathrm{sat}}}{\mathrm{d}T} > 0$, so that (6.2a) holds.

Let us now check if the inequality (6.2b) is ensured. We suppose that (P, τ) lie in the saturation dome, so that the corresponding equilibrium downstream state is a mixture :

$$\varepsilon_1(\tau, P) = \varepsilon_m(\tau, P) = y_l \varepsilon_l(P, \tau_l(P)) + (1 - y_l)\varepsilon_v(P, \tau_v(P)),$$

and we want to know if $\varepsilon_1(P, \tau) - \varepsilon_0(P, \tau) < 0$, the state 0 being of course described by the liquid equation of state. For that, we denote by

$$\delta\varepsilon(y_l) = y_l \varepsilon_l(P, \tau_l(P)) + (1 - y_l)\varepsilon_v(P, \tau_v(P)) - \varepsilon_l\Big(P, y_l\tau_l(P) + (1 - y_l)\tau_v(P)\Big),$$

and we immediately see that $\delta\varepsilon(1) = 0$. It remains to show that $\delta\varepsilon$ is an increasing function

$$\begin{aligned}\frac{\mathrm{d}\delta\varepsilon}{\mathrm{d}y_l}(y_l) \; =& \varepsilon_l(P, \tau_l(P)) - \varepsilon_v(P, \tau_v(P)) \\ & -(\tau_l(P) - \tau_v(P)) \left(\frac{\partial \varepsilon_l}{\partial \tau}\right)_P (P, y_l\tau_l(P) + (1 - y_l)\tau_v(P)).\end{aligned}$$

Integration of the identity $\mathrm{d}\varepsilon + P\mathrm{d}\tau = T\mathrm{d}s$ across the saturation dome leads to

$$\varepsilon_l(P, \tau_l(P)) - \varepsilon_v(P, \tau_v(P)) + P(\tau_l(P) - \tau_v(P)) = T(s_l(P) - s_v(P)),$$

so that

$$\begin{aligned}\frac{\mathrm{d}\delta\varepsilon}{\mathrm{d}y_l}(y_l) \; =& -P(\tau_l(P) - \tau_v(P)) + T(s_l(P) - s_v(P)) \\ & -(\tau_l(P) - \tau_v(P)) \left(\frac{\partial \varepsilon_l}{\partial \tau}\right)_P \Big(P, y_l\tau_l(P) + (1 - y_l)\tau_v(P)\Big)\end{aligned},$$

which can be cast into the following form, thanks for (4.8) and (4.3f)

$$\frac{\mathrm{d}\delta\varepsilon}{\mathrm{d}y_l}(y_l) \; = \; P(\tau_v - \tau_l)\left(\frac{\gamma}{\Gamma} - \frac{T}{P}\frac{\mathrm{d}P_{\mathrm{sat}}}{\mathrm{d}T}\right).$$

As $P > 0$, $\tau_v - \tau_l >$, and as (6.3), $\delta\varepsilon$ increases, so that $\delta\varepsilon \leq \delta\varepsilon(1) = 0$. Thus, (6.2b) holds. □

Remark 6.1. Supposing that (τ, P) is always in the saturation dome is not a strong assumption. Indeed, as the upstream state is few compressible, its specific volume cannot increase a lot across a sonic wave, and it is likely that a metastable liquid with a specific volume equal to the one of a gas at equilibrium cannot exist, except just near the critical point.

Remark 6.2. The condition (6.3) holds at least in the two following framework

1. The terms $\dfrac{\gamma}{\Gamma}$ and $\dfrac{T}{P}\dfrac{\mathrm{d}P_{\mathrm{sat}}}{\mathrm{d}T}$ can easily be compared near the saturation curve. Indeed, if we use (4.3b) with saturated variables, we find

$$\frac{T^2(\gamma g - \Gamma^2)}{P\tau}\frac{\mathrm{d}s_l}{\mathrm{d}T} = \frac{\gamma}{\Gamma} - \frac{T}{P}\frac{\mathrm{d}P_{\mathrm{sat}}}{\mathrm{d}T}, \tag{6.4}$$

   so that we have $\dfrac{\mathrm{d}\delta\varepsilon}{\mathrm{d}T}(1) = (\tau_v - \tau_l)\dfrac{T^2}{\tau}\dfrac{\gamma g - \Gamma^2}{\Gamma}\dfrac{\mathrm{d}s_l}{\mathrm{d}T}$.
   Thus, if the liquid saturation curve is regular (which is always the case) then $\dfrac{\mathrm{d}s_l}{\mathrm{d}T} > 0$, so that the condition (6.3) is ensured.

2. For simple model, as perfect gas or stiffened gas, we have

$$\frac{\gamma}{\Gamma} = \frac{\bar{\gamma}\left(1 + \dfrac{P^\infty}{P}\right)}{\bar{\gamma} - 1},$$

   so that $\dfrac{\gamma}{\Gamma}$ does not depend on the specific volume. Thus, equality (6.4) holds for any τ, so that the condition (6.3) always holds.

Remark 6.3. The same calculations can be made for liquefaction. Then we find, near the vapor saturation curve

$$\frac{\mathrm{d}\delta\varepsilon}{\mathrm{d}T}(1) = (\tau_l - \tau_v)\frac{T^2}{\tau}\frac{\gamma g - \Gamma^2}{\Gamma}\frac{\mathrm{d}s_v}{\mathrm{d}T}.$$

Thus, if the fluid is regular then $\dfrac{\mathrm{d}s_v}{\mathrm{d}T} < 0$, and as $\tau_l - \tau_v < 0$ then $\dfrac{\mathrm{d}\delta\varepsilon}{\mathrm{d}T}(1) > 0$, so that locally we have $\varepsilon_m - \varepsilon_v < 0$, and the Chapman–Jouguet theory can be used. If the fluid is retrograde, then we find that locally $\varepsilon_m - \varepsilon_v > 0$ and the Chapman–Jouguet theory may be used, but by exchanging the upstream and the downstream state. Note that the Hugoniot curves might enter the saturation dome only in the retrograde case.

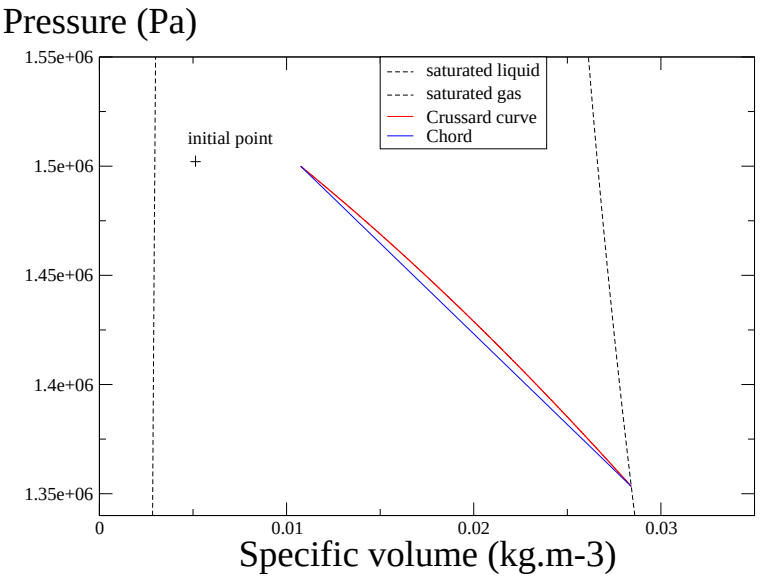

Figure 6.4: Wrong behaviour of the mixture Crussard curve if the condition $\mathscr{G} > 0$ is violated. We notice that the Crussard curve is concave which induces no existence of any CJ point. For a more complicated couple of equation of state, we could expect to observe two or three tangential points if the sign of $\mathscr{G}$ changed two or three times along the Crussard curve.

The Chapman–Jouguet theory relies also a lot on the convexity properties of the Crussard curve (see Proposition 6.2 of section 6.1), which is ensured if the fundamental derivative $\mathscr{G}$ is positive. Nevertheless, even if we suppose that the liquid and the gas equation of state have a positive fundamental derivative, the mixture equation of state can have a negative fundamental derivative, as it was shown numerically in subsection 5.2.4. This non positivity of the fundamental derivative can lead to a wrong behaviour of the Crussard curve as shown in Figure 6.4: the CJ points do not exist any more and all the undercompressive downstream states are strong deflagrations. If the sign of the fundamental derivative changed many times along the Crussard curve, we could expect to observe several CJ points. From now on, we suppose that $\mathscr{G} > 0$.

6.2.2 Entropy growth criterion

As the particles are crossing the front from the liquid area to a mixture or pure phase area, we have to check whether the entropy growth criterion is ensured, i.e. if the entropy of the downstream state (gas or mixture) is greater than the entropy of the upstream state (liquid). We first prove the

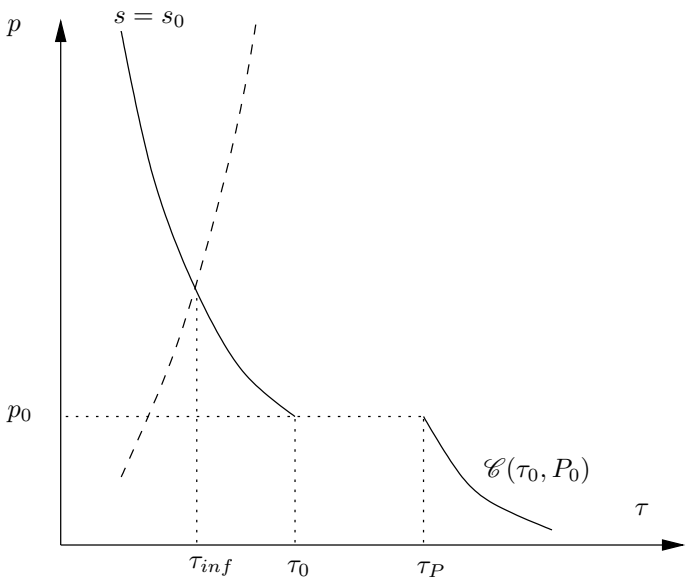

Figure 6.5: Entropy growth criterion. To any point (τ_0, P_0) on a given isentrope $s = s_0$, we associate the point on the Crussard curve (τ_P, P_0). The liquid saturation curve is drawn on dashed lines. When τ_0 is on the liquid saturation curve, we have $\tau_P = \tau_0$, so that $s_P = s_0$. Thus, to show that $s_P \geq s_0$, we only have to prove that entropy of the point P grows when τ_0 increases.

following theorem.

Theorem 6.2. *Let $s = s_0$ a liquid isentrope that crosses the liquid saturation curve. To any metastable point (τ_0, P_0) on that isentrope, we map the point (τ_P, P_0), point of constant pressure deflagration (see Figure 6.5). If we suppose that*

$$\forall (\tau_0, P_0) \qquad \gamma(\tau_0, P_0) > \gamma(\tau_P, P_0) \tag{6.5}$$

then $s(\tau_P, P_0) > s_0$.

Proof. To any point (τ_0, P_0) on this isentrope, we associate the point (τ_P, P_0), point of constant pressure deflagration (see Figure 6.5). For more convenience in the notations, we suppose that (τ_P, P_0) is a mixture state (*i.e.* all the linked quantities have m). τ_P is defined by the implicit equation

$$\varepsilon_m(\tau_P, P_0) - \varepsilon_l(\tau_0, P_0) + P_0(\tau_P - \tau_0) = 0 \tag{6.6}$$

Differentiation of (6.6) with respect to τ_P is equal to $\dfrac{\gamma_m}{\Gamma_m}$, which never vanishes, so that according to the implicit function theorem, τ_P is a $\mathscr{C}^1$ function

of τ_0 and P_0. Moreover, we can calculate its derivative with respect to τ_0 and P_0:

$$\begin{cases} \left(\dfrac{\partial \tau_P}{\partial \tau_0}\right)_{P_0} = \dfrac{\gamma_l}{\gamma_m}\dfrac{\Gamma_m}{\Gamma_l} \\ \left(\dfrac{\partial \tau_P}{\partial P_0}\right)_{\tau_0} = \dfrac{\tau_0}{\gamma_m P_0}\left(\dfrac{\Gamma_m(\Gamma_l+1)}{\Gamma_l} - \dfrac{\tau_P}{\tau_0}(\Gamma_m+1)\right) \end{cases}$$

Besides, as we supposed that the points (P_0, τ_0) belong to the same isentrope, P_0 is actually a function of τ_0 with $\dfrac{\mathrm{d}P_0}{\mathrm{d}\tau_0} = -\dfrac{\gamma_l P_0}{\tau_0}$, so that τ_P is a function of the only variable τ_0 and

$$\begin{aligned} \frac{\mathrm{d}\tau_P}{\mathrm{d}\tau_0} &= \left(\frac{\partial \tau_P}{\partial \tau_0}\right)_{P_0} + \frac{\mathrm{d}P_0}{\mathrm{d}\tau_0}\left(\frac{\partial \tau_P}{\partial P_0}\right)_{\tau_0} \\ &= \frac{\gamma_l}{\gamma_m}\left(-\Gamma_m + \frac{\tau_P}{\tau_0}(\Gamma_m+1)\right) \end{aligned}.$$

Now, we calculate the entropy variation of the point τ_P when the point (P_0, τ_0) follows the isentrope $s = s_0$

$$\begin{aligned} \frac{\mathrm{d}s}{\mathrm{d}\tau_0} &= \frac{\mathrm{d}\tau_P}{\mathrm{d}\tau_0}\left(\frac{\partial s}{\partial \tau}\right)_P + \frac{\mathrm{d}P_0}{\mathrm{d}\tau_0}\left(\frac{\partial s}{\partial P}\right)_\tau \\ &= \frac{\gamma_m P_0}{T\Gamma_m}\left(\frac{\gamma_l \Gamma_m}{\gamma_m}\left(\frac{\tau_P}{\tau_0} - 1\right) + \frac{\tau_P}{\tau_0}\left(\frac{\gamma_l}{\gamma_m} - 1\right)\right). \end{aligned}$$

According to the hypothesis (6.5), $\gamma_l > \gamma_m$. Moreover as we have $\tau_P - \tau_0 > 0$, s is an increasing function of τ_0. Furthermore, in the limit of no overheating, we have

$$\lim_{\tau_0 \to \tau_{\mathrm{inf}}} \tau_P(\tau_0, P_0) = \tau_{inf},$$

where τ_{inf} is the crossing point of the isentrope $s = s_0$ with the saturation curve. Thus $\lim\limits_{\tau_0 \to \tau_{\mathrm{inf}}} s(\tau_P, P_0) = s_0$. As a conclusion

$$\forall \tau_0 \geq \tau_{inf} \qquad s(\tau_P, P_0) \geq s_0,$$

which ends the proof. □

Remark 6.4 (About the hypothesis (6.5))**.**

1. We know that near the saturation curve, we have $\gamma_l > \gamma_m$. For actual data, we have $\gamma_l \gg \gamma_m$. So that we can suppose that any γ is greater than any γ_m.

2. $\gamma_l > \gamma_v$ just means that the liquid phase is very much less compressible than the gas phase (see e.g. [67] chapter XI).

Given an initial point, we know that the entropy grows from the constant pressure point to the Chapman–Jouguet point, so that if the entropy growth criterion holds for the constant pressure deflagration point, it holds for all the downstream states between the constant pressure deflagration point and the Chapman–Jouguet point, *i.e.*

Corollary 6.1. *Under the same hypothesis as the Theorem 6.2, the entropy growth criterion holds for all the weak deflagration points.*

6.2.3 Behaviour of the Crussard curve near the gas saturation curve

In subsection 4.3.1, the behaviour of the isentropes near the saturation curves was studied. The difference of the differential behaviour of the pure phase and the mixture equation of state induced kinks in isentropes. Now, we want to study the behaviour of the Crussard curve when it crosses the vapor saturation curve. It is more difficult than the study of the isentrope, because the Crussard curve does not depend only on the local variables, but also on the starting point (τ_0, P_0).

General study

We denote by C the point in which the Crussard curve crosses the saturation curve, and by

$$\zeta = -\frac{\tau}{P}\frac{\mathrm{d}P}{\mathrm{d}\tau}_{|\mathscr{C}},$$

the adimensioned slope of the Crussard curve.

The first thing we will prove for the behaviour of the Crussard curve near the saturation curve, is that it can be parameterised by τ, under some conditions

Theorem 6.3. *If all the equations of state are convex and if* $\Gamma > 0$*, then* $\zeta > 0$*. With the same hypothesis, the Crussard curve can be parameterised by* τ*, even near the saturation curve.*

Proof. As proved in [42, page 101], we have

$$\zeta = \frac{\dfrac{\gamma}{\Gamma} - \dfrac{\Delta P}{2P}}{\dfrac{1}{\Gamma} + \dfrac{\Delta\tau}{2\tau}} \tag{6.7}$$

Across a deflagration wave, we have $\Delta\tau > 0$ and $\Delta P < 0$. Moreover, we proved that $\Gamma_m > 0$, and we suppose that $\Gamma > 0$. The conditions $\gamma > 0$ and

$\gamma_m > 0$ were already supposed to ensure the convexity of the specific energy. Then $\zeta > 0$. If we combine (6.7) with the identities near the saturation boundary of subsection 4.3.1, we get

$$\frac{\xi - \zeta}{\Gamma}\left(1 + \Gamma\frac{\Delta\tau}{2\tau}\right) = \frac{\xi - \zeta_m}{\Gamma_m}\left(1 + \Gamma_m\frac{\Delta\tau}{2\tau}\right) \tag{6.8}$$

Across a deflagration, we have $\Delta\tau > 0$. Then

$$\frac{\xi - \zeta}{\xi - \zeta_m} > 0$$

which means that the Crussard curve, near a boundary, can be parameterised by τ. As $\zeta > 0$, the Crussard curve is a diffeomorphism of τ in each side of the saturation curve. As the Crussard curve can locally parameterise the Crussard curve near a boundary, we conclude that the Crussard curve is a homeomorphism of τ. □

Remark 6.5. As the Crussard curve is a decreasing homeomorphism in τ, the point of constant pressure deflagration is uniquely defined.

To be more precise on the relative behaviour of the isentropes, the Crussard curve, and the saturation curve, we will prove that

Theorem 6.4. *The relative behaviour of the isentropes and the Crussard curves, which gives the nature of the deflagration on each side of the saturation curve follows the alternative*

- *if $\gamma > \xi$ then*
  - *either $\xi \geq \zeta$, then the deflagration is weak on both sides of the saturation curve,*
  - *or $\xi < \zeta$, then point C cannot be a weak deflagration simultaneously on both sides of the saturation curve.*
- *if $\gamma < \xi$ then*
  - *either $\xi \leq \zeta$, then the deflagration is strong on both of the sides of the saturation curve*
  - *or $\xi > \zeta$, then the deflagration cannot be simultaneously strong on the mixture side, and weak on the pure phase side.*

Proof. Equation (6.8) can be rewritten as

$$\frac{\xi-\zeta}{\xi-\zeta_m}=\frac{\dfrac{1}{\Gamma_m}+\dfrac{\Delta\tau}{2\tau}}{\dfrac{1}{\Gamma}+\dfrac{\Delta\tau}{2\tau}}$$

so that the discontinuity in the slope of the Crussard curve is directly linked with the sign of $\Gamma_m-\Gamma$ (we recall that $\Gamma_m>0$ and that Γ has the same sign as Γ_m near the saturation curves). Equation (4.15) induces a separation into the following cases

- $\gamma>\xi$

  If $\gamma>\xi$ then we also have $\gamma_m>\xi$. As $\gamma_m<\gamma$, we have $\dfrac{\gamma_m-\xi}{\gamma-\xi}\leq 1$, so that $\Gamma_m\leq\Gamma$. Therefore

  $$\frac{\xi-\zeta}{\xi-\zeta_m}\geq 1$$

  Suppose first that $\xi-\zeta\geq 0$. Then $\xi-\zeta\geq\xi-\zeta_m$ so that $\zeta\leq\zeta_m\leq\xi$. In that case, as shown on the Figure 6.6, the relative behaviour of the isentrope and the Crussard curve show that in both sides of the saturation curve, the downstream state is a weak deflagration (see Figure 6.6). In that case, we have $\zeta\leq\zeta_m\leq\xi\leq\gamma_m\leq\gamma$.

  Suppose now that $\xi-\zeta\leq 0$. Then we have $\xi\leq\zeta_m\leq\zeta$. The nature of the deflagration is given by the relative position of the slope of the Crussard curve and the Rayleigh line, so that on the point saturation curve, there are three cases (see Figure 6.7):

  - If the Rayleigh line has a lower slope than both of the slopes of the Crussard curve, then the two parts match with strong deflagrations. Thus, we have $\gamma_m\leq\zeta_m$ and $\gamma\leq\zeta$ (see Figure 6.7, case (a)).
  - If the slope of the Rayleigh line is between the slopes of the Crussard curve, then the mixture Crussard curve matches with strong deflagrations whereas the pure phase Crussard curve matches with weak deflagrations. In that case, we have $\gamma_m\leq\zeta_m$ and $\gamma\geq\zeta$ (see Figure 6.7, case (b)). In that case we have $\xi\leq\zeta_m\leq\gamma_m\leq\gamma\leq\zeta$.
  - If the Rayleigh line has a greater slope than both of the slopes of the Crussard curve then the point C is a weak deflagration with respect to the pure and the mixture Crussard curve. Therefore, we have $\gamma_m\geq\zeta_m$ and $\gamma\geq\zeta$ (see Figure 6.7, case (c)).

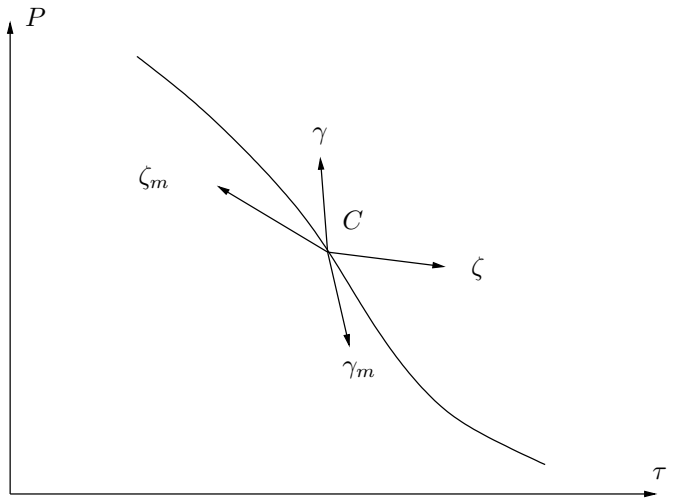

Figure 6.6: Qualitative relative behaviour of the isentrope and of the Crussard curve when they cross the vapor saturation curve in the case 1. Arrows represent half tangent of the Crussard curve (ζ) and of the isentrope (γ)

- $\gamma < \xi$

  If $\gamma < \xi$ then we also have $\gamma_m < \xi$. As we know that $\gamma_m \leq \gamma$, we have $\dfrac{\gamma_m - \xi}{\gamma - \xi} \geq 1$, so that $\Gamma_m \geq \Gamma$ (thanks for equation (4.15)). Therefore

  $$\frac{\xi - \zeta}{\xi - \zeta_m} \leq 1$$

  We suppose first that $\xi - \zeta \leq 0$. Then we immediately have $\zeta \leq \zeta_m$. Thus, we have $\gamma_m \leq \zeta_m$ and $\gamma \leq \zeta$, so that point C matches on both sides of the Crussard curve with strong deflagrations (see Figure 6.8). In that case we have $\zeta_m \leq \zeta \leq \xi \leq \gamma \leq \gamma_m$.

  We suppose now that $\xi - \zeta \geq 0$. Then we have $\zeta_m \leq \zeta \leq \xi$. The nature of the deflagration is given by the relative position of the slope of the Crussard curve and the Rayleigh line, so that three cases may happen (see Figure 6.9):

  – If the Rayleigh line has a lower slope than the slopes on both sides of the Crussard curve in C, then the point C is a weak deflagration with respect to the mixture and the pure phase Crussard curve. We have then $\gamma \leq \zeta$ and $\gamma_m \leq \zeta_m$ (see Figure 6.9, case (a)).

  – If the slope of the Rayleigh line is between the slopes on each side of the Crussard curve, then point C is a strong deflagration for

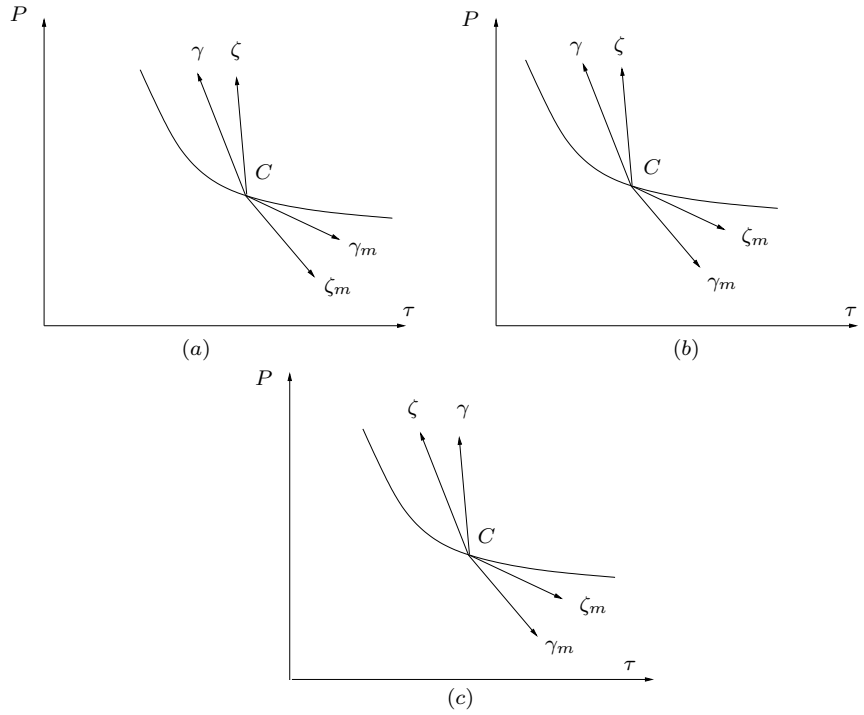

Figure 6.7: Qualitative relative behaviour of the isentrope and of the Crussard curve when they cross the vapor saturation curve, case 2. Arrows represent half tangent of the Crussard curve (ζ) and of the isentrope (γ).

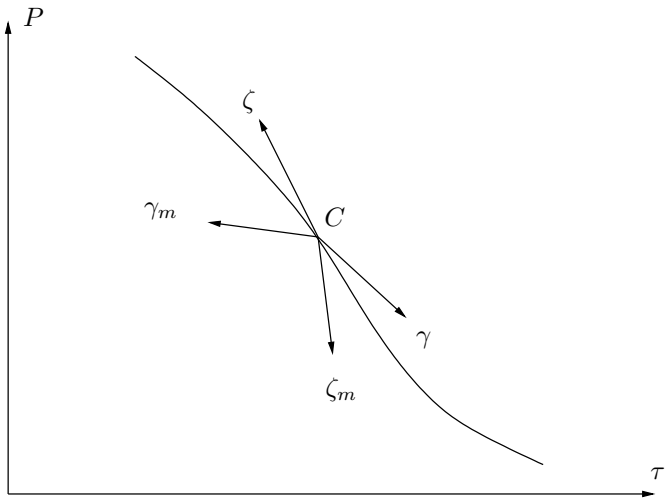

Figure 6.8: Qualitative relative behaviour of the isentrope and of the Crussard curve when they cross the vapor saturation curve, case 3. Arrows represent half tangent of the Crussard curve (ζ) and of the isentrope (γ).

the mixture Crussard curve, and a weak deflagration for the pure phase Crussard curve (see Figure 6.9, case (b)). In that case we have $\gamma_m \leq \zeta_m \leq \zeta \leq \gamma \leq \xi$.

– If the Rayleigh line has a lower slope than both of the slopes of the Crussard curve then the point C is a strong deflagration with respect to the pure and the mixture Crussard curve. Therefore, we have $\gamma_m \geq \zeta_m$ and $\gamma \geq \zeta$ (see Figure 6.9, case (c)).

This ends the proof. □

Ill–posedness of the Chapman–Jouguet closure

The following result comes immediately from the Theorem 6.4

Corollary 6.2. *Let (P_0, τ_0, u_0) be an initial state of liquid at thermodynamic equilibrium, such that the isentrope $\mathscr{C}_s$ coming from this point enters the saturation dome. If $(P_0^\star, \tau_0^\star)$ is a point in $\mathscr{C}_s$, we build $(P^\star, \tau^\star)$ in the following way*

- *if $(P_0^\star, \tau_0^\star)$ is not in the saturation dome then $P^\star = P_0^\star$, and $\tau^\star = \tau_0^\star$,*
- *if $(P_0^\star, \tau_0^\star)$ is in the saturation dome, then it is linked with $(P^\star, \tau^\star)$ with a Chapman–Jouguet deflagration.*

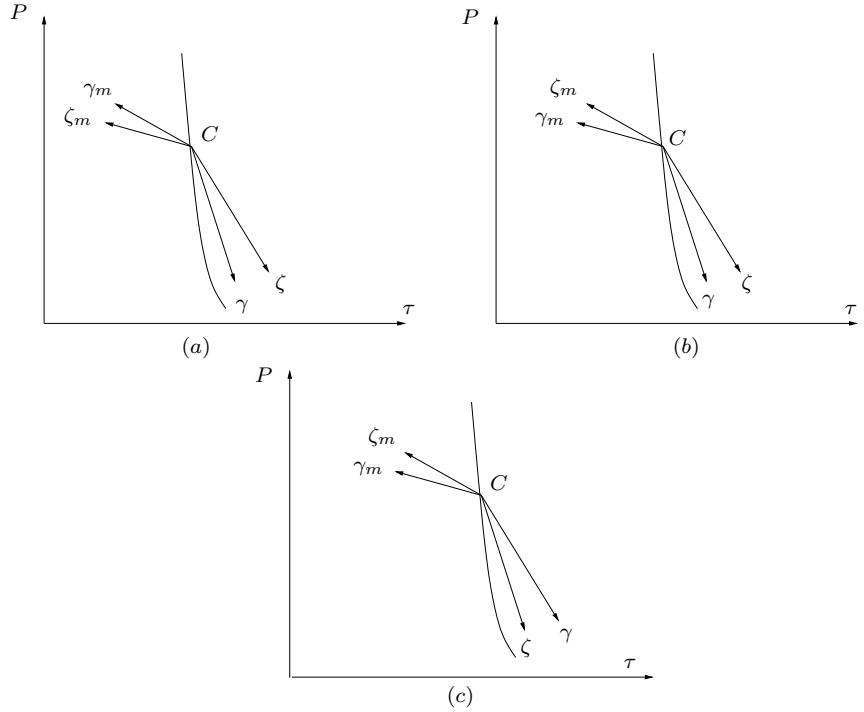

Figure 6.9: Qualitative relative behaviour of the isentrope and of the Crussard curve when they cross the vapor saturation curve, case 4. Arrows represent half tangent of the Crussard curve (ζ) and of the isentrope (γ).

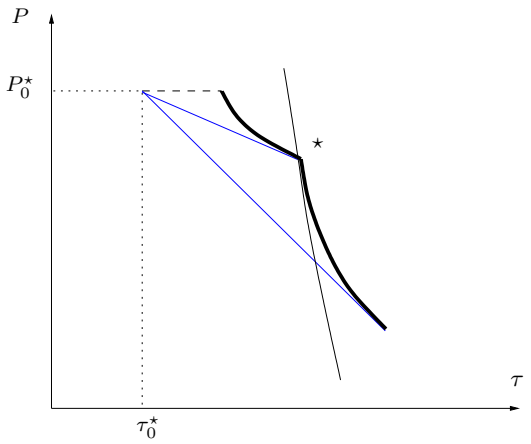

Figure 6.10: Qualitative behaviour of the Rayleigh line and the Crussard curve when the Crussard curve crosses the saturation curve on a mixture Chapman–Jouguet point. As $\zeta_m \leq \zeta$, and as the Rayleigh line is tangential to the mixture Crussard curve, we are in the case $(4.c)$ of the proof of Theorem 6.4. As a consequence, the pure phase side matches with a weak deflagration too, so that there exist another Chapman–Jouguet point.

If $(P^\star, \tau^\star)$ can reach the pure gas phase, then the curve $(P^\star, \tau^\star)$ is discontinuous.

Proof. We suppose that the set described is continuous. As $(P^\star, \tau^\star)$ can reach the saturation dome, it crosses the gas saturation curve on a point (P_c, τ_c). As it is a Chapman-Jouguet point, we have $\gamma_m = \zeta_m$, so that we are in case 4 of Figure 6.9. The case $4.(c)$ is excluded because the Rayleigh line is tangential with the Crussard curve, so that the slope of the Rayleigh line is greater than the slope of the Crussard curve in the pure phase side. Thus, the point $\star$ matches with a weak deflagration with respect to the pure phase Crussard curve. As a consequence, the Crussard curve has another Chapman–Jouguet point that lies in the pure phase area (see Figure 6.10), so that the curve $\mathscr{C}_{CJ}$ has already a branch in the pure gas area. □

Eventually, we can state the following theorem

Theorem 6.5. *With the same hypothesis of Corollary 6.2, if we model the vaporization wave by a Chapman–Jouguet deflagration, then the resulting solution of the Riemann problem is ill–posed in the L^1 sense: the solution does not depend continuously on the initial state.*

Proof. We fix a point for $x < 0$ in the liquid area for which the conditions of Corollary 6.2 hold, and we suppose that on the right, there is some gas.

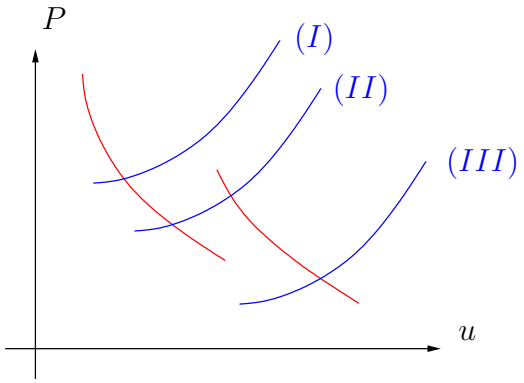

Figure 6.11: In red, the wave curve of the liquid side. In blue, different wave curves for the gas side, depending on the initial state. In the case (I), the gas wave curve intersects the liquid one in one mixture point. In the case (II), the gas wave curve intersects the liquid one in the two branches: one mixture and one pure gas point. In the case (III), the gas wave curve intersects the liquid one only on the pure phase branch.

The Riemann problem is composed (from the left to the right) of a sonic wave, a vaporization wave (if the intermediate state is metastable), a contact discontinuity (across which P and u are constant), and a sonic wave in the gas side. As it is done usually [28], to solve the Riemann problem, we intersect the wave curve of the downstream state (sonic wave and maybe followed by a CJ vaporization) of the left side with the wave curve of the sonic wave of the right side, in the plane (P, u). Corollary 6.2 says that the wave curve of the left side is composed of (at least) two branches (see Figure 6.11). So that the gas wave curve intersects the liquid wave curve either in one mixture point (case (I)), or in two points (case (II)), or in one pure gas point (case (III)). Existence of case (I) and case (III) implies that we must jump from the mixture to the gas branch of the liquid wave curve. But jumping from one branch to the other means that we change a lot the vaporizes state (so the L^1_{loc} norm too), but by changing few the initial state.

□

6.3 Examples

We finish this chapter by drawing the curve $\mathscr{C}_{CJ}$ described in Corollary 6.2 for the models of equation of state of Chapter 4.

6.3.1 Example 1 : two perfect gas equation of state

As an example, we take the model with two perfect gas. As we said before, this model enables to make all the calculation, because the mixture equation of state is explicit.

Mixture CJ–point

In the case when the downstream state is a mixture, the equation of the Crussard curve is the following

$$\frac{P\tau_2}{\Gamma_2} - \frac{P_0\tau_0}{\Gamma_2} + \frac{1}{2}(P+P_0)(\tau-\tau_0) = 0,$$

which gives an expression of τ as a function of P: $\tau = \tau_0 - \dfrac{2\,(P\tau_2 - P_0\tau_0)}{\Gamma_2(P+P_0)}$.

The CJ–point is such that $\dfrac{\mathrm{d}\tau}{\mathrm{d}P}(P_{CJ}) = \dfrac{\tau-\tau_0}{P-P_0}$, so that we find the following equation for P_{CJ}

$$\left(\frac{P}{P_0}\right)^2 - 2\frac{\tau}{\tau_0}\frac{P}{P_0} + 1 = 0,$$

whose undercompressive solution is

$$P_{CJ} = P_0\left(\frac{\tau_0}{\tau_2} - \sqrt{\left(\frac{\tau_0}{\tau_2}\right)^2 - 1}\right).$$

τ_{CJ} is then given by

$$\tau_{CJ} = \tau_2\left(\frac{\tau_0}{\tau_2} + \frac{2\sqrt{\dfrac{\tau_0}{\tau_2} - 1}}{\Gamma_2\left(\dfrac{\tau_0}{\tau_2} + 1 - \sqrt{\left(\dfrac{\tau_0}{\tau_2}\right)^2 - 1}\right)}\right).$$

Of course, this point can be chosen only when the mixture is stable, that means when $\tau_{CJ} \leq \tau_1$.

Vapor CJ–point

The equation of the Crussard curve is then

$$\frac{\tau P}{\Gamma_1} - \frac{\tau_0 P_0}{\Gamma_2} + \frac{1}{2}(P+P_0)(\tau-\tau_0) = 0.$$

As in [39], we first calculate the point of constant specific volume detonation, i.e. the downstream state such as $\tau = \tau_0$: $P_\tau = \dfrac{\Gamma_1}{\Gamma_2} P_0$. If we take the calculations of [39], we get

$$P_{CJ} = \frac{\Gamma_1 P_0}{\Gamma_2}\left(1 - \sqrt{\left(1 - \frac{\Gamma_2}{\Gamma_1}\right)\left(1 + \frac{\Gamma_2}{\Gamma_1} + \frac{2\Gamma_2}{\Gamma_1\left(\gamma_1 + 1\right)}\right)}\right).$$

We remark that P_{CJ} is a linear function of P_0. If we use the equation of the Crussard curve, we get the following expression for τ_{CJ}

$$\tau_{CJ} = \tau_0 \frac{\dfrac{\gamma_2 + 1}{\gamma_2 - 1} P_0 + P_{CJ}}{\dfrac{\gamma_1 + 1}{\gamma_1 - 1} P_{CJ} + P_0}. \tag{6.9}$$

As P_{CJ} is a linear function of P_0, we see that τ_{CJ} is a linear function of τ_0. The CJ–point of pure vapor can be chosen only when $\tau_{CJ} \geq \tau_1$. The two functions τ_{CJ}, for vapor and mixture equation of state are drawn on Figure 6.12, highlighting the fact that they cannot be linked continuously.

How to overcome the problem in this simple case

If we compute the constant pressure deflagration for the pure phase, we find

$$\tau_P = \frac{\Gamma_1(\Gamma_2 + 1)}{\Gamma_2(\Gamma_1 + 1)}\,\tau_0 \tag{6.10}$$

which is a straight line, as the CJ set for pure phase. As the constant pressure set is a continuous set, and as for a given τ_0, we have $\tau_P < \tau_{CJ}$, the constant pressure set cuts $\tau = \tau_1$ for a greater τ than the CJ set. Therefore, the set of the admissible downstream states, for $\tau > \tau_1$ is between the two straight lines (6.9) and (6.10). As a conclusion, the set of the downstream states composed of

- if $\tau < \tau_1$, the CJ mixture downstream states,
- if $\tau > \tau_1$, a straight line going from $(0, 0)$ to the intersection point of the CJ mixture points with $\tau = \tau_1$

is an admissible kinetic closure, because it is subsonic, and continuous, see Figure 6.13.

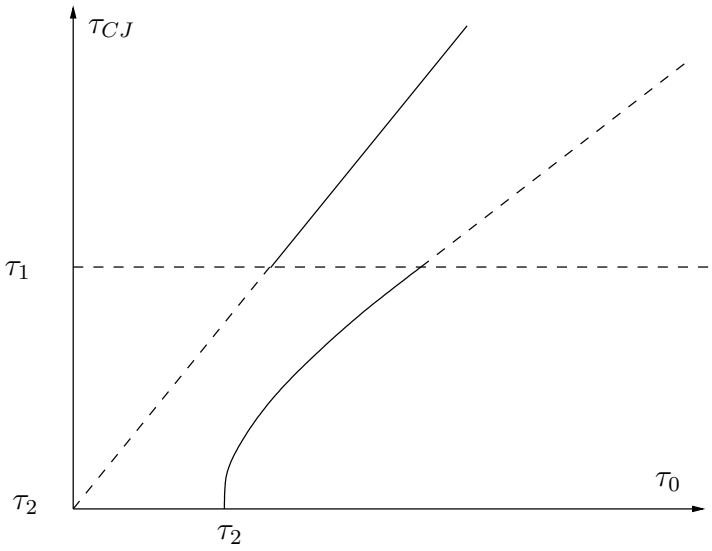

Figure 6.12: Qualitative behaviour of the mixture and the vapor Chapman–Jouguet points for the model with two perfect gas. The horizontal dashed line represents the vapor saturation curve. The increasing line (dashed line, then solid line) is the set of the Chapman–Jouguet points for the vapor equation of state. The other function (solid line, then dashed line) is the set of the mixture Chapman–Jouguet points. The solid lines of the curves correspond to the part in which they match with the equation of state used.

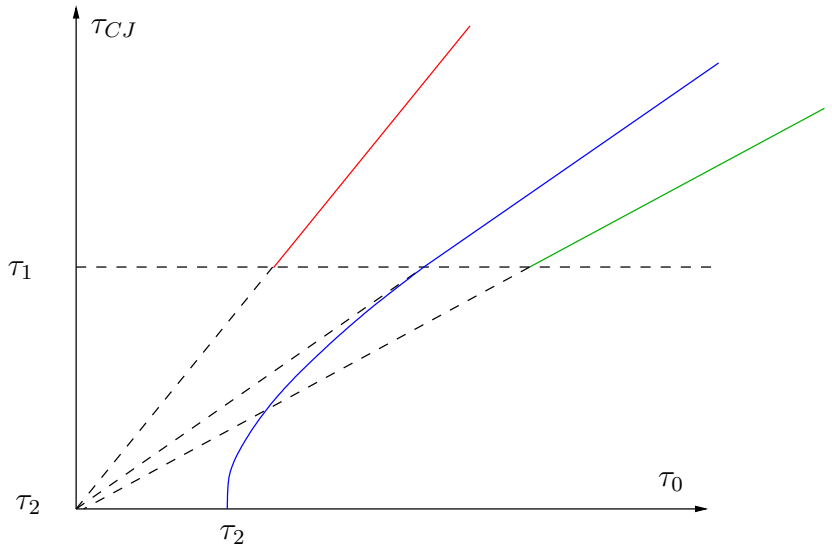

Figure 6.13: For the vaporization involving a mixture for the downstream state, we use the Chapman–Jouguet closure (it is validated in [56]). We draw the set of the pure phase Chapman-Jouguet points (red), and the set of the pure phase, constant pressure points (green). The blue straight line that goes from the intersection of the CJ mixture points with $\tau = \tau_2$ and that would pass by 0 is between the green and the red straight line, so that it corresponds to weak deflagration. As this closure is continuous, it is admissible.

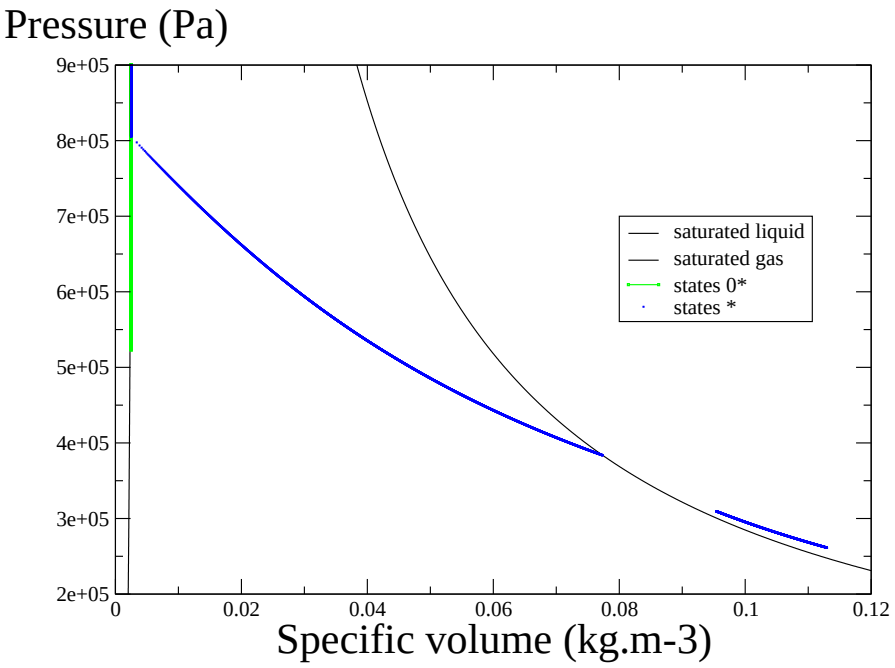

Figure 6.14: Set of all the Chapman–Jouguet points that can be reached from a given point. The isentrope is drawn in green, and is nearly vertical. In blue, the set of all the Chapman Jouguet points was drawn, which shows a jump between the mixture Chapman–Jouguet points and the pure vapor Chapman–Jouguet point.

6.3.2 Example 2 : model with two stiffened gas

As already mentioned, the mixture equation of state cannot be computed when we deal with the two stiffened gas model. Therefore we can only show a numerical computation as an illustration. We chose the model of dodecane for which coefficients lie in Table 4.2. We begin on the point $P_0 = 900000\,\mathrm{Pa}$ with a specific volume of $\tau_0 = 0.0025\,\mathrm{kg.m}^{-3}$. We compute all the states $0^\star$ that can be linked with that initial point via an isentrope. If the state $0^\star$ is overheated (i.e. lie in the saturation dome), then we compute the Chapman–Jouguet point(s) corresponding to a mixture downstream state and/or to a pure vapor downstream state. Numerical results are on Figure 6.14.

6.4 Conclusion

In this chapter, we proposed to take into account metastable states in the solution of the Riemann problem. For that, we used the Chapman–Jouguet theory. We first proved that this theory can be applied. We emphasized the link between the overheat or overcooled of the metastable state and the retrograde and regular behaviour of the fluid. In a particular case, when γ/Γ does not depend on τ, the condition of regular behaviour of the fluid is necessary and sufficient to ensure that the energy of a metastable liquid is lower than the energy of a mixture at thermodynamic equilibrium with the same pressure and specific volume.

For the entropy growth condition, we proved that it is ensured provided $\gamma_l > \gamma_m$ and $\gamma_l > \gamma_v$.

The problem with the deflagration waves is that the Lax characteristic criterion is not ensured, so that the problem is under–determinated. The only thing that we can state with no more hypothesis is that the set of all the downstream states lies in an area limited on the top by the set of all the constant pressure deflagrations, which is continuous, and on below by the set of all the Chapman–Jouguet points, which was proved to be discontinuous thanks for a detailed study of the behaviour of the Crussard curve near the saturation curve. As the set of all the Chapman–Jouguet points is discontinuous, the use of the Chapman–Jouguet closure as in [39] for solving the Riemann problem leads to a solution that does not depend continuously on its initial data in general. A first step to find a right kinetic closure would be for example to study travelling waves for relaxation model as given in [16]. As we know that liquid–vapor phase transition is governed by a competition between relaxation phenomena and thermal conduction, it would be more relevant (but much harder) to study travelling waves with relaxation model and thermal conductivity.

In this chapter, we exposed how to build a solution to the Riemann problem, with pure phases of the same fluid on each side. If the liquid is metastable, we explained how to take into account a vaporization wave. The problem kinetic closure has been solved in the case of a simple academic framework, but remains open for general equation of state. The very difference with the classical Van-der-Waals approach is that the way of building the Riemann problem solution has already been observed [56]. In the next chapter, we explain how to use the solution of the Riemann problem in a multiphase code.

Chapter 7

Numerical scheme and application

7.1 Reminds on the discrete equations method

The discrete equations method [2] was already explained in Chapter 3. We recall here the main ingredients of this scheme: the space in which the flow is computed is meshed by cells $\mathcal{C}_i$ (typically, on a one dimensional domain $[a,b]$ the cells are $\mathcal{C}_i = [a+i\Delta x, a+(i+1)\Delta x]$, with $\Delta x = (b-a)/N$). On each cell and at each time step, the variables are known for each phase:

$$(\alpha_j^{(1)}, \mathbf{U}_j^{(1)}, \alpha_j^{(2)}, \mathbf{U}_j^{(2)})$$

with

$$\mathbf{U}_j^{(k)} = \left(\rho_j^{(k)}, u_j^{(k)}, P_j^{(k)}\right)$$

We consider a family of random subdivision of the cell

$$\mathcal{C}_i = \cup[\xi_k, \xi_{k+1}]$$

we make evolve this random division (see Figure 7.1), and integrate separately each phase. We denote by X the characteristic function of the fluid 1. In section 3.1, we found the following semi-discrete scheme

$$\begin{aligned}
&\frac{\partial(\alpha_i^{(1)}\mathbf{U}_i^{(1)})}{\partial t} \\
&\quad + \frac{1}{\Delta x}\left(\mathcal{E}\left(X\left(x_{i+\frac{1}{2}}, t^+\right)\mathbf{F}\left(\mathbf{U}_{i+\frac{1}{2}}^{\star}\right)\right) - \mathcal{E}\left(X\left(x_{i-\frac{1}{2}}, t^+\right)\mathbf{F}\left(\mathbf{U}_{i-\frac{1}{2}}^{\star}\right)\right)\right) \\
&\quad = \lambda_i\left(\mathbf{F}^{\ell ag}\left(\mathbf{U}_i^{(2)}, \mathbf{U}_i^{(1)}\right) - \mathbf{F}^{\ell ag}\left(\mathbf{U}_i^{(1)}, \mathbf{U}_i^{(2)}\right)\right) \\
&\qquad + \frac{1}{\Delta x}\left(\mathcal{E}\left([X]_0\right)\mathbf{F}^{\ell ag}\left(\mathbf{U}_{i-1}^{+}, \mathbf{U}_i^{-}\right) + \mathcal{E}\left([X]_{N(\omega)}\right)\mathbf{F}^{\ell ag}\left(\mathbf{U}_i^{+}, \mathbf{U}_{i+1}^{-}\right)\right)
\end{aligned} \tag{7.1}$$

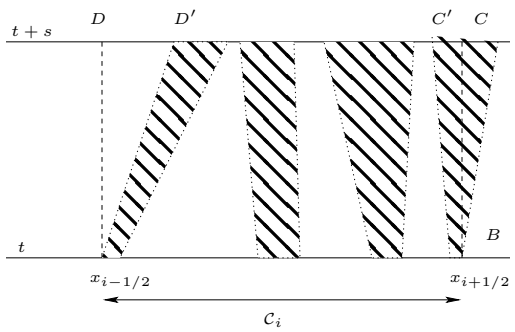

Figure 7.1: Evolution of each phase after a random subdivision of the cell $\mathcal{C}_i$ between time t and $t+s$

where the Lagrangian fluxes correspond to the integration along the surface contact between the phases: the phases are separated before the integration. We remark that the relaxation terms correspond to the case when the fluids are well mixed. In the case of interface problems, they do not appear.

It remains to average the different terms. As seen in section 3.1, the probability distribution of the volume fraction on the boundary between the cell i and $i+1$ is given by

$$\begin{aligned}
\mathcal{P}_{i+\frac{1}{2}}\left(\Sigma_1,\Sigma_1\right) &= \min\left(\alpha_i^{(1)},\alpha_{i+1}^{(1)}\right)\\
\mathcal{P}_{i+\frac{1}{2}}\left(\Sigma_2,\Sigma_2\right) &= \min\left(\alpha_i^{(2)},\alpha_{i+1}^{(2)}\right)\\
\mathcal{P}_{i+\frac{1}{2}}\left(\Sigma_1,\Sigma_2\right) &= \max\left(\alpha_i^{(1)}-\alpha_{i+1}^{(1)},0\right)\\
\mathcal{P}_{i+\frac{1}{2}}\left(\Sigma_2,\Sigma_1\right) &= \max\left(\alpha_i^{(2)}-\alpha_{i+1}^{(2)},0\right)
\end{aligned}$$

Then

- the Eulerian fluxes are evaluated according to which fluid lies on the boundary of the cell

$$\begin{aligned}
\mathcal{E}\left(X\left(x_{i+\frac{1}{2}},t_n^+\right)\mathbf{F}\left(U_{i+\frac{1}{2}}^{\star}\right)\right) = {} & \mathcal{P}_{i+\frac{1}{2}}\left(\Sigma_1,\Sigma_1\right)\mathbf{F}\left(\mathbf{U}_i^{(1)},\mathbf{U}_{i+1}^{(1)}\right)\\
& +\mathcal{P}_{i+\frac{1}{2}}\left(\Sigma_1,\Sigma_2\right)\left(\beta_{i+\frac{1}{2}}^{(1,2)}\right)^{+}\mathbf{F}\left(\mathbf{U}_i^{(1)},\mathbf{U}_{i+1}^{(2)}\right)\\
& +\mathcal{P}_{i+\frac{1}{2}}\left(\Sigma_2,\Sigma_1\right)\left(-\beta_{i+\frac{1}{2}}^{(2,1)}\right)^{+}\mathbf{F}\left(\mathbf{U}_i^{(2)},\mathbf{U}_{i+1}^{(1)}\right)
\end{aligned}$$

- The Lagrangian fluxes are added, if there is a jump of X inside the cell.

$$\begin{aligned}
\mathcal{E}\left(\left[X\right]_{N(\omega)}\right)\mathbf{F}^{\ell ag}\left(\mathbf{U}_i^{N(\omega)},\mathbf{U}_{i+1}^{-}\right) = {} & \mathcal{P}_{i+\frac{1}{2}}\left(\Sigma_1,\Sigma_2\right)\left(\beta_{i+\frac{1}{2}}^{(1,2)}\right)^{-}\mathbf{F}^{\ell ag}\left(\mathbf{U}_i^{(1)},\mathbf{U}_{i+1}^{(2)}\right)\\
& -\mathcal{P}_{i+\frac{1}{2}}\left(\Sigma_2,\Sigma_1\right)\left(\beta_{i+\frac{1}{2}}^{(2,1)}\right)^{-}\mathbf{F}^{\ell ag}\left(\mathbf{U}_i^{(2)},\mathbf{U}_{i+1}^{(1)}\right)
\end{aligned}$$

and for the left one

$$\begin{aligned}\mathcal{E}\left([X]_0\right)\mathbf{F}^{\ell ag}\left(\mathbf{U}_{i-1}^{+},\mathbf{U}_i^0\right) = & -\mathcal{P}_{i-\frac{1}{2}}\left(\Sigma_1,\Sigma_2\right)\left(\beta_{i-\frac{1}{2}}^{(1,2)}\right)^{+}\mathbf{F}^{\ell ag}\left(\mathbf{U}_{i-1}^{(1)},\mathbf{U}_i^{(2)}\right)\\ & +\mathcal{P}_{i-\frac{1}{2}}\left(\Sigma_2,\Sigma_1\right)\left(\beta_{i-\frac{1}{2}}^{(2,1)}\right)^{+}\mathbf{F}^{\ell ag}\left(\mathbf{U}_{i-1}^{(2)},\mathbf{U}_i^{(1)}\right)\end{aligned}$$

The exact values of the β are given in Table 3.1 and Table 3.2. Their meaning is the following:

- An Eulerian flux shall be added provided the fluid is on the boundary of the cell
- A Lagrangian flux shall be added if there is a contact between the fluids.

to be less formal, an Eulerian flux is added on the fluid k if this fluid comes trough the boundary of the cell. A Lagrangian flux is added on the fluid k if there is a contact in the cell between the two fluids, i.e. either if the fluid k is "pushed" by the fluid $\bar{k}$ in the cell, or if the fluid k "pushes" the fluid $\bar{k}$ in the cell.

To summarise, the discrete equation method consists in

1. Cut each cell control in a random subdivision.
2. Make evolve the random subdivision.
3. Integrate the Eulerian system

$$\frac{\partial \mathbf{U}}{\partial t}+\frac{\partial (F(\mathbf{U}))}{\partial x}=0$$

   on the space-time volume, taking care to keep *separate phases*.
4. average.

7.2 How to adapt the DEM to the reactive Riemann problems?

In the above described method, the first and second step will be kept the same. In the third step, the Riemann problem that are to be solved have a pure phase on each side. This is exactly the type that was solved in Chapter 6. In the discrete equations method, four Riemann problems are to be solved at each interface:

- A liquid-liquid Riemann problem,
- A liquid-gas Riemann problem,
- A gas-liquid Riemann problem,
- A gas-gas Riemann problem.

For each of these Riemann problem, we need to solve them, and to integrate the solution by separating the phases. First, we remark that for the liquid-liquid and the gas-gas Riemann problem, the integration does not change, because we chose to keep these Riemann problem inert. We need thus to concentrate on the integration of the liquid-gas and the gas-liquid Riemann problem.

7.2.1 Adaptation for total vaporisation

We suppose that all the Riemann problems are reactive, and that the reaction is total. The average will be kept as the same. We remark that in the integration, everything is the same except for that *the contact surface is replaced by the vaporisation front*. Therefore, the semi-discrete scheme (7.1) becomes

$$\begin{aligned}&\frac{\partial(\alpha_i^{(1)}\mathbf{U}_i^{(1)})}{\partial t}\\&+\frac{1}{\Delta x}\left(\mathcal{E}\left(X\left(x_{i+\frac{1}{2}},t^+\right)\mathbf{F}\left(\mathbf{U}^\star_{i+\frac{1}{2}}\right)\right)-\mathcal{E}\left(X\left(x_{i-\frac{1}{2}},t^+\right)\mathbf{F}\left(\mathbf{U}^\star_{i-\frac{1}{2}}\right)\right)\right)\\&=\frac{1}{\Delta x}\left(\mathcal{E}\left([X]_0\right)\mathbf{F}^{rea}\left(\mathbf{U}^+_{i-1},\mathbf{U}^-_i\right)+\mathcal{E}\left([X]_{N(\omega)}\right)\mathbf{F}^{rea}\left(\mathbf{U}^+_i,\mathbf{U}^-_{i+1}\right)\right)\end{aligned} \tag{7.2}$$

where F^{rea} is the reaction flux $F(\mathbf{U})-\sigma_v\mathbf{U}$, where σ_v is the velocity of the vaporisation front, and $\mathbf{U}$ is taken on any side of the front.

- the Eulerian fluxes are evaluated according to which fluid lies on the boundary of the cell

$$\begin{aligned}\mathcal{E}\left(X\left(x_{i+\frac{1}{2}},t_n^+\right)\mathbf{F}\left(U^\star_{i+\frac{1}{2}}\right)\right)=&\ \mathcal{P}_{i+\frac{1}{2}}\left(\Sigma_1,\Sigma_1\right)\mathbf{F}\left(\mathbf{U}_i^{(1)},\mathbf{U}_{i+1}^{(1)}\right)\\&+\mathcal{P}_{i+\frac{1}{2}}\left(\Sigma_1,\Sigma_2\right)\left(\zeta^{(1,2)}_{i+\frac{1}{2}}\right)^+\mathbf{F}\left(\mathbf{U}_i^{(1)},\mathbf{U}_{i+1}^{(2)}\right)\\&+\mathcal{P}_{i+\frac{1}{2}}\left(\Sigma_2,\Sigma_1\right)\left(-\zeta^{(2,1)}_{i+\frac{1}{2}}\right)^+\mathbf{F}\left(\mathbf{U}_i^{(2)},\mathbf{U}_{i+1}^{(1)}\right)\end{aligned}$$

  The flux indicator for the Eulerian flux is given in Table 7.1.

Table 7.1: Flux indicator for the Eulerian Flux where we denote $\zeta_{i+\frac{1}{2}}^{(l,p)} = \text{sign}\left(\sigma_v\left(U_i^l, U_{i+1}^p\right)\right)$

flow patterns	left and right states	flux indicator
$\Sigma_1 - \Sigma_2$	$U_i^{(1)}, U_{i+1}^{(2)}$	$\left(\zeta_{i+\frac{1}{2}}^{(1,2)}\right)^+$
$\Sigma_1 - \Sigma_1$	$U_i^{(1)}, U_{i+1}^{(1)}$	1
$\Sigma_2 - \Sigma_1$	$U_i^{(2)}, U_{i+1}^{(1)}$	$\left(-\zeta_{i+\frac{1}{2}}^{(2,1)}\right)^+$
$\Sigma_2 - \Sigma_2$	$U_i^{(2)}, U_{i+1}^{(2)}$	0

Table 7.2: Flux indicator for the reactive Flux where we denote $\zeta_{i+\frac{1}{2}}^{(l,p)} = \text{sign}\left(\sigma_v\left(U_i^l, U_{i+1}^p\right)\right)$

flow patterns	Reactive flux	flux indicator
$\Sigma_1 - \Sigma_2$	$F^{rea}\left(U_i^{(1)}, U_{i+1}^{(2)}\right)$	$\left(\zeta_{i+\frac{1}{2}}^{(1,2)}\right)^-$
$\Sigma_1 - \Sigma_1$	$F^{rea}\left(U_i^{(1)}, U_{i+1}^{(1)}\right)$	0
$\Sigma_2 - \Sigma_1$	$F^{rea}\left(U_i^{(2)}, U_{i+1}^{(1)}\right)$	$-\left(-\zeta_{i+\frac{1}{2}}^{(2,1)}\right)^-$
$\Sigma_2 - \Sigma_2$	$F^{rea}\left(U_i^{(2)}, U_{i+1}^{(2)}\right)$	0

- The reactive fluxes are added, if there is a jump of X inside the cell.

$$\mathcal{E}\left([X]_{N(\omega)}\right)\mathbf{F}^{rea}\left(\mathbf{U}_i^{N(\omega)}, \mathbf{U}_{i+1}^-\right) = \mathcal{P}_{i+\frac{1}{2}}\left(\Sigma_1, \Sigma_2\right)\left(\zeta_{i+\frac{1}{2}}^{(1,2)}\right)^-\mathbf{F}^{rea}\left(\mathbf{U}_i^{(1)}, \mathbf{U}_{i+1}^{(2)}\right) - \mathcal{P}_{i+\frac{1}{2}}\left(\Sigma_2, \Sigma_1\right)\left(\zeta_{i+\frac{1}{2}}^{(2,1)}\right)^-\mathbf{F}^{rea}\left(\mathbf{U}_i^{(2)}, \mathbf{U}_{i+1}^{(1)}\right)$$

and for the left one

$$\mathcal{E}\left([X]_0\right)\mathbf{F}^{rea}\left(\mathbf{U}_{i-1}^+, \mathbf{U}_i^0\right) = -\mathcal{P}_{i-\frac{1}{2}}\left(\Sigma_1, \Sigma_2\right)\left(\zeta_{i-\frac{1}{2}}^{(1,2)}\right)^+\mathbf{F}^{rea}\left(\mathbf{U}_{i-1}^{(1)}, \mathbf{U}_i^{(2)}\right) + \mathcal{P}_{i-\frac{1}{2}}\left(\Sigma_2, \Sigma_1\right)\left(\zeta_{i-\frac{1}{2}}^{(2,1)}\right)^+\mathbf{F}^{rea}\left(\mathbf{U}_{i-1}^{(2)}, \mathbf{U}_i^{(1)}\right)$$

The exact value of the flux indicator ζ is given in Table 7.2. Their value are given by the same approach as in section 3.1.

7.2.2 Partial vaporisation

In this subsection, we want to generalise what was done on the previous subsections. The question is: what become the fluxes if there appear a

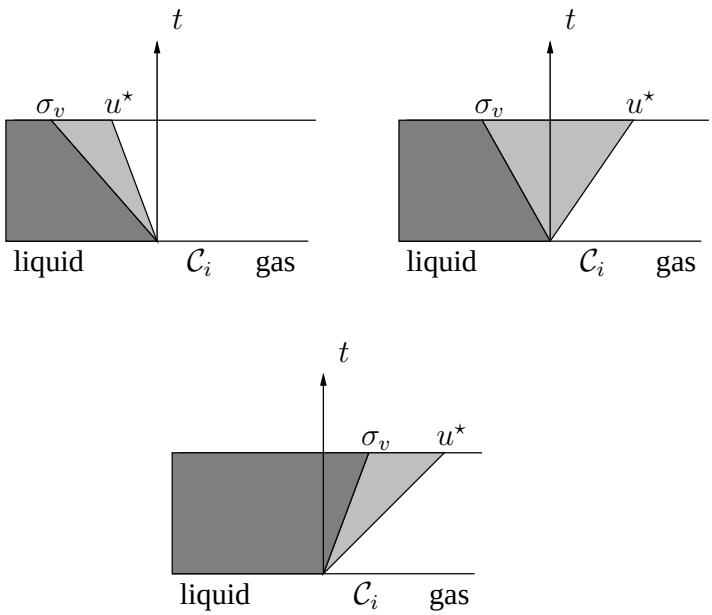

Figure 7.2: The solution of a typical liquid-gas Riemann problem. The darkest zone is a liquid and the white zone is a gas. The grey zone is, in general a mixture of liquid and gas. The discontinuity of X may be across the vaporisation wave σ_v and the contact discontinuity $u^\star$.

mixture zone? In particular, we aim at giving a sense to the integral of X in a mixture area.

We specify this integration for the liquid-gas Riemann problem, on the right boundary of the cell. The other integrations can be deduced from this one by symmetry. In Figure 7.2, we represented all the cases that may happen for this Riemann problem (actually, we draw only what is of interest, i.e. the discontinuities of X. To integrate X in a mixture area, we remark that the flow there is composed of a liquid and a gas, with the same pressure, the same velocity, and a different density. To integrate along X, we restart from the hypothesis that the fluids are locally not miscible. Therefore, the flow can be considered as the limit of the flow described in Figure 7.3: the mixture zone is the limit of a flow composed of either a pure liquid, or a pure gas, moving at the velocity $u^\star$, with the same pressure $P^\star$. Of course, the distribution of the liquid and the gas must be consistent (at least when the size of the bubbles goes to 0) with the volume fraction of each component found when the Riemann problem was solved. Actually, the cut/average procedure described above leads to the fact that for a given realization, we find again an Eulerian, a Lagrangian and a reactive flux, that are weighted with

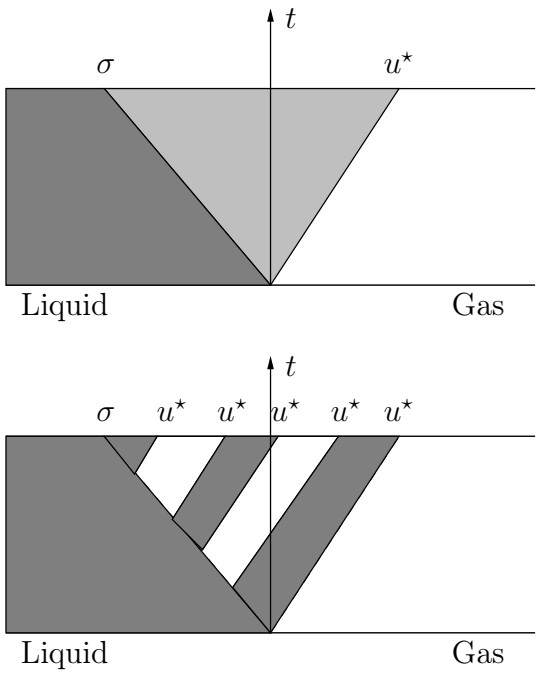

Figure 7.3: The mixture zone of the flow is considered as the limit of a flow of bubbles with the same pressure $P^\star$ and the same velocity $u^\star$. The discontinuity between these bubbles is a contact of velocity $u^\star$. The distribution of the liquid and the gas in the cone $(\sigma t, u^\star t)$ must be consistent, when the size of the bubbles tends to 0, with the volume fraction of the liquid and the gas found when the Riemann problem was solved.

a weight depending on the volume fraction of the fluid concerned. We denote by w^{eul} the weight for the Eulerian flux, $w^{\ell ag}$ the weight for the Lagrangian flux, and w^{rea} the weight for the reactive flux. With these notations, the semi discrete scheme reads

$$\begin{aligned}
&\frac{\partial(\alpha_i^{(1)}\mathbf{U}_i^{(1)})}{\partial t} \\
&\quad + \frac{1}{\Delta x}\left(\mathcal{E}\left(X\left(x_{i+\frac{1}{2}},t^+\right)w_{i+\frac{1}{2}}^{eul}\mathbf{F}\left(\mathbf{U}_{i+\frac{1}{2}}^{\star}\right)\right) - \mathcal{E}\left(X\left(x_{i-\frac{1}{2}},t^+\right)w_{i+\frac{1}{2}}^{eul}\mathbf{F}\left(\mathbf{U}_{i-\frac{1}{2}}^{\star}\right)\right)\right) \\
&\quad = \frac{1}{\Delta x}\left(\mathcal{E}\left([X]_0\, w_0^{rea}\right)\mathbf{F}^{rea}\left(\mathbf{U}_{i-1}^+,\mathbf{U}_i^-\right) + \mathcal{E}\left([X]_{N(\omega)}\, w_{N(\omega)}^{rea}\right)\mathbf{F}^{rea}\left(\mathbf{U}_i^+,\mathbf{U}_{i+1}^-\right)\right) \\
&\qquad + \frac{1}{\Delta x}\left(\mathcal{E}\left([X]_0\, w_0^{\ell ag}\right)\mathbf{F}^{\ell ag}\left(\mathbf{U}_{i-1}^+,\mathbf{U}_i^-\right) + \mathcal{E}\left([X]_{N(\omega)}\, w_{N(\omega)}^{\ell ag}\right)\mathbf{F}^{\ell ag}\left(\mathbf{U}_i^+,\mathbf{U}_{i+1}^-\right)\right)
\end{aligned} \tag{7.3}$$

Now, we denote by $\overset{\star}{\alpha}_i^{(k,l)}$ the volume fraction of the fluid that may disappear in the reaction. The value of this volume fraction is the one found in the mixture zone when the Riemann problem was solved. With this notation, we find

- For the Eulerian flux

$$\begin{aligned}
&\mathcal{E}\left(X\left(x_{i+\frac{1}{2}},t_n^+\right)\mathbf{F}\left(U_{i+\frac{1}{2}}^{\star}\right)\right) \\
&\quad = \mathcal{P}_{i+\frac{1}{2}}\left(\Sigma_1,\Sigma_1\right)\mathbf{F}\left(\mathbf{U}_i^{(1)},\mathbf{U}_{i+1}^{(1)}\right) \\
&\qquad + \mathcal{P}_{i+\frac{1}{2}}\left(\Sigma_1,\Sigma_2\right)\left(\beta_{i+\frac{1}{2}}^{(1,2)}\right)^+ \overset{\star}{\alpha}_{i+\frac{1}{2}}^{(1,2)}\mathbf{F}\left(\mathbf{U}_i^{(1)},\mathbf{U}_{i+1}^{(2)}\right) \\
&\qquad + \mathcal{P}_{i+\frac{1}{2}}\left(\Sigma_2,\Sigma_1\right)\left(-\beta_{i+\frac{1}{2}}^{(2,1)}\right)^+ \overset{\star}{\alpha}_{i+\frac{1}{2}}^{(2,1)}\mathbf{F}\left(\mathbf{U}_i^{(2)},\mathbf{U}_{i+1}^{(1)}\right) \\
&\qquad + \mathcal{P}_{i+\frac{1}{2}}\left(\Sigma_1,\Sigma_2\right)\left(\zeta_{i+\frac{1}{2}}^{(1,2)}\right)^+ (1-\overset{\star}{\alpha}_{i+\frac{1}{2}}^{(1,2)})\mathbf{F}\left(\mathbf{U}_i^{(1)},\mathbf{U}_{i+1}^{(2)}\right) \\
&\qquad + \mathcal{P}_{i+\frac{1}{2}}\left(\Sigma_2,\Sigma_1\right)\left(-\zeta_{i+\frac{1}{2}}^{(2,1)}\right)^+ (1-\overset{\star}{\alpha}_{i+\frac{1}{2}}^{(2,1)})\mathbf{F}\left(\mathbf{U}_i^{(2)},\mathbf{U}_{i+1}^{(1)}\right)
\end{aligned}$$

- For the reactive flux, on the right

$$\begin{aligned}
&\mathcal{E}\left([X]_{N(\omega)}\, w_{N(\omega)}^{rea}\right)\mathbf{F}^{rea}\left(\mathbf{U}_i^{N(\omega)},\mathbf{U}_{i+1}^-\right) \\
&\quad = \mathcal{P}_{i+\frac{1}{2}}\left(\Sigma_1,\Sigma_2\right)\left(\zeta_{i+\frac{1}{2}}^{(1,2)}\right)^- (1-\overset{\star}{\alpha}_{i+\frac{1}{2}}^{(1,2)})\mathbf{F}^{rea}\left(\mathbf{U}_i^{(1)},\mathbf{U}_{i+1}^{(2)}\right) \\
&\qquad - \mathcal{P}_{i+\frac{1}{2}}\left(\Sigma_2,\Sigma_1\right)\left(\zeta_{i+\frac{1}{2}}^{(2,1)}\right)^- (1-\overset{\star}{\alpha}_{i+\frac{1}{2}}^{(2,1)})\mathbf{F}^{rea}\left(\mathbf{U}_i^{(2)},\mathbf{U}_{i+1}^{(1)}\right)
\end{aligned}$$

and for the left one

$$\begin{aligned}\mathcal{E}\left([X]_0\right)\mathbf{F}^{rea}\left(\mathbf{U}_{i-1}^{+},\mathbf{U}_{i}^{0}\right)&\\ =\ -\mathcal{P}_{i-\frac{1}{2}}\left(\Sigma_1,\Sigma_2\right)\left(\zeta_{i-\frac{1}{2}}^{(1,2)}\right)^{+}\left(1-\overset{\star}{\alpha}{}_{i-\frac{1}{2}}^{(1,2)}\right)\mathbf{F}^{rea}\left(\mathbf{U}_{i}^{(1)},\mathbf{U}_{i+1}^{(2)}\right)&\\ +\mathcal{P}_{i-\frac{1}{2}}\left(\Sigma_2,\Sigma_1\right)\left(\zeta_{i-\frac{1}{2}}^{(2,1)}\right)^{+}\left(1-\overset{\star}{\alpha}{}_{i-\frac{1}{2}}^{(2,1)}\right)\mathbf{F}^{rea}\left(\mathbf{U}_{i-1}^{(2)},\mathbf{U}_{i}^{(1)}\right)&\end{aligned}$$

- For the Lagrangian fluxes

$$\begin{aligned}\mathcal{E}\left(\left[X\right]_{N(\omega)}w_{N(\omega)}^{\ell ag}\right)\mathbf{F}^{\ell ag}\left(\mathbf{U}_{i}^{N(\omega)},\mathbf{U}_{i+1}^{-}\right)&\\ =\ \mathcal{P}_{i+\frac{1}{2}}\left(\Sigma_1,\Sigma_2\right)\left(\beta_{i+\frac{1}{2}}^{(1,2)}\right)^{-}\overset{\star}{\alpha}{}_{i+\frac{1}{2}}^{(1,2)}\mathbf{F}^{\ell ag}\left(\mathbf{U}_{i}^{(1)},\mathbf{U}_{i+1}^{(2)}\right)&\\ -\mathcal{P}_{i+\frac{1}{2}}\left(\Sigma_2,\Sigma_1\right)\left(\beta_{i+\frac{1}{2}}^{(2,1)}\right)^{-}\overset{\star}{\alpha}{}_{i+\frac{1}{2}}^{(2,1)}\mathbf{F}^{\ell ag}\left(\mathbf{U}_{i}^{(2)},\mathbf{U}_{i+1}^{(1)}\right)&\end{aligned}$$

and for the left one

$$\begin{aligned}\mathcal{E}\left(\left[X\right]_{0}w_{0}^{\ell ag}\right)\mathbf{F}^{\ell ag}\left(\mathbf{U}_{i-1}^{+},\mathbf{U}_{i}^{0}\right)&\\ =\ -\mathcal{P}_{i-\frac{1}{2}}\left(\Sigma_1,\Sigma_2\right)\left(\beta_{i-\frac{1}{2}}^{(1,2)}\right)^{+}\overset{\star}{\alpha}{}_{i-\frac{1}{2}}^{(1,2)}\mathbf{F}^{\ell ag}\left(\mathbf{U}_{i-1}^{(1)},\mathbf{U}_{i}^{(2)}\right)&\\ +\mathcal{P}_{i-\frac{1}{2}}\left(\Sigma_2,\Sigma_1\right)\left(\beta_{i-\frac{1}{2}}^{(2,1)}\right)^{+}\overset{\star}{\alpha}{}_{i-\frac{1}{2}}^{(2,1)}\mathbf{F}^{\ell ag}\left(\mathbf{U}_{i-1}^{(2)},\mathbf{U}_{i}^{(1)}\right)&\end{aligned}$$

note that in the previous equation, F is the flux of the concerned fluid, *i.e.* the density is the density of the concerned fluid, and the equation of state used to calculate the energy is the equation of state of the concerned fluid. The numerical scheme is the same for the other component, by exchanging the 1 and 2, except for $\overset{\star}{\alpha}$, which is kept the same for the two fluids: it is natural that the scheme is no more symmetric in 1 and 2, because the reaction induces that one of the fluid disappears, whereas the other one appears.

7.2.3 How an α discontinuity should diffuse? Repair procedures

Simple contact

As it is stated in [2, p. 382-385], a contact surface is exactly conserved by the scheme for inert flows. This means that if a contact surface of velocity u and pressure P is computed with the code, and with $\Delta t/\Delta x$ not equal to $1/\left|u\right|$, then the contact is diffused around its exact position, and in this diffusion zone, the velocity of both of the fluids is u, and their pressure is P; the density of each of the fluids is constant in the diffusion zone, see Figure 7.4. We note that this property holds for a contact between pure phases, as much as for a contact between a pure phase and a mixture.

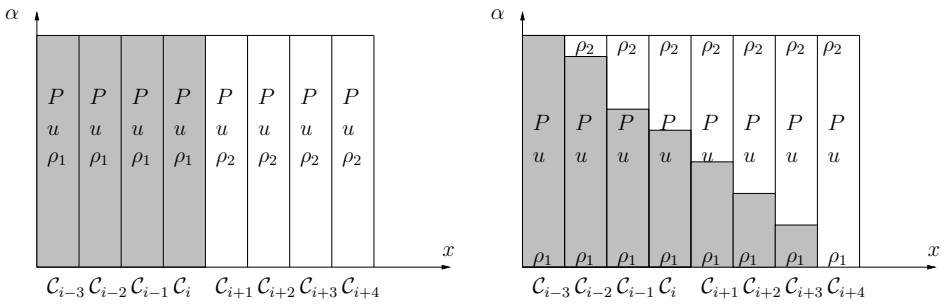

Figure 7.4: A contact surface , characterised by a pressure P and a velocity u is advected at the velocity u. On each side of the contact, the fluid has a constant density, respectively ρ_1 and ρ_2. The contact is initially on the boundary of the cell $\mathcal{C}_i$. After some time, the discontinuity has moved around a new cell k. The contact has diffused, but the pressure of each of the component is still P, the velocity is u, and the density of each of the component is constant.

Liu solution

We recall that in the Liu solution, there are α discontinuities that correspond to shocks, between mixtures and pure gas. In the discrete equations method, only pure phase Riemann problems are solved.

We suppose for example that two neighbour cells are separated by a liquefaction shock, and that this liquefaction is not total. This means that

- On the left, we have a mixture of liquid and gas at thermodynamic equilibrium.
- On the right, we have a pure gas.
- the mixture variables are separated by a shock: $[F(\mathbf{U})-\sigma\mathbf{U}] = 0$, where F and U are the flux and the conservative variable *of the average*.

Then, as the gas-liquid and gas-gas Riemann problem are solved independantly (see Figure 7.5), it is clear that neither the solution of the gas-liquid Riemann problem is a contact with velocity σ, nor the gas-gas Riemann problem. From a more general point of view, it is very rare that replacing a nonlinear problem (the relation $[F(U) - \sigma U] = 0$) by the averaging of two nonlinear problems (the two Riemann problems with pure phase on each side), give the same solution. All the more, what shall be noted is that after averaging, it is very unlikely that the mixture that may appear is still at thermodynamic equilibrium. Nevertheless, we know that in the Liu solution,

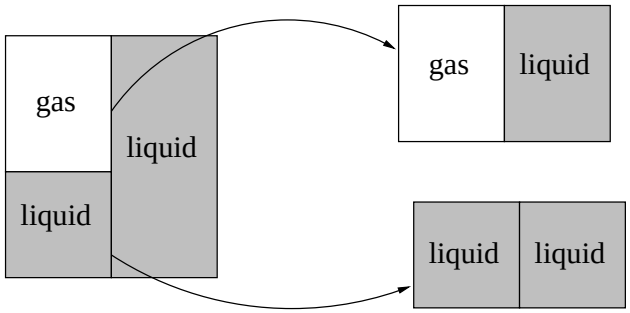

Figure 7.5: In the discrete equations method, only pure phase Riemann problems are solved. For example, if we suppose that on the left, the states are separated by a liquefaction shock, we have $[F(\mathbf{U}) - \sigma\mathbf{U}] = 0$ for the averaged variables. As the Riemann problem is separated into two Riemann problems, the liquefaction shock cannot be exactly advected. This is often the case when a nonlinear problem is replaced by an average of two nonlinear problems.

all the states are at thermodynamical equilibrium. For repairing this, we relax all the mixtures to the thermodynamic equilibrium , i.e. we impose the same temperature, pressure, and thermodynamic potentials by keeping constant the conservative variables.

Chapman-Jouguet solution

For a Chapman-Jouguet phase transition, things become harder. We indeed theoretically have to deal with the problem of metastable liquid, and, if a partial vaporisation occurs, with mixtures at thermodynamic equilibrium. We cannot relax all the fluids as it is done for the Liu solution, because this would induce a return to equilibrium for the metastable liquid. We chose not to do anything, in order to keep the same property as for the contact discontinuity: we let the discontinuity diffuse without doing any relaxation. This allows a good propagation of the total vaporisation waves. For partial vaporisation waves, the problem remains open, up to our knowledge.

7.3 Numerical results

In all the numerical tests, we chose the equation of state of perfect gas, because these are the only ones for which we have an explicit and relevant kinetic closure for the closure of the Riemann problem with metastable va-

porisation. For the Liu solution, the relaxation is much easier with the model with two perfect gas. As said in Chapter 4, the heavier phase must be the one with the smaller polytropic coefficient γ. In the tests, we have

- For the liquid, $\gamma_l = 1.2$
- For the gas, $\gamma_g = 1.9$

For this couple of polytropic coefficient, the (P, τ) phase is divided as follows:

- For $\rho \leq \rho_{\min} \approx 0.566$, the gas is stable.
- For $\rho \geq \rho_{\max} \approx 2.544$, the liquid is stable.

between $\rho_{\max}$ and $\rho_{\min}$, the mixture is stable.

7.3.1 Liquefaction shock

In this first test, we simulate a shock tube involving two shocks in a gas. We impose two sufficiently strong shocks in order to reach the gas saturation curve, and to observe two liquefaction shocks. Both sides have the same pressure, $P = 10^4\,\mathrm{Pa}$ also the same density $\rho = 0.5\,\mathrm{kg.m}^{-3}$. At the initial time, the left side and the right side have opposite velocities: $u = 90\,\mathrm{km.h}^{-1}$ on the left, and $u = -90\,\mathrm{km.h}^{-1}$ on the right. The results are shown on Figure 7.6, at time $t = 2.10^{-3}\,s$. The approximated solution agrees with the analytical solution. On the center, we observe an overshoot on the density, which is an usual problem when Godunov' methods are used for the Euler system on a symmetric case.

7.3.2 Total Chapman–Jouguet vaporization

In this test, we want to compute a vaporisation. Therefore the initial composition is: on the right a gas at rest ($u = 0$, $P = 10^5\,\mathrm{Pa}$, $\rho = 0.5\,\mathrm{kg.m}^{-3}$) and on the left, a liquid with a high pressure ($u = 0$, $P = 10^9\,\mathrm{Pa}$ and $\rho = 3\mathrm{kg.m}^{-3}$). We expect that the difference in pressures will induce a strong rarefaction wave in the liquid, leading it to a metastable state. Then we expect to observe a phase transition wave. The results are shown on Figure 7.7, at time $10^{-4}\,s$. Analytical and numerical solutions agree very well.

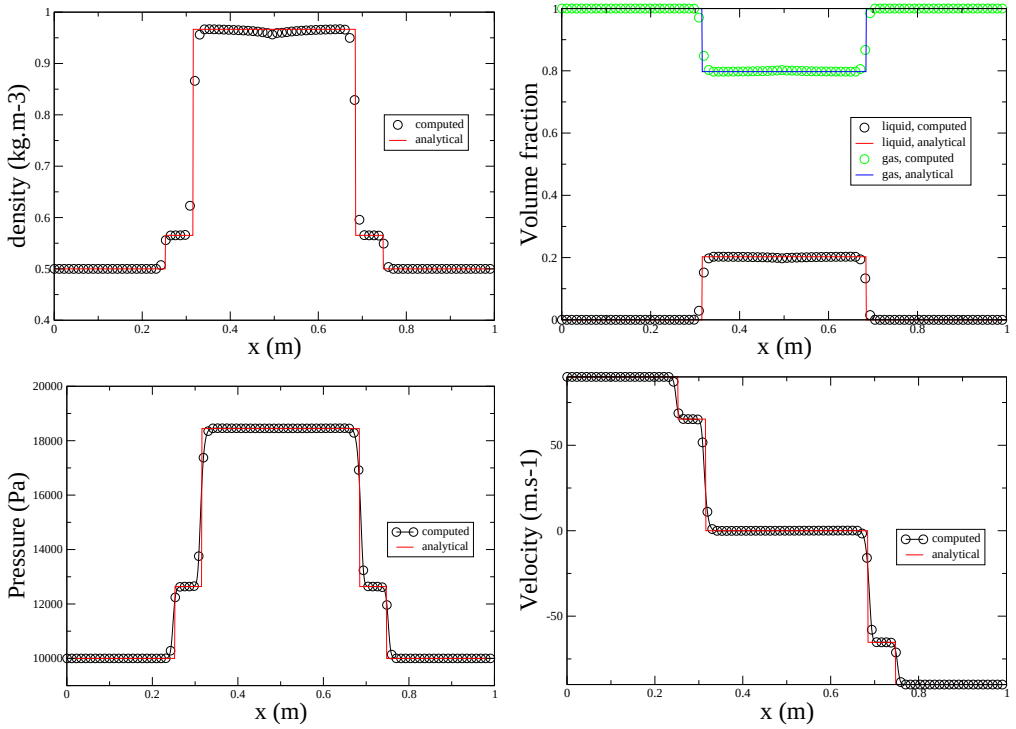

Figure 7.6: Numerical results for the Two shock Riemann problem. Actually, the two shocks are decomposed at the saturation of the gas. On both side, the following shock is a liquefaction shock across which the volume fraction is changed. For all the variables, we observe a good agreement between the analytical solution and the computed one (1000 points).

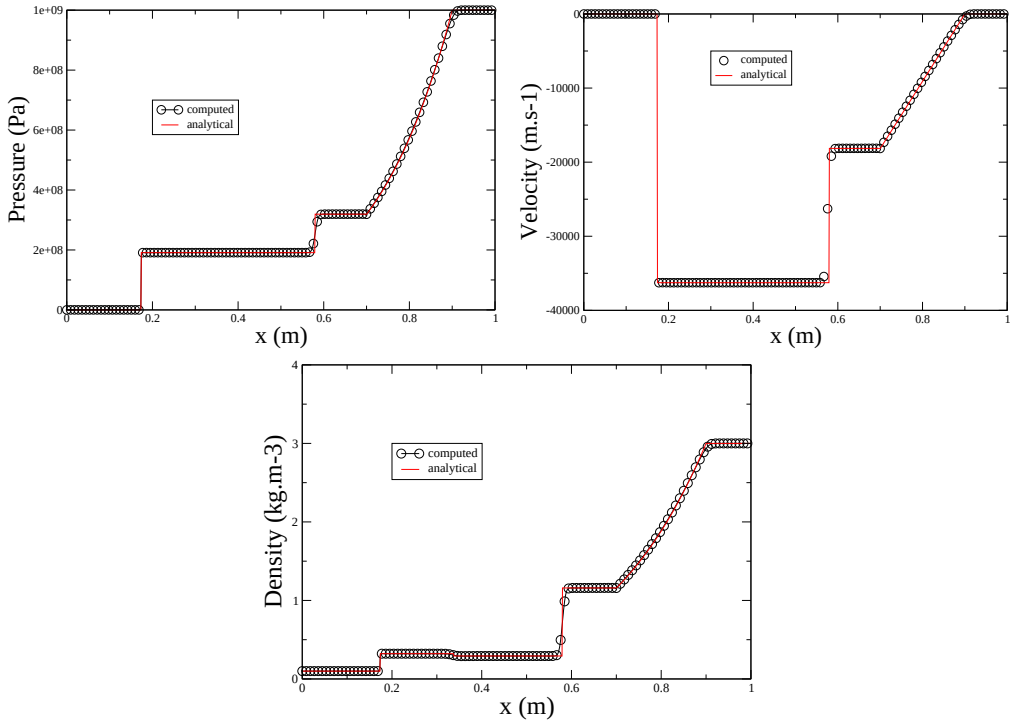

Figure 7.7: Numerical results for the shock tube with high pressure liquid and normal pressure gas. We observe a good agreement between the analytical solution and the computed one (3500 points).

7.4 Application to laser/matter interaction

7.4.1 Physic of laser interaction with matter

In this section, we are concerned with a simulation in the conditions of laser matter interaction.

A matter (solid) lies in its vapour. This solid is enlightened by an high energy laser. This laser propagates in the vapour, whereas in the solid, it cannot propagate further than a critical density ρ_c, due to the skin effect. The laser energy is released in the matter, and induces a vaporisation, and other hydrodynamic and thermal effects that we aim at simulating.

In this context: the following phenomena are to be taken into account

- The laser propagation: it is modelled as an energy released in the matter, at the given critical density ρ_c. It means that only solutions with thermal equilibrium will be possible ($T_e = T_i$) and that characteristic time of laser pulse has to be of the nanosecond. It excludes picosecond and sub-picosecond laser pulse duration into which matter is at strong thermal non equilibrium, and where volume ablation can arise. In our case, The laser intensity I will vary from $6\ 10^7$ to $8\ 10^7\,\mathrm{W\,m^{-2}}$, and we define $\rho_c = 1.75\,\mathrm{kg\,m^{-3}}$.

- The matter and its vapour are modelled by compressible fluids, the modelling is justified by the extreme conditions of the experiment. In our modelling, we chose the same equation of state as for the previous tests, i.e. perfect gas for both of the phases, and

$$\begin{array}{ll} \text{solid} & \gamma = 1.2 \\ \text{vapor} & \gamma = 1.9 \end{array}$$

- For the solid matter, we also need to take into account the thermal conductivity. In this context, the Spitzer-Härm nonlinear conduction holds [58]. Non-linear thermal conductivity is defined by

$$\kappa = \kappa_0 T^\alpha,$$

with $\kappa_0 = 2\ 10^{-13}\,\mathrm{W\,m^{-1}K^{-1-\alpha}}$ and $\alpha = 3/2$.

7.4.2 Analytical model

In order to find an analytical solution, we are interested in finding a simplified problem model. Major hypothesis is that the ablation front can be viewed as a discontinuous wave, and that all laser energy is released at a given density.

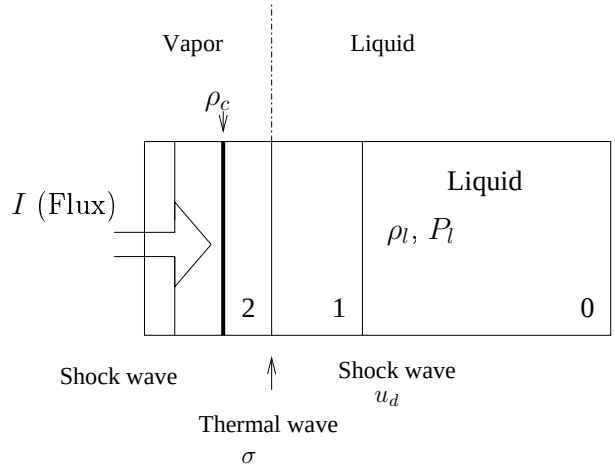

Figure 7.8: Sequence of waves in the laser energy deposition test case at $t > 0$, the laser comes from the left. Energy is released at critical density ρ_c, transported in the solid by thermal conduction, with an ablation (vaporisation) when $T > T_{sat}$.

As it is observed in experiments, the problem to be solved is composed of four states. Initial liquid state (0), shocked liquid state (1), a state between the thermal wave (2) and ablated state at critical density, see Figure 7.8. Actually, what is observed is that the distance between the thermal wave and the ablation front is very narrow. In our model, we consider that it is infinitely thin. Therefore, we can write the conservation equations between the state (1) and the state at density ρ_c. These relations are the Rankine-Hugoniot relations, except for the energy equations, in which the source term I must be added. Thus energy jump relation across ablation wave writes

$$\frac{1}{2}\left(\sigma - u_1\right)^2 + C_{v1}{}' T_1' + \frac{p_1}{\rho_1'} + Q = \frac{1}{2}\left(\sigma - u_2\right)^2 + C_{v2} T_2 + \frac{p_2}{\rho_2}. \tag{7.4}$$

In (7.4), the Q depends on the context:

- In classical flame front theory, Q (specific energy unit) is a constant source term depending on temperature (Arrhenius theory).
- whereas in the ablation theory, the energy release Q depends on mass flux J across the ablation front. From resolution of energy equation we have $Q = I/J$.

So that it is natural to wonder on the validity of a Chapman-Jouguet closure in the context of ablation.

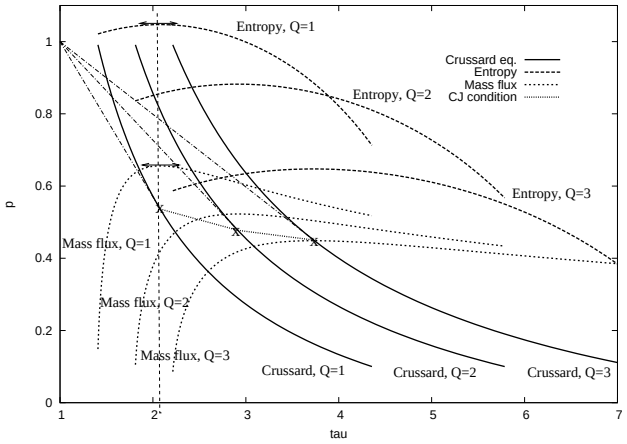

Figure 7.9: Chapman-Jouguet closures for a flame front problem. From an initial state p_1, τ_1, we have presented three Crussard curves with $Q = 1, 2, 3$ as parameter. We see here that Chapman-Jouguet condition which gives point p_2, τ_2 are equivalent: the tangent point on Crussard curve, the maximum mass flux, or the maximum entropy.

In a combustion context (constant Q), it has been shown that an admissible closure relation is the sonic Chapman-Jouguet velocity, i.e. $(u_1 - \sigma)^2 = \gamma p_1/\rho_1)$, as the consequence of existence of one tangent points on the Crussard curve. We have to recall here that Crussard curve defines all states mathematically admissible from an energy balance, and that the Chapman-Jouguet point is a point where we get maximum mass flux, and maximum entropy. We have plotted the Crussard curves, the mass flux curves and the entropy curve for $Q = 1, 2, 3$ (specific energy) in Figure 7.9. These plots are for perfect gas ($\gamma = 5/3$) and for initial point $p_1 = 1$, $\tau_1 = 1$.

In a laser type problem the source term Q is no longer constant. It depends on mass flux since $Q = I/J$. Crussard curves can always been obtained for a given I (power per surface unit), but J depends on p_2, τ_2. Some simplified models for ablation use a Chapman-Jouguet closure [12, 30] to determine the velocity of the ablation wave. In these models, it is expressed that Chapman-Jouguet point is also the point where all laser energy is released. We have plotted some Crussard curves to verify this assumption with $I = 1, 2, 3$ (power per surface unit) as parameter in Figure 7.10. We see that Chapman-Jouguet condition which gives point p_2, τ_2 admits two tangent points in subsonic regime, which is a different behaviour from the one for combustion front. Fortunately, only one of these two tangent points admits also a maximum of entropy or and mass flux condition. So even though

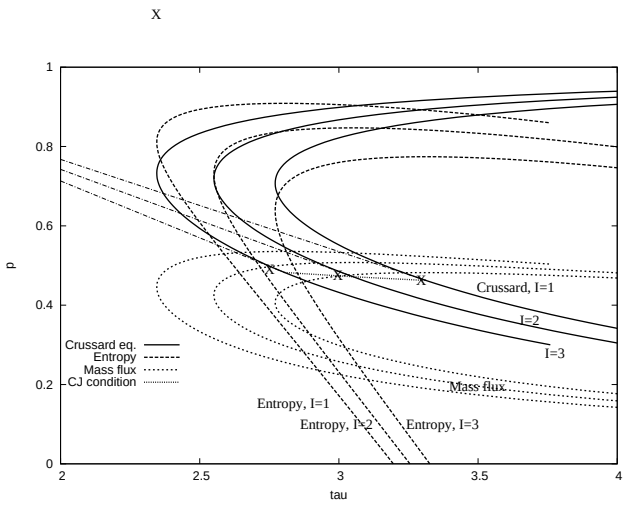

Figure 7.10: Chapman-Jouguet closures for an ablation front created by laser. From an initial state p_1, τ_1, we have presented three Crussard curves with $I = 1, 2, 3$ as parameter. We see here that Chapman-Jouguet condition which gives point p_2, τ_2 can be the tangent point on Crussard curve and the maximum mass flux or the maximum entropy.

Q is no longer constant in ablation type problems, we have concluded that Chapman-Jouguet closure could be employed in laser ablation problem. To summarise, the analytical model for the sequence of wave from the right until the ablation front is

1. a shock,

2. and a discontinuity between the shocked matter and the vapour, modelling the ablation front.

The model is closed by a Chapman-Jouguet relation for the ablation front, and by a downstream state with $\rho = \rho_c$.

Remark 7.1. The velocity of the ablation front can be computed following [25, 12, 32]

$$\sigma = \left[\frac{2Q\rho_c \left(\gamma_g + 1\right)\left(A_l - 1\right)}{\gamma_g A_g A_l \rho_0} \right]^{\frac{1}{2}},$$

where $A = (\gamma+1)/(\gamma-1)$, a relation between shock speed and ablation front speed

$$\sigma = \left(\frac{A_l - 1}{A_l} \right) u_s,$$

and an expression for volume energy release

$$Q = I^{\frac{2}{3}} \left(\frac{A_g}{2\rho_c^2} \right)^{\frac{1}{3}}.$$

We will use the more convenient expression of σ written

$$\sigma = \sqrt{\frac{4}{\gamma_l + 1} \left(1 - \frac{1}{\gamma_g} \right) \frac{\rho_c}{\rho_0} \left[\frac{\gamma_g + 1}{\gamma_g - 1} \frac{1}{2\rho_c^2} \right]^{\frac{1}{3}} I^{\frac{2}{3}}}. \tag{7.5}$$

This agrees very well with the usual models that can be found in [21, 27], in particular, the scaling law of the velocity of the ablation front is $I^{1/3}$. Ablation pressure is deduced from jump relations

$$p_2 \approx \frac{2Q\rho_c}{\gamma_g A_g}. \tag{7.6}$$

Expressions for ablation velocity and ablated matter pressure (7.5) and (7.6) will be used to estimate the behaviour of the numerical results obtained with the multi-wave solver.

7.4.3 Numerical results

The laser intensity I will vary from 6 10^7 to 8 10^7 $\mathrm{W\,m^{-2}}$. The multi-wave solver has been coupled with the resolution of thermal flux, with a two-step time integration. The first half step for hydrodynamic, the second half step for thermal diffusion. The length of the domain is 0.5m. The two domains have equal length (0.25m) at initial time.

Using this set of variables, we can compute from the analytical model the approximate laws for ablation and shock wave velocities

$$\sigma \approx 0.691\ I^{1/3}\ \mathrm{m\,s^{-1}},$$

and

$$u_s = 0.76\ I^{1/3}\ \mathrm{m\,s^{-1}}.$$

From the analytical model we can also settle down scaling laws for pressure of ablated matter

$$p_2 = 0.461\ I^{2/3}\ \mathrm{Pa}.$$

Temperature of ablated matter will be deduced from equation of state $T_2 = p_2/\rho_2/r_l$. These scaling laws for pressure and density will allow us to verify the accuracy of the multi-wave solver results.

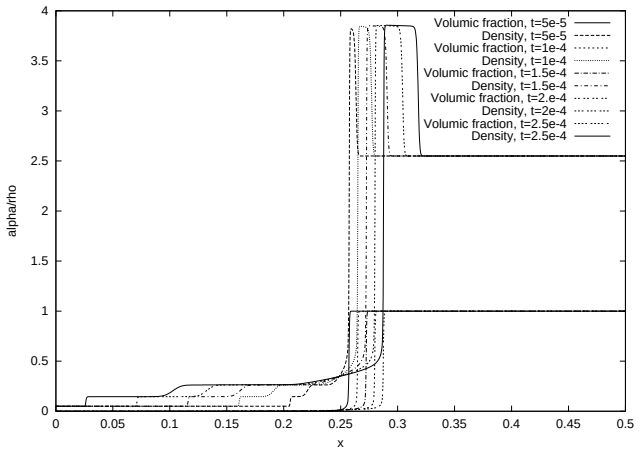

Figure 7.11: Density and volume fraction profiles versus x obtained with multi-wave solver from time $t = 5.\ 10^{-5}$ s to $t = 1.\ 10^{-4}$ s by time step of $5.\ 10^{-5}$ s.

Three laser intensity have been used ($I = 6\ 10^7\,\mathrm{W\,m^{-2}}$, $7\ 10^7\,\mathrm{W\,m^{-2}}$ and $8\ 10^7\,\mathrm{W\,m^{-2}}$) from initial time to $t = 2.5\ 10^{-4}$ s.

First of all, we present results from multi-wave solver: density of mean fluid and pressure profiles versus x for $I = 6\ 10^7\ \mathrm{W\,m^{-2}}$, from time $t = 5.\ 10^{-5}$ s to final time by time step of $5.\ 10^{-5}$s (Fig. 7.11).

The energy release induces the formation of a shock wave followed by a thermal wave into which phase transition occurs (ablation of matter). Just behind the ablation wave is the expansion wave. The shock travelling to the left in the low pressure chamber is a strong shock wave. We must point out that we do not have a full vaporisation across ablation wave, but the vaporisation is completed in the expansion wave.

A criterion to localise the ablation had to be chosen in order to compute the velocity of ablation front. We have taken a criterion on volume fraction, $\alpha \approx 0.5$, to estimate the position of the ablation wave at each time. Ablation front velocity has been finally computed with

$$\sigma = u_1 + \frac{\Delta x|_{\alpha=0.5}}{\Delta t}.$$

For $I = 6\ 10^7\,\mathrm{W\,m^{-2}}$ we evaluate $\sigma_{\mu wave} \approx 245\,\mathrm{m\,s^{-1}}$ that we have to compare to the velocity predicted by approximate model

$$\sigma_{mod} = 0.691\ I^{1/3} = 270\ \mathrm{m\,s^{-1}}.$$

These values are in good agreement and point out the good behaviour of the multi-wave solver in the case of a laser energy release.

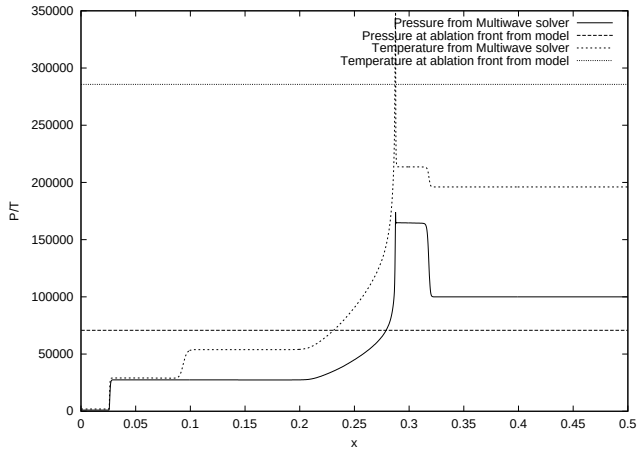

Figure 7.12: Pressure and temperature profile versus x at time $t = 2.5\ 10^4\,\mathrm{s}$, comparison of solution from multi-wave solver to level predicted by analytical model.

This good behaviour can be exhibited also on pressure and temperature profile versus x at time $t = 2.5\ 10^4\,\mathrm{s}$ that are presented in Figure 7.12. In this figure, we have also plotted the pressure and temperature predicted by approximate model.

This gap can be explained by some hypothesis of the model, especially strong shock wave ahead of the ablation wave, and full vaporisation of the liquid in the ablation wave. This is not the case numerically where the multi-wave solver predicts a residual volume fraction of liquid of 0.05.

The quality of results obtained with multi-wave solver is confirmed for higher laser intensities ($I = 7\ 10^7\,\mathrm{W\,m^{-2}}$, and $I = 8\ 10^7\,\mathrm{W\,m^{-2}}$). For these fluxes we have also compared ablation front velocity obtained with multi-wave solver with the one predicted by approximate model.

For $I = 7\ 10^7\,\mathrm{W\,m^{-2}}$ we have $\sigma_{\mu w} \approx 262\,\mathrm{m\,s^{-1}}$ for $\sigma_{mod} \approx 284\,\mathrm{m\,s^{-1}}$, and for $I = 8\ 10^7\,\mathrm{W\,m^{-2}}$ we have $\sigma_{\mu w} \approx 283\,\mathrm{m\,s^{-1}}$ for $\sigma_{mod} \approx 297\,\mathrm{m\,s^{-1}}$.

Finally we compare density and volume fraction profiles versus x at time $t = 2\ 10^{-4}\,\mathrm{s}$ for the three intensities used in these simulations ($I = 6\ 10^7\,\mathrm{W\,m^{-2}}$, $I = 7\ 10^7\,\mathrm{W\,m^{-2}}$, and $I = 8\ 10^7\,\mathrm{W\,m^{-2}}$). The multi-wave solver and the analytical models results are closely related.

The larger the laser intensity is, the stronger are the shock wave and the ablation front velocity. We do not notice any numerical oscillations and the level are pretty good.

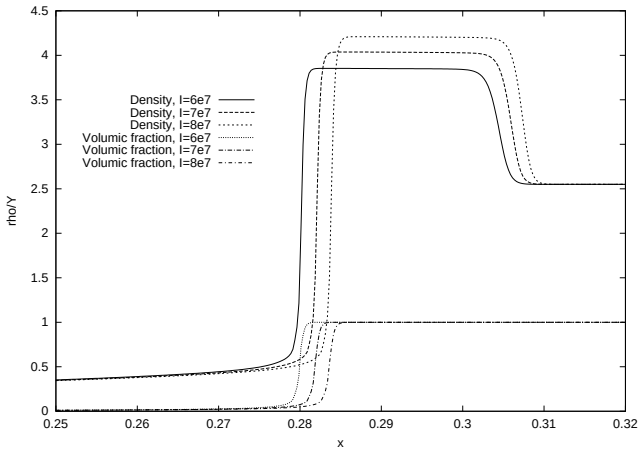

Figure 7.13: Comparison of density and volume fraction profiles versus x at time $t = 2\ 10^{-4}\,\mathrm{s}$ for $I = 6\ 10^{7}\,\mathrm{W\,m^{-2}}$, $I = 7\ 10^{7}\,\mathrm{W\,m^{-2}}$, and $I = 8\ 10^{7}\,\mathrm{W\,m^{-2}}$, multi-wave solver results.

7.5 Conclusions and prospects

In this chapter, we showed how to extend the numerical scheme of [2] to take into account self similar transformations, as vaporisation fronts. The extension is fully done in the case of total vaporisation fronts, but there remains problems for partial vaporisation fronts.

In this part, we made the extension only for vaporisation fronts that are induced by a contact between a liquid and its vapour. Another sort of phase transition, that was not modelled in this part, is the nucleation, i.e. the apparition of a gas in a liquid. Nucleation and the vaporisation modelled here are very different phenomena. The problem of modelling nucleation lies only in explaining why a bubble appears there and not there. Such explanation exists, but lies on capillarity.

Taking into account capillarity would induce a strong modification, starting in the thermodynamic modelling: in Chapter 4, the optimisation of the total entropy was made under the constraints of constant total energy, mass and volume. If the capillarity is taken into account, the total energy and the total entropy are no more equal to the sum of each component' energy and entropy: part of the energy and entropy are stocked in the interface. Therefore, the function that is to be optimised (the entropy), and one of the constraint (the energy) are modified, so that the Lagrangian equations (4.6) are modified too. We expect for example that such an optimisation will lead to an equation similar to

$$P_l - P_v = \frac{2\sigma}{R}$$

where σ is the surface tension, and R is the radius of curvature of the local interface. Thus, we see that such a model should take into account the local topology of the bubbles.

For the solution of the Riemann problem (Chapter 6), the introduction of the capillarity might be used to explain the relative stability of metastable states, and could be a first modelling step to try to solve the kinetic closure problem by the travelling wave way,as it was explained in the conclusion of Chapter 6. Taking into account nucleation would also mean studying the reactive liquid–liquid Riemann problem; actually, the difference would essentially relies on the choice of the kinetic closure.

At a numerical point of view, the modelling of nucleation induces that a bubble, when it appears, can be strongly smaller than a computing cell. Computing such a flow could be done by the following multiscale algorithm: for a given time step δt,

- Compute the average flow for the time step δt
- Mesh the cells $\mathcal{C}_i$ where nucleation occurs (the mesh of the cell must be at the scale of an inside bubble) and use the code in each domain $\mathcal{C}_i$, with wall limit conditions. This second time step essentially aims at computing the growth of the small bubbles, and other phenomena, as coalescence. Actually, there should be many computations, because the exact location of the bubbles is not known, so that a Monte-Carlo method shall be led for this step. Note that this second time step would be easily parallelised. However costly might be this step, it is likely that few cell can be concerned: nucleation, at least homogeneous nucleation often appears only in very particular locations, for example near inhomogeneities of the walls.

Part III

Correctors in stochastic homogenization

Table of Contents

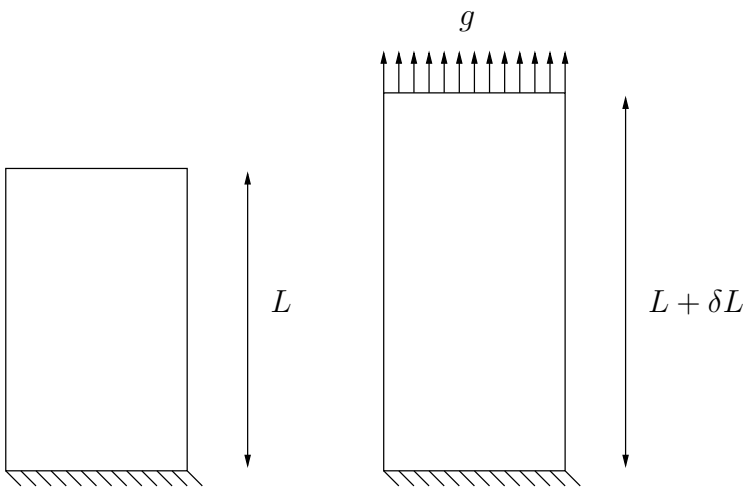

Figure 7.14: An ensemble of pieces with the same geometry are tested with the same force g.

This part of the PhD was made during the CEMRACS 2006. The project was proposed by EADS. This work was led under the supervision of Pr. Bal and Pr. Garnier, and I would especially thank them for everything I learnt in this period.

The problem, as it was proposed by EADS was the following: some mechanical pieces are built with a composite medium. This medium is made of a synthetic resin in which some short carbon fiber are put. The pieces built are submitted to a vertical constraint g, and their lengthening δL is measured (see Figure 7.14). Experimentally, a strong dispersion of the results is observed. The behavior of these pieces is modeled by the system of linear elasticity

$$\begin{cases} \text{div}\boldsymbol{\sigma} = 0 & \text{sur} \quad \mathscr{O} \\ \boldsymbol{\sigma} = \boldsymbol{A}\epsilon & \text{sur} \quad \mathscr{O} \\ \epsilon = \dfrac{1}{2}\left(\boldsymbol{\nabla u} + \boldsymbol{\nabla}^t \boldsymbol{u}\right) & \text{sur} \quad \mathscr{O} \\ \boldsymbol{u} = 0 & \text{sur} \quad \Gamma_1 \\ \boldsymbol{\sigma} \cdot \boldsymbol{n} = 0 & \text{sur} \quad \Gamma_2 \\ \boldsymbol{\sigma} \cdot \boldsymbol{n} = g & \text{sur} \quad \partial\mathscr{O} \setminus \Gamma_1 \cup \Gamma_2 \end{cases}$$

where

- $\boldsymbol{\sigma}$ is the stress tensor.
- $\boldsymbol{u}$ is the acceleration.
- $\boldsymbol{\epsilon}$ is the linearized strain tensor.

- $\boldsymbol{A}$ is the elsaticity tensor.
- g is the external applied force.

The tensor A locally depends on the concentration and th orientation of the carbon fibers. To simplify, we are interested in the following system on $(0,1)$.

$$\begin{cases} -\nabla \cdot a(\mathbf{x},\omega)\nabla u = 0, & \mathbf{x} \in (0,1)^2, \qquad \omega \in \Omega, \\ \dfrac{\partial u}{\partial x} = 0, & \text{if} \quad x = 0 \quad \text{and} \quad x = 1, \\ u = 0 & y = 0, \\ a((x,1),\omega)\dfrac{\partial u}{\partial y} = g \equiv 1 & y = 1. \end{cases} \tag{7.7}$$

where $(a(\mathbf{x},\omega))_{\mathbf{x}}$ is a stationnary random process that model the distribution of the carbon fibers. If we suppose that the characteristic length of the fibers, l, which is also the correlation radius of the process a is small compared with the length L of Ω, then an asymptotic development can be computed when $\varepsilon = l/L$ tends to 0. If the convergence to a deterministic solution $\bar{u}$ (that explain the convergence to a mean lenghtnening) is well known [34], few result concern the correctors [13], *i.e.* the behavior of $u - \bar{u}$, which measure the dispersion of the results.

In these chapters, we will be interested only in the one dimensional case, for which an explicit solution can be computed. Therefore, the main effort will be concentrated in the asymptotic expansion of oscillating integrals. In the Chapter 8, we will find a corrector when the autocorrelation is not integrable, and equivalent to a K/t^{α} with $\alpha < 1$. In each case, the theoretical results will be validated by numerical simulations. The convergence results will be proved for oscillating integrals, and then will be extended for the solutions of one dimensional linear elliptic equations with Dirichlet conditions. As the solution of (7.7) in one dimension is a stochastic integral, the results of Chapter 8 can be applied in that context. This chapter is submitted in [6].

Chapter 8

Non mixing case

8.1 Introduction

Homogenization theory for second-order elliptic equations with highly oscillatory coefficients is well developed, both for periodic and random coefficients; see e.g. [9, 34]. The analysis of correctors, which measure the difference between the heterogeneous solution and the homogenized solution, is more limited.

In the periodic setting, the solution of so-called cell problems allow us to obtain explicit expressions for the correctors. Denoting by ε the size of the cell of periodicity of the oscillatory coefficients, the amplitude of the corrector for a second-order equation is typically of order ε [9, 34].

In the random setting, the situation is complicated by the fact that the local problems are no longer defined on compact cells. And as it turns out, the amplitude of the correctors is no longer of size ε in general, where ε now measures the correlation length of the random heterogeneities. Relatively few general estimates are available in the literature on the size of the correctors; see [66]. For the one-dimensional second-order elliptic equation (see (8.1) below), much more is known because of the availability of explicit expressions for the solutions (see (8.3) below). The analysis of correctors was taken up in [13], where it is shown that the correctors' amplitude is of order $\sqrt{\varepsilon}$ provided that the random coefficients have sufficiently short-range correlations so that, among other properties, their correlation function is integrable. Moreover, the corrector may be shown to converge in distribution in the space of continuous paths to a Gaussian process, which may be written as a stochastic integral with respect to Brownian motion. This result is recalled in Theorem 8.2 below. The work [13] also proposes error estimates for the corrector in the case of longer-range correlations, when the correla-

tion function of the random coefficients is no longer integrable. The limiting behavior of the corrector is however not characterized.

This chapter reconsiders the analysis of correctors for the one-dimensional equation when the correlation function of the random coefficients is no longer integrable, and more precisely takes the form $R(\tau) \sim \tau^{-\alpha}$ as $\tau \to \infty$ for some $0 < \alpha < 1$. Longer-range correlations are modeled by smaller values of α. A prototypical example of a continuous, stationary process with long-range correlation is a normalized Gaussian process g_x with a correlation function $R_g(\tau) = \mathscr{E}\{g_x g_{x+\tau}\}$ that decays as $\tau^{-\alpha}$. The random coefficients for the elliptic equation we consider in this chapter are mean zero stationary processes that can be written as $\varphi(x) = \Phi(g_x)$, where $\Phi(t)$ belongs to a large class of functions. Under appropriate assumptions on Φ, the correlation function of g also decays as $\tau^{-\alpha}$ as $\tau \to \infty$.

For the random coefficients described above, we show that the corrector to homogenization has an amplitude of order ε^{α} and converges in distribution to a Gaussian process that may be represented as a stochastic integral with respect to a fractional Brownian motion W_t^H with Hurst index $H = 1 - \frac{\alpha}{2}$. The limit $\alpha \to 1$ thus converges to the case of integrable correlation function. Note however that in the limit of very long-range correlations as $\alpha \to 0$, the influence of the corrector becomes more and more important. The main tool in our derivation is a careful convergence analysis in distribution of oscillatory integrals of the form $\int_0^1 K(x,t)\varepsilon^{-\frac{\alpha}{2}}\phi(\frac{t}{\varepsilon})dt$ to a stochastic integral with respect to fractional Brownian motion, where $K(x,t)$ is a known kernel and $\phi(t)$ is a random process with long-range correlations.

The rest of the chapter is structured as follows. section 8.2 presents the heterogeneous and homogeneous one-dimensional elliptic equations and describes our hypotheses on the random coefficients. The section concludes by a statement of Theorem 8.1, which is our main result. The analysis of random oscillatory integrals of the form $\int_0^1 F(t)\varepsilon^{-\frac{\alpha}{2}}\phi(\frac{t}{\varepsilon})dt$ is carried out in section 8.3. Theorem 8.3 shows their convergence to stochastic integrals with respect to fractional Brownian motion W_t^H. section 8.4 shows how the results of section 8.3 extend to the analysis of the processes of the form $\int_0^1 K(x,t)\varepsilon^{-\frac{\alpha}{2}}\phi(\frac{t}{\varepsilon})dt$ that arise in the analysis of the correctors to homogenization. The convergence in distribution in the space of continuous paths of such processes to a Gaussian processes is summarized in Theorem 8.4. The theoretical results are backed up by numerical simulations in section 8.5. After a detailed description of the construction of random processes with given long-range correlations, we demonstrate the convergence of random oscillatory integrals and of homogenization correctors to their appropriate limits as stochastic integrals with respect to fractional Brownian motion. Some concluding remarks are given in section 8.7.

8.2 One-dimensional homogenization

8.2.1 Homogenization problem

We are interested in the solution to the following elliptic equation with random coefficients

$$\begin{aligned} &-\frac{d}{dx}\Big(a\Big(\frac{x}{\varepsilon},\omega\Big)\frac{d}{dx}u^\varepsilon\Big) = f(x), \qquad 0\le x\le 1, \quad \omega\in\Omega,\\ &u^\varepsilon(0,\omega)=0, \qquad u^\varepsilon(1,\omega)=q. \end{aligned} \tag{8.1}$$

Here $a(x,\omega)$ is a stationary ergodic random process such that $0<a_0\le a(x,\omega)\le a_0^{-1}$ a.e. for $(x,\omega)\in(0,1)\times\Omega$, where $(\Omega,\mathcal{F},\mathcal{P})$ is an abstract probability space. The source term $f\in W^{-1,\infty}(0,1)$ and $q\in\mathbb{R}$. Classical theories for elliptic equations then show the existence of a unique solution $u(\cdot,\omega)\in H^1(0,1)$ $\mathcal{P}-$a.s.

As the scale of the micro-structure ε converges to 0, the solution $u^\varepsilon(x,\omega)$ converges $\mathcal{P}$-a.s. weakly in $H^1(0,1)$ to the deterministic solution $\bar u$ of the homogenized equation

$$\begin{aligned} &-\frac{d}{dx}\Big(a^*\frac{d}{dx}\bar u\Big) = f(x), \qquad 0\le x\le 1,\\ &\bar u(0)=0, \qquad \bar u(1)=q. \end{aligned} \tag{8.2}$$

The effective diffusion coefficient is given by $a^*=\big(\mathscr{E}\{a^{-1}(0,\cdot)\}\big)^{-1}$, where $\mathscr{E}$ is mathematical expectation with respect to $\mathcal{P}$. See e.g. [34, 36, 45].

The above one-dimensional boundary value problems admit explicit solutions. Introducing $a^\varepsilon(x)=a(\frac{x}{\varepsilon})$ and $F(x)=\int_0^x f(y)dy$, we have:

$$u^\varepsilon(x,\omega)=c^\varepsilon(\omega)\int_0^x\frac{1}{a^\varepsilon(y,\omega)}dy-\int_0^x\frac{F(y)}{a^\varepsilon(y,\omega)}dy, \qquad c^\varepsilon(\omega)=\frac{q+\displaystyle\int_0^1\frac{F(y)}{a^\varepsilon(y,\omega)}dy}{\displaystyle\int_0^1\frac{1}{a^\varepsilon(y,\omega)}dy} \tag{8.3}$$

$$\bar u(x)=c^*\frac{x}{a^*}-\int_0^x\frac{F(y)}{a^*}dy, \qquad c^*=a^*q+\int_0^1F(y)dy. \tag{8.4}$$

Our aim is to characterize the behavior of $u^\varepsilon-\bar u$ as $\varepsilon\to 0$.

8.2.2 Hypothesis on the random process a

In order to characterize the behavior of the corrector $u^\varepsilon-\bar u$ as $\varepsilon\to 0$, we need additional assumptions on the random process $a(x,\omega)$. Let us define the mean zero stationary random process

$$\varphi(x,\omega)=\frac{1}{a(x,\omega)}-\frac{1}{a^*}. \tag{8.5}$$

Hypothesis [H]. We assume that φ is of the form

$$\varphi(x) = \Phi(g_x), \tag{8.6}$$

where Φ is a bounded function such that

$$\int \Phi(g) e^{-\frac{g^2}{2}} dg = 0, \tag{8.7}$$

and g_x is a stationary Gaussian process with mean zero and variance one. The autocorrelation function of g

$$R_g(\tau) = \mathscr{E}\{g_x g_{x+\tau}\}$$

is assumed to have a heavy tail of the form

$$R_g(\tau) \sim \kappa_g \tau^{-\alpha} \text{ as } \tau \to \infty, \tag{8.8}$$

where $\kappa_g > 0$ and $\alpha \in (0, 1)$.

Remark 8.1. This hypothesis is satisfied by a large class of random coefficients. For instance, if we take $\Phi = \text{sgn}$, then φ models a two-component medium. If we take $\Phi = \tanh$ or $\arctan$, then φ models a continuous medium with bounded variations.

The autocorrelation function of the random process a has a heavy tail, as stated in the following proposition.

Proposition 8.1. *The process φ defined by* (8.6) *is a stationary random process with mean zero and variance V_2. Its autocorrelation function*

$$R(\tau) = \mathscr{E}\{\varphi(x)\varphi(x+\tau)\} \tag{8.9}$$

has a heavy tail of the form

$$R(\tau) \sim \kappa \tau^{-\alpha} \text{ as } \tau \to \infty, \tag{8.10}$$

where $\kappa = \kappa_g V_1^2$,

$$V_1 = \mathscr{E}\{g_0 \Phi(g_0)\} = \frac{1}{\sqrt{2\pi}} \int g \Phi(g) e^{-\frac{g^2}{2}} dg\,, \tag{8.11}$$

$$V_2 = \mathscr{E}\{\Phi^2(g_0)\} = \frac{1}{\sqrt{2\pi}} \int \Phi^2(g) e^{-\frac{g^2}{2}} dg\,. \tag{8.12}$$

Proof. The fact that φ is a stationary random process with mean zero and variance V_2 is straightforward in view of the definition of φ. In particular, (8.7) implies that φ has mean zero.
For any x, τ, the vector $(g_x, g_{x+\tau})^T$ is a Gaussian random vector with mean $(0,0)^T$ and 2×2 covariance matrix

$$C = \begin{pmatrix} 1 & R_g(\tau) \\ R_g(\tau) & 1 \end{pmatrix}.$$

Therefore the autocorrelation function of the process φ is

$$\begin{aligned} R(\tau) &= \mathscr{E}\big\{\Phi(g_x)\Phi(g_{x+\tau})\big\} = \frac{1}{2\pi\sqrt{\det C}} \iint \Phi(g_1)\Phi(g_2) \exp\Big(-\frac{g^T C^{-1} g}{2}\Big) d^2 g \\ &= \frac{1}{2\pi\sqrt{1-R_g^2(\tau)}} \iint \Phi(g_1)\Phi(g_2) \exp\Big(-\frac{g_1^2+g_2^2-2R_g(\tau)g_1g_2}{2(1-R_g^2(\tau))}\Big) dg_1 dg_2 \,. \end{aligned}$$

For large τ, the coefficient $R_g(\tau)$ is small and we can expand the value of the double integral in powers of $R_g(\tau)$, which gives the autocorrelation function of φ. □

To simplify the notations, we do not write explicitly the ω-dependence anymore and we denote $\varphi^\varepsilon(x) = \varphi(\frac{x}{\varepsilon})$.

8.2.3 Analysis of the error

The purpose of this section is to show that the error term $u^\varepsilon - \bar{u}$ has two different types of contributions. It contains integrals of random processes with long term memory effects and lower-order terms. The analysis of integrals of random processes with long term memory effects is carried out in the next sections. Here we simply state the following lemma, which gives the order of magnitude of these integrals.

Lemma 8.1. *Let $\varphi(x)$ be a mean zero stationary random process of the form (8.6). There exists $K > 0$ such that, for any $F \in L^\infty(0,1)$, we have*

$$\sup_{x\in[0,1]} \mathscr{E}\Big\{\Big|\int_0^x \varphi^\varepsilon(t)F(t)dt\Big|^2\Big\} \le K\|F\|_\infty^2 \varepsilon^\alpha \,. \tag{8.13}$$

This lemma will be proved in subsection 8.4.2. A corollary of this lemma is the following estimate:

Corollary 8.1. *Let $\varphi(x)$ be a mean zero stationary random process of the form (8.6) and $f \in W^{-1,\infty}(0,1)$. The solutions u^ε in (8.3) and $\bar{u}$ in (8.4) are such that*

$$u^\varepsilon(x) - \bar{u}(x) = -\int_0^x \varphi^\varepsilon(y)F(y)dy + (c^\varepsilon - c^*)\frac{x}{a^*} + c^*\int_0^x \varphi^\varepsilon(y)dy + r^\varepsilon(x), \quad (8.14)$$

where

$$\sup_{x\in[0,1]} \mathscr{E}\{|r^\varepsilon(x)|\} \leq K\varepsilon^\alpha\,, \quad (8.15)$$

for some $K > 0$. Similarly, we have that

$$c^\varepsilon - c^* = a^*\int_0^1 \Big(F(y) - \int_0^1 F(z)dz - a^*q\Big)\varphi^\varepsilon(y)dy + \rho^\varepsilon, \quad (8.16)$$

where

$$\mathscr{E}\{|\rho^\varepsilon|\} \leq K\varepsilon^\alpha\,, \quad (8.17)$$

for some $K > 0$.

Proof. We first establish the estimate for $c^\varepsilon - c$. We write

$$c^\varepsilon - c^* = \frac{\int_0^1 F(y)\Big(\frac{1}{a^\varepsilon(y)} - \frac{1}{a^*}\Big)dy}{\int_0^1 \frac{1}{a^\varepsilon(y)}dy} + \Big(q + \frac{1}{a^*}\int_0^1 F(y)dy\Big)\Big(\frac{1}{\int_0^1 \frac{1}{a^\varepsilon(y)}dy} - \frac{1}{\frac{1}{a^*}}\Big),$$

which gives (8.16) with

$$\rho^\varepsilon = \frac{a^*}{\int_0^1 \frac{1}{a^\varepsilon(y)}dy}\left[(a^*q + \int_0^1 F(y)dy)\left(\int_0^1 \varphi^\varepsilon(y)dy\right)^2 - \int_0^1 F(y)\varphi^\varepsilon(y)dy\int_0^1 \varphi^\varepsilon(y)dy\right].$$

Since $\int_0^1 \frac{1}{a^\varepsilon(y)}dy$ is bounded from below a.e. by a positive constant a_0, we deduce from Lemma 8.1 and the Cauchy-Schwarz estimate that $\mathscr{E}\{|\rho^\varepsilon|\} \leq K\varepsilon^\alpha$. The analysis of $u^\varepsilon - \bar{u}$ follows the same lines. We write

$$u^\varepsilon(x) - \bar{u}(x) = c^\varepsilon\int_0^x \frac{1}{a^\varepsilon(y)}dy - \int_0^x \frac{F(y)}{a^\varepsilon(y)}dy - c^*\frac{x}{a^*} + \int_0^x \frac{F(y)}{a^*}dy,$$

which gives (8.14) with

$$\begin{aligned} r^\varepsilon(x) &= (c^\varepsilon - c^*)\int_0^x \varphi^\varepsilon(y)dy \quad (8.18)\\ &= r_1^\varepsilon(x) + r_2^\varepsilon(x), \end{aligned}$$

where we have defined

$$\begin{aligned} r_1^\varepsilon(x) &= \left[a^* \int_0^1 \Big(F(y) - \int_0^1 F(z)dz - a^* q\Big)\varphi^\varepsilon(y)dy\right]\left[\int_0^x \varphi^\varepsilon(y)dy\right], \\ r_2^\varepsilon(x) &= \rho^\varepsilon \left[\int_0^x \varphi^\varepsilon(y)dy\right]. \end{aligned}$$

The Cauchy-Schwarz estimate and Lemma 8.1 give that $\mathscr{E}\{|r_1^\varepsilon(x)|\} \leq K\varepsilon^\alpha$. Besides, φ^ε is bounded by $\|\Phi\|_\infty$, so $|r_2^\varepsilon(x)| \leq \|\Phi\|_\infty |\rho^\varepsilon|$. The estimate on ρ^ε then shows that $\mathscr{E}\{|r_2^\varepsilon(x)|\} \leq K\varepsilon^\alpha$. □

Roughly speaking, the previous corollary shows that the error term $u^\varepsilon(x) - \bar{u}(x)$ involves integrals of random coefficients, which are of order $\varepsilon^{\alpha/2}$, up to lower-order terms of order ε^α.

8.2.4 Homogenization theorem

The results we obtain in the following sections allow for the following characterization of the correctors.

Theorem 8.1. *Let u^ε and $\bar{u}$ be the solutions in* (8.3) *and* (8.4)*, respectively, and let $\varphi(x)$ be a mean zero stationary random process of the form* (8.6)*. Then $u^\varepsilon - \bar{u}$ is a random process in $\mathcal{C}(0,1)$, the space of continuous functions on $[0,1]$. We have the following convergence in distribution in the space of continuous functions $\mathcal{C}(0,1)$*

$$\frac{u^\varepsilon(x) - \bar{u}(x)}{\varepsilon^{\frac{\alpha}{2}}} \xrightarrow{\text{distribution}} \sqrt{\frac{\kappa}{H(2H-1)}}\mathcal{U}^H(x), \tag{8.19}$$

where

$$\mathcal{U}^H(x) = \int_{\mathbb{R}} K(x,t)dW_t^H, \tag{8.20}$$

$$K(x,t) = \mathbf{1}_{[0,x]}(t)\big(c^* - F(t)\big) + x\Big(F(t) - \int_0^1 F(z)dz - a^* q\Big)\mathbf{1}_{[0,1]}(t). \tag{8.21}$$

Here $\mathbf{1}_{[0,x]}$ is the characteristic function of the set $[0,x]$ and W_t^H is a fractional Brownian motion with Hurst index $H = 1 - \frac{\alpha}{2}$.

The proof of this theorem is postponed to subsection 8.4.3.

For convenience of the reader, we give a quick and partial review of the integration theory with respect to a fractional Brownian motion. The fractional

Brownian motion W_t^H is a mean zero Gaussian process with autocorrelation function

$$\mathscr{E}\{W_t^H W_s^H\} = \frac{1}{2}\big(|t|^{2H} + |s|^{2H} - |s-t|^{2H}\big). \tag{8.22}$$

In particular, the variance of W_t^H is $\mathscr{E}\{|W_t^H|^2\} = |t|^{2H}$. The increments of W_t^H are stationary but not independent for $H \neq \frac{1}{2}$. Moreover, W_t^H admits the following spectral representation

$$W_t^H = \frac{1}{2\pi C(H)} \int_{\mathbb{R}} \frac{e^{i\xi t} - 1}{i\xi |\xi|^{H-\frac{1}{2}}} d\hat{W}(\xi), \quad t \in \mathbb{R}, \tag{8.23}$$

where

$$C(H) = \Big(\frac{1}{2H \sin(\pi H)\Gamma(2H)}\Big)^{1/2} \tag{8.24}$$

and $\hat{W}$ is the Fourier transform of a standard Brownian motion W, that is, a complex Gaussian measure such that

$$\mathscr{E}\big\{d\hat{W}(\xi)\overline{d\hat{W}(\xi')}\big\} = 2\pi\delta(\xi - \xi')d\xi d\xi' .$$

Note that the constant $C(H)$ is defined such that $\mathscr{E}\{(W_1^H)^2\} = 1$, because it is the result of the computation of the integral

$$C(H)^2 = \frac{1}{2\pi} \int_{\mathbb{R}} \frac{|e^{i\xi} - 1|^2}{|\xi|^{2H+1}} d\xi .$$

The integral with respect to the fractional Brownian motion is defined for a large class of deterministic functions F (see [51] for an extensive review). Functions in $L^1(\mathbb{R}) \cap L^2(\mathbb{R})$ are in the class of integrable functions when $H \in (1/2, 1)$, which is the range of values of H considered in Theorem 8.1. Using the representation (8.23), we have, in distribution, for any $F \in L^1(\mathbb{R}) \cap L^2(\mathbb{R})$,

$$\int_{\mathbb{R}} F(t) dW_t^H = \frac{1}{2\pi C(H)} \int_{\mathbb{R}} \frac{\hat{F}(\xi)}{|\xi|^{H-\frac{1}{2}}} d\hat{W}(\xi) ,$$

where the Fourier transform $\hat{F}(\xi)$ of a function $F(t)$ is defined by

$$\hat{F}(\xi) = \int_{\mathbb{R}} e^{it\xi} F(t) dt . \tag{8.25}$$

If $F, G \in L^1(\mathbb{R}) \cap L^2(\mathbb{R})$, then the random vector $(\int_{\mathbb{R}} F(t)dW_t^H, \int_{\mathbb{R}} G(t)dW_t^H)$ is a mean zero Gaussian vector with covariance

$$\mathscr{E}\Big\{ \int_{\mathbb{R}} F(t) dW_t^H \int_{\mathbb{R}} G(t) dW_t^H \Big\} = \frac{1}{2\pi C(H)^2} \int_{\mathbb{R}} \frac{\hat{F}(\xi)\overline{\hat{G}(\xi)}}{|\xi|^{2H-1}} d\xi .$$

As a consequence, in Theorem 8.1, the limit process $\mathcal{U}^H(x)$ is a mean zero Gaussian process with autocorrelation function

$$\mathscr{E}\{\mathcal{U}^H(x)\mathcal{U}^H(y)\} = \frac{1}{2\pi C(H)^2}\int_{\mathbb{R}} \frac{\hat{K}(x,\xi)\overline{\hat{K}(y,\xi)}}{|\xi|^{2H-1}}d\xi\,, \tag{8.26}$$

where $\hat{K}(x,\xi)$ is the Fourier transform with respect to t of $K(x,t)$. Finally, if we use the notation

$$\int_0^x F(s)dW_t^H = \int_{\mathbb{R}} \mathbf{1}_{[0,x]}(s)F(s)dW_t^H\,,$$

then the limit process $\mathcal{U}^H(x)$ defined by (8.20) can also be written as

$$\mathcal{U}^H(x) = c^*W_x^H - \int_0^x F(t)dW_t^H + x\int_0^1 F(t)dW_t^H - x\left(\int_0^1 F(z)dz - a^*q\right)W_1^H\,.$$

The result of Theorem 8.1 should be contrasted to the convergence result for processes with short term memory. In that case, we obtain the following theorem.

Theorem 8.2. *Let u^ε and $\bar{u}$ as in Theorem 8.1 and $\varphi(x)$ be a mean zero stationary random process of the form* (8.6)*. If the correlation function R_g of g is integrable (instead of being equivalent to $\tau^{-\alpha}$ at infinity), then R is also integrable. The corrector $u^\varepsilon - \bar{u}$ is a random process in $\mathcal{C}[0,1]$ and we have the following convergence in $\mathcal{C}(0,1)$*

$$\frac{u^\varepsilon(x) - \bar{u}(x)}{\sqrt{\varepsilon}} \xrightarrow{\text{distribution}} \left(2\int_0^\infty R(\tau)d\tau\right)^{1/2}\mathcal{U}(x), \tag{8.27}$$

where

$$\mathcal{U}(x) = \int_{\mathbb{R}} K(x,t)dW_t, \tag{8.28}$$

$K(x,t)$ is given by (8.21)*, and W_t is standard Brownian motion.*

The limit process $\mathcal{U}(x)$ can also be written in the form

$$\mathcal{U}(x) = c^*W_x - \int_0^x F(t)dW_t + x\int_0^1 F(t)dW_t - x\left(\int_0^1 F(z)dz - a^*q\right)W_1\,.$$

Such a result is based on standard techniques of approximation of oscillatory integrals [37] and was first derived in [13]. In the next sections, we focus our attention to the analysis of random variables or random processes defined in terms of integrals of random processes with long-term memory.

8.3 Convergence of random integrals

In this section, we aim at proving the following theorem.

Theorem 8.3. *Let φ be of the form (8.6) and let $F \in L^1(\mathbb{R}) \cap L^\infty(\mathbb{R})$. We define the mean zero random variable M_F^ε by*

$$M_F^\varepsilon = \varepsilon^{-\frac{\alpha}{2}} \int_{\mathbb{R}} \varphi^\varepsilon(t) F(t) dt \,. \tag{8.29}$$

Then the random variable M_F^ε converges in distribution as $\varepsilon \to 0$ to the mean zero Gaussian random variable M_F^0 defined by

$$M_F^0 = \sqrt{\frac{\kappa}{H(2H-1)}} \int_{\mathbb{R}} F(t) dW_t^H \,, \tag{8.30}$$

where W_t^H is a fractional Brownian motion with Hurst index $H = 1 - \frac{\alpha}{2}$.

The limit random variable M_F^0 is a Gaussian random variable with mean zero and variance

$$\mathscr{E}\{|M_F^0|^2\} = \frac{\kappa}{H(2H-1)} \times \frac{1}{2\pi C(H)^2} \int_{\mathbb{R}} \frac{|\hat{F}(\xi)|^2}{|\xi|^{2H-1}} d\xi \,. \tag{8.31}$$

In order to prove Theorem 8.3, we will prove in subsection 8.3.1 that the variance of M_F^ε converges as $\varepsilon \to 0$ to the variance of M_F^0. In subsection 8.3.2 we will prove the convergence in distribution by using the Gaussian property of the underlying process g_x.

8.3.1 Convergence of the variances

We begin with a key technical lemma that will be used in the proof of the convergence theorem.

Lemma 8.2. *1. There exist $T, K > 0$ such that the autocorrelation function $R(\tau)$ of the process φ satisfies*

$$|R(\tau) - V_1^2 R_g(\tau)| \leq K R_g(\tau)^2$$

for all $|\tau| \geq T$.
2. There exist T, K such that

$$|\mathscr{E}\{g_x \Phi(g_{x+\tau})\} - V_1 R_g(\tau)| \leq K R_g^2(\tau)$$

for all $|\tau| \geq T$.

Proof. The first point is a refinement of what we proved in Proposition 8.1: we found that the autocorrelation function of the process φ is

$$R(\tau) \;=\; \frac{1}{2\pi\sqrt{1-R_g^2(\tau)}}\iint \Phi(g_1)\Phi(g_2)\exp\Big(-\frac{g_1^2+g_2^2-2R_g(\tau)g_1g_2}{2(1-R_g^2(\tau))}\Big)dg_1dg_2\,.$$

For large τ, the coefficient $R_g(\tau)$ is small and we can expand the value of the double integral in powers of $R_g(\tau)$, which gives the result of the first item. The proof of the second item follows the same lines. We first write

$$\mathscr{E}\big\{g_x\Phi(g_{x+\tau})\big\} = \frac{1}{2\pi\sqrt{1-R_g^2(\tau)}}\iint g_1\Phi(g_2)\exp\Big(-\frac{g_1^2+g_2^2-2R_g(\tau)g_1g_2}{2(1-R_g^2(\tau))}\Big)dg_1dg_2\,,$$

and we expand the value of the double integral in powers of $R_g(\tau)$. □

For any $F\in L^1(\mathbb{R})\cap L^\infty(\mathbb{R})$ we define the mean zero random variable $M_F^{\varepsilon,g}$ by

$$M_F^{\varepsilon,g} = \varepsilon^{-\frac{\alpha}{2}}\int_{\mathbb{R}} g_{\frac{t}{\varepsilon}}F(t)dt\,. \tag{8.32}$$

The purpose of this subsection is to determine the limits of the variances of the variables M_F^{ε} and $M_F^{\varepsilon,g}$.

Lemma 8.3. *Let $F\in L^1(\mathbb{R})\cap L^\infty(\mathbb{R})$ and let g_x be the Gaussian random process described in Hypothesis [H]. Then*

$$\lim_{\varepsilon\to 0}\mathscr{E}\big\{\big|M_F^{\varepsilon,g}\big|^2\big\} = \frac{\kappa_g 2^{-\alpha}\Gamma(\frac{1-\alpha}{2})}{\sqrt{\pi}\Gamma(\frac{\alpha}{2})}\int_{\mathbb{R}}\frac{|\hat F(\xi)|^2}{|\xi|^{1-\alpha}}d\xi\,. \tag{8.33}$$

Proof. We write the square of the integral as a double integral, which gives

$$\mathscr{E}\Big\{\Big|\int_{\mathbb{R}}F(y)g_{\frac{y}{\varepsilon}}dy\Big|^2\Big\} = \int_{\mathbb{R}^2}R_g\big(\frac{y-z}{\varepsilon}\big)F(y)F(z)dydz\,.$$

This implies the estimate

$$\begin{aligned}\Big|\mathscr{E}\big\{\big|M_F^{\varepsilon,g}\big|^2\big\} - \int_{\mathbb{R}^2}\frac{\kappa_g}{|y-z|^\alpha}F(y)F(z)dydz\Big| \\ \le \int_{\mathbb{R}^2}\Big|\varepsilon^{-\alpha}R_g\big(\frac{y-z}{\varepsilon}\big) - \frac{\kappa_g}{|y-z|^\alpha}\Big|\,|F(y)||F(z)|dydz\,.\end{aligned}$$

By (8.8), for any $\delta>0$, there exists T_δ such that, for all $|\tau|\ge T_\delta$,

$$\big|R_g(\tau)-\kappa_g\tau^{-\alpha}\big|\le\delta\tau^{-\alpha}\,.$$

We decompose the integration domain into three subdomains D_1, D_2, and D_3:

$$\begin{aligned} D_1 &= \left\{(y,z)\in\mathbb{R}^2\,,\,|y-z|\le T_\delta\varepsilon\right\}\,,\\ D_2 &= \left\{(y,z)\in\mathbb{R}^2\,,\,T_\delta\varepsilon<|y-z|\le 1\right\}\,,\\ D_3 &= \left\{(y,z)\in\mathbb{R}^2\,,\,1<|y-z|\right\}\,. \end{aligned}$$

First,

$$\begin{aligned} &\int_{D_1}\left|\varepsilon^{-\alpha}R_g\big(\frac{y-z}{\varepsilon}\big)-\frac{\kappa_g}{|y-z|^\alpha}\right||F(y)||F(z)|dydz\\ &\quad\le\int_{D_1}\left|\varepsilon^{-\alpha}R_g\big(\frac{y-z}{\varepsilon}\big)\right||F(y)||F(z)|dydz+\int_{D_1}\kappa_g|y-z|^{-\alpha}|F(y)||F(z)|dydz\\ &\quad\le 2\varepsilon^{-\alpha}\|R_g\|_\infty\int_{\mathbb{R}}\int_0^{T_\delta\varepsilon}|F(y+z)|dy|F(z)|dz+2\kappa_g\int_{\mathbb{R}}\int_0^{T_\delta\varepsilon}y^{-\alpha}|F(y+z)|dy|F(z)|dz\\ &\quad\le 2\varepsilon^{-\alpha}\|R_g\|_\infty\|F\|_\infty\|F\|_1\int_0^{T_\delta\varepsilon}dy+2\kappa_g\|F\|_\infty\|F\|_1\int_0^{T_\delta\varepsilon}y^{-\alpha}dy\\ &\quad\le\|F\|_\infty\|F\|_1\left(2T_\delta R_g(0)+\frac{2\kappa_g T_\delta^{1-\alpha}}{1-\alpha}\right)\varepsilon^{1-\alpha}\,, \end{aligned}$$

where we have used the fact that $R_g(\tau)$ is maximal at $\tau=0$, and the value of the maximum is equal to the variance of g. Second,

$$\begin{aligned} \int_{D_2}\left|\varepsilon^{-\alpha}R_g\big(\frac{y-z}{\varepsilon}\big)-\frac{\kappa_g}{|y-z|^\alpha}\right||F(y)||F(z)|dydz &\le \delta\int_{D_2}|y-z|^{-\alpha}|F(y)||F(z)|dydz\\ &\le 2\delta\|F\|_\infty\|F\|_1\int_{T_\delta\varepsilon}^1 y^{-\alpha}dy\\ &\le \frac{2\delta\|F\|_\infty\|F\|_1}{1-\alpha}\,, \end{aligned}$$

and finally

$$\begin{aligned} \int_{D_3}\left|\varepsilon^{-\alpha}R_g\big(\frac{y-z}{\varepsilon}\big)-\frac{\kappa_g}{|y-z|^\alpha}\right||F(y)||F(z)|dydz &\le \delta\int_{D_3}|y-z|^{-\alpha}|F(y)||F(z)|dydz\\ &\le \delta\int_{D_3}|F(y)||F(z)|dydz\\ &\le \delta\|F\|_1^2\,. \end{aligned}$$

Therefore, there exists $K>0$ such that

$$\limsup_{\varepsilon\to 0}\left|\mathscr{E}\left\{\left|M_F^{\varepsilon,g}\right|^2\right\}-\int_{\mathbb{R}^2}\frac{\kappa_g}{|y-z|^\alpha}F(y)F(z)dydz\right|\le K\left(\|F\|_\infty^2+\|F\|_1^2\right)\delta\,.$$

Since this holds true for any $\delta > 0$, we get

$$\lim_{\varepsilon\to 0}\left|\mathscr{E}\left\{\left|M_F^{\varepsilon,g}\right|^2\right\} - \int_{\mathbb{R}^2}\frac{\kappa_g}{|y-z|^\alpha}F(y)F(z)dydz\right| = 0\,.$$

We recall that the Fourier transform of the function $|x|^{-\alpha}$ is

$$\widehat{|x|^{-\alpha}}(\xi) = c_\alpha|\xi|^{\alpha-1}\,, \qquad c_\alpha = \int_{\mathbb{R}}\frac{e^{it}}{|t|^\alpha}dt = \frac{\sqrt{\pi}2^{1-\alpha}\Gamma(\frac{1-\alpha}{2})}{\Gamma(\frac{\alpha}{2})}\,. \tag{8.34}$$

Using the Parseval equality, we find that

$$\int_{\mathbb{R}^2}\frac{1}{|y-z|^\alpha}F(y)F(z)dydz = \frac{c_\alpha}{2\pi}\int_{\mathbb{R}}\frac{|\hat{F}(\xi)|^2}{|\xi|^{1-\alpha}}d\xi\,.$$

The right-hand side is finite, because 1) $F \in L^1(\mathbb{R})$ so that $\hat{F}(\xi) \in L^\infty(\mathbb{R})$, 2) $F \in L^1(\mathbb{R}) \cap L^\infty(\mathbb{R})$ so $F \in L^2(\mathbb{R})$ and $\hat{F} \in L^2(\mathbb{R})$, and 3) $\alpha \in (0,1)$. □

Lemma 8.4. *Let $F \in L^1(\mathbb{R})\cap L^\infty(\mathbb{R})$ and let the process $\varphi(x)$ be of the form* (8.6)*. Then we have:*

$$\lim_{\varepsilon\to 0}\mathscr{E}\Big\{(M_F^\varepsilon - V_1 M_F^{\varepsilon,g})^2\Big\} = 0\,.$$

Proof. We write the square of the integral as a double integral:

$$\mathscr{E}\Big\{(M_F^\varepsilon - V_1 M_F^{\varepsilon,g})^2\Big\} = \varepsilon^{-\alpha}\int_{\mathbb{R}^2}F(y)F(z)Q(\frac{y}{\varepsilon},\frac{z}{\varepsilon})dydz\,,$$

where

$$Q(y,z) = \mathscr{E}\Big\{\Phi(g_y)\Phi(g_z) - V_1\Phi(g_y)g_z - V_1 g_y\Phi(g_z) + V_1^2 g_y g_z\Big\}\,.$$

By Lemma 8.2 and (8.8), there exist K, T such that $|Q(y,z)| \le K|y-z|^{-2\alpha}$ for all $|x-y| \ge T$. Besides, Φ is bounded and g_x is square-integrable, so there exists K such that, for all $y, z \in \mathbb{R}$, $|Q(y,z)| \le K$. We decompose the integration domain $\mathbb{R}^2$ into three subdomains D_1, D_2, and D_3:

$$\begin{aligned} D_1 &= \left\{(y,z)\in\mathbb{R}^2\,,\, |y-z| \le T\varepsilon\right\}\,,\\ D_2 &= \left\{(y,z)\in\mathbb{R}^2\,,\, T\varepsilon < |y-z| \le 1\right\}\,,\\ D_3 &= \left\{(y,z)\in\mathbb{R}^2\,,\, 1 < |y-z|\right\}\,. \end{aligned}$$

We get the estimates

$$\begin{aligned} \left|\int_{D_1}F(y)F(z)Q(\frac{y}{\varepsilon},\frac{z}{\varepsilon})dydz\right| &\le K\int_{D_1}|F(y)||F(z)|dydz\\ &\le 2K\int_{\mathbb{R}}\int_0^{T\varepsilon}|F(y+z)|dy|F(z)|dz\\ &\le 2K\|F\|_\infty\|F\|_1 T\varepsilon\,, \end{aligned}$$

$$\begin{aligned}
\left|\int_{D_2} F(y)F(z)Q(\frac{y}{\varepsilon},\frac{z}{\varepsilon})dydz\right| &\leq K\int_{D_2}\left|\frac{y}{\varepsilon}-\frac{z}{\varepsilon}\right|^{-2\alpha}|F(y)||F(z)dydz \\
&\leq 2K\varepsilon^{2\alpha}\int_{\mathbb{R}}\int_{T\varepsilon}^{1} y^{-2\alpha}|F(y+z)|dy|F(z)|dz \\
&\leq 2K\|F\|_1\|F\|_\infty\varepsilon^{2\alpha}\int_{T\varepsilon}^{1} y^{-2\alpha}dy \\
&\leq 2K\|F\|_1\|F\|_\infty\begin{cases} \frac{1}{1-2\alpha}\varepsilon^{2\alpha} \text{ if } \alpha<1/2 \\ |\ln(T\varepsilon)|\varepsilon \text{ if } \alpha=1/2 \\ \frac{T^{1-2\alpha}}{2\alpha-1}\varepsilon \text{ if } \alpha>1/2 \end{cases}
\end{aligned}$$

$$\begin{aligned}
\left|\int_{D_3} F(y)F(z)Q(\frac{y}{\varepsilon},\frac{z}{\varepsilon})dydz\right| &\leq K\int_{D_3}\left|\frac{y}{\varepsilon}-\frac{z}{\varepsilon}\right|^{-2\alpha}|F(y)||F(z)dydz \\
&\leq 2K\varepsilon^{2\alpha}\int_{\mathbb{R}}\int_{1}^{\infty} y^{-2\alpha}|F(y+z)|dy|F(z)|dz \\
&\leq 2K\varepsilon^{2\alpha}\int_{\mathbb{R}}\int_{1}^{\infty} |F(y+z)|dy|F(z)|dz \\
&\leq 2K\|F\|_1^2\varepsilon^{2\alpha}\,,
\end{aligned}$$

which gives the desired result:

$$\lim_{\varepsilon\to 0}\varepsilon^{-\alpha}\left|\int_{\mathbb{R}^2} F(y)F(z)Q(\frac{y}{\varepsilon},\frac{z}{\varepsilon})dydz\right| = 0\,.$$

□

The following proposition is now a straighforward corollary of Lemma 8.3 and Lemma 8.4 and the fact that $\kappa = \kappa_g V_1^2$.

Proposition 8.2. *Let $F \in L^1(\mathbb{R})\cap L^\infty(\mathbb{R})$ and let the process $\varphi(x)$ be of the form* (8.6)*. Then we find that:*

$$\lim_{\varepsilon\to 0}\mathscr{E}\left\{\left|M_F^\varepsilon\right|^2\right\} = \frac{\kappa 2^{-\alpha}\Gamma(\frac{1-\alpha}{2})}{\sqrt{\pi}\Gamma(\frac{\alpha}{2})}\int_{\mathbb{R}}\frac{|\hat{F}(\xi)|^2}{|\xi|^{1-\alpha}}d\xi\,. \tag{8.35}$$

Remark 8.2. The limit of the variance of M_F^ε is (8.35) and the variance of M^0 is (8.31). These two expressions are reconciled by using the identity $1-\alpha = 2H-1$ and standard properties of the Γ function, namely $\Gamma(H)\Gamma(H+\frac{1}{2}) = 2^{1-2H}\sqrt{\pi}\Gamma(2H)$ and $\Gamma(1-H)\Gamma(H) = \pi(\sin(\pi H))^{-1}$. We get

$$\frac{2^{-\alpha}\Gamma(\frac{1-\alpha}{2})}{\sqrt{\pi}\Gamma(\frac{\alpha}{2})} = \frac{2^{-2+2H}\Gamma(H-\frac{1}{2})}{\sqrt{\pi}\Gamma(1-H)} = \frac{2^{-2+2H}\Gamma(H+\frac{1}{2})}{\sqrt{\pi}(H-\frac{1}{2})\Gamma(1-H)} = \frac{\Gamma(2H)\sin(\pi H)}{\pi(2H-1)}\,.$$

By (8.24) this shows that

$$\frac{2^{-\alpha}\Gamma(\frac{1-\alpha}{2})}{\sqrt{\pi}\Gamma(\frac{\alpha}{2})}2\pi = \frac{1}{H(2H-1)C(H)^2}\,,$$

and this implies that the variance (8.31) of M_F^0 is exactly the limit (8.35) of the variance of M_F^ε:

$$\lim_{\varepsilon\to 0}\mathscr{E}\left\{\left|M_F^\varepsilon\right|^2\right\} = \mathscr{E}\left\{\left|M_F^0\right|^2\right\}.$$

8.3.2 Convergence in distribution

We can now give the proof of Theorem 8.3.

Step 1. The sequence of random variables $M_F^{\varepsilon,g}$ defined by (8.32) *converges in distribution as $\varepsilon \to 0$ to*

$$M_F^{0,g} = \sqrt{\frac{\kappa_g}{H(2H-1)}}\int_{\mathbb{R}} F(t)dW_t^H\,.$$

Since the random variable $M_F^{\varepsilon,g}$ is a linear transform of a Gaussian process, it has Gaussian distribution. Moreover, its mean is zero. The same statements hold true for $M_F^{0,g}$. Therefore, the characteristic functions of $M_F^{\varepsilon,g}$ and $M_F^{0,g}$ are

$$\mathscr{E}\left\{e^{i\lambda M_F^{\varepsilon,g}}\right\} = \exp\left(-\frac{\lambda^2}{2}\mathscr{E}\left\{(M_F^{\varepsilon,g})^2\right\}\right)\,,\quad \mathscr{E}\left\{e^{i\lambda M_F^{0,g}}\right\} = \exp\left(-\frac{\lambda^2}{2}\mathscr{E}\left\{(M_F^{0,g})^2\right\}\right)\,,$$

where $\lambda\in\mathbb{R}$. Convergence of the characteristic functions implies that of the distributions [14]. Therefore, it is sufficient to show that the variance of $M_F^{\varepsilon,g}$ converges to the variance of $M_F^{0,g}$ as $\varepsilon\to 0$. This follows from Lemma 8.3.

Step 2: M_F^ε converges in distribution to M_F^0 as $\varepsilon\to 0$.

Let $\lambda\in\mathbb{R}$. Since $M_F^0 = V_1 M_F^{0,g}$, we have

$$\begin{aligned}\left|\mathscr{E}\left\{e^{i\lambda M_F^\varepsilon}\right\} - \mathscr{E}\left\{e^{i\lambda M_F^0}\right\}\right| \;\le\; &\left|\mathscr{E}\left\{e^{i\lambda M_F^\varepsilon}\right\} - \mathscr{E}\left\{e^{i\lambda V_1 M_F^{\varepsilon,g}}\right\}\right| \\ &+ \left|\mathscr{E}\left\{e^{i\lambda V_1 M_F^{\varepsilon,g}}\right\} - \mathscr{E}\left\{e^{i\lambda V_1 M_F^{0,g}}\right\}\right| \quad (8.36)\end{aligned}$$

Since $|e^{ix}-1|\le|x|$ we can write

$$\left|\mathscr{E}\left\{e^{i\lambda M_F^\varepsilon}\right\} - \mathscr{E}\left\{e^{i\lambda V_1 M_F^{\varepsilon,g}}\right\}\right| \le |\lambda|\mathscr{E}\left\{|M_F^\varepsilon - V_1 M_F^{\varepsilon,g}|\right\} \le |\lambda|\mathscr{E}\left\{(M_F^\varepsilon - V_1 M_F^{\varepsilon,g})^2\right\}^{1/2},$$

which goes to zero by the result of Lemma 8.4. This shows that the first term of the right-hand side of (8.36) converges to 0 as $\varepsilon\to 0$. The second term of the right-hand side of (8.36) also converges to zero by the result of Step 1. This completes the proof of Theorem 8.3.

8.4 Convergence of random processes

Let F_1, F_2 be two functions in $L^\infty(0,1)$. We consider the random process $M^\varepsilon(x)$ defined for any $x \in [0,1]$ by

$$M^\varepsilon(x) = \varepsilon^{-\frac{\alpha}{2}} \left(\int_0^x F_1(t)\phi^\varepsilon(t)dt + x \int_0^1 F_2(t)\phi^\varepsilon(t)dt \right) . \tag{8.37}$$

With the notation (8.29) of the previous section, we have

$$M^\varepsilon(x) = M^\varepsilon_{F_x} = \varepsilon^{-\frac{\alpha}{2}} \int_{\mathbb{R}} F_x(t)\phi^\varepsilon(t)dt \,,$$

where

$$F_x(t) = F_1(t)\mathbf{1}_{[0,x]}(t) + xF_2(t)\mathbf{1}_{[0,1]}(t) \tag{8.38}$$

is indeed a function in $L^1(\mathbb{R}) \cap L^\infty(\mathbb{R})$.

Theorem 8.4. *Let φ be a random process of the form (8.6) and let $F_1, F_2 \in L^\infty(0,1)$. Then the random process $M^\varepsilon(x)$ defined by (8.37) converges in distribution as $\varepsilon \to 0$ in the space of the continuous functions $\mathcal{C}(0,1)$ to the continuous Gaussian process*

$$M^0(x) = \sqrt{\frac{\kappa}{H(2H-1)}} \int_{\mathbb{R}} F_x(t)dW_t^H \,, \tag{8.39}$$

where F_x is defined by (8.38) and W_t^H is a fractional Brownian motion with Hurst index $H = 1 - \frac{\alpha}{2}$.

The limit random process M^0 is a Gaussian process with mean zero and autocorrelation function

$$\mathscr{E}\big\{M^0(x)M^0(y)\big\} = \frac{\kappa}{H(2H-1)} \times \frac{1}{2\pi C(H)^2} \int_{\mathbb{R}} \frac{\hat{F}_x(\xi)\overline{\hat{F}_y(\xi)}}{|\xi|^{2H-1}} d\xi \,. \tag{8.40}$$

The proof of Theorem 8.4 is based on a classical result on the weak convergence of continuous random processes [11]:

Proposition 8.3. *Suppose $(M^\varepsilon)_{\varepsilon\in(0,1)}$ are random processes with values in the space of continuous functions $\mathcal{C}(0,1)$ with $M^\varepsilon(0) = 0$. Then M^ε converges in distribution to M^0 provided that:*

(i) for any $0 \le x_1 \le \ldots \le x_k \le 1$, the finite-dimensional distribution $(M^\varepsilon(x_1), \cdots, M^\varepsilon(x_k))$ converges to the distribution $(M^0(x_1), \ldots, M^0(x_k))$ as $\varepsilon \to 0$.

(ii) $(M^\varepsilon)_{\varepsilon\in(0,1)}$ *is a tight sequence of random processes in* $\mathcal{C}(0,1)$*. A sufficient condition for tightness of* $(M^\varepsilon)_{\varepsilon\in(0,1)}$ *is the Kolmogorov criterium:* $\exists\delta,\beta,C>0$ *such that*

$$\mathscr{E}\big\{\big|M^\varepsilon(s)-M^\varepsilon(t)\big|^\beta\big\}\le C|t-s|^{1+\delta}\,, \tag{8.41}$$

uniformly in $\varepsilon,t,s\in(0,1)$*.*

We split the proof of Theorem 8.4 into two parts: in the next subsection, we prove the point (i), and next, we prove (ii).

8.4.1 Convergence of the finite-dimensional distributions

For the proof of convergence of the finite-dimensional distributions, we want to show that for each set of points $0\le x_1\le\cdots\le x_k\le 1$ and each $\Lambda=(\lambda_1,\dots,\lambda_k)\in\mathbb{R}^k$, we have the following convergence result for the characteristic functions:

$$\mathscr{E}\Big\{\exp\Big(i\sum_{j=1}^k\lambda_jM^\varepsilon(x_j)\Big)\Big\}\xrightarrow{\varepsilon\to0}\mathscr{E}\Big\{\exp\Big(i\sum_{j=1}^k\lambda_jM^0(x_j)\Big)\Big\}\,. \tag{8.42}$$

Convergence of the characteristic functions implies that of the joint distributions [14]. Now the above characteristic function may be recast as

$$\mathscr{E}\Big\{\exp\Big(i\sum_{j=1}^k\lambda_jM^\varepsilon(x_j)\Big)\Big\}=\mathscr{E}\Big\{\exp i\Big(\varepsilon^{-\frac{\alpha}{2}}\int_{\mathbb{R}}\varphi^\varepsilon(t)F_\Lambda(t)dt\Big)\Big\}\,, \tag{8.43}$$

where

$$F_\Lambda(t)=\Big(\sum_{j=1}^k\lambda_j\mathbf{1}_{[0,x_j]}(t)\Big)F_1(t)+\Big(\sum_{j=1}^k\lambda_jx_j\Big)\mathbf{1}_{[0,1]}(t)F_2(t)\,.$$

Since $F_\Lambda\in L^\infty(\mathbb{R})\cap L^1(\mathbb{R})$ when $F_1,F_2\in L^\infty(0,1)$, we can apply Theorem 8.3 which gives

$$\mathscr{E}\Big\{\exp\Big(i\sum_{j=1}^k\lambda_jM^\varepsilon(x_j)\Big)\Big\}\xrightarrow{\varepsilon\to0}\mathscr{E}\Big\{\exp i\Big(\sqrt{\frac{\kappa}{H(2H-1)}}\int_{\mathbb{R}}F_\Lambda(t)dW_t^H\Big)\Big\}\,,$$

which in turn establishes (8.42).

8.4.2 Tightness

It is possible to control the increments of the process M^ε, as shown by the following proposition.

Proposition 8.4. *There exists K such that, for any $F_1, F_2 \in L^\infty(0,1)$ and for any $x, y \in [0,1]$,*

$$\sup_{\varepsilon\in(0,1)} \mathscr{E}\big\{\big|M^\varepsilon(y)-M^\varepsilon(x)\big|^2\big\} \le K\Big(\|F_1\|_\infty^2|y-x|^{2-\alpha}+\|F_2\|_\infty^2|y-x|^2\Big)\,, \quad (8.44)$$

where M^ε is defined by (8.37).

Proof. The proof is a refinement of the ones of Lemma 8.3 and Lemma 8.4. We can split the random process M^ε into two components: $M^\varepsilon(x) = M^{\varepsilon,1}(x)+ M^{\varepsilon,2}(x)$, with

$$M^{\varepsilon,1}(x) = \varepsilon^{-\frac{\alpha}{2}} \int_0^x F_1(t)\phi^\varepsilon(t)dt\,, \qquad M^{\varepsilon,2}(x) = x\varepsilon^{-\frac{\alpha}{2}} \int_0^1 F_2(t)\phi^\varepsilon(t)dt\,.$$

We have

$$\mathscr{E}\big\{\big|M^\varepsilon(y)-M^\varepsilon(x)\big|^2\big\} \le 2\mathscr{E}\big\{\big|M^{\varepsilon,1}(y)-M^{\varepsilon,1}(x)\big|^2\big\}+2\mathscr{E}\big\{\big|M^{\varepsilon,2}(y)-M^{\varepsilon,2}(x)\big|^2\big\}\,.$$

The second moment of the increment of $M^{\varepsilon,2}$ is given by

$$\mathscr{E}\big\{\big|M^{\varepsilon,2}(y) - M^{\varepsilon,2}(x)\big|^2\big\} = |x-y|^2\varepsilon^{-\alpha}\int_{[0,1]^2} R\big(\frac{z-t}{\varepsilon}\big)F_2(z)F_2(t)dzdt\,.$$

Since there exists $K>0$ such that $|R(\tau)| \le K\tau^{-\alpha}$ for all τ, we have

$$\begin{aligned}\varepsilon^{-\alpha}\int_{[0,1]^2} R\big(\frac{z-t}{\varepsilon}\big)F_2(z)F_2(t)dzdt &\le K\int_{[0,1]^2}|z-t|^{-\alpha}|F_2(z)||F_2(t)|dzdt\\ &\le K\|F_2\|_\infty^2\int_{-1}^1|z|^{-\alpha}dz = \frac{2K}{1-\alpha}\|F_2\|_\infty^2\,,\end{aligned}$$

which gives the following estimate

$$\mathscr{E}\big\{\big|M^{\varepsilon,2}(y) - M^{\varepsilon,2}(x)\big|^2\big\} \le \frac{2K}{1-\alpha}\|F_2\|_\infty^2|x-y|^2\,.$$

The second moment of the increment of $M^{\varepsilon,1}$ for $x<y$ is given by

$$\mathscr{E}\big\{\big|M^{\varepsilon,1}(y) - M^{\varepsilon,1}(x)\big|^2\big\} = \varepsilon^{-\alpha}\int_{[x,y]^2} R\big(\frac{z-t}{\varepsilon}\big)F_1(z)F_1(t)dzdt\,.$$

We will distinguish the cases $|y-x| \leq \varepsilon$ and $|y-x| \geq \varepsilon$.

First case. Let us assume that $|y-x| \leq \varepsilon$. Since R is bounded by V_2, we have

$$\mathscr{E}\left\{\left|M^{\varepsilon,1}(y) - M^{\varepsilon,1}(x)\right|^2\right\} \leq V_2 \|F_1\|_\infty^2 \varepsilon^{-\alpha} |y-x|^2 .$$

Since $|y-x| \leq \varepsilon$, this implies

$$\mathscr{E}\left\{\left|M^{\varepsilon,1}(y) - M^{\varepsilon,1}(x)\right|^2\right\} \leq V_2 \|F_1\|_\infty^2 |y-x|^{2-\alpha} .$$

Second case. Let us assume that $|y-x| \geq \varepsilon$. Since R can be bounded by a power-law function $|R(\tau)| \leq K\tau^{-\alpha}$ we have

$$\begin{aligned}
\mathscr{E}\left\{\left|M^{\varepsilon,1}(y) - M^{\varepsilon,1}(x)\right|^2\right\} &\leq K\|F_1\|_\infty^2 \int_{[x,y]^2} |z-t|^{-\alpha} dzdt \\
&\leq 2K\|F_1\|_\infty^2 \int_x^y \int_0^{y-x} t^{-\alpha} dtdz \\
&\leq \frac{2K}{1-\alpha} \|F_1\|_\infty^2 |y-x|^{2-\alpha} ,
\end{aligned}$$

which completes the proof. □

This Proposition allows us to get two results.

1) By applying Proposition 8.4 with $F_2 = 0$ and $y = 0$, we prove Lemma 8.1.

2) By applying Proposition 8.4, we obtain that the increments of the process M^ε satisfy the Kolmogorov criterium (8.41) with $\beta = 2$ and $\delta = 1-\alpha > 0$. This gives the tightness of the family of processes M^ε in the space $\mathcal{C}(0,1)$.

8.4.3 Proof of Theorem 8.1

We can now give the proof of Theorem 8.1. The error term can be written in the form

$$\varepsilon^{-\frac{\alpha}{2}} \left(u^\varepsilon(x) - \bar{u}(x)\right) = \varepsilon^{-\frac{\alpha}{2}} \left(\int_0^x F_1(t)\varphi^\varepsilon(t)dt + x \int_0^1 F_2(t)\varphi^\varepsilon(t)dt \right) + \widetilde{r}^\varepsilon(x) ,$$

where $F_1(t) = c^* - F(t)$, $F_2(t) = F(t) - \int_0^1 F(z)dz - a^*q$, and $\widetilde{r}^\varepsilon(x) = \varepsilon^{-\alpha/2}[r^\varepsilon(x) + \rho^\varepsilon a^{*-1}x]$. The first term of the right-hand side is of the form (8.37). Therefore, by applying Theorem 8.4, we get that this process converges in distribution in $\mathcal{C}(0,1)$ to the limit process (8.20). It remains to show that the random process $\widetilde{r}^\varepsilon(x)$ converges as $\varepsilon \to 0$ to zero in $\mathcal{C}(0,1)$ in probability.

We have

$$\mathscr{E}\{|\widetilde{r}^{\varepsilon}(x)-\widetilde{r}^{\varepsilon}(y)|^2\} \leq 2\varepsilon^{-\alpha}\mathscr{E}\{|r^{\varepsilon}(x)-r^{\varepsilon}(y)|^2\} + 2a^{*-2}\varepsilon^{-\alpha}\mathscr{E}\{|\rho^{\varepsilon}|^2\}|x-y|^2\,,$$

From the expression (8.18) of r^{ε}, and the fact that c^{ε} can be bounded uniformly in ε by a constant c_0, we get

$$\varepsilon^{-\alpha}\mathscr{E}\{|r^{\varepsilon}(x)-r^{\varepsilon}(y)|^2\} \leq 2\varepsilon^{-\alpha}c_0\mathscr{E}\left\{\left|\int_x^y \varphi^{\varepsilon}(t)dt\right|^2\right\}.$$

Applying Proposition 8.4 we obtain that there exists $K>0$ such that

$$\varepsilon^{-\alpha}\mathscr{E}\{|r^{\varepsilon}(x)-r^{\varepsilon}(y)|^2\} \leq K|x-y|^{2-\alpha}\,.$$

Besides, since ρ^{ε} can be bounded uniformly in ε by a constant ρ_0, we have $\mathscr{E}\{|\rho^{\varepsilon}|^2\} \leq \rho_0\mathscr{E}\{|\rho^{\varepsilon}|\} \leq K\varepsilon^{\alpha}$ for some $K>0$. Therefore, we have established that there exists $K>0$ such that

$$\mathscr{E}\{|\widetilde{r}^{\varepsilon}(x)-\widetilde{r}^{\varepsilon}(y)|^2\} \leq K|x-y|^{2-\alpha}\,,$$

uniformly in ε, x, y. This shows that $\widetilde{r}^{\varepsilon}(x)$ is a tight sequence in the space $\mathcal{C}(0,1)$ by the Kolmogorov criterium (8.41). Furthermore, the finite-dimensional distributions of $\widetilde{r}^{\varepsilon}(x)$ converges to zero because

$$\sup_{x\in[0,1]} \mathscr{E}\big\{|\widetilde{r}_{\varepsilon}(x)|\big\} \stackrel{\varepsilon\to 0}{\longrightarrow} 0$$

by (8.15) and (8.17). Proposition 8.3 then shows that $\widetilde{r}^{\varepsilon}(x)$ converges to zero in distribution in $\mathcal{C}(0,1)$. Since the limit is deterministic, the convergence actually holds true in probability.

8.5 Numerical results for Theorem 8.2

In this section we numerically study the convergence of the error in the case in which $F=0$, $q=1$, and the driving process $\varphi(x)$ has an integrable autocorrelation function. The solutions of the random elliptic equation (8.1) and of the homogenized equation (8.2) are given by

$$u_{\varepsilon}(x) = \frac{1}{\int_0^1 \frac{1}{a_{\varepsilon}}\,dy}\int_0^x \frac{1}{a_{\varepsilon}}\,dy \quad ; \quad \bar{u}(x) = x\,.$$

Using the decomposition $\varphi_{\varepsilon} = \frac{1}{a_{\varepsilon}} - \frac{1}{a_*}$ and assuming that $a_*=1$, we have

$$u_{\varepsilon}(x) = \frac{x+\int_0^x \varphi_{\varepsilon}\,dy}{1+\int_0^1 \varphi_{\varepsilon}\,dy}\,.$$

We will study the the convergence at $x = 1/2$, where we have

$$u_\varepsilon(1/2) = \frac{\frac{1}{2} + \int_0^{\frac{1}{2}} \varphi_\varepsilon \, dy}{1 + \int_0^1 \varphi_\varepsilon \, dy} \overset{\varepsilon \to 0}{\longrightarrow} \frac{1}{2} = \bar{u}(1/2).$$

8.5.1 Generation of the driving process

We will carry out numerical simulations in the case in which the random process $\varphi(x)$ is of the form $\Phi(g_x)$ with g_x a stationary Ornstein-Uhlenbeck process and $\Phi(x) = (1/2)\mathrm{sgn}(x)$ (see Figure 8.1). This is a simple model for a two-component random medium.

The Ornstein-Uhlenbeck is the random process solution of the stochastic differential equation [14]

$$dg_x = -g_x dx + \sqrt{2} dW_x \,,$$

where W_x is a standard Brownian motion. If we suppose that g_0 is a Gaussian random variable with mean 0 and variance 1 independent of the driving Brownian motion, then $(g_x)_{x \geq 0}$ is a stationary zero-mean Gaussian process with the autocorrelation function $\mathscr{E}\{g_x g_{x+\tau}\} = \exp(-|\tau|)$. Moreover, it is a Markovian process, which makes it easy to simulate a realization of the Ornstein-Uhlenbeck process $(g_{k\Delta x})_{k \geq 0}$ sampled at times $(k\Delta x)_{k \geq 0}$ by the following recursive procedure:
- $g_0 = G_0$,
- $g_{(k+1)\Delta x} = e^{-\Delta x} g_{k\Delta x} + \sqrt{1 - \mathrm{e}^{-2\Delta x}} G_{k+1}$,
where $(G_k)_{k \geq 0}$ is a sequence of independent and identically distributed Gaussian random variables with mean 0 and variance 1. Note that the simulation is exact, whatever the value of the grid step Δx is.

Lemma 8.5. *If g_x is the stationary Ornstein-Uhlenbeck process and $\varphi(x) = (1/2)\mathrm{sgn}(g_x)$, then $\varphi(x)$ is a stationary, zero-mean random process with the autocorrelation function*

$$R(\tau) = \mathscr{E}\{\varphi(x+\tau)\varphi(x)\} = \frac{1}{4}\left(1 - \frac{2}{\pi}\arctan(\sqrt{\mathrm{e}^{2|\tau|} - 1})\right).$$

Proof. Since $g \mapsto \mathrm{sgn}(g)$ is an odd function, it is obvious that $\varphi(x)$ has mean zero. Denoting $a_\tau = e^{-|\tau|}$ and $b_\tau = \sqrt{1 - e^{-2|\tau|}}$, the autocorrelation function

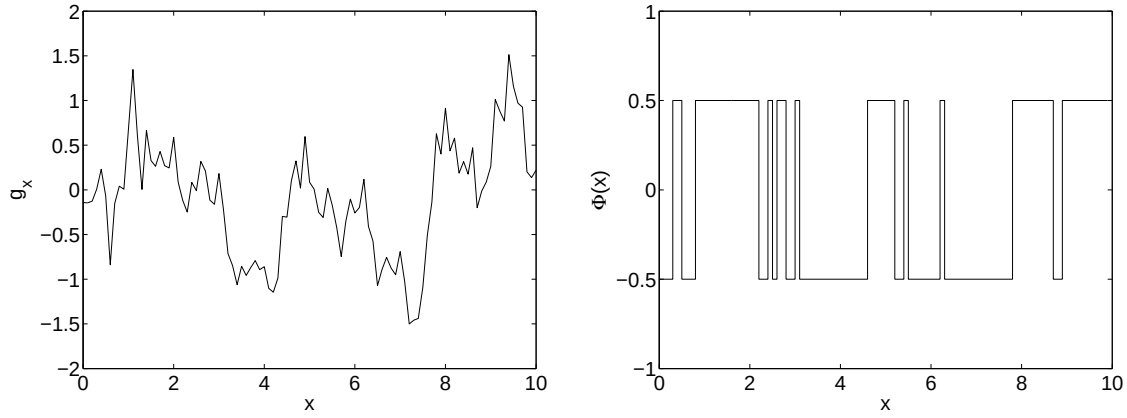

(a) **(b)**

Figure 8.1: Simulation of the Ornstein-Uhlenbeck process g_x (picture (a)) and the induced bounded process $\varphi(x) = (1/2)\mathrm{sgn}(g_x)$ (picture (b)).

of $\varphi(x)$ can be computed as follows:

$$\begin{aligned}
R(\tau) &= \mathscr{E}\{\Phi(g_0)\Phi(g_\tau)\} = \frac{1}{4}\,\mathscr{E}\{\mathrm{sgn}(g_0)\mathrm{sgn}(g_\tau)\} \\
&= \frac{1}{4}\frac{1}{2\pi}\int_{\mathbb{R}^2} \mathrm{sgn}(x)\mathrm{sgn}(a_\tau x + b_\tau y)\,\mathrm{e}^{-\frac{x^2+y^2}{2}}\,dxdy \\
&= \frac{1}{4}\frac{2}{2\pi}\int_{\mathbb{R}^+\times\mathbb{R}} \mathrm{sgn}(x)\mathrm{sgn}(a_\tau x + b_\tau y)\,\mathrm{e}^{-\frac{x^2+y^2}{2}}\,dxdy \\
&= \frac{1}{4\pi}\int_0^\infty \int_{\theta=-\pi/2}^{-\pi/2+\theta_\tau} (-1)\,\rho\mathrm{e}^{-\frac{\rho^2}{2}}\,d\theta d\rho + \frac{1}{4\pi}\int_0^\infty \int_{\theta=\theta_\tau}^{\pi/2} 1\,\rho\mathrm{e}^{-\frac{\rho^2}{2}}\,d\theta d\rho \\
&= \frac{1}{4\pi}\left[-\theta_\tau + (\pi - \theta_\tau)\right] = \frac{1}{4}\left(1 - \frac{2}{\pi}\theta_\tau\right),
\end{aligned}$$

with $\theta_\tau = \arctan(b_\tau/a_\tau) = \arctan(\sqrt{\mathrm{e}^{2|\tau|}-1})$. □

8.5.2 Convergence of the corrector

We now study the convergence of $u_\varepsilon(1/2)$ to $\bar{u}(1/2)$. The value of the integral $\int_0^1 F(s)\varphi_\varepsilon(s)\,ds$ is approximated by the standard quadrature formula

$$\int_0^1 F(s)\varphi_\varepsilon(s)\,ds = \int_0^1 F(s)\varphi\left(\frac{s}{\varepsilon}\right)\,ds = \varepsilon\int_0^{1/\varepsilon} F(\varepsilon y)\varphi(y)\,dy \approx \varepsilon\sum_{i=0}^{n} F(i\varepsilon\Delta x)\varphi(i\Delta x)\Delta x,$$

with $n = [1/(\varepsilon\Delta x)]$ and $\Delta x = 0.1$ in our simulations.

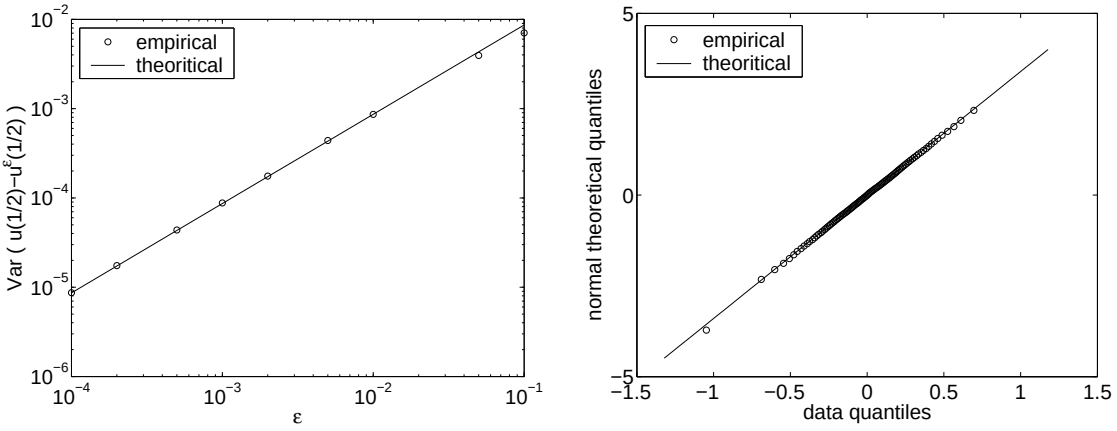

(a) **(b)**

Figure 8.2: Picture (a): Variance of $(u_\varepsilon - u)(1/2)$ as a function of ε, in log-log scale. The convergence rate of the variance in log log scale has a slope equal to one, which proves that the convergence is proportional to ε. Picture (b): Normal QQ plot for the distribution of $\varepsilon^{-1/2}(u^\varepsilon - \bar{u})\,(1/2)$ with $\varepsilon = 0.0001$, which confirms the Gaussian behavior of the error.

We first estimate the convergence order of the variance of $(u_\varepsilon - \bar{u})(1/2)$ when $\varepsilon \to 0$. The following values are given to ε:

$$\varepsilon \in \{0.0001,\, 0.0002,\, 0.0005,\, 0.001,\, 0.002,\, 0.005,\, 0.01,\, 0.05,\, 0.1\}.$$

For each ε, we carry out 10^4 experiments and compute the empirical variance. The results are shown on Figure 8.2a. The asymptotic theory predicts that the convergence is linear in ε:

$$\mathrm{Var}\big\{u_\varepsilon(1/2) - \bar{u}(1/2)\big\} = \sigma^2\varepsilon + o(\varepsilon)\,, \qquad \sigma^2 = 2a_* \int_0^\infty R(\tau)\,d\tau \approx 0.0865.$$

The computation of a linear regression of the empirical variance with respect to ε, with the two, three, etc.. first points give 0.0865, 0.0875, 0.0870, which is less than 1% different from the theory.

We now check the convergence in law of $\frac{1}{\sqrt{\varepsilon}}\,(u_\varepsilon(1/2) - \bar{u}(1/2))$. Theorem 8.2 predicts that

$$\frac{1}{\sqrt{\varepsilon}}\,(u_\varepsilon(x) - \bar{u}(x)) \xrightarrow{law} \left(2\int_0^\infty R(\tau)\,d\tau\right)^{1/2} \mathcal{U}(x),$$

with $\mathcal{U}(x) = a_* W_x - a_* x W_1$, so that in our case

$$\frac{1}{\sqrt{\varepsilon}}\,(u_\varepsilon(1/2) - \bar{u}(1/2)) \xrightarrow{law} G,$$

where G is a Gaussian random variable with mean zero and variance

$$\sigma^2 = 2\int_0^\infty R(\tau)\,d\tau\,\mathrm{Var}\big\{\mathcal{U}(1/2)\big\} = 2a_*\int_0^\infty R(\tau)\,d\tau \approx 0.0865$$

On Figure 8.2b we perform a comparison of the distribution of $\frac{1}{\sqrt{\varepsilon}}\,(u_\varepsilon(1/2) - \bar{u}(1/2))$ for $\varepsilon = 10^{-4}$ with the one of G by plotting the normal QQ plot which shows perfect agreement (a normal QQ plot is a scatterplot with the quantiles of the sample on the horizontal axis and the expected normal quantiles on the vertical axis).

8.6 Numerical results for Theorem 8.1

8.6.1 Generation of the driving process

To test the result of Theorem 8.1, we need to generate a Gaussian process with heavy tail. We choose to generate the increments of a fractional Brownian motion: $g_x = W^H_{x+1} - W^H_x$. As a fractional Brownian motion is not a Markovian process, it cannot be generated iteratively. However many different methods have been developed to simulate fractional Brownian motions, based on integral representations in terms of standard Brownian motions, spectral representations, or wavelet decompositions (see the review [7]). In this chapter we use the Choleski method, that is the simplest method to implement. It is based on the following facts:
1) the fractional Brownian motion W^H_x and the process g_x are Gaussian processes,
2) the autocorrelation function of the fractional Brownian motion is known (see (8.22)), so that it is possible to calculate the covariance matrix C of the Gaussian vector $(g_{k\Delta x})_{k=0,\dots,N}$,
3) if X is a vector of independent and identically distributed random variables with Gaussian distribution, mean 0, and variance 1, then MX is a zero-mean Gaussian vector with covariance matrix MM^T.

The Choleski method consists in
1) computing a square root $\sqrt{C}$ of the covariance matrix C of the Gaussian vector $(g_{k\Delta x})_{k=0,\dots,N}$,
2) generating a vector X of $N+1$ independent and identically distributed Gaussian random variables with mean 0 and variance 1,
3) computing the vector $\sqrt{C}X$.

This method is exact, in the sense that the simulated vector $\sqrt{C}X$ has the distribution of $(g_{k\Delta x})_{k=0,\dots,N}$, whatever the grid step Δx is. The method is, however, computationaly expensive. In fact, only the computation of the

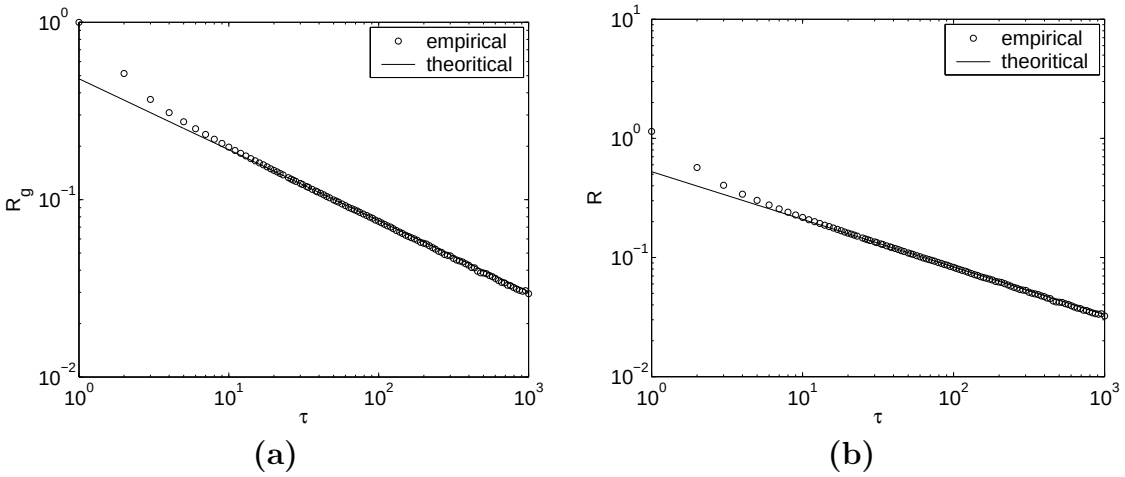

Figure 8.3: A series of 10^5 numerical simulations of the vector $(g_{k\Delta x})_{k=0,\dots,N}$ is carried out, in the case in which $g_x = W^H_{x+1} - W^H_x$, $H = 0.8$, $N = 2000$, and $\Delta x = 1$. Picture (a): The empirical autocorrelation of g_x is compared with the theoretical asymptotic behavior $\tau \mapsto H(2H-1)\tau^{2H-2}$. Picture (b): The empirical autocorrelation of $\varphi(x)$ is compared with the theoretical asymptotic behavior $\tau \mapsto V_1^2 H(2H-1)\tau^{2H-2}$.

square root of the matrix C is costly. Once this computation has been carried out, it is straightfoward to generate a sequence of independent and identically distributed random vectors with the distribution of $(g_{k\Delta x})_{k=0,\dots,N}$.

In the following we apply the Choleski method to generate 10^5 realizations of the vector $(g_{k\Delta x})_{k=0,\dots,N}$ with $\Delta x = 1$ and $N = 2000$. The Hurst parameter is equal to 0.8. The empirical autocorrelation function is shown on Figure 8.3 and compared with its theoretical asymptotic behavior $\tau \mapsto H(2H-1)\tau^{2H-2}$ $[\tau \to \infty]$. When τ becomes large, the fluctuations becomes large compared with $R(\tau)$, because $R(\tau) \to 0$. A linear regression made on the interval $[10, 100]$ gives the power law fit Kt^β, with $K = 0.4901$ and $\beta = 0.3964$, which is in agreement with the theoretical values $K = 0.48$ and $\beta = 0.4$.

We suppose that the random medium is described by the stationary random process

$$\frac{1}{a(x)} = \frac{9}{2} + \frac{8}{\pi}\arctan(g_x) \tag{8.45}$$

The asymptotic behavior of its autocorrelation function is theoretically given by (8.11) with

$$V_1 = \frac{1}{\sqrt{2\pi}}\,\frac{8}{\pi}\int_{-\infty}^{+\infty} x\arctan(x)\mathrm{e}^{-\frac{x^2}{2}}\,dx \approx 1.6694$$

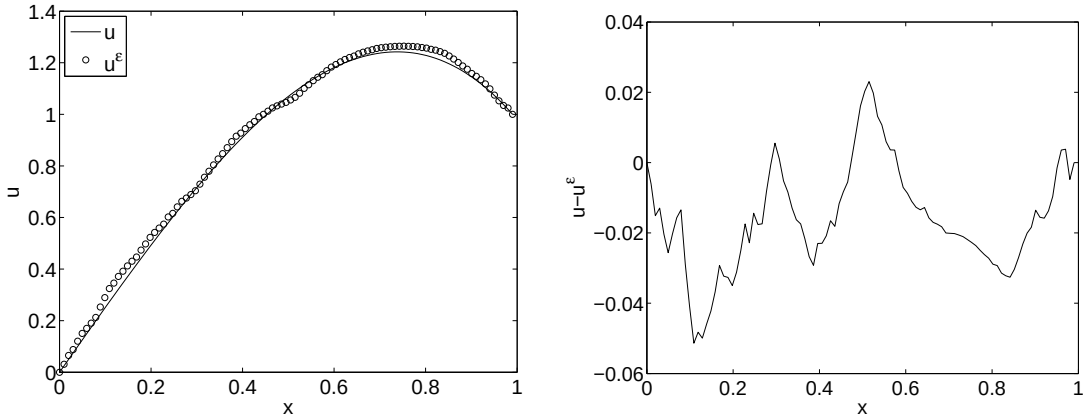

(a) **(b)**

Figure 8.4: Picture (a) compares the homogenized solution (solid line) with the solution of (8.1) obtained for $\varepsilon = 0.0033$ and for a particular realization of the random process φ (circles). Picture (b) plots the difference between u^ε and $\bar{u}$.

The empirical autocorrelation function of the process determined by a series of 10^5 experiments is shown in Figure 8.3, where the theoretical curve and the empirical one agree very well.

8.6.2 Convergence of the corrector

We now study the convergence of the solution of the homogenization problem (8.1) when $\varepsilon \to 0$. We choose $F(x) = x^2$ and $q = 1$. If $a(x)$ is given by (8.45), then we have $a^\star = 2/9$. A solution obtained with a particular realization of the random process with $\varepsilon = 0.0033$ is shown on Figure 8.4 and compared with the theoretical solution of the homogenized problem.

We estimate the convergence order of the variance of the error $(u_\varepsilon - u)(1/2)$ when $\varepsilon \to 0$. The following values are given to ε:

$$\varepsilon \in \{0.0033,\ 0.0017,\ 0.0011,\ 0.00091,\ 0.00077,\ 0.00062,\ 0.0004\} \qquad (8.46)$$

For each value of ε, we make 10^4 experiments, compute the empirical variance of the error, and compare with the asymptotic theoretical variance predicted by Theorem 8.1:

$$\mathrm{Var}\big\{u_\varepsilon(1/2) - \bar{u}(1/2)\big\} = \sigma_H^2 \varepsilon^{2-2H} + o(\varepsilon^{2-2H}) \qquad (8.47)$$

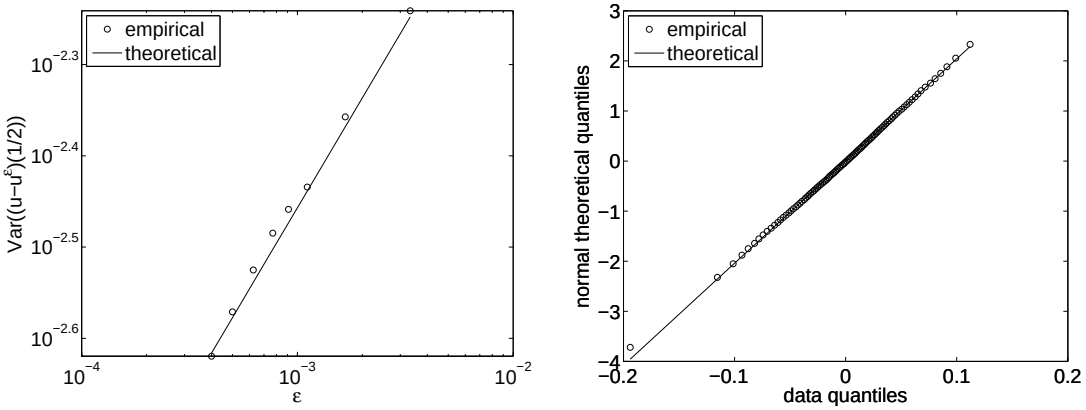

Figure 8.5: Picture (a): Empirical variance of $(u_\varepsilon - \bar{u})(1/2)$ as a function of ε, in log-log scale (circles), compared with the asymptotic theoretical variance (8.47) predicted by Theorem 8.1. Picture (b): Normal QQ plot for $(u^\varepsilon - \bar{u})(1/2)$ with $\varepsilon = 0.0004$, which confirms the Gaussian behavior of the error.

with $2 - 2H = 0.4$ and

$$\sigma_H^2 = \mathrm{Var}\left(\sqrt{\frac{\kappa}{H(2H-1)}}\int_{\mathbb{R}} K\left(\frac{1}{2}, t\right) dW_t^H\right) \approx 0.0553$$

The results are shown on Figure 8.5a, which shows good agreement. More quantitatively, a linear regression of the logarithm of the empirical variance of the error with respect to $\log \varepsilon$ gives:

$$\mathrm{Var}\big\{u^\varepsilon(1/2) - \bar{u}(1/2)\big\} \approx 0.0581\varepsilon^{0.4041} \tag{8.48}$$

which agrees very well with (8.47). Finally, we can check that the distribution of the limit process is Gaussian by observing that the normal QQ plot in Figure 8.5b is indeed a straight line.

8.7 Conclusions

In this chapter, we investigated the correctors in one dimensional homogenization, for a large class of random process. These process are the image of a Gaussian process. Thanks to Hypothesis [H], and the Gaussian behavior of g_x, we managed to have accurate estimates of oscillatory integrals involving this process. These estimates allowed us to prove the convergence of the

explicit solution of a generic one dimensional elliptic problem with Dirichlet conditions.

The first outlook we could do would be to apply the work done here to other integrable systems, such as a wave problem in a random medium, or the linear Schrödinger equation. We could also try to find less restrictive conditions on the process. Last, we could investigate (at least numerically) the case when there does not exist explicit formula, for example an elliptic problem in dimension 2.

Conclusion

In this thesis, we proposed numerical methods for approximating multiphase flows with or without phase transition. Two crucial issues on these models are that they are nonconservative, and that they include some modelling terms that often depend on the physical context.

In the first part, a multiphase flow model was derived in the case when all the fluids have locally the same pressure and velocity, by asymptotic expansion of the seven equations model. In that case, there is no more modelling problem. Nevertheless, the derived system has a nonconservative term, which is a mathematical and a numerical problem. This problem was overcome by returning to the origin of the system: we used a numerical scheme able to deal with the seven equations model, and checked if the asymptotic expansion could be led at a discrete scale, as for the continuous system. The numerical scheme derived was tested with both academic and physical tests. It was proved to be very accurate for these problems.

In the second part, we were interested in the modelling of phase transition. We first compared two types of models: the Van-der-Waals one, and a model built by entropy optimisation with two given convex equations of state. We gave a necessary condition to ensure the convexity of the mixture equation of state. After having compared the properties of the two models, we chose the second one, which is better adapted for metastable states. Then we investigated the Riemann problem with such an equation of state. Based on experiments, we used the Chapman-Jouguet theory to model the vaporisation wave. We gave some conditions in which the assumptions necessary for using the Chapman Jouguet theory hold. We found also a condition for ensuring the entropy growth criterion. Then we proved that the usual closure, i.e. the Chapman-Jouguet closure could not be used in general, and we proposed a relevant closure in the case of a simple model of two perfect gas. Finally, we extended the numerical scheme initially made for multiphase flows in the case of reacting multiphase flows. The scheme was validated on shock tube tests, and it was used in the context of laser interaction with matter.

In the third part, we investigated correctors in stochastic homogenisation, for a simple one dimensional elliptic problem

$$\begin{cases} -\dfrac{d}{dx}\Big(a\Big(\dfrac{x}{\varepsilon},\omega\Big)\dfrac{d}{dx}u^\varepsilon\Big) = f(x), & 0 \leq x \leq 1, \quad \omega \in \Omega, \\ u^\varepsilon(0,\omega) = 0, \qquad u^\varepsilon(1,\omega) = q. \end{cases}$$

where a is an ergodic random process. Under some hypothesis on a and if the autocorrelation of a is equivalent to κ/τ^α, we proved a convergence in law of the corrector to a stochastic process, weighted by ε^α. The theoretical results were validated by numerical simulations.

Outlook

We recall the main outlook that were proposed at the end of each part.

Multiphase flows

As stated at the end of Chapter 3, the main challenge in multiphase flows is to compute a multiphase shock. For this purpose, many solutions can be considered

- In [54], shock jump relations were derived for multiphase flows which were validated on many experiments. One of the challenge is to derive a numerical scheme that can compute the regular waves of the five equations model, and the analytical shock relations.

- More generally, if we have an hyperbolic problem in nonconservative form
$$\frac{\partial \mathbf{U}}{\partial t} + A(\mathbf{U}) \frac{\partial \mathbf{U}}{\partial x} = 0,$$
and prescribed shock relations, how can we derive a numerical scheme that can reproduce the regular solutions of the system, and the prescribed shock relations?

- in [43], the seven equations model is expanded at the ε order: this gives a parabolic regularization of the five equations model. With this regularization, travelling waves can be studied to derive shock relations. This work is in progress with Hervé Guillard (INRIA Sophia Antipolis) on a simplified isothermal model.

Phase transition

For phase transition, several aims can be followed

- First, the numerical scheme derived in Chapter 7 is not able to propagate mixture evaporation fronts. This might be due to the decoupling of the Riemann problems. One way to couple again the different Riemann problem could be to choose a kinetic closure for the Liquid-Gas Riemann problem that would depend on the initial volume fraction of each of the components.

- Some efforts should also be made in the derivation of a relevant kinetic closure for arbitrary equation of state. For that, travelling waves could be derived with the system of [16]. But in this system, the terms that

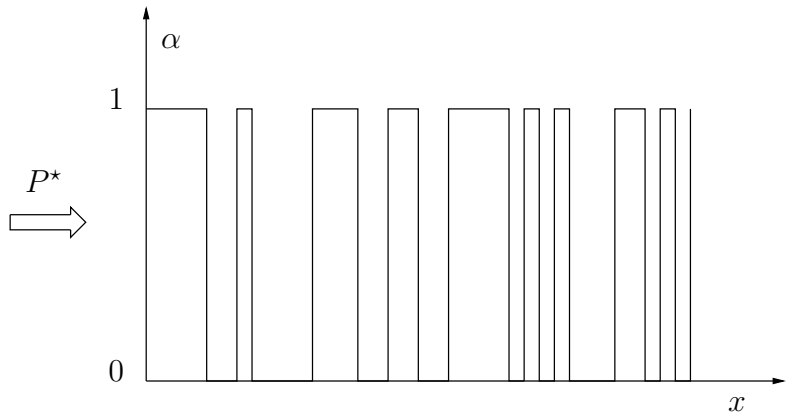

Figure 8.6: For a given realization, we compute the solution, with an imposed pressure $P^\star$ on the left.

appear are $\mu_1 - \mu_2$, $P_1 - P_2$ and $T_1 - T_2$, which means that metastable states are not equilibrium states of these source terms. That is why an effort should be made in the thermodynamic to find a source term for which metastable states are equilibrium states.

- We could also try to find a kinetic closure modelling nucleation.

Stochastic homogenization

The model derived in Chapter 1 relies formally on stochastic homogenisation. As stated in Chapter 8, the process $sgn(g_x)$ (where g_x is a stochastic process) models a two components medium. For a given realization, we could mesh the inclusions and compute an approximated solution with a code, by imposing a constant pressure on the left for example, see Figure 8.6. The first thing we can expect to observe for a long time simulation is a relaxation of the pressure and velocity. Then by making many simulations, and taking the mathematical expectancy, we can wonder whether the averaged solution is self-similar. We note that all the modelling of this simulation relies on the initial stochastic process. Then we could study the convergence order, and the effect of the autocorrelation function on the computed shock velocity.

Bibliography

[1] R. Abgrall, M. Papin, and L. Hallo. A scheme for compressible two-phase flows and interface problems. In *Chen, Zhangxin (ed.) et al., Current trends in scientific computing. ICM 2002 Beijing satellite conference on scientific computing, August 15-18, 2002, Xi'an, China. Providence, RI: American Mathematical Society (AMS). Contemp. Math. 329, 1-12* . 2003.

[2] R. Abgrall and R. Saurel. Discrete equations for physical and numerical compressible multiphase mixtures. *J. Comput. Phys.*, 186(2):361–396, 2003.

[3] Rémi Abgrall and Vincent Perrier. Numerical approximation of multiphase flows. In *Third International Conference on Computational Fluid Dynamics*, Lecture Notes in Physics. Springer-Verlag, 2004.

[4] Rémi Abgrall and Vincent Perrier. Asymptotic expansion of a multiscale numerical scheme for compressible multiphase flows. *Multiscale Model. Simul.*, 5, 2006.

[5] M.R. Baer and J.W. Nunziato. A two-phase mixture theory for the deflagration-to-detonation transition (DDT) in reactive granular materials. *Int. J. Multiphase Flow*, 12:861–889, 1986.

[6] Guillaume Bal, Josselin Garnier, Sébastien Motsch, and Vincent Perrier. Random integrals and correctors in homogenization. *Asymptotic Analysis*, 2007. Submitted.

[7] Jean-Marc Bardet, Gabriel Lang, Georges Oppenheim, Anne Philippe, and Murad S. Taqqu. Generators of long-range dependent processes: a survey. In *Theory and applications of long-range dependence*, pages 579–623. Birkhäuser Boston, Boston, MA, 2003.

[8] Michaël Baudin. *Méthodes de relaxation pour la simulation des écoulements diphasiques dans les conduites pétrolières*. PhD thesis, Université de Paris 6, Institut Français du Pétrole, Novembre 2003.

[9] Alain Bensoussan, Jacques-L. Lions, and George C. Papanicolaou. Boundary layers and homogenization of transport processes. *Publ. Res. Inst. Math. Sci.*, 15(1):53–157, 1979.

[10] Christophe Berthon and Frédéric Coquel. Nonlinear projection methods for multi-entropies Navier-Stokes systems. In *Innovative methods for numerical solutions of partial differential equations (Arcachon, 1998)*, pages 278–304. World Sci. Publ., River Edge, NJ, 2002.

[11] Patrick Billingsley. *Convergence of probability measures*. Wiley Series in Probability and Statistics: Probability and Statistics. John Wiley & Sons Inc., New York, second edition, 1999. A Wiley-Interscience Publication.

[12] J-L Bobin. Flame propagation and overdense heating in a laser created plasma. *Physics of Fluids*, 14(11):2341–2354, 1971.

[13] A. Bourgeat and A. Piatnitski. Estimates in probability of the residual between the random and the homogenized solutions of one-dimensional second-order operator. *Asymptot. Anal.*, 21(3-4):303–315, 1999.

[14] Leo Breiman. *Probability*, volume 7 of *Classics in Applied Mathematics*. Society for Industrial and Applied Mathematics (SIAM), Philadelphia, PA, 1992. Corrected reprint of the 1968 original.

[15] Herbert B. Callen. *Thermodynamics and an Introduction to Thermostatistics*. John Wiley & Sons Inc., New York, second edition, 1985.

[16] Florian Caro. *Modélisation et simulation numérique des transitions de phase liquide–vapeur*. PhD thesis, École Polytechnique, CEA Saclay, November 2004.

[17] F. Coquel and F. Perthame. Relaxation of energy and approximate Riemann solvers for general pressure laws in fluid dynamics. *SIAM J. Numer. Anal.*, 35(6):2223–2249, 1998.

[18] R. Courant and K. O. Friedrichs. *Supersonic Flow and Shock Waves*. Interscience Publishers, Inc., New York, N. Y., 1948.

[19] Gianni Dal Maso, Philippe G. Lefloch, and François Murat. Definition and weak stability of nonconservative products. *J. Math. Pures Appl. (9)*, 74(6):483–548, 1995.

[20] Donald A. Drew and Stephen L. Passman. *Theory of multicomponent fluids*, volume 135 of *Applied Mathematical Sciences*. Springer-Verlag, New York, 1999.

[21] J. Duderstadt and Moses A. G. *Inertial Confinement Fusion*. J. Wiley and sons, 1982.

[22] S. Evje and K.K. Fjelde. Hybrid flux-splitting schemes for a two-phase flow model. *J. Comput. Phys.*, 175(2):674–701, 2002.

[23] Jean-Pierre Fouque, Josselin Garnier, and Georges Papanicolaou. *Wave propagation and time reversal in randomly layered media*. Springer, first edition, 2007.

[24] Erwin Franquet. *Modélisation Eulérienne d'écoulements multiphasiques en présence d'ondes de choc, de détonations, et d'interfaces matérielles. Application aux matériaux énergétiques nanostructurés*. PhD thesis, Université de Provence, Institut Universitaire des Systèmes Thermiques Industriels, 2006.

[25] A.R. Fraser. Radiation fronts. *Proc. Roy. Soc. London*, A 245:536–545, 1958.

[26] Thierry Gallouët, Jean-Marc Hérard, and Nicolas Seguin. Numerical modeling of two-phase flows using the two-fluid two-pressure approach. *Math. Models Methods Appl. Sci.*, 14(5):663–700, 2004.

[27] S.J. Gitomer, R.L Morse, and B.S. Newberger. Structure and scaling laws of laser-driven ablative implosions. *Physics of Fluids*, 20(2):234–238, 1977.

[28] Edwige Godlewski and Pierre-Arnaud Raviart. *Numerical approximation of hyperbolic systems of conservation laws*, volume 118 of *Applied Mathematical Sciences*. Springer-Verlag, New York, 1996.

[29] Hervé Guillard and Mathieu Labois. Numerical modelling of compressible two–phase flows. In *P. Wesseling (ed.) et al., European Conference on Computational Fluid Dynamics. ECCOMAS CFD 2006*. 2006.

[30] Ludovic Hallo, Vincent Perrier, and Rémi Abgrall. Application of a multiwave solver to ICF like problems. 46th APS, 2004.

[31] Philippe Helluy and Thomas Barberon. Finite volume simulation of cavitating flows. *Computer & Fluids*, 34(7):832–858, August 2005.

[32] T.P. Hughes. *Plasmas and laser light*. Adam and Hilger publisher, 1975.

[33] Stephane Jaouen. *Étude mathématique et numérique de la stabilité pour des modèles hydrodynamiques avec transition de phase*. PhD thesis, Université Pierre et Marie Curie, CEA Bruyères–le–Châtel, November 2001.

[34] V. V. Jikov, S. M. Kozlov, and O. A. Oleĭnik. *Homogenization of differential operators and integral functionals*. Springer-Verlag, Berlin, 1994. Translated from the Russian by G. A. Yosifian [G. A. Iosif′yan].

[35] R.Z. Khas'minskij. A limit theorem for the solutions of differential equations with random right-hand sides. *Teor. Veroyatn. Primen.*, 11:444–462, 1966.

[36] S. M. Kozlov. The averaging of random operators. *Mat. Sb. (N.S.)*, 109(151)(2):188–202, 327, 1979.

[37] Harold J. Kushner. *Approximation and weak convergence methods for random processes, with applications to stochastic systems theory*. MIT Press Series in Signal Processing, Optimization, and Control, 6. MIT Press, Cambridge, MA, 1984.

[38] Olivier Le Métayer, Jacques Massoni, and Richard Saurel. Élaboration de lois d'état d'un liquide et de sa Vapeur pour les Modèles d'écoulements Diphasiques. *Int. J. Thermal. Sci.*, 43:265–276, 2003.

[39] Olivier Le Métayer, Jacques Massoni, and Richard Saurel. Modelling evaporation fronts with reactive Riemann solvers. *J. Comput. Phys.*, 205(2):567–610, 2005.

[40] Andrew Majda and Robert L. Pego. Stable viscosity matrices for systems of conservation laws. *J. Differential Equations*, 56(2):229–262, 1985.

[41] S.P. Marsh. *LASL Shock Hugoniot data*. Los Alamos series on dynamic material properties. University of California Press, Berkeley, 1980.

[42] Ralph Menikoff and Bradley J. Plohr. The Riemann problem for fluid flow of real materials. *Rev. Modern Phys.*, 61(1):75–130, 1989.

[43] Angelo Murrone. *Modèles bi-fluides à six et sept équations pour les écoulements diphasiques à faible nombre de Mach*. PhD thesis, Université de Provence, CEA Cadarache et INRIA Sophia Antipolis, Décembre 2003.

[44] Angelo Murrone and Hervé Guillard. A five equation reduced model for compressible two-phase flow problems. *J. Comput. Phys.*, 202(2):664–698, 2005.

[45] Georges Papanicolaou and Srinivasa Varadhan. Boundary value problems with rapidly oscillating random coefficients. In *Random fields (Esztergom, 1979), Colloq. Math. Soc. János Bolyai*, pages 835–873. North Holland, New York, 1981.

[46] Mikaël Papin. *Contribution à l'étude d'écoulements supersoniques particulaires. Étude et validation d'un modèle diphasique discret.* PhD thesis, Université de Bordeaux 1, Mathématiques appliquées de Bordeaux and CEA-CESTA, Juin 2005.

[47] Mikael Papin and Rémi Abgrall. Fermetures entropiques pour les systèmes bifluides à sept équations. *C. R. Méc. Acad. Sci. Paris*, 333:838–842, 2005.

[48] Vincent Perrier. The Chapman-Jouguet closure for the Riemann problem with vaporization. *SIAM Journal on Appl. Math.*, 2006. In revision.

[49] Vincent Perrier, Rémi Abgrall, and Ludovic Hallo. A numerical scheme for the modelling of condensation and flash vaporization in compressible multi-phase flows. In *Numerical Mathematics and Advanced Applications (ENUMATH 2005)*. Springer, 2005.

[50] Vincent Perrier, Ludovic Hallo, and Rémi Abgrall. A several waves solver for phase transition in laser-matter interaction. In *28th European Conference on laser interaction with matter*, 2004.

[51] Vladas Pipiras and Murad S. Taqqu. Integration questions related to fractional Brownian motion. *Probab. Theory Related Fields*, 118(2):251–291, 2000.

[52] Robert D. Richtmyer and K. W. Morton. *Difference methods for initial-value problems*. Second edition. Interscience Tracts in Pure and Applied Mathematics, No. 4. Interscience Publishers John Wiley & Sons, Inc., New York-London-Sydney, 1967.

[53] Richard Saurel and Rémi Abgrall. A multiphase Godunov method for compressible multifluid and multiphase flows. *J. Comput. Phys.*, 150(2):425–467, 1999.

[54] Richard Saurel, Olivier Le Métayer, Jacques Massoni, and Sergey Gavrilyuk. Shock jumps conditions for multiphase mixtures with stiff mechanical relaxation. *Inter. Jour. Shock Waves*, 2006. submitted.

[55] Denis Serre. *Systems of conservation laws. I: Hyperbolicity, entropies, shock waves.* Cambridge University Press, Cambridge, 1999.

[56] José Roberto Simões-Moreira and Joseph E. Shepherd. Evaporation waves in superheated dodecane. *J. Fluid Mech.*, 382:63–86, 1999.

[57] M. Slemrod. Dynamic phase transitions in a van der Waals fluid. *J. Differential Equations*, 52(1):1–23, 1984.

[58] L. Spitzer and R. Harm. Transport phenomena in a completely ionized gas. *Phys. Rev.*, 89:977–981, 1953.

[59] Philip A. Thomson. A fundamental derivative in gasdynamics. *Phys. Fluids*, 14:1843–1849, 1971.

[60] Philip A. Thomson, Garry C. Carofano, and Yoon-Gon Kim. Shock waves and phase changes in a large heat capacity fluid emerging from a tube. *J. Fluid. Mech.*, 166:57–92, 1986.

[61] Philip A. Thomson, Humberto Chaves, G.E.A. Meier, Yoon-Gon Kim, and H.D. Speckman. Wave splitting in a fluid of large heat capacity. *J. Fluid. Mech.*, 185:385–414, 1987.

[62] Eleuterio F. Toro. *Riemann solvers and numerical methods for fluid dynamics.* Springer-Verlag, Berlin, second edition, 1999. A practical introduction.

[63] I. Toumi. A weak formulation of Roe's approximate Riemann solver. *J. Comput. Phys.*, 102(2):360–373, 1992.

[64] Burton Wendroff. The Riemann problem for materials with nonconvex equations of state. I. Isentropic flow. *J. Math. Anal. Appl.*, 38:454–466, 1972.

[65] Burton Wendroff. The Riemann problem for materials with nonconvex equations of state. II. General flow. *J. Math. Anal. Appl.*, 38:640–658, 1972.

[66] V. V. Yurinskiĭ. Averaging of symmetric diffusion in a random medium. *Sibirsk. Mat. Zh.*, 27(4):167–180, 215, 1986.

[67] Ya. B. Zel'dovich and Yu. P. Raizer. *Physics of shock waves and high temperature hydrodynamic phenomena*, volume II. Academic press, New York and London, 1967.